



National Library
of Canada

Bibliothèque nationale
du Canada

Canadian Theses Service Service des thèses canadiennes

Ottawa, Canada
K1A 0N4

NOTICE

The quality of this microform is heavily dependent upon the quality of the original thesis submitted for microfilming. Every effort has been made to ensure the highest quality of reproduction possible.

If pages are missing, contact the university which granted the degree.

Some pages may have indistinct print especially if the original pages were typed with a poor typewriter ribbon or if the university sent us an inferior photocopy.

Reproduction in full or in part of this microform is governed by the Canadian Copyright Act, R.S.C. 1970, c. C-30, and subsequent amendments.

AVIS

La qualité de cette microforme dépend grandement de la qualité de la thèse soumise au microfilmage. Nous avons tout fait pour assurer une qualité supérieure de reproduction.

S'il manque des pages, veuillez communiquer avec l'université qui a conféré le grade.

La qualité d'impression de certaines pages peut laisser à désirer, surtout si les pages originales ont été dactylographiées à l'aide d'un ruban usé ou si l'université nous a fait parvenir une photocopie de qualité inférieure.

La reproduction, même partielle, de cette microforme est soumise à la Loi canadienne sur le droit d'auteur, SRC 1970, c. C-30, et ses amendements subséquents.

UNIVERSITY OF ALBERTA

MOISTURE DEPOSITION FROM AIR FLOW
THROUGH WALL CAVITIES

BY

KENT GEORGE NIKEL



A THESIS SUBMITTED TO THE FACULTY OF
GRADUATE STUDIES AND RESEARCH
IN PARTIAL FULFILMENT OF THE REQUIREMENTS FOR
THE DEGREE OF MASTER OF SCIENCE

DEPARTMENT OF MECHANICAL ENGINEERING

EDMONTON, ALBERTA

FALL 1991



National Library
of Canada

Bibliothèque nationale
du Canada

Canadian Theses Service Service des thèses canadiennes

Ottawa, Canada
K1A 0N4

The author has granted an irrevocable non-exclusive licence allowing the National Library of Canada to reproduce, loan, distribute or sell copies of his/her thesis by any means and in any form or format, making this thesis available to interested persons.

The author retains ownership of the copyright in his/her thesis. Neither the thesis nor substantial extracts from it may be printed or otherwise reproduced without his/her permission.

L'auteur a accordé une licence irrévocable et non exclusive permettant à la Bibliothèque nationale du Canada de reproduire, prêter, distribuer ou vendre des copies de sa thèse de quelque manière et sous quelque forme que ce soit pour mettre des exemplaires de cette thèse à la disposition des personnes intéressées.

L'auteur conserve la propriété du droit d'auteur qui protège sa thèse. Ni la thèse ni des extraits substantiels de celle-ci ne doivent être imprimés ou autrement reproduits sans son autorisation.

ISBN 0-315-70172-2

UNIVERSITY OF ALBERTA

RELEASE FORM

NAME OF AUTHOR: KENT GEORGE NIKEL

TITLE OF THESIS: MOISTURE DEPOSITION FROM AIR FLOW
THROUGH WALL CAVITIES

DEGREE: MASTER OF SCIENCE

YEAR THIS DEGREE GRANTED: 1991

PERMISSION IS HEREBY GRANTED TO THE UNIVERSITY OF
ALBERTA LIBRARY TO REPRODUCE SINGLE COPIES OF THIS THESIS AND
TO LEND OR SELL SUCH COPIES FOR PRIVATE, SCHOLARLY OR
SCIENTIFIC RESEARCH PURPOSES ONLY.

THE AUTHOR RESERVES OTHER PUBLICATION RIGHTS, AND
NEITHER THE THESIS NOR EXTENSIVE EXTRACTS FROM IT MAY BE
PRINTED OR OTHERWISE REPRODUCED WITHOUT THE AUTHOR'S
WRITTEN PERMISSION.

Kent, Nikel

#204, 10750-78 Avenue.

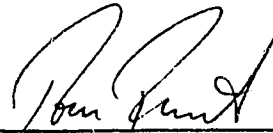
Edmonton, Alberta T6E 1P6

Date: July 11/91

UNIVERSITY OF ALBERTA

FACULTY OF GRADUATE STUDIES AND RESEARCH

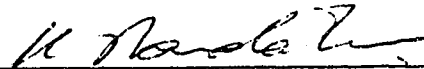
THE UNDERSIGNED CERTIFY THAT THEY HAVE READ, AND RECOMMEND
TO THE FACULTY OF GRADUATE STUDIES AND RESEARCH FOR
ACCEPTANCE, A THESIS ENTITLED MOISTURE DEPOSITION FROM
AIR FLOW THROUGH WALL CAVITIES
SUBMITTED BY KENT GEORGE NIKEL
IN PARTIAL FULFILMENT OF THE REQUIREMENTS FOR THE DEGREE OF
MASTER OF SCIENCE IN MECHANICAL ENGINEERING.



Dr. T.W. Forest, Supervisor



Dr. D.J. Wilson, Co-Supervisor



Dr. K. Nandakumar

Date: July 8/91

To
Marian Nickel
For your love and patience

ABSTRACT

Significant damage to residential buildings can result from moisture trapped within wall cavities. Most of the moisture entering wall cavities is due to air leakage through cracks around baseboards or electrical fittings. The entering moisture deposits on the exterior sheathing, and over time, rotting and the growth of micro-organisms can occur.

Air flow through the wall cavity is modeled as two-dimensional flow through a porous medium. The air flow transports moisture into the cavity which then diffuses toward the exterior sheathing, where it deposits. The air-vapour flow is assumed to have constant properties and behaves according to Darcy's Law for flow through porous medium, while the diffusion of moisture within the cavity is governed by Fick's Law. The governing equations for heat and mass transfer are solved analytically with imposed boundary conditions on each side of the cavity. The heat and mass equations are independent, except for the boundary condition for partial pressure of water vapour at the condensing surface. One side of the cavity is isothermal and impermeable to mass diffusion while the other side is isothermal and acts as a limited moisture source/sink.

The resulting solutions for the heat and mass transfer equations were compared to measurements in a test house. The thermal boundary layers from the warm inlet air flow, become fully developed a short distance into the cavity. Conduction dominates heat transfer beyond the thermally developing region. The wall temperature predicted when convective heat transfer within the wall was neglected agreed closely with the temperature predicted using the convective heat transfer model.

Deposition of moisture occurs at the insulation-sheathing interface. Most of the moisture entering the wall cavity, either by exfiltration or infiltration, deposits near the inlet. Infiltration was shown to be capable of either depositing or removing moisture from the exterior sheathing. Accumulation of moisture within the porous medium is negligible for typical indoor relative humidity and temperature conditions found throughout Canada.

The moisture deposition model was able to follow the trends recorded in the measured data and gave reasonable estimates for the measured deposition. A sensitivity analysis was conducted on the parameters that most affected the model: flow rate, cavity dimensions, porous medium properties, and wall boundary conditions. The range of inlet relative humidities and wall temperatures over which the moisture deposition model was valid was determined and found to encompass the majority of conditions experienced by Canadian housing.

ACKNOWLEDGEMENTS

I would like to acknowledge the continuing advice and assistance of Drs. Forest and Wilson in the preparation of this work. Their help has been greatly appreciated.

This work was financed in part by the R.M. Hardy Engineering Enrichment Fund; and an American Society of Heating, Refrigerating, and Air Conditioning Engineers' Grant-In-Aid.

TABLE OF CONTENTS

	Page
LIST OF TABLES	xii
LIST OF FIGURES	xiv
NOMENCLATURE	xxi
 1 INTRODUCTION	 1
1.1 Historical Development and Literature Review	4
1.2 Features of the Heat and Mass Transfer Models	6
 2 DEVELOPMENT OF THE HEAT AND MASS TRANSFER MODELS FOR FLOW THROUGH INSULATION FILLED CAVITIES	 8
2.1 Basic Assumptions and Simplifications for the Models	8
2.1.1 Construction of the real and idealized wall cavities	9
2.1.2 Cavity air flow and entrance and exit effects	10
2.1.3 Indoor and outdoor conditions	11
2.1.4 Latent heat energy	11
2.1.5 The porous medium	12
2.1.6 Flow through porous medium — Darcy's Law	13
2.1.7 Heat transfer through porous medium in wall cavities	14
2.1.8 Mass transfer and porous medium	18
2.2 Development of the Heat Transfer Model	19
2.2.1 Boundary conditions specific to the heat transfer problem	19
2.2.2 Deriving the temperature profile and temperature gradient expressions	20
2.2.3 Behaviour of the temperature profile solution	26
2.2.4 Determining the number of terms to retain in the temperature profile equations	28
2.2.5 Changing the flow velocity through the wall cavity	30

2.2.6	Changing the inlet plane temperature profile	31
2.2.7	Overall heat balance for an insulation-filled cavity	32
2.3	Development of the Mass Diffusion Model	36
2.3.1	Boundary conditions specific to the mass diffusion problem	37
2.3.2	Deriving the partial pressure profile and gradient expressions	38
2.3.3	The mass flux solution	43
2.3.4	An examination of the partial pressure and mass flux equations	44
2.3.4.1	Partial pressure profiles and heat fluxes for exfiltration	45
2.3.4.2	Partial pressure profiles and heat fluxes for infiltration	47
2.3.5	Determining the number of terms to retain in the summation	48
2.3.6	Effect of flow rate on the humidity ratio profile	49
2.3.7	Region of validity for the mass diffusion model	50
2.3.7.1	Background development for determining the region of validity	50
2.3.7.2	Calculating the region of validity	52
2.3.7.3	Mapping of the region of validity	53
2.3.7.4	Comparison of measured home relative humidities and the region of validity for the moisture deposition model	54
3	EXPERIMENTAL METHODS AND MODEL EVALUATION	80
3.1	Review of Experimental Apparatus, Method, and Data Obtained	80
3.1.1	Description of the wall test panel	81
3.1.2	Measuring moisture deposition	82
3.1.3	Measuring temperatures	84
3.1.4	Indoor and outdoor relative humidity and humidity ratios	84
3.1.5	Flow through the wall cavities	85
3.2	Heat Transfer Model Testing	87
3.2.1	The ASHRAE-based steady-state heat transfer models	88
3.2.1.1	The basic ASHRAE heat transfer model	88
3.2.1.2	The modified ASHRAE heat transfer model	89

3.2.1.3 Comparing the basic and modified ASHRAE heat transfer models	90
3.2.2 Comparing the modified ASHRAE heat transfer model to the internal forced convective heat transfer model	92
3.3 Testing the Moisture Deposition Model	93
3.3.1 The outer cavity wall boundary condition	94
3.3.1.1 The internal moisture limit concept	94
3.3.1.2 Selecting an appropriate internal moisture limit and calculating moisture deposition boundary conditions	97
3.3.2 Moisture deposition in the upper wall zones	98
3.3.3 Moisture deposition in the lower wall zones	102
3.3.4 Effect of the moisture deposition model's region of validity on the test results	103
3.3.5 Summary of the moisture deposition model testing	103
 4 PARAMETRIC STUDIES OF THE SENSITIVITY OF THE MOISTURE DEPOSITION MODEL TO VARIATIONS IN INPUT PARAMETERS	132
4.1 Initial Parameters for the Sensitivity Study	132
4.2 The Effect of Varying the Internal Moisture Limit on Moisture Deposition	133
4.2.1 The effect of internal moisture limits on wall relative humidity	134
4.2.2 Choosing an internal moisture limit below the base case 20% IML	136
4.2.3 Choosing an internal moisture content above the base case 20% IML	137
4.3 Dependence of Moisture Deposition on Changes in Distribution of Flow	139
4.4 Effect of Changing Mass Diffusivity on Moisture Deposition	141
4.5 The Effect of Changing Wall Height on Moisture Deposition	144
4.6 The Effect of Changing Cavity Width on Moisture Deposition	146
4.7 Summary of Sensitivity Study	148
 CONCLUSIONS AND RECOMMENDATIONS	165

REFERENCES	169
APPENDIX A: Results of the Moisture Deposition Measurements	173
APPENDIX B: Determining the Flow Division Between the Upper and Lower Wall Sections.	177
APPENDIX C: ASHRAE-Based Calculations	183
C.1 Steady-State Heat Transfer	183
C.2 Steady-State Moisture Diffusion	185
C.3 Determining the Mass of Water Entering the Cavity by Convection	187
C.4 Determining the Saturated Partial Pressure	189
APPENDIX D: Estimating the Amount of Energy Released by Condensation . .	191
APPENDIX E: Alternate Solutions to the Governing Differential Equation for Heat Transfer	192

LIST OF TABLES

Table	Page
2.1 Typical Rayleigh numbers for closed and open wall cavities filled with glass fibre insulation.	56
2.2 Base case parameters and variables used to examine the exact solution for temperature profiles and heat fluxes within a porous medium filled cavity. The cavity is shown in Figure 2.2. The walls have no thermal resistance.	57
2.3 Base case parameters and variables used to examine the exact solution for partial pressure profiles and mass fluxes within a porous medium filled cavity. The cavity is shown in Figure 2.3.	58
3.1 Construction details of Alberta Home Heating Research Facility test House 6.	105
3.2 Summary of velocity flow data and calculated flow velocities in the north wall test cavity. The upper wall cavity had 2/3 of the total flow. . .	106
3.3 Summary of velocity flow data and calculated flow velocities in the south wall test cavity. The upper wall cavity had 2/3 of the total flow. . .	107
3.4 Comparison of the measured moisture deposition in each zone of the upper wall section and the predictions of the moisture deposition model.	108
3.5 Comparison of the measured moisture deposition in each zone of the lower wall section and the predictions of the moisture deposition model.	109
4.1 Base case parameters used in the sensitivity analysis for the north wall test panel, upper and lower sections.	149
4.2 Mass accumulation predicted on the outer cavity wall after 550 hours using the base case parameters.	150
A.1 Moisture accumulated at the moisture plugs in the north wall 169 hours (seven days) after testing began.	174
A.2 Moisture accumulated at the moisture plugs in the north wall 314 hours (thirteen days) after testing began.	175

Table	Page
A.3 Moisture accumulated at the moisture plugs in the north wall 501 hours (twenty-one days) after testing began.	176
B.1 Physical properties used in evaluating the flow division through the wall cavity.	182
B.2 Summary of flow distributions with various driving pressures and crack sizes.	182
C.1 Parameters used for the example ASHRAE steady state conduction temperature calculations.	184
C.2 Calculated temperatures and temperature drops between the layers of a typical multi-layered wall.	184
C.3 Temperature, relative humidity, and partial pressures on the surfaces of a typical wall cavity.	186
C.4 Calculated vapour diffusion through the wall cavity using the ASHRAE steady state method.	186
C.5 Values of the coefficients used to determine the water vapour saturation pressure and gradient	190

LIST OF FIGURES

Figure	Page
2.1 A comparison of a typical real wall cavity and the idealized parallel plate wall cavity.	59
2.2 Description of the wall cavity used to develop the heat transfer model. The inlet velocity is constant across the cavity depth and the temperature profile is linear.	60
2.3 Description of wall cavity used to derive the moisture transport equations. The inlet velocity and partial pressure profiles are linear. The left side boundary is impermeable to moisture.	61
2.4 Pressure distribution across a building wall due to stack and wind action.	62
2.5 The velocity profile for flow in an open cavity and for flow through porous medium	63
2.6 (a) Exact temperature profile for exfiltrating flow through a porous medium filled wall cavity as the vertical distance from the inlet plane increases. (b) Horizontal heat flux corresponding to the gradient of the temperature profiles shown in (a). The flow becomes thermally developed approximately 20 cm from the inlet.	64
2.7 (a) Exact temperature profile for infiltrating flow through a porous medium filled wall cavity as the vertical distance from the inlet plane increases. (b) Horizontal heat flux corresponding to the gradient of the temperature profiles shown in (a). The flow becomes thermally developed approximately 20 cm from the inlet.	65
2.8 (a) Temperature profiles evaluated with varying the number of terms retained in Eqn. (2.33) (b) Error in temperature caused when retaining a small number of terms. The curves were evaluated 1 cm from the inlet. The base solution retained 20 terms ($N = 20$).	66
2.9 (a) Horizontal heat flux determined from the slope of the temperature profiles when evaluated using an increasing number of retained terms in Eqn. (2.34). (b) Error in heat flux caused when retaining a small number of terms. The curves were evaluated 1 cm from the inlet. Thermal conductivity for the porous medium was $0.0425 \text{ W}\cdot\text{m}^{-1}\cdot\text{K}^{-1}$. The base solution retained 20 terms ($N = 20$).	67

- 2.10 Effect on temperature profiles of increasing the exfiltrating flow velocity. With an increased flow rate the temperature profiles are more horizontal indicating a larger temperature difference from the conduction solution (zero flow). Evaluated at 1 cm from the inlet. 68
- 2.11 Temperature profiles for exfiltrating flow when the inlet temperature is greater than the warm wall temperature. Flow entering with a temperature higher than the warm wall boundary temperature will cause a bowing of the temperature profile. Evaluated at 1 cm from the inlet. . . . 69
- 2.12 Temperature profiles for infiltrating flow when the inlet temperature is less than the cold wall temperature. Flow entering with a temperature lower than the cold wall boundary temperature will cause a bowing of the temperature profile. Evaluated at 1 cm from the inlet. 70
- 2.13 (a) Partial pressure profiles for exfiltrating flow through a porous medium filled wall cavity. (b) Mass flux of moisture through the porous medium. (Exfiltration: $T_{room} = 20^{\circ}\text{C}$; $\phi_{room} = 50\%$; $T_c = -20^{\circ}\text{C}$; $\phi_c = 100\%$; $w = 0.001 \text{ m}\cdot\text{s}^{-1}$; $D = 2.56\cdot 10^{-5} \text{ m}^2\cdot\text{s}^{-1}$; $N = 20$) . . . 71
- 2.14 (a) Partial pressure profiles for infiltrating flow through a porous medium filled wall cavity. (b) Mass flux of moisture through the porous medium. (Infiltration: $T_{out} = -30^{\circ}\text{C}$; $\phi_{out} = 80\%$; $T_c = -20^{\circ}\text{C}$; $\phi_c = 100\%$; $w = 0.001 \text{ m}\cdot\text{s}^{-1}$; $D = 2.56\cdot 10^{-5} \text{ m}^2\cdot\text{s}^{-1}$; $N = 20$) 72
- 2.15 (a) Variation in the partial pressure profile (Eqn. (2.70)) when retaining an increasing number of terms. (b) Error in the calculated partial pressures. (Exfiltration: $T_{room} = 20^{\circ}\text{C}$; $\phi_{room} = 50\%$; $T_c = -20^{\circ}\text{C}$; $\phi_c = 100\%$; $w = 0.001 \text{ m}\cdot\text{s}^{-1}$; $D = 2.56\cdot 10^{-5} \text{ m}^2\cdot\text{s}^{-1}$; $\Delta z = 1 \text{ cm}$) 73
- 2.16 (a) Variation in mass flux (Eqn. (2.71)) when retaining an increasing number of terms. (b) Error in the calculated mass fluxes. (Exfiltration: $T_{room} = 20^{\circ}\text{C}$; $\phi_{room} = 50\%$; $T_c = -20^{\circ}\text{C}$; $\phi_c = 100\%$; $w = 0.001 \text{ m}\cdot\text{s}^{-1}$; $D = 2.56\cdot 10^{-5} \text{ m}^2\cdot\text{s}^{-1}$; $\Delta z = 1 \text{ cm}$) 74
- 2.17 Variation in humidity ratio profiles for increasing exfiltration velocity. (Exfiltration: $T_{room} = 20^{\circ}\text{C}$; $\phi_{room} = 50\%$; $T_c = -20^{\circ}\text{C}$; $\phi_c = 100\%$; $D = 2.56\cdot 10^{-5} \text{ m}^2\cdot\text{s}^{-1}$; $n = 20$; $\Delta z = 1 \text{ cm}$) 75

Figure	Page
2.18 Three possible partial pressure profile conditions within the wall cavity. (a) shows that the model is valid and deposition occurs at the outer cavity wall ($\phi_{inlet} = 30\%$). (b) shows the transition point where deposition in the insulation may occur ($\phi_{inlet} = 50\%$). (c) indicates that the model is invalid and deposition will occur within the insulation ($\phi_{inlet} = 70\%$).	76
2.19 Region of validity for the moisture deposition model for very high exfiltration velocity. (Exfiltration: $T_{room} = 20^{\circ}\text{C}$; $D = 2.56 \cdot 10^{-5} \text{ m}^2 \cdot \text{s}^{-1}$; $N = 20$; $w = 0.01 \text{ m} \cdot \text{s}^{-1}$)	77
2.20 Region of validity for the moisture deposition model for slow flow rates. (Exfiltration: $T_{room} = 20^{\circ}\text{C}$; $D = 2.56 \cdot 10^{-5} \text{ m}^2 \cdot \text{s}^{-1}$; $N = 20$; $w = 0.0001 \text{ m} \cdot \text{s}^{-1}$)	78
2.21 Typical relative humidities and temperature distributions for Canadian homes, Kent <i>et al.</i> (1966), superimposed on the region of validity for the moisture deposition model. ($T_{room} = 20^{\circ}\text{C}$; $w = 0.01 \text{ m} \cdot \text{s}^{-1}$)	79
3.1 Alberta Home Heating Research Facility House 6 used in experimentally validating the moisture deposition model.	110
3.2 Plan view of House 6 at the Alberta Home Heating Research Facility showing the location of the wall test panels in the north and south walls.	111
3.3 Front view of the north wall test panel showing construction details, placement of the moisture plugs, and the location of the exfiltration site.	112
3.4 Side view and construction details of the north wall test panel. The annular slit orifice plate flowmeter acts as the exfiltration site on the interior wall of the test panel.	113
3.5 Labelling of the individual moisture plugs and grouping of the plugs into zones. Each zone consists of three horizontal plugs. Zones 1 to 3 constitute the upper wall section while zones 4 to 6 constitute the lower wall section.	114
3.6 Daily averaged indoor—outdoor temperature difference for AHHRF House 6 from 26 January to 18 February 1988. The indoor temperature was maintained at $20^{\circ}\text{C} \pm 1.5^{\circ}\text{C}$	115

Figure	Page
3.7 Daily averaged indoor and outdoor humidity ratios for House 6 at the AHHRF from 26 January to 18 February 1988. The indoor relative humidity was maintained at $40\% \pm 3\%$ while the indoor temperature was maintained at $20^{\circ}\text{C} \pm 1.5^{\circ}\text{C}$	116
3.8 The flow rate of moist air through the north wall cavity in House 6 at the AHHRF from 1400h, 26 January 1988 to 1100h, 18 February 1988. Data was recorded eighty times each hour and then averaged over the hour.	117
3.9 The flow rate of moist air through the south wall cavity in House 6 at the AHHRF from 1400h, 26 January 1988 to 1100h, 18 February 1988. Data was recorded eighty times each hour and then averaged over the hour.	118
3.10 A comparison of the actual measured temperatures on the outer cavity wall for the north test panel with the ASHRAE-based models. The basic model used no solar data while the modified model used solar data.	119
3.11 A comparison of the actual measured temperatures on the outer cavity wall for the south test panel with the ASHRAE-based models. The basic model used no solar data while the modified model used solar data.	120
3.12 Comparison of measured temperatures on the outer cavity wall with predictions made using the internal convection (non-steady state) model and the modified ASHRAE steady-state model. Both models include solar radiation and wind speed effects.	121
3.13 The 20% internal moisture limit ramp function used for determining the relative humidity on the outer cavity wall given wood moisture contents. Saturated conditions are reached when the wood moisture content exceeds 20%.	122
3.14 Outer cavity wall wood moisture content and corresponding relative humidity using a 20% internal moisture limit. Curves are for the upper section of the north wall test panel.	123
3.15 Outer cavity wall wood moisture content and corresponding relative humidity using a 20% internal moisture limit. Curves are for the lower section of the north wall test panel.	124

Figure	Page
3.16 Cumulative moisture deposition on the north test panel outer cavity wall in zone 1 when using a 20% internal moisture limit. The solid line indicates the model predicted depositions. Shown also is the corresponding total flow rate through the north test panel.	125
3.17 Cumulative moisture deposition on the north test panel outer cavity wall in zone 2 when using a 20% internal moisture limit. The solid line indicates the model predicted depositions. Shown also is the corresponding total flow rate through the north test panel.	126
3.18 Cumulative moisture deposition on the north test panel outer cavity wall in zone 3 when using a 20% internal moisture limit. The solid line indicates the model predicted depositions. Shown also is the corresponding total flow rate through the north test panel.	127
3.19 Contribution of exfiltration and infiltration to cumulative moisture deposition in zone 3 during the test period.	128
3.20 Cumulative moisture deposition on the north test panel outer cavity wall in zone 4 when using a 20% internal moisture limit. The solid line indicates the model predicted depositions. Shown also is the corresponding total flow rate through the north test panel.	129
3.21 Cumulative moisture deposition on the north test panel outer cavity wall in zone 5 when using a 20% internal moisture limit. The solid line indicates the model predicted depositions. Shown also is the corresponding total flow rate through the north test panel.	130
3.22 Cumulative moisture deposition on the north test panel outer cavity wall in zone 6 when using a 20% internal moisture limit. The solid line indicates the model predicted depositions. Shown also is the corresponding total flow rate through the north test panel.	131
4.1 The internal moisture limit ramp functions used for comparing the sensitivity of the moisture deposition model to changes in the outer cavity wall boundary conditions.	151
4.2 A comparison of the relative humidity boundary conditions for various internal moisture limits used in the sensitivity studies. Each curve corresponds to a prescribed internal moisture limit for the upper wall section where the base case has an internal moisture limit of 20%.	152

Figure	Page
4.3 Cumulative moisture deposition in zone 1 as the internal moisture limit is increased from 15% to 60%. The upper cavity had 2/3 of the total flow shown in the upper graph.	153
4.4 Cumulative moisture deposition in zone 2 as the internal moisture limit is increased from 15% to 60%. The upper cavity had 2/3 of the total flow shown in the upper graph.	154
4.5 Cumulative moisture deposition in zone 3 as the internal moisture limit is increased from 15% to 60%. The upper cavity had 2/3 of the total flow shown in the upper graph.	155
4.6 Cumulative moisture deposition in zone 4 as the internal moisture limit is increased from 15% to 60%. The lower cavity had 1/3 of the total flow shown in the upper graph.	156
4.7 Cumulative moisture deposition in zone 5 as the internal moisture limit is increased from 15% to 60%. The lower cavity had 1/3 of the total flow shown in the upper graph.	157
4.8 Cumulative moisture deposition in zone 6 as the internal moisture limit is increased from 15% to 60%. The lower cavity had 1/3 of the total flow shown in the upper graph.	158
4.9 Cumulative moisture deposition in (a) zone 1 and (b) zone 3 for increasing and decreasing the total flow rate by 10%. An increased flow rate in the upper wall section increases moisture deposition and moisture evaporation. (IML = 20%)	159
4.10 Cumulative moisture deposition in (a) zone 4 and (b) zone 6 for increasing and decreasing the total flow rate by 10%. Increasing the flow in the lower wall section correspondingly decreases the flow in the upper wall section.	160
4.11 Cumulative moisture deposition in (a) zone 1 and (b) zone 3 for doubling and halving the mass diffusivity (D). Deposition in zone 1 is dominated by exfiltration while deposition in zone 3 is dominated by infiltration. (IML = 20%)	161

Figure	Page
4.12 Cumulative moisture deposition in zone 3 for (a) one-half and (b) twice the standard mass diffusivity. Each graph shows the contribution to the total moisture deposition by exfiltration and infiltration. For low diffusivities exfiltration is prominent. For high diffusivities moisture deposition by infiltration dominates.	162
4.13 Cumulative moisture deposition in (a) zone 1 and (b) zone 3 for increasing wall height. Increasing the wall height moves zone 3 further from the upper leakage site and therefore reduces the effect of infiltration on moisture deposition. Zone 1 is unaffected by changing the wall height. (IML = 20%)	163
4.14 Cumulative moisture deposition in (a) zone 1 and (b) zone 3 for decreasing cavity width. A narrower cavity increases the mass flux causing increased deposition in the lower zone and increased evaporation in the upper zone. (IML = 20%)	164
B.1 Schematic of an analogous resistance diagram for flow through the wall cavity.	181

NOMENCLATURE

A_c	Crack area [m^2]
A_v	Area of the wall in the vertical plane [m^2]
A_m	Cross sectional area of the porous media perpendicular to the flow direction [m^2]
C_A	Mass concentration of component A [$\text{kg}\cdot\text{m}^{-3}$]
C_p	Specific heat at constant pressure for air [$\text{J}\cdot\text{kg}^{-1}\cdot\text{K}^{-1}$]
C_w	Mass concentration of water vapour [$\text{kg}\cdot\text{m}^{-3}$]
D	Mass diffusivity of water vapour into air [$\text{m}^2\cdot\text{s}^{-1}$]
d	Depth of wall cavity between the inside and outside walls [m]
g	Gravitational acceleration [$\text{m}\cdot\text{s}^{-2}$]
H	Height of wall cavity [m]
h_a	Convective heat transfer coefficient for the interior wall [$\text{W}\cdot\text{m}^{-2}\cdot\text{K}^{-1}$]
h_d	Convective and radiation heat transfer coefficient for exterior wall [$\text{W}\cdot\text{m}^{-2}\cdot\text{K}^{-1}$]
h_v	Vertical height travelled per unit time [$\text{m}\cdot\text{h}^{-1}$]
I_D	Diffuse solar radiation [$\text{W}\cdot\text{m}^{-2}$]
I_{DN}	Direct normal solar radiation [$\text{W}\cdot\text{m}^{-2}$]
I_R	Reflected solar radiation [$\text{W}\cdot\text{m}^{-2}$]
I_T	Total solar radiation [$\text{W}\cdot\text{m}^{-2}$]
IML	Internal moisture limit [%]
K	Permeability of porous medium [m^2]
k	Thermal conductivity of porous medium [$\text{W}\cdot\text{m}^{-1}\cdot\text{K}^{-1}$]
L	Width of cavity [m]
M	Permeance coefficient [$\text{ng}\cdot\text{s}^{-1}\cdot\text{m}^{-1}\cdot\text{Pa}^{-1}$]
M_{air}	Molecular mass of air [$\text{kg}\cdot\text{kmol}^{-1}$]
M_w	Molecular mass of water [$\text{kg}\cdot\text{kmol}^{-1}$]
m_{air}	Mass of air [kg]

m_w	Mass of water [kg]
\dot{m}	Mass flow rate [kg·s ⁻¹]
\dot{m}''	Mass flux as defined by Fick's Law [kg·m ⁻² ·s ⁻¹]
MC _v	Wood moisture content by volume
MC _{wt}	Wood moisture content by weight
N	Number of terms to retain in summation
n	Orifice flow exponent (1/2 = turbulent flow, 1 = laminar flow)
n	Summation index
ΔP_c	Pressure difference across a crack [Pa]
ΔP_m	Pressure difference across the porous media filled cavity [Pa]
ΔP_{wall}	External-internal pressure difference [Pa]
p_{atm}	Total atmospheric pressure [Pa]
$p_w(x,z)$	Partial pressure of water vapour at position (x,z) [Pa]
$p_{w,c}$	Partial pressure of water vapour on outer cavity wall [Pa]
$p_{w,out}$	Partial pressure of water vapour outside [Pa]
$p_{w,room}$	Partial pressure of water vapour inside [Pa]
p_{ws}	Partial pressure of water vapour at saturation [Pa]
$p_{ws,c}$	Partial pressure of water vapour at saturation on outer cavity wall [Pa]
Q	Volume flow rate [m ³ ·s ⁻¹]
Q_I	Volume flow rate through the crack in wall I [m ³ ·s ⁻¹]
Q_{II}	Volume flow rate through the crack in wall II [m ³ ·s ⁻¹]
q	Heat [W]
q''	Heat flux [W·m ⁻²]
Ra^*	Darcy-modified Rayleigh number for closed cavities filled with porous medium
Ra_w	Rayleigh number for open cavities filled with porous medium
R_0	Universal gas constant [J·kmol ⁻¹ ·K ⁻¹]
R_I	Thermal resistance of the interior wall [K·m ² ·W ⁻¹]
R_{II}	Thermal resistance of the exterior wall [K·m ² ·W ⁻¹]

ΔT_E	Temperature difference between the inlet and the inner cavity wall for exfiltrating flow [K]
ΔT_I	Temperature difference between the inlet and the outer cavity wall for infiltrating flow [K]
ΔT_{wall}	Temperature difference across the wall cavity [K]
T	Property averaged temperature, $\frac{T_{room} + T_c}{2}$ [K]
$T_{(x,z)}$	Temperature at position (x,z) [K]
T_a	Temperature of interior wall [K]
T_b	Temperature of inner cavity wall [K]
T_c	Temperature of outer cavity wall [K]
T_d	Temperature of exterior wall [K]
T_I	Temperature of inlet profile at inner cavity wall boundary [K]
T_{II}	Temperature of inlet profile at outer cavity wall boundary [K]
T_{room}	Temperature of the inside room [K]
T_{out}	Temperature outside [K]
u	Velocity in the x direction [$m \cdot s^{-1}$]
v	Velocity in the y direction [$m \cdot s^{-1}$]
W	Humidity ratio [$g_{water} \cdot (kg_{dry air})^{-1}$]
w	Velocity in the z direction [$m \cdot s^{-1}$]
x	Horizontal position (depth) coordinate measured from the inner cavity wall [m]
\bar{x}	Non-dimensionalized depth (x/d)
y	Horizontal position (width) coordinate [m]
z	Vertical position coordinate [m]
\bar{z}	Non-dimensionalized height (z/H)
Δz	Distance from the inlet plane in the flow direction [m]

GREEK SYMBOLS

α	Thermal diffusivity of fluid-saturated porous media [$\text{m}^2 \cdot \text{s}^{-1}$]
α_d	Absorptance of surface d for solar radiation [dimensionless]
β	Coefficient of thermal expansion [K^{-1}]
λ	Separation constant
μ	Dynamic viscosity [$\text{kg} \cdot \text{m}^{-1} \cdot \text{s}^{-1}$]
ν	Kinematic viscosity [$\text{m}^2 \cdot \text{s}^{-1}$]
ρ	Density [$\text{kg} \cdot \text{m}^{-3}$]
ρ_w	Density of water vapour [$\text{kg} \cdot \text{m}^{-3}$]
θ	Non-dimensional temperature difference
θ_i	Incident solar angle
ϕ_c	Relative humidity on outer cavity wall [$p_{w,c}/p_{ws,c}$]
ϕ_{room}	Relative humidity inside [$p_{w,\text{room}}/p_{ws,\text{room}}$]
ϕ_{out}	Relative humidity outside [$p_{w,\text{out}}/p_{ws,\text{out}}$]

SUBSCRIPTS

<i>a</i>	Interior wall
<i>b</i>	Inner cavity wall
<i>c</i>	Outer cavity wall
<i>d</i>	Exterior wall
<i>f</i>	Fluid in media (air)
<i>I</i>	Interior (warm) wall
<i>II</i>	Exterior (cold) wall
<i>out</i>	Outside of building
<i>w</i>	Water
<i>air</i>	Air

SUPERSCRIPTS

"	Flux [m^{-1}]
---	--------------------------

CHAPTER 1

INTRODUCTION

Since the mid 1970s it has been the aim of home designers and builders to design and construct the most energy efficient homes possible. To do this, homes have been built with thicker walls to hold more insulation, high-efficiency flue-less furnaces, sealed windows, and tightly sealed walls and ceilings. To their credit, the cost of heating (or cooling) the newer homes are considerably less than the homes built in the 1950s and 1960s. However, what the modern designers failed to consider was the effect a "tight" house would have on indoor temperature and humidity levels. Present home designs are capable of maintaining a constant temperature but often fail at maintaining relative humidity at a comfortable and healthy level. Sterling *et al.* (1985) recommend an indoor relative humidity level of between 40 and 50% at 20°C. During winter months, the indoor relative humidity rarely exceeds 30% at 20°C.

A typical method of maintaining a constant indoor temperature is to seal the leakage sites that allow warm indoor air to exfiltrate, or cold outdoor air to infiltrate. While this certainly helps to reduce energy costs, it fails to maintain a healthy indoor environment; stale, humid indoor air remains trapped within the house and the relative humidity level rises as moisture is continually added to the indoor air. Some of the sources of moisture in homes, and the amount they contribute, are cooking (≈ 0.5 l/meal), cleaning (≈ 1 l/day), and showering (≈ 0.3 l/shower), ASHRAE (1988). The single largest source of moisture is from the respiration of the occupants: a typical human generates ≈ 4 l/day, ASHRAE (1988). For a family of four, the total amount of moisture entering the indoor air, per day, would be over 15 l. This excess moisture must be removed from the house before moisture related damage can begin to occur.

Moisture can be removed from "tight" homes using a mechanical ventilation system (typically exhaust fans). However, when indoor air is vented to the outdoors, not only is the excess moisture removed, but so is the warm indoor air. This defeats

the energy conservation aspect of the house design. Installing an air-to-air heat exchanger on the outlet of the exhaust fan would recoup some of the heat energy lost. However, since the majority of newer homes do not have a ventilation system dedicated to removing moist indoor air, they rely solely on periodic use of stove-top exhaust fans or open windows to remove built-up moisture. This type of ventilation is often insufficient to prevent moisture related damage from occurring.

One moisture related problem associated with newer, unventilated homes and older homes, is the build-up of moisture within wall cavities. The problem is more acute during winter months when warm, humid air exfiltrates into the wall cavity and deposits on the exterior sheathing. In spring, melting results in damage to the building materials in the wall.

Moist air can enter the wall cavity from the indoor environment through two mechanisms: vapour diffusion and vapour convection. Vapour diffusion occurs due to the difference in partial pressure of water vapour between the humid indoor environment and the dry outdoor environment. Convection occurs due to an indoor-outdoor total pressure differential which drives air out of the home. Studies have shown that vapour convection through walls carries 10 to 4000 times as much water vapour than does vapour diffusion, TenWolde and Suleski (1984). House designers try to reduce the amount of moisture entering walls by specifying the use of vapour retarders during construction. Vapour retarders, usually made of a thin polyethylene sheet, resist the diffusion of moisture and, if securely sealed to the wood frame of the house and free of punctures, will act as an air barrier by eliminating air flow through the wall cavity. The key point here is that the vapour retarder must be free of all leaks. If it is not, air will flow through the barrier and into the wall, bringing moisture along with it.

Ideally, if a home is built properly, there will be no breaks in the vapour retarder, no air flow through the wall cavity, and moisture will be forced out of the home using mechanical ventilation. However, in the real world, homes do not use mechanical ventilation, vapour retarders are poorly installed, and air leaks through wall cavities. Moisture can therefore accumulate in the wall cavity over the heating

season and then melt or evaporate in warmer outdoor temperatures. Any moisture that does not evaporate will run down the inside of the wall and, over time, cause damage to both the wooden studs framing the house and the insulation within the wall. The damage to wood involves rotting, and in addition, if the wood remains damp for extended periods, the possibility of mould growth exists. Insulation will lose its thermal resistance, making it ineffective in saving energy for the home owner. These consequences are tied directly to climatic conditions.

Moisture related problems are more common in areas where the outdoor winter conditions are mild and the year-round outdoor relative humidities are high, as opposed to areas which have severe winters and low year-round ambient relative humidities. Coastal areas fall into the former category while the Prairies fall into the latter category. During the winter months, the indoor relative humidity in coastal areas is capable of reaching levels in excess of 50%. If the humid air enters the wall cavity, large amounts of moisture will be deposited and absorbed by the wood frame of the house and the exterior sheathing. In spring, the ambient temperature increases, and because the ambient relative humidity is high, the ambient air is incapable of desorbing moisture from the exterior sheathing. Thus, the wooden studs in the wall cavity would have a tendency to retain any absorbed moisture, and wood rot may result. In the dryer prairies, even in winter, it is extremely difficult to maintain high indoor relative humidities. Typical relative humidities during winter are less than 30%, Kent *et al.* (1966), and therefore, less moisture enters the wall cavity. The moisture that does accumulate over the winter months tends to evaporate rapidly as the ambient temperatures increase during the dry summer.

Historically, in older homes the accumulation of moisture within building envelopes has been a serious and potentially dangerous situation. Imperfections in the building envelope during construction make newer homes susceptible to this same moisture damage. What the designer of new homes needs is a model to predict the deposition of moisture within wall cavities in order to better understand the problem.

1.1 Historical Development and Literature Review

Several models have been devised to analyze and predict the moisture performance of walls. The most common model is the simple ASHRAE (1989) method for vapour diffusing through a multi-layered wall. The ASHRAE model divides the wall into a number of parallel elements, each of which has a resistance to moisture diffusion. The elements are connected in series in order to calculate the total amount of moisture able to diffuse through the wall. However, this model is extremely limited in scope as it fails to include convective transport of moisture through the wall cavity by air exfiltration and infiltration. Other models have been devised to overcome this deficiency.

TenWolde (1985) presented a model which incorporated water vapour movement in multi-layered walls by diffusion and convection. The analysis was based on a one-dimensional analytical solution to the heat and mass diffusion equations.

TenWolde's model was capable of tracking the progress of the condensation front as it moved through the porous insulation. The forced flow part of TenWolde's model allowed for flow only in the direction of the moisture diffusion, i.e. perpendicular to the cavity. However, in most wall structures the flow is not parallel to the diffusion of moisture. Usually the leakage path induces air flow in the vertical direction, while heat and moisture continue to migrate in the horizontal direction. When a leak exists in a wall structure it becomes the dominant entrance or exit for moisture and the effect of diffusion through walls often becomes negligible, TenWolde and Suleski (1984). Ogniewicz and Tien (1981) conducted a one-dimensional numerical study of condensation in vertical porous insulation, but again, only with horizontal flow.

Much research is being dedicated to developing a model for heat transfer through a vertical cavity with combined natural and forced convection. Bejan (1984) discusses analytical solutions for forced convection and natural convection in closed cavities. Each type of convective heat transfer is dealt with independently and are not combined in a single open vertical cavity. A full numerical approach was presented

by Burns *et al.* (1977) and Burns and Tien (1978) for combined natural and forced convection.

In their study, a wall structure filled with a porous material was analyzed with various temperature boundary conditions and leakage configurations. A method was presented to obtain a Nusselt number correlation for typical wall cavities. Burns and Tien's correlation could be used to determine the heat transfer through the wall cavity and hence the boundary conditions for the moisture deposition model under development in this thesis. Unfortunately, their model predicts only the overall heat transfer across the entire wall. It is not possible to separate the amount of heat entering the cavity through forced air flow from the amount entering through conduction, and so it is not possible to determine the internal cavity wall temperatures which are required to set the moisture boundary condition.

A second numerical model which includes heat and mass transfer with convection and diffusion was discussed by Ojanen and Kohonen (1989). Ojanen and Kohonen solved the complete Navier-Stokes equations in three-dimensions using a finite difference grid. Because a finite difference grid method is used, the model is capable of handling air flow aberrations such as turning flows, corners, partial barriers, flow around electrical sockets, etc. However, a fairly detailed representation of the wall cavity, which in most practical applications is difficult to obtain, is required in order to give accurate results. The Kohonen model is being used by the Canadian National Research Council (NRC) as their reference model.

The Canada Mortgage and Housing Corporation (CMHC) uses the computer model WALLDRY as their reference model. WALLDRY was developed by Schuyler *et al.* (1989) and can simulate heat, air, and moisture flow through a wall cavity. The model is based on a finite difference method. The model includes the effects of latent and sensible heat gain. The model geometry is for a standard wood framed wall similar in nature to the one presented in this thesis with no flow through the insulation filled cavity.

1.2 Features of the Heat and Mass Transfer Models

The heat and mass transfer models presented here are based on an analytical solution of the governing differential equations for flow through a porous medium filled vertical cavity. The model uses approximate boundary conditions on the sides of the cavity to simulate the actual variable boundary conditions present in real walls. During exfiltration and infiltration, moisture can be either deposited on, or evaporated from, the wall bounding the cavity.

The basic assumptions underlining the development of this model are: (the appropriate chapter references are in brackets)

1. The heat and mass transfer models are two-dimensional representations of a three-dimensional problem.
2. An air-vapour flow enters through a crack on one side of the cavity, travels vertically through the cavity, and exits through a crack on the opposite side of the cavity. (Section 2.1.2)
3. The vertical cavity is filled with a homogeneous and air-vapour saturated porous medium (glass fibre insulation). (Section 2.1.5)
4. The air-vapour flow through the insulation-filled cavity is laminar plug flow with a uniform velocity profile and behaves according to Darcy's Law. (Section 2.1.6)
5. Heat is conducted across the insulation-filled cavity in the horizontal direction and is convected along the cavity by air flowing in the vertical direction. Natural convection is neglected. (Section 2.1.7)
6. The inlet temperature profile is linear (usually constant). The two sides of the wall cavity are isothermal. (Section 2.2.1)
7. The effects of latent heat generation due to phase change on the moist-air properties (temperature, viscosity) are insignificant. (Section 2.1.4)
8. The inlet partial pressure profile is uniform. The inner cavity wall is impermeable to moisture, while the outer cavity wall is allowed to absorb or desorb moisture as required. (Section 2.3.1)

9. Moisture within the cavity diffuses horizontally through the porous medium according to Fick's Law and is convected in the vertical direction. (Section 2.1.8)
10. Moisture can only deposit on the exterior sheathing. (Section 2.3)
11. Partial pressure at the exterior sheathing is related to wood moisture content. This relation specifies the wall boundary condition. (Section 3.3.1)

Two models are developed in this thesis to improve the design of wall assemblies. The first model, presented in Section 2.2, deals with forced convection and conduction heat transfer across the wall cavity. The second model, presented in Section 2.3, is a moisture deposition model for flow through insulation-filled wall cavities. The models are not coupled and may be used independently. Chapter 3 reviews the data used to verify the models and compares the model's predicted results to actual field test data. A parametric sensitivity study is conducted in Chapter 4, comparing the moisture deposition model performance to variations in the input parameters.

The moisture deposition model was used to study the behaviour of walls exposed to an air-vapour flow. In verifying the moisture deposition model, the air flows entering the wall cavity were determined from tests on an actual wall cavity. In real houses this data is not generally known, however, by linking the moisture model to an air infiltration model, the air flows through the buildings walls can be estimated and the moisture deposition calculated.

CHAPTER 2

DEVELOPMENT OF THE HEAT AND MASS TRANSFER MODELS FOR FLOW THROUGH INSULATION FILLED CAVITIES

This section deals with developing steady-state models capable of predicting heat transfer and moisture deposition in a vertical wall cavity filled with a porous medium. The model accounts for vertical air flow through the cavity, while allowing heat and mass to diffuse horizontally across the cavity. These horizontal fluxes are driven by an indoor-outdoor temperature gradient and an indoor-outdoor vapour pressure gradient.

The overall model consists of two separate parts: the heat transfer model and the mass transfer model. The heat transfer model is used to predict the outer cavity wall surface temperature which can then be used in specifying the outer cavity wall partial pressure boundary condition in the mass transfer model. The effect of water vapour diffusion on the overall heat transfer within the cavity is small and will not be investigated. Although the heat and mass transfer models are not strictly independent, they will be dealt with separately since the only imposed connection is through the surface temperature of the outer cavity wall.

The development of the model will proceed initially by discussing the basic assumptions and simplifications used for the wall cavity, including a consideration of the effects of porous medium on heat and mass transfer. The heat transfer model will then be discussed in detail, followed by the mass transfer model.

2.1 Basic Assumptions and Simplifications for the Models

The heat and mass transfer models are based on a porous medium filled vertical wall cavity. The cavity is assumed to be sealed except for one leakage site in the interior wall and one leakage site in the exterior wall. In order to use an analytical approach to model the cavity certain assumptions and simplifications had to be made.

The assumptions and simplifications that were made for the idealized wall cavity, and the basis for them, are discussed in this section.

2.1.1 Construction of the real and idealized wall cavities

The vertical wall cavity can be of any general construction provided it is rectangular with a large aspect ratio (height/depth $\gg 1$) and a fixed width. A typical wall cavity, found in most wood-framed residential homes, would have a height of 2.4 m and a depth of 0.09 m, which corresponds to an aspect ratio of about 27. The standard spacing between the vertical studs in a wood-framed wall would be 0.4 m. Figure 2.1 compares a real multi-layered wall cavity with the idealized wall cavity which the models are based on.

The real wall is broken down into a series of sub-walls as shown in Fig. 2.2. The interior wall (subscript *a*) faces the warm and humid room and is in both thermal and moisture equilibrium with the room. The interior wall is usually constructed out of gypsum wallboard or wood panelling. The inner cavity wall (subscript *b*) is a vapour barrier which faces the cavity and prevents the passage of moisture, but not the passage of heat. The outer cavity wall (subscript *c*) consists of wood sheathing of which one surface faces the cavity and the other surface faces the exterior wall (see Fig. 2.1). The outer cavity wall is generally colder than the inner cavity wall. The exterior wall (subscript *d*) is the exterior siding and faces the cold and dry outdoor environment. The exterior wall is directly exposed to solar radiation and is contact with the prevailing winds. The interior wall and the inner cavity wall are referred to jointly as wall *I* while the outer cavity wall and the exterior wall are referred to as wall *II*. It was shown by Burns and Tien (1978) that the top and bottom ends exert only a minor effect on the overall cavity heat transfer and can be considered as insulated boundaries. The wall has a finite width limited by the end studs. The effect of these end studs are neglected in the heat transfer model.

The real wall cavity is modeled as two parallel plates shown in Fig. 2.1. Both plates are maintained at constant temperatures, with the interior wall being warmer

than the exterior wall. The warm wall would be equivalent to the impermeable inner cavity wall shown in Fig. 2.2 while the cold wall is the outer cavity wall shown in Fig. 2.2. In the space between the walls is the porous medium.

Figure 2.2 shows the details of the wall cavity configuration used to create the heat transfer model. A similar configuration, Fig. 2.3, was used to develop the moisture diffusion model. For the moisture diffusion model, the cold wall (outer cavity wall) has a fixed partial pressure for water vapour and the warm wall (inner cavity wall) is impermeable to moisture so that there is no mass flux through the boundary.

2.1.2 Cavity air flow and entrance and exit effects

During the construction of typical wall assemblies leaks appear which allow air flow to pass through the cavity. Air passing from the inside to the outside is called exfiltration while the reverse action, air passing from outside to inside, is called infiltration. Leakage air flow through the cavity is caused by a combination of stack effect and a wind induced internal-external pressure difference.

Figure 2.4, ASHRAE (1989), shows the pressure profile along a vertical wall due to stack and wind action. In Fig. 2.4(a) is shown the pressure difference across a vertical wall due only to stack action. Above the neutral pressure level exfiltration occurs, and below the neutral pressure level infiltration occurs. No flow occurs at the neutral pressure level. Wind action causes more exfiltration to occur on the leeward side than the windward side, as shown in Fig. 2.4(b) and (c). A strong wind may cause the neutral pressure level to occur at any height along the wall. When a typical wall cavity is exposed to the combined stack and wind effects, a pressure difference between the inside pressure at $z = 0$ (height of interior leakage site) and the outdoor pressure at $z = H$ (height of exterior leakage site) develops causing air to flow through the cavity in the vertical direction.

Most leakage sites in the interior wall occur along the baseboard or around electrical fittings. Exterior leaks are generally located where the exterior sheathing is fastened to the frame of the house. The leaks can either be long slender cracks or

larger jagged openings where the flow through the crack is proportional to the pressure difference across the crack raised to an exponent between 0.5 and 1.0, Walker (1991). The leakage sites in walls occur in the vertical plane which forces the air flow to enter the cavity in the horizontal direction. Assuming that the vapour barrier is punctured at the same spot as the interior crack, the air flow will enter the porous medium. The jet of air entering the porous medium will begin to disperse and its velocity will decrease. When the air flow impinges on the outer cavity wall, the flow will turn toward the exit leakage site. The details of air stream behaviour in the entrance and exit region of the cavity is beyond the scope of this work. It will be assumed that the air enters the cavity at the ends, as shown in Fig. 2.2, with a uniform velocity profile and proceeds in only the z direction. Forced convective flow in the x or y direction is not permitted. A discussion regarding the behaviour of uniform flow with porous medium can be found in Section 2.1.6.

2.1.3 Indoor and outdoor conditions

The indoor and outdoor conditions are assumed to be constant. The indoor temperature T_{room} and the indoor relative humidity ϕ_{room} fix the indoor partial pressure of water vapour $p_{w,room}$ and the saturated partial pressure $p_{ws,room}$. Similarly, the outdoor temperature T_{out} and the outdoor relative humidity ϕ_{out} fix the outdoor partial pressure of water vapour $p_{w,out}$ and the saturated partial pressure $p_{ws,out}$. When the flow through the cavity is exfiltration, the indoor conditions set the cavity inlet conditions; during infiltration, the outdoor conditions set the inlet conditions. The inlet conditions are represented by the subscript *inlet*.

2.1.4 Latent heat energy

When moisture vapour in the air condenses or freezes upon reaching a cold surface, energy is released. This energy is referred to as latent heat and is capable of increasing the local area temperature. An increased temperature would reduce the driving force for deposition and therefore reduce the amount of moisture depositing.

If the amount of latent energy released at the cold wall is small, then the temperature of the cold wall will not be significantly altered and the amount of moisture being deposited will not be affected. In Appendix D an estimate of the latent energy released within the wall cavity due to a change of state was performed, indicating that the amount of energy released was 3 orders of magnitude less than steady-state heat conduction. This result is substantiated by TenWolde (1985) who discusses latent energy release in his one-dimensional diffusion model and concludes that the effect of latent heat release is negligible when the outer cavity wall is close to the outside temperature (this is the case for most typical walls). For most typical applications, neglecting the effects of latent heat gain is reasonable. Since the cavity does not experience a significant temperature change, the properties of the air and porous medium also do not change significantly due to latent heat gain.

2.1.5 The porous medium

Any porous medium can be used within the wall cavity provided it meets four basic requirements (adapted from Bejan (1984)):

1. The porous medium is homogeneous. The solid material and the air permeating through the pores must be evenly distributed throughout the porous medium.
2. The medium is isotropic. Permeability, K , thermal conductivity, k , and mass diffusivity, D , must not depend on the orientation of the porous medium.
3. At any point in the porous medium, the solid matrix is in thermal equilibrium with the fluid filling the pores.
4. The local Reynolds number based on average velocity and $K^{1/2}$ does not exceed $O(1)$, i.e. the Darcy law applies in its original form. The Darcy flow model will be discussed in Section 2.1.6.

It must also be assumed that the working fluid permeating the porous medium, an air-vapour mixture, can be treated as an ideal gas.

2.1.6 Flow through porous medium — Darcy's Law

Flow through a porous medium is not the same as flow through an open duct. In open duct flow, the flow resistance is concentrated at the boundaries. As uniform flow enters the cavity, a velocity boundary layer begins to form at the walls (non-slip boundary condition). As the boundary layer grows, the velocity profile develops into a parabola with the maximum velocity at the centre of the duct. Figure 2.5 shows the development of the velocity boundary layer in an open cavity.

When a porous medium is added to the cavity, the flow development changes. Due to the nature of porous medium, the flow resistance is spread evenly across the entire cavity. As a uniform flow enters the cavity, it encounters equal resistance at the centre and at the edges. The flow remains uniform and proceeds as laminar plug flow. Figure 2.5 shows the constant velocity profile for flow through porous medium. On a microscopic level there exists velocity boundary layers within the pores of the medium. However, on a macroscopic level the effect is not noticeable and the flow is uniform and constant. Bejan (1984) shows that the boundary layer at the walls cannot exist "beyond a few pore lengths." The benefit of having a uniform and constant flow rate through the cavity is that the solution of the general energy equation, presented in Section 2.2.2, is far simpler than when a parabolic profile is used.

The flow rate through a homogeneous porous medium is directly proportional to the pressure gradient along the medium. Darcy, see Bejan (1984), in 1856 proposed a law, based on experimental observations, which governs flow in porous medium. Darcy's Law can be stated as

$$w = \frac{K}{\mu} \left(-\frac{dP}{dz} \right) \quad (2.1)$$

where w is the velocity in the z direction, K is the permeability of the medium, μ is the dynamic viscosity of the fluid, and dP/dz is the pressure gradient driving the flow. The permeability, K , is an empirical constant which must be determined for each porous medium. When a porous medium with a low permeability, tightly packed

with small pore sizes, is used in a cavity, the flow rate for a given pressure gradient will be smaller than when a high permeability material is used. The typical range of permeability for glass fibre insulation is 1×10^{-10} to $100 \times 10^{-10} \text{ m}^2$, Burns *et al.* (1978), which corresponds to glass fibre insulation densities from 240 to $2.5 \text{ kg}\cdot\text{m}^{-3}$, respectively, Jackson and James (1986). Typical $10 \text{ kg}\cdot\text{m}^{-3}$ glass fibre insulation would have a permeability of $31 \times 10^{-10} \text{ m}^2$, Jackson and James (1986).

Darcy's law, Eqn. (2.1), is used as the basis for the flow calculations in the heat and mass transfer models. Darcy's law can be used if the Reynolds number, based on $K^{1/2}$ as the length scale, is less than order 1. This is expressed as,

$$\frac{wK^{1/2}}{\nu} < 1 \quad (2.2)$$

where ν is the kinematic viscosity of the fluid. For typical glass fibre filled wall cavities ($K = 31 \times 10^{-10} \text{ m}^2$; $w \leq 0.01 \text{ m}\cdot\text{s}^{-1}$; $\nu = 1.6 \times 10^{-5} \text{ m}^2\cdot\text{s}^{-1}$), the Reynolds number would be 0.03.

2.1.7 Heat transfer through porous medium in wall cavities

Heat transfer within open cavities can occur by three methods: radiation, conduction, and convection. The introduction of a porous medium into the cavity alters each of these forms of heat transfer.

For the purposes of this analysis, radiation heat transfer has not been explicitly considered. Radiation heat transfer between the walls and within the porous medium account for a significant fraction of the total heat transfer and is usually included in an "effective" thermal conductivity, Bankvall (1972).

Conductive heat transfer from the warm wall to the cold wall is decreased by the addition of a porous medium. Resistance to heat energy transfer is increased by adding trapped air spaces (pores) through which the energy being conducted from the warm wall to the cold wall must pass. As the porous medium approaches the permeability of a solid (K becomes very small), the conductive heat transfer increases as heat

is able to bypass the air spaces and travel by conduction through the contacting fibres; for high permeabilities, conduction is mainly through the air pores. Glass fibre insulation is a typical porous medium used in wall cavities in which almost all conduction is through the air spaces.

Both forced and natural convection heat transfer are affected by the presence of a porous medium within the cavity. In a closed but empty cavity the temperature differential created by heating one wall and cooling the opposite wall sets up a natural convective cell. Heat is transferred from the warm wall to the cold wall by this action. Adding a porous medium to the wall cavity restricts the ability of the air to move freely and hence natural convective cells require larger temperature differences in order to form. Therefore the porous medium causes a reduction or elimination of heat transfer by natural convection.

To determine if natural convection is a significant heat transfer mechanism in closed porous medium filled cavities the Darcy-modified Rayleigh number is used. The Darcy-modified Rayleigh number, Bejan (1980) is defined as

$$Ra^* = \frac{g \beta K (T_b - T_c) d}{\alpha \nu} \quad (2.3)$$

where g is gravity, $\beta = 1/T$ is the coefficient of thermal expansion of air, d is the cavity depth, T_b and T_c are the temperatures of the inner and outer cavity walls respectively, and α is the thermal diffusivity of the fluid saturated porous medium. For closed cavities filled with a porous medium, the point at which heat transfer begins to be affected by natural convection is considered the critical value for the Rayleigh number. In contrast with open cavities, the onset of natural convection is not sudden and therefore the critical point is not distinct. For cavities with aspect ratios varying from 10 to about 40, the critical Rayleigh number ranges from 10 to 17 typically being about 15. For comparison, a square cavity ($H/d = 1$) would have a critical Rayleigh number of about 7. Using a typical permeability of $31 \times 10^{-10} \text{ m}^2$, corresponding to a glass fibre density of $10 \text{ kg}\cdot\text{m}^{-3}$, Jackson and James (1986), the Darcy-modified Rayleigh number, for a temperature difference of 40 K, would be about 0.8,

two orders of magnitude less than the critical value of 15. This indicates that natural convection cannot occur in a typical closed wall cavity.

It can be inferred that because natural convective cells cannot form when there is no flow through a cavity, a uniform flow imposed through the cavity should not cause a convective cell to be created. However, buoyancy driven flow along each side of the cavity, when superimposed on the forced cavity flow, may cause the velocity profile to be approximately linear and not uniform as assumed in the development of this work.

When there is an imposed air flow through the wall cavity, the Rayleigh number can no longer be defined as Eqn. (2.3), which is for a closed cavity. The Rayleigh number due to an imposed flow, Ra_w , is defined as the ratio of buoyancy to viscous forces in the permeable medium, expressed as,

$$Ra_w = \frac{\rho g \beta \frac{\Delta T}{2} h \left(\frac{d}{2}\right) L}{\left(\frac{w \mu h}{K}\right) \left(\frac{d}{2}\right) L} \quad (2.4)$$

where d is the cavity depth and L is the cavity width. The buoyancy force acts only over half of the cavity depth since the mean temperature plane is located in the centre of the cavity. The numerator of Eqn. (2.4) is the pressure difference driving the air flow through the cavity due to internal buoyancy effects, while the denominator is the imposed pressure difference from Darcy's Law for flow through porous medium. The imposed velocity w includes the stack-effect buoyancy driven flow from the room to outdoors. Ra_w accounts only for differences in buoyancy across the cavity and not along it. Equation (2.4) can be rewritten as,

$$Ra_w = \frac{g \beta K \Delta T}{2 w \nu} \quad (2.5)$$

which is of the same general form as the Rayleigh number for a closed cavity,

$$Ra^* = \frac{g \beta K \Delta T}{\left(\frac{\alpha}{d}\right) v} \quad (2.6)$$

In the denominator of Eqn. (2.5) the velocity, w , is imposed on the cavity while for the closed cavity the natural velocity scale, α/d , is for internal buoyancy driven flow. Small values of Ra_w indicate that the buoyancy effect is small as compared to the forced flow and the velocity profile across the cavity remains uniform as first predicted. Large values of Ra_w indicate a large internal buoyancy force difference and the probability that non-uniform flow may be present in the cavity. Table 2.1 compares the Rayleigh numbers for open and closed cavities using different insulation permeabilities.

For a closed cavity with very loose fill, $K = 500 \times 10^{-10} \text{ m}^2$, Ra^* is less than the critical value of 15, Bankvall (1972). This indicates that natural convective cells cannot be set up by the temperature difference between the cold and warm walls. In the same cavity with an imposed flow velocity of $0.01 \text{ m}\cdot\text{s}^{-1}$, Ra_w is 0.25. This signifies that the buoyancy force in the cavity is as much as 25% of the flow induced force. Under these conditions, the velocity profile may not be uniform across the cavity. However, at this value of K , the insulation density is $1.0 \text{ kg}\cdot\text{m}^{-3}$, which is much less than typical values for wall insulation.

In more typical cases, $K \approx 30 \times 10^{-10} \text{ m}^2$, $Ra^* = 0.81$, and $Ra_{imposed} = 0.016$. Natural convection in a closed cavity is not possible ($Ra^* < 15$) and the internal buoyancy force in a cavity with flow is only 1.6% of the imposed pressure force. The internal buoyancy forces are negligible. The effect of natural convection on heat transfer in typical porous medium filled cavities is not significant and is not included in the development of the heat transfer model.

Forced convection due to the induced air flow passing through the cavity is included in the model. The porous medium acts to reduce the flow rate of the air passing through the cavity, compared to open cavities, by adding resistance to the flow, and hindering the ability of the air flow to remove or add heat.

2.1.8 Mass transfer and porous medium

In open cavities or rooms, moisture tends to spread rapidly from regions of high vapour pressure to regions of lower vapour pressure by convective and diffusion. This rapid transport occurs due to large air flows which are capable of carrying the moisture from regions of high partial pressure to regions of low partial pressure. When higher vapour pressure flow encounters a surface with a vapour pressure below the saturation temperature, condensation will occur. An example of this is when condensation forms on windows due to the vapour pressure on the cold window surface being lower than the vapour pressure of the warm, humid room air.

Moisture can enter wall cavities by either diffusion through the inner cavity wall or by being transported along with a leakage air flow. Since wall cavities are constructed using a vapour retarder, which is impermeable to vapour diffusion, fastened to the inner side of the cavity (Fig. 2.3) very little moisture can enter the cavity by diffusion. The amount of moisture able to diffuse through a vapour retarder is about $0.011 \text{ g}\cdot\text{h}^{-1}$ (Appendix C.2). Convective air flows are the largest source of moisture in wall cavities, typically bringing in excess of $0.95 \text{ g}\cdot\text{h}^{-1}$ (Appendix C.3).

In wall cavities filled with porous material, molecular diffusion is the prominent mechanism for transporting free moisture in the horizontal direction. Molecular diffusion is governed by Fick's Law and is more fully discussed in Section 2.3.2. The resistance to moisture diffusion is characterized by using a mass diffusivity coefficient, D . A dense porous medium would have a small mass diffusivity, representing an increased resistance to vapour diffusion, resulting in a smaller mass flux. Conversely, a loosely packed cavity would have a larger mass diffusivity, decreased flow resistance, and increased mass transfer. For glass fibre insulation, the mass diffusivities range from $1.61 \times 10^{-5} \text{ m}^2\cdot\text{s}^{-1}$ for $165 \text{ kg}\cdot\text{m}^{-3}$ glass fibre board, Tveit (1966), to $3.32 \times 10^{-5} \text{ m}^2\cdot\text{s}^{-1}$ for $10 \text{ kg}\cdot\text{m}^{-3}$ glass fibre batts, ASHRAE (1989). There appears to be a discrepancy in these measured values since the diffusivity of water vapour through still air ($2.5 \times 10^{-5} \text{ m}^2\cdot\text{s}^{-1}$, Perry and Chilton (1983)) should be the upper limit for the mass diffusivity term. This discrepancy warrants further investigation.

The diffusivity of water vapour in air was chosen to be the base value for the moisture diffusion model.

2.2 Development of the Heat Transfer Model

The heat transfer analysis is based on laminar plug flow between two infinite walls filled with porous medium, as shown in Fig. 2.2. Heat transfer between infinite walls in open ducts with flow is discussed by McCuen (1962), Reynolds *et al.* (1963), and Lundberg *et al.* (1963). The solution method presented by McCuen (1962) was adapted to solve analytically the governing differential equation for two-dimensional heat transfer in the vertical wall with porous insulation and cavity flow in Section 2.2.2.

2.2.1 Boundary conditions specific to the heat transfer problem

As mentioned previously (Section 2.1.1), the idealized cavity is bound by two isothermal surfaces shown in Fig. 2.2. The inner cavity wall is the warmer wall and is located at $x = 0$. The temperature boundary condition is $T(0,z) = T_b$ along the entire height of the cavity. The outer cavity wall, located at $x = d$, is the colder wall. The temperature boundary condition for the cold wall is $T(d,z) = T_c$ along the entire height of the cavity. Located at the entrance plane, $z = 0$, is the entering flow which can have a linear temperature variation with x . The linear temperature profile can be expressed as

$$T(x,0) = -(T_I - T_{II}) \frac{x}{d} + T_I$$

where x is the position across the cavity depth, T_I is the temperature at the inner cavity wall position, T_{II} is the temperature at the outer cavity wall position, and d is the depth of the cavity. T_I and T_{II} do not necessarily correspond to the actual surface temperatures T_b or T_c , respectively. If they do, then the entering temperature profile would be the profile corresponding to steady-state conduction.

2.2.2 Deriving the temperature profile and temperature gradient expressions

Heat transfer is expressed mathematically in Fourier's Law of heat conduction,

$$q''(x,z) = -k \frac{\partial T}{\partial x} \bigg|_{x,z} \quad (2.7)$$

where q'' is the heat flux per unit area, k is the thermal conductivity, and $\partial T/\partial x$ is the temperature gradient driving the heat flux. The heat flux can be determined if the temperature profile across the cavity is known. It is possible to solve analytically for the temperature profile across the wall cavity by utilizing the steady-state energy equation, or:

$$\rho C_p \left(\underset{1}{u} \frac{\partial T}{\partial x} + \underset{2}{v} \frac{\partial T}{\partial y} + \underset{3}{w} \frac{\partial T}{\partial z} \right) = k \left(\underset{4}{\frac{\partial^2 T}{\partial x^2}} + \underset{5}{\frac{\partial^2 T}{\partial y^2}} + \underset{6}{\frac{\partial^2 T}{\partial z^2}} \right) + \underset{7}{\dot{q}} \quad (2.8)$$

where ρ is the density of the fluid (air), C_p is the specific heat for air at constant pressure, u , v , w are the velocities in the x , y , z directions respectively, k is the thermal conductivity of the medium, and \dot{q} accounts for any internal generation of heat energy within the system. The most general form of the energy equation should include terms representing the energy transferred by moisture movement within the cavity, however, because these effects are neglected, Eqn. (2.8) is sufficient.

In the case of steady-state conduction and forced convection in a porous medium filled cavity the steady-state energy equation can be reduced from its more general three-dimensional form to a simpler two-dimensional form. In Eqn. (2.8), terms 1 and 2 deal with convection heat transfer in the x and y directions, respectively. The model assumes that there is no flow in the x or y directions (Section 2.1.1) and hence terms 1 and 2 can be neglected. Term 3 accounts for the convective heat transfer in the z direction which is not negligible and which will be retained. Terms 4, 5, and 6 in Eqn. (2.8) deal with conduction in the x , y , and z directions, respectively. The conduction terms in the y and z directions, in the developing thermal region, are considerably smaller than the conduction term in the x direction, and for

this reason, terms 5 and 6 are considered negligible. Term 8, accounts for any internal heat generation within the wall cavity. Since the effects of latent heat are being neglected (Section 2.1.4) this term can be set to zero.

Applying the restrictions listed above, the governing equation reduces to

$$w \frac{\partial T}{\partial z} = \alpha \frac{\partial^2 T}{\partial x^2} \quad (2.9)$$

where α is the thermal diffusivity for the fluid saturated porous medium ($k/(\rho C_p)$). In order to solve Eqn. (2.9) boundary conditions must be specified for the warm wall, cold wall, and inlet plane. These boundary conditions as a function of x and z were explained in Section 2.2.1 and reprinted here for clarity,

$$T(0, z) = T_b \quad ; \quad T(d, z) = T_c \quad ; \quad T(x, 0) = -(T_I - T_W) \frac{x}{d} + T_I \quad (2.10)$$

The solution to the governing Eqn. (2.9) is facilitated by non-dimensionalizing the temperature and length scales,

$$\theta = \frac{T - T_c}{T_b - T_c} \quad , \quad \bar{x} = \frac{x}{d} \quad , \quad \bar{z} = \frac{z}{H} \quad (2.11)$$

where θ is the non-dimensional temperature difference, \bar{x} is the non-dimensional depth, and \bar{z} is the non-dimensional height term. The boundary conditions in Eqn. (2.10) can be expressed as,

$$\theta(0, \bar{z}) = 1 \quad ; \quad \theta(1, \bar{z}) = 0 \quad ; \quad \theta(\bar{x}, 0) = \frac{[-(T_I - T_W)\bar{x} + T_I] - T_c}{T_b - T_c} \quad (2.12)$$

The boundary conditions shown in Eqn. (2.12) present a problem because they are not homogeneous. However, due to the linearity of the governing Eqn. (2.9), it is possible to perform a transformation on the dependent variable θ such that the boundary conditions become homogeneous. First, Eqn. (2.9) is rewritten in terms of the non-dimensional variables,

$$\frac{w}{H} \left[(T_b - T_c) \frac{\partial \theta}{\partial \bar{z}} + \frac{\partial T_b}{\partial \bar{z}} \right] - \frac{\alpha}{d^2} \left[(T_b - T_c) \frac{\partial^2 \theta}{\partial \bar{x}^2} + \frac{\partial^2 T_b}{\partial \bar{x}^2} \right] \quad (2.13)$$

which reduces to,

$$\frac{\partial \theta}{\partial \bar{z}} - \frac{\alpha H}{w d^2} \frac{\partial^2 \theta}{\partial \bar{x}^2} \quad (2.14)$$

since T_b and T_c are constants.

The next step is to use a transformation developed by Sparrow, *et al.* (1958) and later employed by McCuen (1962). Sparrow initially developed the transformation to solve a turbulent heat transfer problem in the entrance region of a pipe. McCuen then adapted the method to solve for laminar heat transfer between parallel plates with a constant wall temperature boundary condition. McCuen's adapted transformation was to let

$$\bar{\theta} = \theta - \theta_{ss} \quad (2.15)$$

where $\bar{\theta}$ is the transformed non-dimensional temperature difference, θ is the non-dimensional temperature difference defined in Eqn. (2.11), and θ_{ss} is the steady-state conduction temperature profile. McCuen's transformation assumes that far downstream from the initial entrance plane, convection effects dissipate and the heat transfer between the warm and cold walls is by steady-state conduction only. This can occur since the two isothermal boundaries are held at different temperatures, with heat energy entering the cavity through the inner cavity wall (warm boundary) and exiting through the outer cavity wall (cold boundary).

The steady-state temperature profile is determined by the conduction equation,

$$\frac{\partial^2 \theta_{ss}}{\partial \bar{x}^2} = 0 \quad (2.16)$$

which has the general solution $\theta_{ss} = A + B\bar{x}$, where application of the boundary

conditions $\theta_{ss}(0) = 1$ at $\bar{x} = 0$, and $\theta_{ss}(1) = 0$ at $\bar{x} = 0$, yields the specific solution,

$$\theta_{ss} = 1 - \bar{x} \quad (2.17)$$

Then by substituting Eqn. (2.15) into Eqn. (2.14), the following differential equation with homogeneous boundary conditions is obtained,

$$\left[\frac{\partial \bar{\theta}}{\partial \bar{z}} + \frac{\partial \theta_{ss}}{\partial \bar{z}} \right] - \frac{\alpha H}{wd^2} \left[\frac{\partial^2 \bar{\theta}}{\partial \bar{x}^2} + \frac{\partial^2 \theta_{ss}}{\partial \bar{x}^2} \right] \quad (2.18)$$

which, since the partial derivative of θ_{ss} with respect to \bar{z} is zero and the second partial derivative of θ_{ss} with respect to \bar{x} is zero, Eqn. (2.18) reduces to

$$\frac{\partial \bar{\theta}}{\partial \bar{z}} - \frac{\alpha H}{wd^2} \frac{\partial^2 \bar{\theta}}{\partial \bar{x}^2} \quad (2.19)$$

with the homogeneous boundary conditions,

$$\bar{\theta}(0, \bar{z}) = 0 ; \quad \bar{\theta}(1, \bar{z}) = 0 ; \quad \bar{\theta}(\bar{x}, 0) = \frac{[-(T_l - T_{ll})\bar{x} + T_l] - T_c}{T_b - T_c} = 1 - \bar{x} \quad (2.20)$$

Equation (2.19) can now be solved by using the method of separation of variables where X is a function of only \bar{x} and Z is a function of only \bar{z} . By letting,

$$\bar{\theta}(\bar{x}, \bar{z}) = X(\bar{x}) \cdot Z(\bar{z}) \quad (2.21)$$

Eqn. (2.19) is rewritten as two ordinary differential equations,

$$\frac{wd^2}{\alpha H} \frac{1}{Z} \frac{dZ}{d\bar{z}} = -\lambda^2 \quad (2.22)$$

$$\frac{1}{X} \frac{d^2 X}{d\bar{x}^2} = -\lambda^2 \quad (2.23)$$

Equation (2.22) is dependant only on \bar{z} and Eqn. (2.23) is dependent only on \bar{x} . The term $-\lambda^2$ is the separation constant. The separation constant could take on values of

zero, positive, or negative, with each one yielding a possible solution to Eqn. (2.19). However, the only physically realistic solution (which also satisfies the boundary conditions) is when the separation constant is strictly negative. Refer to the Appendix E for a discussion of the other solutions.

Integrating Eqn. (2.22), where A is a constant of integration, results in

$$Z(\bar{z}) = A \exp\left[-\frac{\alpha H}{w d^2} \lambda^2 \bar{z}\right] \quad (2.24)$$

Equation (2.23) is more difficult to solve; however, Eqn. (2.23) is a linear homogeneous second order differential equation of the form,

$$\frac{d^2 X}{d\bar{x}^2} + \lambda^2 X = 0 \quad (2.25)$$

which is an eigenvalue problem, Powers (1979). The characteristic equation is of the form,

$$m^2 + \lambda^2 = 0$$

for which the solution is,

$$X(\bar{x}) = B \sin(\lambda \bar{x}) + C \cos(\lambda \bar{x}) \quad (2.26)$$

Equations (2.24) and (2.26) can now be multiplied together, as expressed in Eqn. (2.21), to arrive at the general solution for Eqn. (2.19),

$$\bar{\theta}(\bar{x}, \bar{z}) = (B \sin(\lambda \bar{x}) + C \cos(\lambda \bar{x})) \exp\left[-\frac{\alpha H}{w d^2} \lambda^2 \bar{z}\right] \quad (2.27)$$

Applying the isothermal boundary condition $\bar{\theta}(0, \bar{z}) = 0$ at the inner cavity wall to Eqn. (2.27) yields,

$$\bar{\theta}(0, \bar{z}) = 0 = (B \cdot 0 + C \cdot 1) \exp\left[-\frac{\alpha H}{w d^2} \lambda^2 \bar{z}\right] \quad (2.28)$$

from which it is apparent that the constant $C = 0$. The second isothermal boundary

condition on the outer cavity wall, $\bar{\theta}(1, \bar{z}) = 0$, applied to Eqn. (2.27) together with the known solution, $C = 0$, results in,

$$\bar{\theta}(1, \bar{z}) = 0 = B \sin \lambda \exp \left[-\frac{\alpha H}{wd^2} \lambda^2 \bar{z} \right] \quad (2.29)$$

Since $B \neq 0$ the term $\sin(\lambda)$ must equal zero for all λ . This can only be accomplished for eigenvalues of $\lambda = n\pi$, $n = 0, 1, 2, 3, \dots$

The general solution can now be written as,

$$\bar{\theta}(\bar{x}, \bar{z}) = \sum_{n=0}^{\infty} B_n \sin(\lambda_n \bar{x}) \exp \left[-\frac{\alpha H}{wd^2} \lambda_n^2 \bar{z} \right] \quad (2.30)$$

which satisfies the first two boundary conditions concerning the isothermal walls.

Application of the third boundary condition, the linear variation of the inlet temperature profile, results in the following equation,

$$\frac{[-(T_I - T_H)\bar{x} + T_I] - T_c}{T_b - T_c} = 1 - \bar{x} = \sum_{n=0}^{\infty} B_n \sin(n\pi\bar{x}) \quad (2.31)$$

which is a Fourier sine series; hence,

$$B_n = 2 \int_0^1 \left(\frac{[-(T_I - T_H)\bar{x} + T_I] - T_c}{T_b - T_c} = 1 - \bar{x} \right) \sin(n\pi\bar{x}) d\bar{x} \quad (2.32)$$

Expanding the coefficients of B_n yields

$$B_0 = 0 ; \quad B_n = 2 \left(\frac{T_c - T_H}{T_b - T_c} \frac{\cos(n\pi)}{n\pi} + \frac{T_I - T_b}{T_b - T_c} \frac{1}{n\pi} \right), \quad n = 1, 2, 3, \dots \quad (2.33)$$

Combining Eqns. (2.30) and (2.33) and performing the reverse transformation from $\bar{\theta}$ to θ , the final non-dimensionalized temperature profile is obtained:

$$\theta(\bar{x}, \bar{z}) = 1 - \bar{x} + \sum_{n=1}^{\infty} 2 \left(\frac{T_c - T_H}{T_b - T_c} \frac{\cos(n\pi)}{n\pi} + \frac{T_I - T_b}{T_b - T_c} \frac{1}{n\pi} \right) \sin(n\pi\bar{x}) \exp \left[-\frac{\alpha H (n\pi)^2 \bar{z}}{wd^2} \right] \quad (2.34)$$

Since heat fluxes must also be calculated later, the non-dimensionalized temperature

gradient is:

$$\frac{\partial \theta(\bar{x}, \bar{z})}{\partial \bar{x}} = -1 + \sum_{n=1}^{\infty} 2 \left(\frac{T_c - T_H}{T_b - T_c} \cos(n\pi) + \frac{T_I - T_b}{T_b - T_c} \right) \cos(n\pi \bar{x}) \exp \left[-\frac{\alpha H(n\pi)^2 \bar{z}}{wd^2} \right] \quad (2.35)$$

The dimensional temperature profile is,

$$T(x, z) = (T_b - T_c) \left(1 - \frac{x}{d} + \sum_{n=1}^{\infty} 2 \left(\frac{T_c - T_H}{T_b - T_c} \frac{\cos(n\pi)}{n\pi} + \frac{T_I - T_b}{T_b - T_c} \frac{1}{n\pi} \right) \sin\left(\frac{n\pi x}{d}\right) \exp \left[-\frac{\alpha(n\pi)^2 z}{wd^2} \right] \right) + T_c \quad (2.36)$$

expressed in degrees Kelvin, and the dimensional temperature gradient is,

$$\frac{\partial T(x, z)}{\partial x} = \frac{T_b - T_c}{d} \left(-1 + \sum_{n=1}^{\infty} 2 \left(\frac{T_c - T_H}{T_b - T_c} \cos(n\pi) + \frac{T_I - T_b}{T_b - T_c} \right) \cos\left(\frac{n\pi x}{d}\right) \exp \left[-\frac{\alpha(n\pi)^2 z}{wd^2} \right] \right) \quad (2.37)$$

expressed in degrees Kelvin per metre.

The solutions for Eqns. (2.36) and (2.37) require using an infinite number of terms in the summation. An approximate solution can be obtained by performing the summation over a fixed number of terms from $n = 1$ to N , where n and N are integers.

2.2.3 Behaviour of the temperature profile solution

Before proceeding further, it is useful to take a closer look at the temperature profiles and heat flux equations to determine how valid these solutions are in light of the assumptions made. Equations (2.36) and (2.37) have not been validated by using measured temperature or heat flux data since detailed data is not presently available. Instead, it will be shown that the temperature profiles and heat fluxes behave in a manner consistent with physical reasoning.

The examination was conducted using the test cavity shown in Fig. 2.2. Table 2.2 lists the values used to test the temperature profile and heat flux equations, including the physical dimensions of the cavity. Also listed is a typical range for the physical parameters used. For these calculations, the inlet temperature profile was assumed constant ($T_I = T_H = 20^\circ\text{C}$) and equal to the inner cavity wall temperature,

T_b .

For exfiltration the inlet plane is at the bottom of the cavity as shown in Fig. 2.2 and the inlet conditions are the room conditions. The air flows in the positive z direction. For infiltration the entrance plane is at the top of the cavity and the inlet conditions correspond to the outdoor conditions. The air flows in the negative z direction.

The results for wall cavities experiencing both exfiltration and infiltration will be presented since the equations require a different inlet temperature profile. Figure 2.6 shows the developing temperature profile and corresponding heat flux for exfiltration, Fig. 2.7 shows the developing temperature profile and corresponding heat flux for infiltration. Referring to Fig. 2.6(a), the temperature profiles are shown at points 1 cm, 2 cm, 3 cm, and 20 cm from the inlet opening. As the flow proceeds through the cavity, the thermal boundary layer develops, extending from the cold outer surface across the cavity to the warm inner wall. Initially, at $\Delta z = 1$ cm, the profiles extend horizontally from the warm wall until reaching the thermal boundary layer extending from the cold outer cavity wall. The horizontal profile indicates that the temperature is the same throughout the layer of porous material not contained within the thermal boundary layer. Figure 2.6(b) shows that the heat flux at $x = 0$ equals zero therefore no heat is being added to the layer next to the warm wall. Within the boundary layer the temperature profile shown in Fig. 2.6(a) drops down slowly towards the colder outer cavity wall. As Δz increases, the flow becomes more developed and the layer of air next to the warm wall becomes increasingly smaller until at $\Delta z = 20$ cm the flow is thermally fully developed. At $\Delta z = 20$ cm the temperature profile across the cavity is the same as for steady-state conduction with no convection.

The same general trends are seen in the data for infiltration. In Fig. 2.7(a) the temperature profile at $\Delta z = 1$ cm extends horizontally from the cold outer cavity wall, indicating a constant temperature, and then increases in temperature until reaching the inner cavity wall. In both Figs. 2.6 and 2.7, the thermal boundary layers grow rapidly, with the temperature profiles becoming fully developed approximately

20 cm into the cavity. The distance into the cavity at which the temperature profile becomes fully developed is not the same for all conditions. However, in many of the cases tested the flow became thermally developed in less than 1/3 the height of the cavity.

The heat fluxes shown in Figs. 2.6(b) and 2.7(b) were calculated using Eqn. (2.7) with a thermal conductivity of $0.0425 \text{ W}\cdot\text{m}^{-1}\cdot\text{K}^{-1}$. Positive heat flux indicates heat being transferred from left to right through the wall assembly. In Fig. 2.6(b), the heat flux through the inner wall close to the entrance is very small since the thermal boundary layer has not yet reached the inner wall. In a very short distance, less than 20 cm, the flow becomes thermally developed and the heat flux through the inner wall and out of the outer wall are equal.

For exfiltrating flow the heat flux on the left boundary starts at zero where the temperature gradient between the boundary and the cavity is small and rises to the thermally developed value when $z = 20 \text{ cm}$. The heat flux on the right boundary is initially high when the temperature gradient is large, and then drops to the pure conduction thermally developed value. The reverse is true for the infiltration case, where the left boundary flux is initially high, indicating heat being transferred from the warm wall into the colder, cavity while on the right surface the heat flux is low since the temperature gradient between the inlet flow and the right boundary is small.

The addition of a forced flow through the wall cavity does not alter the fully developed heat flux calculations. Once the plug flow becomes thermally fully developed the constant heat flux between the warm and cold walls is pure conduction. The induced flow only tends to affect a small region, about $2d$ long, near the entrance to the cavity which is small in comparison to the rest of the cavity. For the test case, the developing region was about 1/4 of the total cavity height.

2.2.4 Determining the number of terms to retain in the temperature profile equations

In order to solve accurately for the temperature profile, Eqns. (2.36) and (2.37) must be solved using an infinite number of terms in the summation (the sum-

mation goes from $n = 1$ to ∞). Unfortunately, it would be impossible to retain an infinite number of terms so a compromise must be reached. The solutions shown in Figs. 2.6 and 2.7 were calculated using 20 terms in the summation ($N = 20$). An interesting question arises as to how many terms must be retained for an approximate solution of sufficient accuracy (5% of the exact solution). A small number of retained terms would allow Eqns. (2.36) and (2.37) to be used with a hand calculator.

Figure 2.8 shows the exfiltration temperature profiles and the corresponding error in temperature profiles when the number of retained terms is four or less. By retaining only one term in addition to the zero order or steady-state term in Eqn. (2.36), the temperature profile had a maximum absolute error of 2.4 K in comparison to the base case solution which retained twenty terms. By retaining two terms the temperature error was reduced to a maximum of 0.2 K. By keeping four terms the maximum temperature error was less than 0.01 K.

Of greater interest is how rapidly the heat flux term converges. Figure 2.9(a) shows the variation in horizontal heat flux for the same number of retained terms as before (1, 2, and 4). Figure 2.9(b) shows the error expressed in watts per square metre when compared to the base case of retaining twenty terms for exfiltrating flow. By retaining only a single term, the error fluctuated between -8 and $+6 \text{ W}\cdot\text{m}^{-2}$ (-42% and $+32\%$, respectively, of the steady-state conduction heat flux) with the greatest error occurring at the boundaries and at the centre of the cavity. By retaining two terms in the summation the error was reduced significantly to a maximum of $\pm 1 \text{ W}\cdot\text{m}^{-2}$ (5% of the steady-state conduction heat flux). The error caused by retaining four or more terms was less than the 10^{-6} resolution of the computer. The large relative errors at the boundaries place a severe limitation on the number of terms that have to be retained. Practical application of Eqn. (2.37) requires at least four terms in the summation to be retained for this example. Retaining four terms is sufficient if the flow velocity is less than $0.01 \text{ m}\cdot\text{s}^{-1}$ and if the point where the profile is determined is more than 1 cm from the entrance plane.

Both Eqns. (2.36) and (2.37) contain a summation of trigonometric terms multiplied by an exponential term. The exponential factor is a function of thermal

diffusivity, elevation, flow velocity, and cavity depth. Since thermal diffusivity is a constant for a particular porous medium, the effect of changing thermal diffusivity was not investigated. As expected, the errors shown in Figs. 2.8 and 2.9 show a sinusoidal variation about the exact solution, due to these trigonometric terms. As the number of terms retained in the summations increase, the fluctuations are smoothed out. The sinusoidal terms are only weakly dependent on cavity geometry and virtually independent of the physical properties of the porous medium.

The convergence of Eqns. (2.36) and (2.37) depend on the height, flow velocity, and cavity depth. The height, z , and velocity, w , terms appear only in the exponential part of the summation. As z increases and/or w decreases, the exponential term goes to zero leaving only the thermally developed pure conduction solution. In the denominator of the exponential term, the depth is squared, indicating that a small decrease in depth corresponds to a large decrease in the exponential term. This again leads to the pure conduction solution. The number of terms necessary to retain in the summation decrease as the pure conduction solution is reached.

2.2.5 Changing the flow velocity through the wall cavity

Figure 2.10 shows the effect of changing the exfiltration velocity through the wall cavity. All curves are evaluated at $\Delta z = 1$ cm. For high velocity flow, $w = 0.004 \text{ m}\cdot\text{s}^{-1}$ (corresponding to a pressure differential across the wall cavity of 20 Pa), the thermal boundary layer grows more slowly than for low velocity flow, $w = 0.0005 \text{ m}\cdot\text{s}^{-1}$. Figure 2.10 shows that the temperature of the high velocity flow remains constant until 6 cm across the cavity indicating that the thermal boundary layer extends 3 cm across the cavity from the outer cavity wall. When there is no flow through the cavity, the thermally developed regime starts at the cavity entrance plane and extends for the entire cavity height. This corresponds to a state of pure conduction. High velocity flow will force the onset of the thermally developed regime further along the height of the cavity.

2.2.6 Changing the inlet plane temperature profile

So far, the discussion has been for an exfiltration inlet temperature which was the same as the warm wall (20°C) and an infiltration inlet temperature the same as the cold wall (-20°C). In typical wall assemblies each layer shown in Fig. 2.1 would have a different steady-state temperature. The interior wall would typically be 2° colder than the room air and 1° or 2° warmer than the inner cavity wall. The largest temperature drop occurs across the cavity occurs through the insulation. For a total indoor-outdoor temperature difference of 40°C , typically the temperature drop across the porous medium would be 34°C or 85% of the total. The outside wall and the outer cavity wall are generally closer in temperature than the inner cavity wall and the interior wall. Appendix C.1 lists the typical steady-state temperatures for a wall cavity exposed to a 40°C temperature differential between indoors and outdoors.

Air entering real wall cavities, either through exfiltration or infiltration, will not have the same temperature as the inner or outer cavity wall, as has been assumed for this model. Figure 2.11 shows the temperature profile when the inlet temperature for exfiltration (the indoor temperature) is 5.0°C above the inner cavity wall temperature of 20°C . The entire temperature profile, evaluated at $\Delta z = 1\text{ cm}$, is shifted upwards and to the right. As the warmer room air enters the cavity, two thermal boundary layers develop, one on each side of the cavity. Because the thermal boundary layers on each side of the cavity do not grow at the same rate, the maximum temperature across the cavity does not occur in the centre of the cavity. The boundary layer on the colder outer cavity wall grows more rapidly than the warm wall boundary layer, resulting in a maximum cavity temperature being closer to the warm wall. The inner cavity wall and the outer cavity wall remove heat from the flow until the flow is fully thermally developed and the conduction temperature profile is obtained.

Figure 2.12 shows temperature profiles across the test cavity when the infiltrating inlet temperature is -30°C and the cold wall boundary temperature is -20°C . When the inlet temperature is the same as the outer cavity wall temperature (-20°C),

only one thermal boundary layer is present within the cavity. The boundary layer grows along the inner cavity wall and eventually reaches the outer cavity wall. As in the previous case for exfiltration, two thermal boundary layers will develop within the cavity when the inlet temperature is different than the outer cavity wall temperature. The minimum flow temperature within the cavity when $T_{inlet} = -30^{\circ}\text{C}$ and $T_c = -20^{\circ}\text{C}$ occurs closer to the outer cavity wall than the inner cavity wall as would be expected since the inlet temperature is close to the outer cavity wall temperature. As shown by the change in slope of the temperature profile curves in Fig. 2.12, the heat fluxes at the boundaries have increased. Heat is being added to the flow from the warm inner wall and being removed at the cold outer cavity wall.

2.2.7 Overall heat balance for an insulation-filled cavity

The temperature profile and temperature gradient equations presented in Section 2.2.2 require prior knowledge of the surface temperatures in order to set the boundary conditions. In most cases this information will not be known. It is therefore necessary to perform an overall heat balance on the cavity to determine the inner and outer cavity wall temperatures, T_b and T_c respectively. The analysis developed in this section parallels the solution method presented in the ASHRAE Fundamentals Handbook (1989).

The wall cavity, shown in Fig. 2.2, is entirely filled with an homogeneous fluid-saturated porous medium, glass fibre batt insulation. The side walls are isothermal and the top and bottom of the cavity are insulated. The heat balance is concerned with only forced convection and conduction heat transfer as outlined in Section 2.1.7. The amount of heat generated by the change of state of the moist air will not be included (see Section 2.1.4).

Heat is transferred across the wall by conduction between the wall layers shown in Fig. 2.2 and by forced convection between the inner and outer cavity walls. The analysis of the overall wall heat balance begins by characterizing the heat transfer mechanisms through the interior wall and the exterior wall so as to arrive at a heat

flux going through both the inner cavity wall and the outer cavity wall. In order for the energy balance to be satisfied, the heat flux entering the cavity must equal the heat flux leaving the cavity since no sources or sinks for heat energy are allowed within the cavity.

Heat is transferred from the warm room to the inner cavity wall in three steps. First, heat must pass from the room, which is held at a constant temperature T_{room} , to the interior wall, which is at temperature T_a . This is represented by,

$$q_{room-a} = A_v h_a (T_{room} - T_a) \quad (2.38)$$

where q_{room-a} is the heat energy (watts) being transferred from the room to the interior wall, A_v is the vertical area through which the heat is transferred ($H \times L$), and h_a is the convective heat transfer coefficient for the interior wall bounded by still air.

The heat at the interior wall migrates to the inner cavity wall by conduction,

$$q_{a-b} = \frac{A_v}{R_l} (T_a - T_b) \quad (2.39)$$

where q_{a-b} is the heat transferred from the interior wall to the inner cavity wall, R_l is the thermal resistance of wall l shown in Fig. 2.2, and T_b is the temperature of the inner cavity wall.

By combining Eqns. (2.38) and (2.39) one can write the overall equation for heat transfer from the room to the inner cavity wall as,

$$q_l = \frac{T_{room} - T_b}{\frac{1}{A_v h_a} + \frac{R_l}{A_v}} \quad (2.40)$$

where q_l is the heat being transferred from the room to the inner cavity wall.

Heat energy is transferred from the outer cavity wall to the exterior wall by conduction,

$$q_{c \rightarrow d} = \frac{A_v}{R_{II}} (T_c - T_d) \quad (2.41)$$

where $q_{c \rightarrow d}$ is the heat transferred from the outer cavity wall to the exterior wall, R_{II} is the thermal resistance of wall II shown in Fig. 2.2, T_c is the temperature of the outer cavity wall, and T_d is the temperature of the exterior wall.

The heat balance for the exterior wall is complicated by two effects: a wind sensitive surface heat transfer coefficient, h_d , and solar radiation. ASHRAE (1968) published a correlation linking wind speed with the exterior heat transfer coefficient. The solar energy is handled by utilizing existing equations taken directly from the ASHRAE Fundamentals Handbook (1989), Chapters 26 & 27. The wind speed correlation for the exterior heat transfer coefficient is given by

$$h_d = 5.68(-0.002 V^2 + 0.315 V + 1.45) \quad (2.42)$$

where the wind speed, V , is given in miles per hour and the heat transfer coefficient is given in $\text{W} \cdot \text{m}^{-2} \cdot \text{K}^{-1}$. The typical range of h_d for wind speeds from 0 to $10 \text{ m} \cdot \text{s}^{-1}$ is 8.2 to $42.6 \text{ W} \cdot \text{m}^{-2} \cdot \text{K}^{-1}$ respectively.

The exterior wall may experience large amounts of short wave solar radiation which affects the amount and direction of heat transfer through the wall. The total short wave solar radiation incident on the exterior wall per square metre, expressed as I_T , can be broken down into three components,

$$I_T = I_{DN} \cos \theta_i + I_D + I_R \quad (2.43)$$

where I_{DN} is the direct normal radiation, I_D is the diffuse sky radiation, I_R is the reflected radiation, and θ_i is the angle of incidence. South-facing walls will be exposed to all three components of radiation while north-facing walls will only be exposed to diffuse and reflected solar radiation. In order to account for absorption of the wall surface for solar radiation, the solar absorptivity, α_d , of the material can be introduced.

The overall heat transfer from the exterior wall to the outdoors including solar

radiation affects can be expressed as,

$$q_{d-out} = A_v h_d (T_d - T_{out}) - A_v \alpha_d I_T \quad (2.44)$$

where h_d is defined in Eqn. (2.42).

Combining Eqns. (2.41) and (2.44) results in the equation for heat transfer through wall II,

$$q_{II} = \frac{T_c - T_{out} - \frac{\alpha_d}{h_d} I_T}{\frac{R_{II}}{A_v} + \frac{1}{A_v h_d}} \quad (2.45)$$

where q_{II} is the heat being transferred from the outer cavity wall to the outdoors.

To complete the discussion of the overall heat balance across the cavity, it is necessary to balance the heat entering the cavity with the heat leaving the cavity. The heat flux passing through the inner cavity wall is given by Eqn. (2.40). The heat flux for the inner cavity wall can also be determined by utilizing Fourier's law, Eqn. (2.7), and integrating the temperature gradient along the cavity's height, resulting in the equality,

$$\frac{q_I}{A_v} = \frac{T_{room} - T_b}{\frac{1}{h_a} + R_I} = -k \int_0^H \frac{\partial T(x,z)}{\partial x} \Big|_{x=0} dz \quad (2.46)$$

A similar balancing equation can be formulated for the outer cavity wall, where the heat flux through the outer cavity wall must be equal to the heat flux leaving the cavity (Eqn. (2.45)). The heat flux balance on the outer cavity wall is,

$$\frac{q_{II}}{A_v} = \frac{T_c - T_{out} - \frac{\alpha_d I_T}{h_d}}{R_{II} + \frac{1}{h_d}} = -k \int_0^H \frac{\partial T(x,z)}{\partial x} \Big|_{x=d} dz \quad (2.47)$$

Equations (2.46) and (2.47) are coupled by the temperature terms T_b and T_c and the temperature gradient terms, $\partial T/\partial x$, which are also functions of T_b and T_c . The temperature gradient terms include the effects of convection heat transfer at the surfaces of the cavity. It is necessary to solve Eqns. (2.46) and (2.47) by using a Gauss-Seidel iterative procedure. The solution converges rapidly and only requires a few iterations when indoor and outdoor air temperatures are used as initial estimates for the boundary temperatures.

The results from performing the overall heat balance on a typical wall cavity is presented in Section 3.2.

2.3 Development of the Mass Diffusion Model

The mass transfer model is based on an analytical solution of the differential equations governing diffusion through porous media. The working fluid will be assumed to be air, which can be treated as an ideal gas. The diffusing component will be water vapour. The partial pressure gradient of water vapour will be used as the driving force for mass diffusion instead of the more traditional mass concentration gradient. The reason for using partial pressures will be discussed in Section 2.3.2. As mentioned in Section 2.1 and shown in Fig. 2.3 the flow entering the cavity is assumed to be laminar plug flow with a constant velocity profile. The inlet flow is assumed to have a uniform partial pressure profile across the depth of the cavity.

The development of the mass diffusion model will proceed by initially discussing the specific boundary conditions for the model. A detailed derivation of the governing mass diffusion equations determining the partial pressure profiles and gradients through a wall cavity filled with porous media will be discussed. The derived

equations will be examined and discussed. Following, will be a further discussion on the region of validity of the present solution method.

2.3.1 Boundary conditions specific to the mass diffusion problem

The wall assembly being used to test the mass diffusion model is shown in Fig. 2.3. This wall is identical to the wall used in Section 2.2 to develop the heat transfer equations. The three boundary conditions needed to solve the governing differential equations for mass transfer deal with partial pressures and not temperatures. The partial pressure within the cavity is a function of its x and z positions, expressed as $p_w(x,z)$.

The inner cavity wall, at $x = 0$, is actually a vapour barrier which is attached to the interior wall as shown in Fig. 2.3. Since the vapour barrier is assumed to be impermeable to moisture vapour, no moisture will diffuse into the cavity through the interior wall. This boundary condition corresponds to a zero mass flux condition,

$$\frac{\partial p_w(0,z)}{\partial x} = 0 \quad (2.48)$$

By allowing no moisture to diffuse through the inner cavity wall, moisture may only enter the cavity via the leaking air flow. Calculations in Appendix C.2 show that the amount of moisture which may diffuse through a real vapour barrier is considerably smaller than the amount of moisture which the leakage flow is capable of carrying into the cavity. The effects of moisture diffusion and moisture convection are not additive, TenWolde (1985), and when both forms of transport are present, convective transport tends to dominate.

The second boundary condition is that the outer cavity wall, located at $x = d$ as shown in Fig. 2.3, has a set vapour pressure given by $p_w(d,z) = p_{w,c}$. The value of $p_{w,c}$ depends on the absorption and desorption characteristics of the wall. It will be shown in Section 3.3.1.1 that the outer cavity wall boundary condition can be chosen in such a way so as to limit the walls ability to add or remove moisture from the

flow.

A third boundary condition concerns the partial pressure of the inlet flow. As was discussed previously in Section 2.1, the flow entering the cavity is laminar plug flow with a uniform velocity profile. The inlet temperature profile is assumed to be linear (see Section 2.2.1) and therefore constant. Since the inlet temperature and relative humidity are assumed to be constant (Section 2.1.3), the inlet partial pressure must also be constant. Figure 2.3 shows a graphical representation of the constant inlet partial pressure profile. The boundary condition can be expressed as $p_w(x,0) = p_{w,inlet}$ where $p_{w,inlet}$ is the inlet partial pressure.

2.3.2 Deriving the partial pressure profile and gradient expressions

The molecular diffusion of any material component through another material was first described by Adolph Fick in 1855, see Bejan (1984). From his observations he formulated a basic law analogous to Fourier's law for heat transfer. The basic Fick's Law can be expressed as:

$$\dot{m}'' = -D \frac{\partial C_A}{\partial x} \quad (2.49)$$

where \dot{m}'' is the mass flux, D is the mass diffusivity, and $\partial C_A / \partial x$ is the horizontal concentration gradient of the diffusing component A. C_A is the mass concentration of component A per unit volume. For the purposes of this analysis the diffusing component, A, is water vapour.

With ideal gas mixtures, Fick's Law can be rewritten using partial pressures instead of concentrations. It is simpler to measure temperature and relative humidity, in order to determine the partial pressure of water vapour, than it is to measure the mass concentration of moist air. The ideal gas law for water vapour can be written as

$$p_w V = m_w \frac{R_0 T}{M_w} \quad (2.50)$$

where p_w is the partial pressure of water vapour, V is the volume, m_w is the mass of

water vapour, R_0 is the universal gas constant, T is the temperature, and M_w is the molecular mass of water. By rearranging Eqn. (2.50) an expression for mass concentration, in terms of partial pressure of water vapour, can be obtained,

$$C_w = \frac{m_w}{V} = \frac{M_w}{R_0 T} p_w \quad (2.51)$$

where C_w is the mass concentration of water vapour. By utilizing Eqn. (2.51), the partial pressure version of Fick's Law for water vapour diffusing through a porous material can be stated as

$$\dot{m}'' = -D \frac{M_w}{R_0 T} \frac{\partial p_w}{\partial x} \quad (2.52)$$

where $\partial p_w / \partial x$ is the horizontal gradient of the partial pressure of water vapour.

The mass and heat flux equations, Eqns. (2.52) and (2.7) respectively, are of the same form. The mass flux term is analogous to the heat flux term just as the vapour pressure gradient is analogous to the temperature gradient. The heat flux equation uses the thermal diffusivity as a proportionality constant while the mass flux equation uses a similar mass diffusivity term. The similarity between the mass flux and heat flux equations allows a similar analysis to be conducted on mass transfer as was done on heat transfer in Section 2.2. The effects of a porous medium on mass diffusion has already been discussed in Section 2.1.8.

The general steady-state differential equation governing diffusion of a gas through a solid is also analogous to the governing differential equation for heat transfer presented earlier in Section 2.2, and can be expressed as

$$u \frac{\partial C_w}{\partial x} + v \frac{\partial C_w}{\partial y} + w \frac{\partial C_w}{\partial z} = D \left(\frac{\partial^2 C_w}{\partial x^2} + \frac{\partial^2 C_w}{\partial y^2} + \frac{\partial^2 C_w}{\partial z^2} \right) \quad (2.53)$$

where u , v , w are the velocities in the x , y , z directions respectively. Equation (2.53) can be rewritten using partial pressures,

$$\frac{M_w}{R_0 T} \left(u \frac{\partial p_w}{\partial x} + v \frac{\partial p_w}{\partial y} + w \frac{\partial p_w}{\partial z} \right) - D \frac{M_w}{R_0 T} \left(\frac{\partial^2 p_w}{\partial x^2} + \frac{\partial^2 p_w}{\partial y^2} + \frac{\partial^2 p_w}{\partial z^2} \right) \quad (2.54)$$

Using the same arguments as in Section 2.2.2, namely, the velocities in the x and y directions are zero and allowing for mass diffusion in only the x direction (refer to Fig. 2.3) results in the simplified steady-state moisture diffusion equation,

$$w \frac{\partial p_w}{\partial z} = D \frac{\partial^2 p_w}{\partial x^2} \quad (2.55)$$

which will be solved analytically. The term $M_w \cdot (R_0 \cdot T)^{-1}$ has been factored out from both sides of the equation. The temperature term, T , is assumed not to be a function of x but rather is the mean temperature between the room and the outer cavity wall. If the temperature term is retained and is considered a function of x , the governing equation becomes much more difficult to solve and would require a numerical solution. It was decided to stay with an analytical solution and base the solution on the mean temperature within the cavity. Other fluid properties, such as density and viscosity, were also evaluated at the mean temperature.

The partial pressure and length scales in Eqn. (2.55) can be non-dimensionalized such that,

$$\bar{p}_w(\bar{x}, \bar{z}) = \frac{p_w(x, z) - p_{w,c}}{p_{w,inlet} - p_{w,c}} ; \quad \bar{x} = \frac{x}{d} ; \quad \bar{z} = \frac{z}{H} \quad (2.56)$$

It follows that the boundary conditions for the diffusion problem discussed in Section 2.3.1 and reprinted here for completeness,

$$\frac{\partial p_w(0, z)}{\partial x} = 0 ; \quad p_w(d, z) = p_{w,c} ; \quad p_w(x, 0) = p_{inlet} \quad (2.57)$$

can be non-dimensionalized such that,

$$\frac{\partial \bar{p}_w(0, \bar{z})}{\partial \bar{x}} = 0 ; \quad \bar{p}_w(1, \bar{z}) = 0 ; \quad \bar{p}_w(\bar{x}, 0) = 1 \quad (2.58)$$

The stated boundary conditions: zero mass flux at the inner cavity wall, fixed partial pressure at the outer cavity wall, and fixed partial pressure at the inlet plane are homogeneous and therefore require no transformation on the dependent variable, as was necessary in the heat transfer section.

The governing differential equation can be rewritten in terms of the non-dimensional parameters such that,

$$-\frac{DH}{wd^2} \frac{\partial^2 \bar{p}_w(\bar{x}, \bar{z})}{\partial \bar{x}^2} \quad (2.59)$$

which can be solved by using the separation of variables method where,

$$\bar{p}_w(\bar{x}, \bar{z}) = X(\bar{x}) \cdot Z(\bar{z}) \quad (2.60)$$

X is a function of only \bar{x} and Z is a function of only \bar{z} . The separation constant, λ^2 , is taken to be strictly negative such that,

$$\frac{wd^2}{DH} \frac{1}{Z(\bar{z})} \frac{dZ(\bar{z})}{d\bar{z}} = -\lambda^2 \quad (2.61)$$

and

$$\frac{1}{X(\bar{x})} \frac{d^2 X(\bar{x})}{d\bar{x}^2} = -\lambda^2 \quad (2.62)$$

Solving Eqns. (2.61) and (2.62) for $Z(\bar{z})$ and $X(\bar{x})$ respectively yields:

$$Z(\bar{z}) = A \exp \left[-\frac{DH}{d^2 w} \lambda^2 \bar{z} \right] \quad (2.63)$$

and,

$$X(\bar{x}) = C \cos(\lambda \bar{x}) + E \sin(\lambda \bar{x}) \quad (2.64)$$

where A , C , and E are constants of integration. The general solution for \bar{p}_w can be arrived at by substituting Eqns. (2.63) and (2.64) into Eqn. (2.60) to yield

$$\bar{p}_w(\bar{x}, \bar{z}) = (C \cos(\lambda \bar{x}) + E \sin(\lambda \bar{x})) \exp \left[-\frac{DH}{d^2 w} \lambda^2 \bar{z} \right] \quad (2.65)$$

Applying the boundary condition which states that the inner cavity wall is impermeable to moisture, Eqn. (2.48), it can be shown that the constant E in Eqn. (2.65) must equal zero. Applying the second boundary condition, $\bar{p}_w(1, \bar{z}) = 0$, and since $C \neq 0$, the resulting equation turns into an eigenvalue problem where $\cos(\lambda) = 0$ and

$$\lambda_n = \frac{(2n - 1)\pi}{2}, \quad n = 1, 2, 3, \dots \quad (2.66)$$

Equation (2.65) can be rewritten as,

$$\bar{p}_w(\bar{x}, \bar{z}) = \sum_{n=1}^{\infty} B_n \cos(\lambda_n \bar{x}) \exp \left[-\frac{DH}{d_s^2 w} \lambda_n^2 \bar{z} \right] \quad (2.67)$$

where B_n can be solved for by invoking the last boundary condition, $\bar{p}_w(\bar{x}, 0) = 1$, with the resulting equation being a Fourier cosine series,

$$\bar{p}_w(\bar{x}, 0) = 1 = \sum_{n=0}^{\infty} B_n \cos(\lambda_n \bar{x}) \quad (2.68)$$

where $B_0 = 0$ and

$$B_n = 2 \int_0^1 \cos(\lambda_n \bar{x}) d\bar{x} = \frac{2 \sin \lambda_n}{\lambda_n} \quad (2.69)$$

Combining Eqns. (2.67) and (2.69) yields the solution for the non-dimensional partial pressure profile,

$$\bar{p}_w(\bar{x}, \bar{z}) = \sum_{n=1}^{\infty} \frac{2 \sin \lambda_n}{\lambda_n} \cos(\lambda_n \bar{x}) \exp \left[-\frac{DH}{d^2 w} \lambda_n^2 \bar{z} \right] \quad (2.70)$$

The non-dimensional partial pressure gradient, with respect to \bar{x} , is given by,

$$\frac{\partial \bar{p}_w(\bar{x}, \bar{z})}{\partial \bar{x}} = \sum_{n=1}^{\infty} -2 \sin \lambda_n \sin(\lambda_n \bar{x}) \exp \left[-\frac{DH}{d^2 w} \lambda_n^2 \bar{z} \right] \quad (2.71)$$

At any point within the flow field the partial pressure for water vapour can be determined by using the non-dimensional parameter \bar{p}_w as shown below,

$$p_w(x, z) = (p_{w, \text{inlet}} - p_{w, c}) \bar{p}_w(\bar{x}, \bar{z}) + p_{w, c} \quad (2.72)$$

Expanding Eqn. (2.72) results in the partial pressure profile solution,

$$p_w(x, z) = p_{w, c} + (p_{w, \text{inlet}} - p_{w, c}) \sum_{n=1}^{\infty} \frac{2 \sin \lambda_n}{\lambda_n} \cos \left(\frac{\lambda_n x}{d} \right) \exp \left[-\frac{D \lambda_n^2 z}{w d^2} \right] \quad (2.73)$$

The partial pressure gradient can be expressed as,

$$\frac{\partial p_w(x, z)}{\partial x} = (p_{w, \text{inlet}} - p_{w, c}) \sum_{n=1}^{\infty} \frac{-2 \sin \lambda_n}{d} \sin \left(\frac{\lambda_n x}{d} \right) \exp \left[-\frac{D \lambda_n^2 z}{w d^2} \right] \quad (2.74)$$

The solutions for Eqns. (2.73) and (2.74) require using an infinite number of terms in the summation. An approximate solution can be obtained by performing the summation over a fixed number of terms from $n = 1$ to N , where n and N are integers.

2.3.3 The mass flux solution

As mentioned previously, the mass flux at any point within the flow field can be determined by using Fick's Law. Fick's Law was given in Eqn. (2.52) and is repeated here for completeness,

$$\dot{m}'' = -D \frac{M_w}{R_0 T} \frac{\partial p_w}{\partial x} \quad (2.75)$$

The mass flux can be calculated since the partial pressure gradient term, given in equation (2.74), is known. The total mass deposited on a surface can be determined by integrating equation (2.75) along z such that,

$$\dot{m}_w = -D L \frac{M_w}{R_0 T} \int \frac{\partial p_w}{\partial x} dz \quad (2.76)$$

where L is the cavity width. The integration of $\partial p_w / \partial x$ from $z = i$ to j results in the following equation:

$$\dot{m}_w = -D L \frac{M_w}{R_0 T} (p_{w,inlet} - p_{w,c}) \sum_{n=1}^{\infty} \frac{-2 \sin \lambda_n}{d} \sin\left(\frac{\lambda_n x}{d}\right) \left(\frac{-w d^2}{D \lambda_n^2} \right) \left(\exp\left[-\frac{D \lambda_n^2 j}{w d^2}\right] - \exp\left[-\frac{D \lambda_n^2 i}{w d^2}\right] \right) \quad (2.77)$$

2.3.4 An examination of the partial pressure and mass flux equations

The behaviour of the partial pressure profile and partial pressure gradient terms derived in Section 2.3.2 directly influence the amount of mass deposited on any surface. It is therefore necessary to understand the behaviour and limitations of the derivations. The partial pressure profile and subsequent mass flux will be discussed as the profiles develop through the cavity.

Figure 2.3 shows a typical wall cavity which was used to test the partial pressure equations. Table 2.3 lists the values used for the test as well as a typical range of values. The values in Table 2.3 are equivalent to the values used in examining the temperature profile equations presented in Section 2.2.2, wherever possible.

The mass diffusivity, D , used to examine the behaviour of the moisture diffusion equations was that for water vapour diffusing through still air, 2.56×10^{-5}

$\text{m}^2 \cdot \text{s}^{-1}$, Perry (1963). Increasing or decreasing the diffusivity changes the rate at which mass is deposited, but does not change the development of the profiles.

Figure 2.3 shows the flow entering the cavity at $z = 0$ with a constant inlet partial pressure, $p_{w,\text{inlet}}$, and constant velocity, w . For exfiltration, the inlet conditions would equal the room conditions. For infiltration, the inlet conditions would match the outdoor conditions. As the flow proceeds vertically through the cavity, moisture brought into the cavity with the flow is carried by convection along the cavity and diffuses horizontally across the cavity. Upon reaching a cold interface, where the vapour pressure of water is lower than that of the diffusing moisture, condensation or sublimation will occur. In most practical cases the cold interface is the outer cavity wall and condensation will accumulate on the surface of the wall. If the wall temperature is less than 0°C then the condensing moisture would accumulate as ice. In certain instances the wall vapour pressure may be larger than the inlet vapour pressure and moisture will be desorbed from the wall surface. Desorption of water from the outer cavity wall occurs more frequently during infiltration than exfiltration.

2.3.4.1 Partial pressure profiles and heat fluxes for exfiltration

Figure 2.13 shows the developing partial pressure profiles for exfiltrating flow through a porous medium filled wall cavity (see Fig. 2.3) and the corresponding mass flux based on the partial pressure gradient. The inlet temperature was 20°C and the inlet relative humidity was 50%. The outer cavity wall conditions were -20°C and 100% relative humidity. For the chosen inlet conditions, 0.95 g of moisture enter the cavity per hour.

At $\Delta z = 1 \text{ cm}$, the partial pressure profile in Fig. 2.13(a) shows a partial pressure at $x = 0$, the inner cavity wall, equal to the inlet partial pressure (1170 Pa). The partial pressure gradient along the inner cavity wall is zero, which corresponds to a zero mass flux, as shown in Fig. 2.13(b). Moving from the inner wall to the outer wall, the partial pressure profile in Fig. 2.13(a) decreases in value until at the outer cavity wall, $x = 9 \text{ cm}$, the partial pressure is equal to the wall boundary pressure of

103 Pa. Figure 2.13(b) indicates that the mass flux at the outer cavity wall, for an elevation of 1 cm, is $0.0066 \text{ g}\cdot\text{m}^{-2}\cdot\text{s}^{-1}$. As Δz increases, the partial pressure profiles in Fig. 2.13(a), drop indicating that moisture is being removed from the flow. At the same time the mass fluxes decrease, indicating a slowing of the amount of mass being deposited on the outer cavity wall. At an elevation of 10 cm the mass flux is $0.0026 \text{ g}\cdot\text{m}^{-2}\cdot\text{s}^{-1}$, 40% of the mass flux which is experienced at $\Delta z = 1 \text{ cm}$. At $\Delta z = 40 \text{ cm}$ the mass flux is 6% of the mass flux when $\Delta z = 1 \text{ cm}$. At the exit plane of the cavity, $\Delta z = 75 \text{ cm}$, the partial pressure profile across the cavity is nearly linear and equal to the cold wall partial pressure. This indicates that most, but not all of the moisture in the flow has been removed. The mass flux at $\Delta z = 74 \text{ cm}$ is less than $0.0002 \text{ g}\cdot\text{m}^{-2}\cdot\text{s}^{-1}$, but still greater than zero meaning that moisture is leaving the cavity with the air flow.

Figure 2.13(b) clearly shows that the largest mass fluxes occur within the first few centimetres of the cavity, $\Delta z < 10 \text{ cm}$. Further up the cavity the mass fluxes decrease rapidly. Timusk and Doshi (1985) report in their experimental investigation that most moisture accumulation in cavities occurs close to the entrance hole. The results of this moisture deposition model are consistent with Timusk and Doshi's findings.

For the conditions chosen in Table 2.3, the exfiltrating flow deposited moisture on the outer cavity wall. It is possible to have conditions in which moisture could be removed from the outer cavity wall during exfiltration. However, in northern climates, where indoor temperatures are typically higher than outdoor temperatures, it would be extremely rare to have moisture being removed from the outer cavity wall due to exfiltration. In the summer time when the outdoor temperature is typically higher than the indoor temperature it is possible to have moisture removed from the cavity during exfiltration.

2.3.4.2 Partial pressure profiles and heat fluxes for infiltration

Figure 2.14 shows the developing partial pressure and mass flux profiles for infiltrating flow through a porous medium filled wall cavity. The wall cavity used is shown in Fig. 2.3 where the inlet conditions are the outdoor conditions and the flow enters from the top, $z = 75$ cm, not the bottom, $z = 0$, as drawn. Δz is measured from the entrance plane in the direction of the flow. The inlet temperature was -30°C with a relative humidity of 80%. The outer cavity wall temperature was -20°C with a relative humidity of 100%. In most cases the difference between the outer cavity wall temperature and the outdoor temperature would be less than 10° . A large temperature difference was chosen for this analysis in order to make the effects of infiltration mass deposition more noticeable. The specified inlet conditions allow for the inlet air flow to carry $70\ \mu\text{g}$ of water per hour into the cavity.

In Fig. 2.14(a) the partial pressure profiles are shown for increasing distances from the entrance plane. At $\Delta z = 1$ cm, the partial pressure at the inner cavity wall is 30 Pa, the same as the inlet condition. There is no mass flux through the inner cavity wall since the wall is impermeable to moisture. At the outer cavity wall the partial pressure is 103 Pa, corresponding to the boundary conditions. It can be seen that the slope of the partial pressure profile in Fig. 2.14(a) is positive, which indicates that the mass flux ($-D \partial p_w / \partial x$) will be negative. Moisture is being removed from the outer cavity wall. Further along the cavity, $\Delta z > 1$ cm, the partial pressure at the inner cavity wall rises as more moisture is absorbed from the outer cavity wall by the air flow. Eventually, the flow becomes saturated and the partial pressure profile becomes horizontal ($\Delta z = 74$ cm). In Fig. 2.14(b) the mass flux profiles are negative at $x = 9$ cm, indicating that moisture is being removed from the wall. At $x = 0$, the mass flux is zero due to the boundary conditions imposed on the inner cavity wall.

In most typical winter situations the outer cavity wall temperature will be slightly higher than the outdoor temperature and therefore the outer cavity wall partial pressure will be higher than the outdoor partial pressure. This will lead to moisture being removed from the outer cavity wall as shown in Fig. 2.14. However, it is not

uncommon to have a situation where the outdoor partial pressure is higher than the outer cavity wall partial pressure even though the outer cavity wall temperature is higher than the outdoor temperature. In this type of situation, moisture will be deposited on the cavity wall during infiltration.

2.3.5 Determining the number of terms to retain in the summation

The partial pressure profiles and mass flux terms defined in Eqns. (2.73) and (2.74) were calculated using a summation term in the expression. For Figs. 2.15 and 2.16 the number of terms retained in the summation was twenty ($N = 20$), plus the steady-state term. Retaining twenty terms would make hand calculations cumbersome. It would be useful to reduce the number of retained terms to a manageable number.

Figure 2.15 shows the effect on the partial pressure profiles for exfiltration of reducing the number of terms retained in the summation from eight to one. The error in retaining only one term is as large as 350 Pa or 30% of the inlet partial pressure (1170 Pa). By retaining two terms the maximum error is reduced to 90 Pa or 7.7% of the inlet partial pressure. Retaining four terms further reduces the maximum error to less than 3 Pa or 0.3% of the inlet partial pressure. When eight terms are retained, in addition to the steady-state term, the partial pressure solution is the same, to six significant digits, as the solution for retaining 20 terms. For the typical range of conditions outlined in Table 2.3, retaining four terms is sufficient to obtain less than 5% error in calculated partial pressures.

The same results hold for the mass flux as for the partial pressure profiles. In Fig. 2.16 the effect on mass flux is shown as the number of retained terms increases from one to eight. When only one term is retained in the summation, the maximum error was $0.0034 \text{ g}\cdot\text{m}^{-2}\cdot\text{s}^{-1}$ or 52% of the mass flux measured at $x = 9 \text{ cm}$. By increasing the retained terms to 2, the error dropped to $0.0013 \text{ g}\cdot\text{m}^{-2}\cdot\text{s}^{-1}$ or 20%. Retaining four terms dropped the error to $0.00007 \text{ g}\cdot\text{m}^{-2}\cdot\text{s}^{-1}$ or 1%. Retaining eight terms yielded the same solution, to six significant digits, as retaining twenty terms. For the

typical range of conditions outlined in Table 2.3, retaining four terms is sufficient to obtain less than 2% error in calculated mass fluxes.

Figures 2.15 and 2.16 indicate that by retaining only four terms plus the steady-state term in Eqns. (2.73) and (2.74) a suitable solution can be determined. However, other factors exist that may make it advantageous to retain more than the minimum number of terms. Fluctuating flow rates, changing inlet conditions, and different physical characteristics of the wall cavity will all affect the number of terms that must be retained within the summation. Over the range of values tested and listed in Table 2.3, it was found that retaining four terms was adequate.

2.3.6 Effect of flow rate on the humidity ratio profile

The humidity ratio, W , can be determined by knowing the partial pressure of water vapour and the combined partial pressures of water and dry air. According to ASHRAE (1989) the definition for humidity ratio is,

$$W = \frac{M_w}{M_{air}} \frac{p_w}{p_{atm} - p_w} \times 1000 \quad (2.78)$$

expressed in grams water per kilogram dry air, where M_w and M_{air} are the molecular masses of water and air respectively, and p_{atm} is the total atmospheric pressure. By knowing the partial pressure profile, the humidity ratio profile may be determined. The area under the humidity profile is the amount of water present in the air flow.

Figure 2.17 shows how the humidity ratio profile, and hence the partial pressure profile, behaves as the flow rate through the cavity is increased. A slow flow rate allows the moisture in the flow more time to diffuse to the outer cavity wall and therefore, reduces the area under the curve. A smaller area under the curve signifies less moisture in the flow. A faster flow rate reduces the amount of time the moisture has to diffuse to the outer cavity wall and hence increases the area under the curve. An increased flow rate will cause the moisture to be deposited further up the wall, while a slow flow rate will allow more deposition to occur closer to the entrance plane.

2.3.7 Region of validity for the mass diffusion model

Inherent in the derivation of the partial pressure profile solution was the assumption that the migration of moisture within the cavity was diffusion driven and that moisture can only condense or freeze at the outer cavity wall. Therefore, the model developed here is only strictly valid when mass transfer occurs by diffusion and when no moisture condenses within the porous medium. The mass diffusion model is valid over a large range of inlet relative humidity and for widely varying external temperatures. A plot showing the inlet relative humidity and wall temperature conditions for which the model is valid has been established and will be discussed in this section.

2.3.7.1 Background development for determining the region of validity

A common assumption concerning mass deposition in wall cavities, which has been substantiated in experimental studies, Timusk and Doshi (1985), is that the majority of moisture accumulates at the outer cavity wall. Since mass diffusion is driven by a vapour pressure gradient, moisture will tend to migrate towards the area within the cavity with the lowest vapour pressure. For winter conditions, the outer wall cavity has the lowest vapour pressure and temperature within the cavity. The outer cavity wall also has a higher resistance to mass diffusion than the porous medium. As moisture diffuses through the porous medium toward the cold wall, it meets an increased resistance and deposits excess moisture on the surface (the model assumes that this moisture is subsequently absorbed by the wall (see Section 3.3.1.1)) while some moisture continues to migrate through the wall to the outdoors. It is possible, however, that the moisture vapour within the cavity may begin to condense within the porous medium before reaching the cold outer wall. If conditions exist such that condensation occurs in the insulation then the method presented in Section 2.3.2 to determine the partial pressure profiles becomes invalid. Another problem with condensation occurring within the porous medium is that resistance to air flow increases and the assumptions of uniform cavity resistance and air flow (Darcy's Law, Section

2.1.6) become invalid. Condensation will occur within the porous medium at the location where the local partial pressure of water vapour meets or exceeds the local partial pressure of water vapour at saturation for the same temperature.

The equation for determining the temperature profile for flow in a porous medium was discussed in Section 2.2.2 and shown as Eqn. (2.36). What was not mentioned in Section 2.2.2 was that, along with the developing temperature profile, a second profile, the saturated partial pressure profile, was also developing. The saturated partial pressure is defined as the maximum partial pressure for water vapour that can exist in an air-water vapour mixture at a given temperature. As the temperature drops, the maximum amount of moisture that can be retained in the air (at saturation) drops. It was shown in Section 2.2.3 that the temperature profile reaches the steady-state profile a short distance into the cavity. The saturated partial pressure profile would reach a steady-state profile as the temperature profile does. However, the saturated partial pressure profile does not have the same shape as the temperature profile.

In order for the diffusion model to be valid, the partial pressure profile must not cross the saturated partial pressure profile and become super-saturated. Determining whether the partial pressure profile crosses the saturated pressure profile can be accomplished in two ways. One method is to compare the gradient of the partial pressure profile with the gradient of the saturated pressure profile at the outer wall surface. If the saturated partial pressure gradient is larger than the partial pressure gradient, then the two profiles must have crossed at some point within the cavity. The gradient method is limited to the case where the outer wall cavity is maintained at a saturated condition ($\phi_c = 100\%$). In most practical cases the outer wall cavity will not be saturated (see Section 3.3.1.1 for a more complete discussion) therefore a different method must be used.

The second method simply compares the saturated partial pressure to the actual partial pressure at finite intervals across the cavity. If at any point the partial pressure exceeds the saturated partial pressure for the same temperature the model is considered invalid. The saturated partial pressure can be determined using the ASHRAE

equations shown in Appendix C.4. This method is more cumbersome than the gradient method, which only requires calculations at the outer wall boundary and not throughout the cavity. However, the finite interval method is more useful as it can handle any outer cavity wall surface relative humidity (vapour pressure).

2.3.7.2 Calculating the region of validity

The region of validity for the mass diffusion model was calculated using the finite-interval method discussed in Section 2.3.7.1. The partial pressure profile and the saturated partial pressure profile were calculated along the cavity height and then compared to determine if super-saturated conditions existed. Shown in Fig. 2.18 are the developing partial pressure profiles and the developing saturated partial pressure profiles for three different inlet relative humidities. The inlet relative humidity was 30, 50, and 70% for Fig. 2.18(a), (b), and (c) respectively. The outer cavity wall temperature was -10°C which corresponds to a saturated partial pressure of 260 Pa. The surface relative humidity was set at 75% ($p_{w,c} = 195 \text{ Pa}$; $p_{ws,c} = 260 \text{ Pa}$). All profiles were evaluated at $\Delta z = 6 \text{ cm}$ from the entrance plane for exfiltrating flow. The evaluation point at 6 cm was selected so that the affects of changing the inlet parameters could be easily recognized. The test cavity is shown in Fig. 2.3.

Figure 2.18(a) shows the partial pressure and saturated pressure profile for an inlet relative humidity of 30%. It can be seen that the profiles do not cross. The model is valid at this point ($\Delta z = 6 \text{ cm}$). To determine if the model is valid for the stated inlet conditions ($\phi_{\text{inlet}} = 30\%$) it would be necessary to check the pressure profiles along the entire wall height to see if the profiles crossed at any other elevation. Figure 2.18(b) shows the two profiles at the same elevation but with the inlet relative humidity increased to 50%. The partial pressure profile touches the saturated profile at $x = 8.5 \text{ cm}$ from the inner cavity wall. This contact would indicate that moisture deposition may occur within the porous medium as well as on the outer cavity wall. The model would therefore be considered invalid for an inlet relative humidity of 50%. Figure 2.18(c) shows the effect of increasing the inlet relative humid-

ity to 70%. The model is clearly invalid since the two profiles cross at $x = 6.5$ cm. Moisture would be expected to be deposited within the porous medium. Although it is not possible with this model to predict where the moisture is likely to be deposited, Timusk and Doshi (1985) have shown that when moisture is deposited within glass fibre insulation it tends to gather next to the outer cavity wall.

The criteria used in determining the region of validity for this model is considered to be conservative. What was taken as a failure condition in Fig. 2.18(b) could also have been considered as non-failure. The reason for taking the conservative approach is that once the developing partial pressure profile approaches or crosses the saturated profile then the model becomes invalid. In the region next to the wall condensation may be occurring within the insulation which is beyond the scope of this model to handle.

2.3.7.3 Mapping of the region of validity

Simply knowing when the model is invalid is insufficient. It is far better to know when the model is valid and hence, when the model can be used with confidence. Using the calculation method outlined previously (Section 2.3.7.2) a range of inlet and wall conditions were evaluated for two different flow rates in order to determine the limits for the model. The model was run using an inlet relative humidity varying from 5 to 100% at a fixed temperature of 20°C. The outer wall cavity temperature varied from -30 to +10°C.

Figure 2.19 shows the region of validity for the mass diffusion governed model when the maximum flow velocity is $0.01 \text{ m}\cdot\text{s}^{-1}$. Shown in the figure are curves for outer cavity wall relative humidities of 25, 50, 75, and 100%. The area beneath and to the right of the solid line indicates the region where the model is completely valid with an outer cavity wall relative humidity of 100%. For lower relative humidities on the outer wall the region of validity increases. For example, with a wall temperature of -10 °C and 100% relative humidity, the maximum permissible inlet relative humidity is $\approx 36\%$ at an indoor temperature of 20°C. If the outer wall rela-

tive humidity is decreased to 25% then the maximum permissible indoor relative humidity would increase to $\approx 60\%$. Another factor affecting the area of validity for the model is the flow rate through the cavity. Figure 2.20 shows the region of validity for the same conditions as in Fig. 2.19, except that the flow velocity through the cavity is reduced by a factor of 100, to $0.0001 \text{ m}\cdot\text{s}^{-1}$. Most porous medium filled cavities do not experience flow velocities larger than $0.01 \text{ m}\cdot\text{s}^{-1}$, which can be taken as an extreme upper limit on flow velocities (measured flow velocities in wall cavities are discussed in Section 3.1.5). At -10°C the permissible inlet relative humidity in Figure 2.20 is $\approx 45\%$ for a saturated wall condition and $\approx 83\%$ for a wall at 25% of saturation. By directly comparing Figs. 2.19 and 2.20 it can be seen that the slower flow velocity yields a larger region of validity.

2.3.7.4 Comparison of measured home relative humidities and the region of validity for the moisture deposition model

Use of the moisture deposition model requires that the inlet relative humidity and the outer cavity wall temperature fall into the region shown in Fig. 2.19, which represents moisture deposition only on the outer cavity wall. Kent *et al.* (1966) studied the humidity variations in a number of Canadian homes and determined a range of relative humidities that typical homes would experience as a function of outdoor temperature. Superposed on Fig. 2.19 and shown in Fig. 2.21 is the region defined by Kent *et al.* indicating the typical indoor relative humidities experienced in Canadian homes and the region of validity for the model. Figure 2.21 indicates that the model can be relied on to give confident results when the outer wall cavity temperature drops to as low as -18°C , depending on the inlet relative humidity. The model's range could be extended to as low as -26°C , depending on the outer cavity wall relative humidity and the inlet relative humidity.

The relative humidity on the outer cavity wall does not have to be at saturation (100%). Most often the wall is not saturated and a boundary condition less than 100% relative humidity is more representative of the wall's ability to absorb moisture.

In Section 3.3.1 the outer cavity wall boundary conditions are discussed in more detail.

Table 2.1 Typical Rayleigh numbers for closed and open wall cavities filled with glass fibre insulation.

Density ($\text{kg}\cdot\text{m}^{-3}$)	Permeability ($\text{m}^2 \times 10^{-10}$)	ΔT (K)	Vertical velocity ($\text{m}\cdot\text{s}^{-1}$)	Ra^*	Ra_w
1.0	500	40	0.010	13.122	0.25
2.5	100	40	0.010	2.624	0.05
5	50	40	0.010	1.312	0.025
10	31	40	0.010	0.814	0.016
15	10	40	0.010	0.262	0.006
50	5	40	0.010	0.131	0.002
240	1	40	0.010	0.026	0.001

Table 2.2 Base case parameters and variables used to examine the exact solution for temperature profiles and heat fluxes within a porous medium filled cavity. The cavity is shown in Figure 2.2. The walls have no thermal resistance.

Symbol	Description	Value	Typical Range
H	Height [m]	0.75	--
L	Width [m]	0.34	--
d	Depth [m]	0.09	--
H/d	Aspect ratio	8.33	--
z	Elevation of outlet (exfiltration) [m]	0	--
z	Elevation of inlet (infiltration) [m]	0.75	--
α	Thermal diffusivity [$\text{m}^2\cdot\text{s}^{-1}$]	$3.49\cdot 10^{-5}$	1.6 to $4.9\cdot 10^{-5}$
k	Thermal conductivity of insulation [$\text{W}\cdot\text{m}^{-1}\cdot\text{K}^{-1}$]	0.0425	0.02 to 0.06
T_{room}	Indoor temperature [$^{\circ}\text{C}$]	20	15 to 30
T_{out}	Outdoor temperature [$^{\circ}\text{C}$]	-20	-40 to 0
T_b	Inner cavity wall temperature [$^{\circ}\text{C}$]	20	15 to 30
T_c	Outer cavity wall temperature [$^{\circ}\text{C}$]	-20	-40 to 0
w	Velocity [$\text{m}\cdot\text{s}^{-1}$]	0.001	0 to 0.01
Ra^*	Darcy-modified Rayleigh number	10.3	up to 10.3

Table 2.3 Base case parameters and variables used to examine the exact solution for partial pressure profiles and mass fluxes within a porous medium filled cavity. The cavity is shown in Figure 2.3.

Symbol	Description	Value	Typical Range
H	Height [m]	0.75	--
L	Width [m]	0.34	--
d	Depth [m]	0.09	--
z	Elevation of inlet (exfiltration) [m]	0	--
z	Elevation of inlet (infiltration) [m]	0.75	--
D	Mass diffusivity [$\text{m}^2 \cdot \text{s}^{-1}$]	$2.56 \cdot 10^{-5}$	$1.61 \cdot 10^{-5}$ ^a to $3.31 \cdot 10^{-5}$ ^b
T_{room}	Indoor temperature [$^{\circ}\text{C}$]	20	15 to 30
ϕ_{room}	Indoor relative humidity [%]	50	10 to 60
$p_{w,\text{room}}$	Indoor partial pressure of water vapour [Pa]	1170	171 to 2548
T_{out}	Outdoor temperature [$^{\circ}\text{C}$]	-30	-40 to 0 ^c
ϕ_{out}	Outdoor relative humidity [%]	80	20 to 100
$p_{w,\text{out}}$	Outdoor partial pressure of water vapour [Pa]	30.4	3 to 611
T_b	Inner cavity wall temperature [$^{\circ}\text{C}$]	20	15 to 30
T_c	Outer cavity wall temperature [$^{\circ}\text{C}$]	-20	-40 to 0
ϕ_c	Outer cavity wall relative humidity [%]	100	0 to 100 ^d
$p_{w,c}$	Outer cavity wall vapour pressure [Pa]	103	3 to 611
w	Velocity [$\text{m} \cdot \text{s}^{-1}$]	0.001	0 to 0.01

^aTveit (1969) typical glass fibre.

^bASHRAE Fundamentals (1989), page 22.13, typical mineral wool batt.

^cTypical winter conditions in Edmonton.

^dDependent on material type and surface covering.

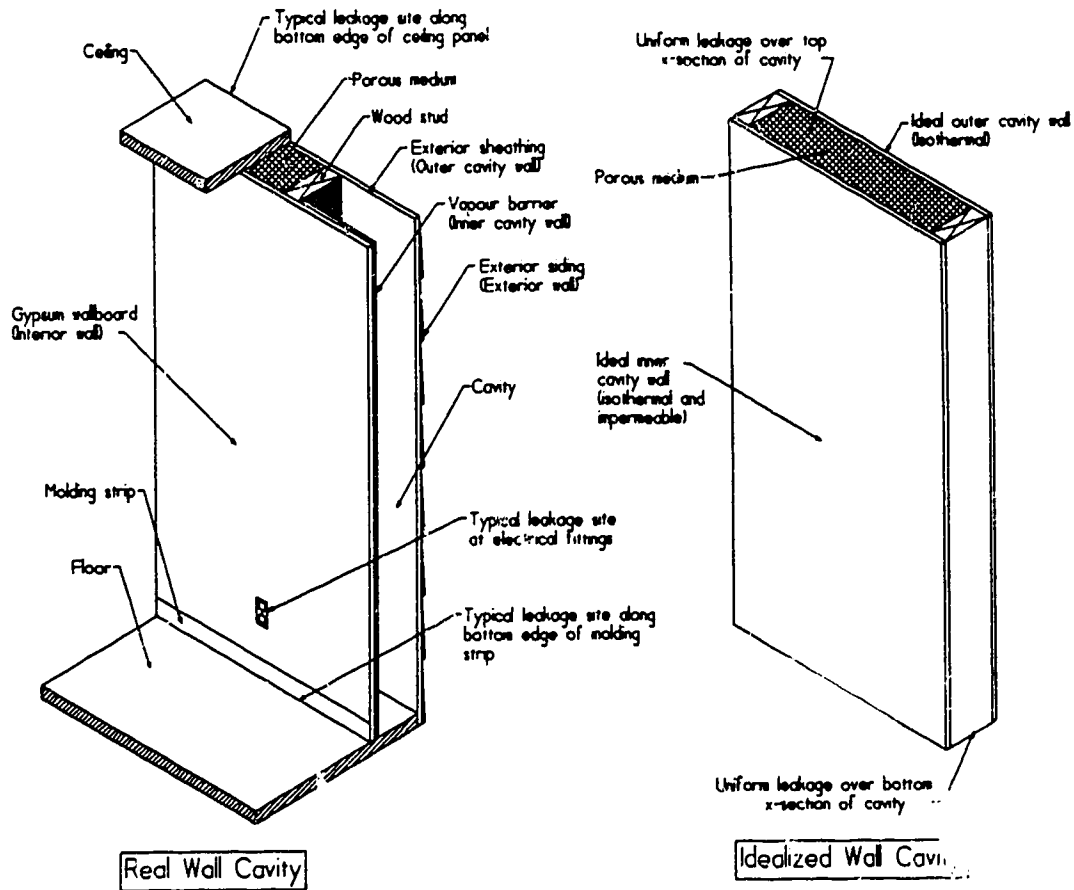


Figure 2.1 A comparison of a typical real wall cavity and the idealized parallel plate wall cavity.

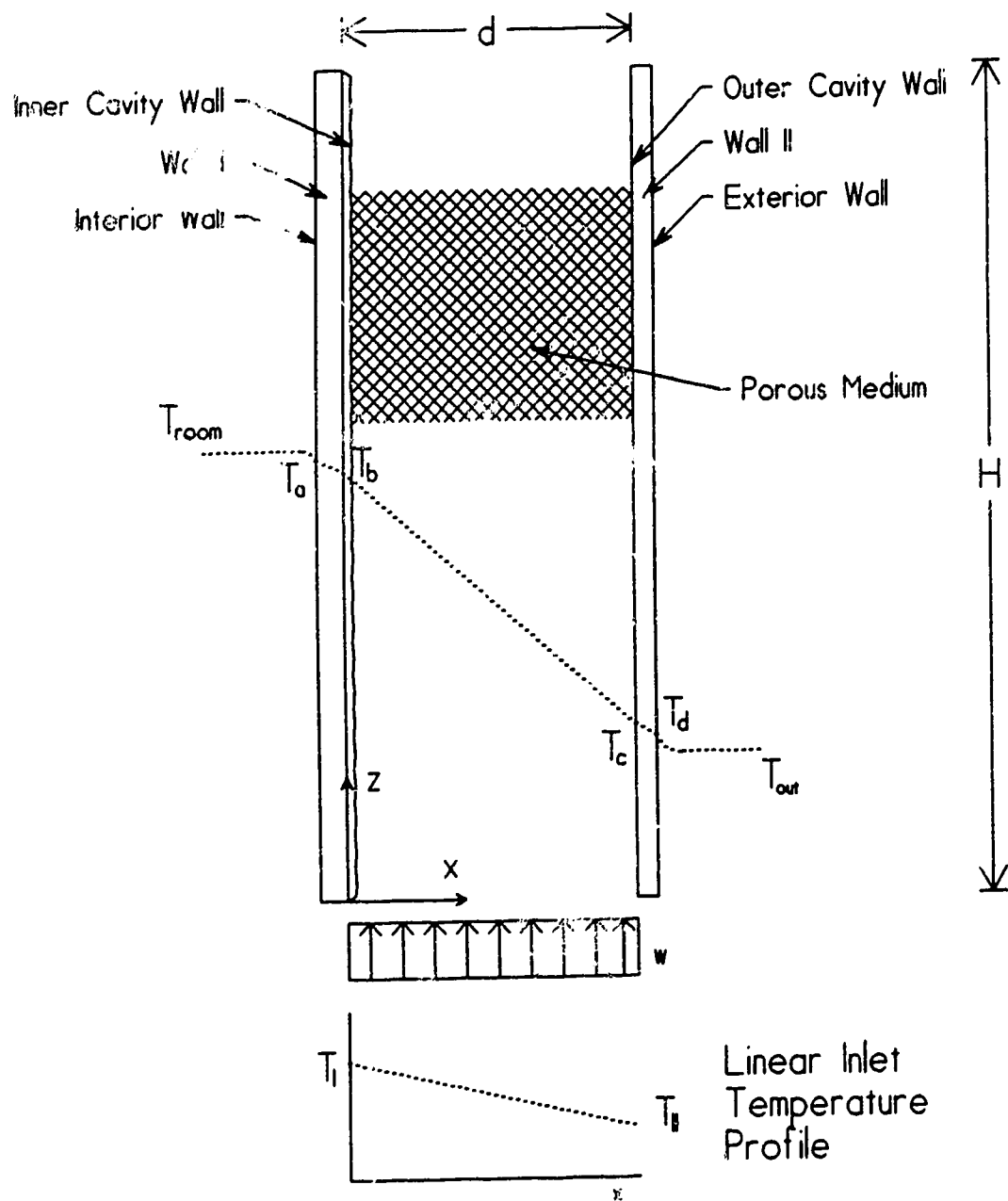


Figure 2.2 Description of the wall cavity used to develop the heat transfer model. The inlet velocity is constant across the cavity depth and the temperature profile is linear.

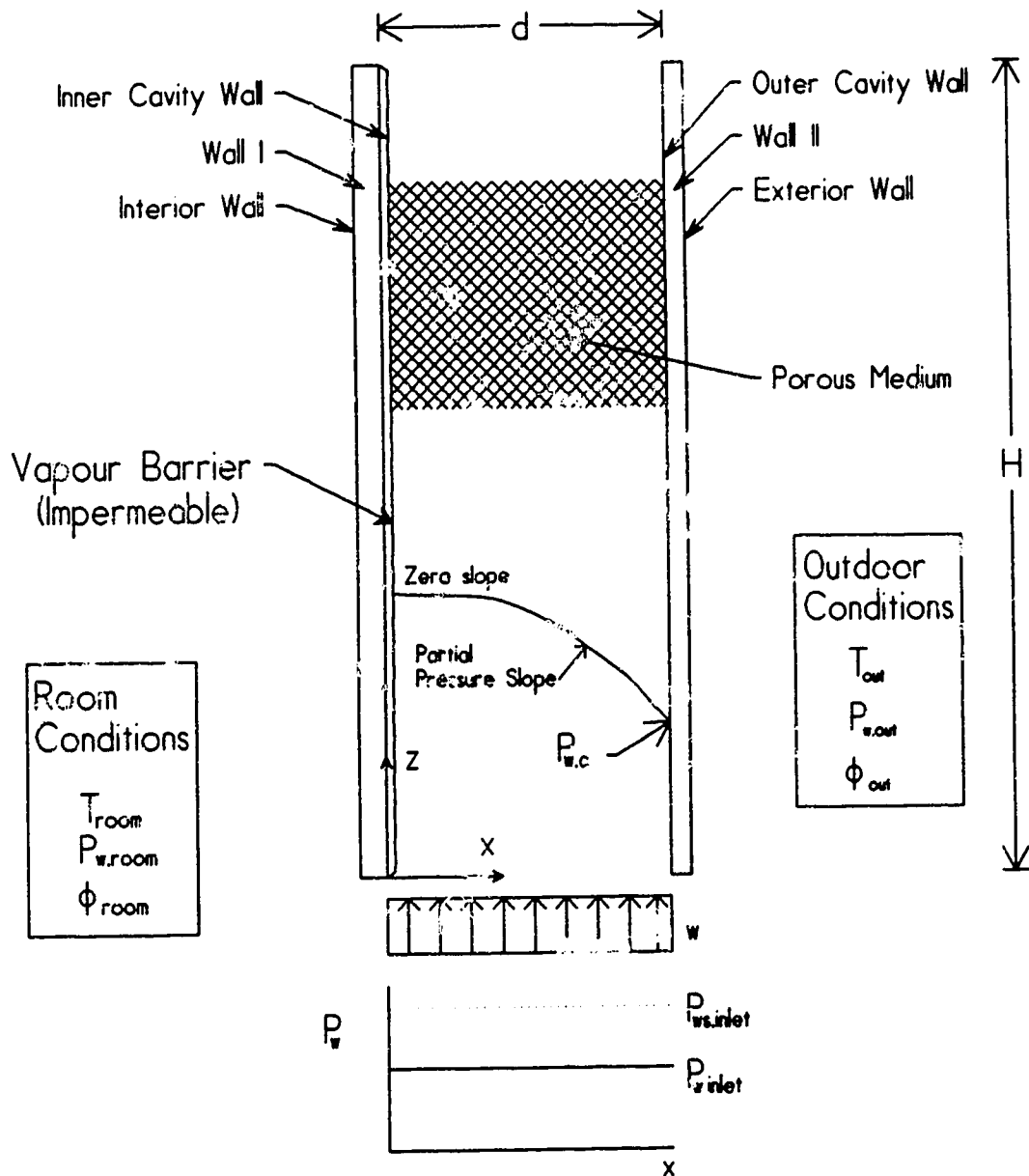


Figure 2.3 Description of wall cavity used to derive the moisture transport equations. The inlet velocity and partial pressure profiles are linear. The left side boundary is impermeable to moisture.

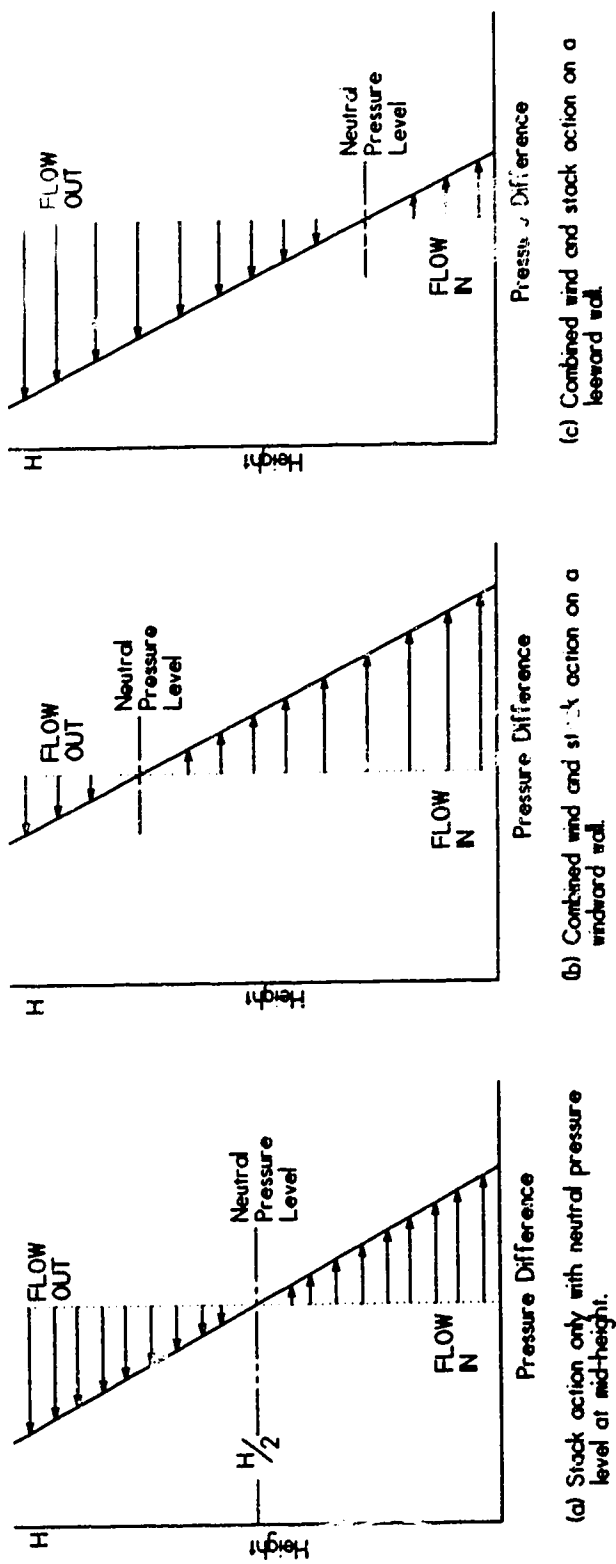


Figure 2.4 Pressure distribution across a building wall due to stack and wind action.

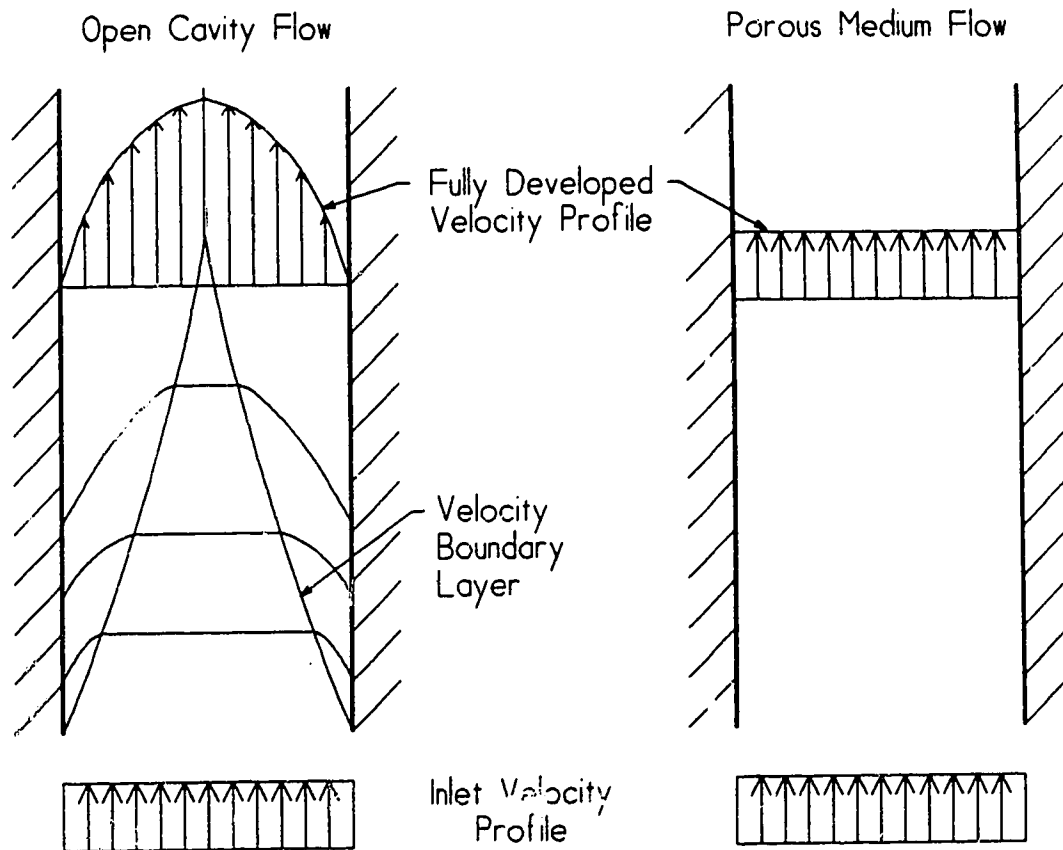


Figure 2.5 The velocity profile for flow in an open cavity and for flow through porous medium.

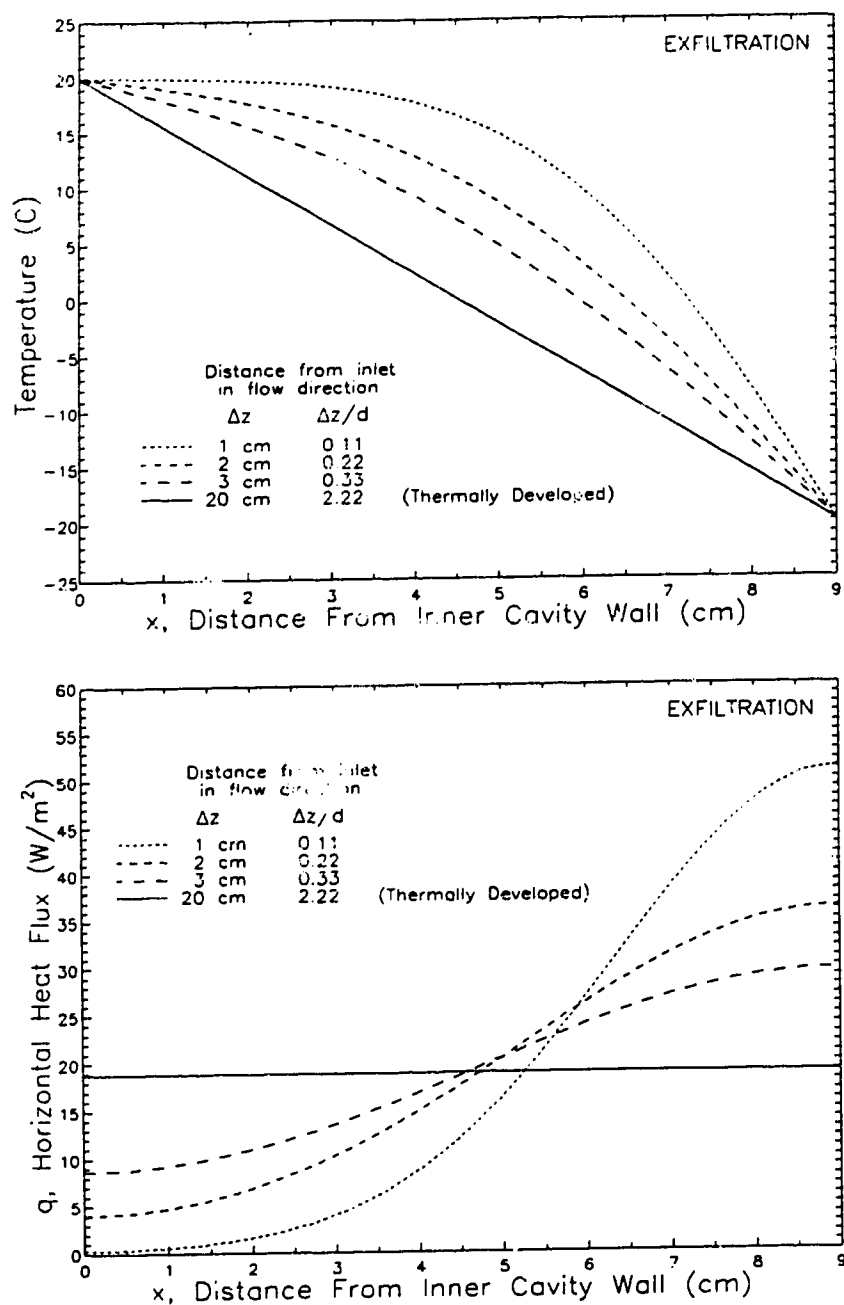


Figure 2.6 (a) Exact temperature profile for exfiltrating flow through a porous medium filled wall cavity as the vertical distance from the inlet plane increases. (b) Horizontal heat flux corresponding to the gradient of the temperature profiles shown in (a). The flow becomes thermally developed approximately 20 cm from the inlet.

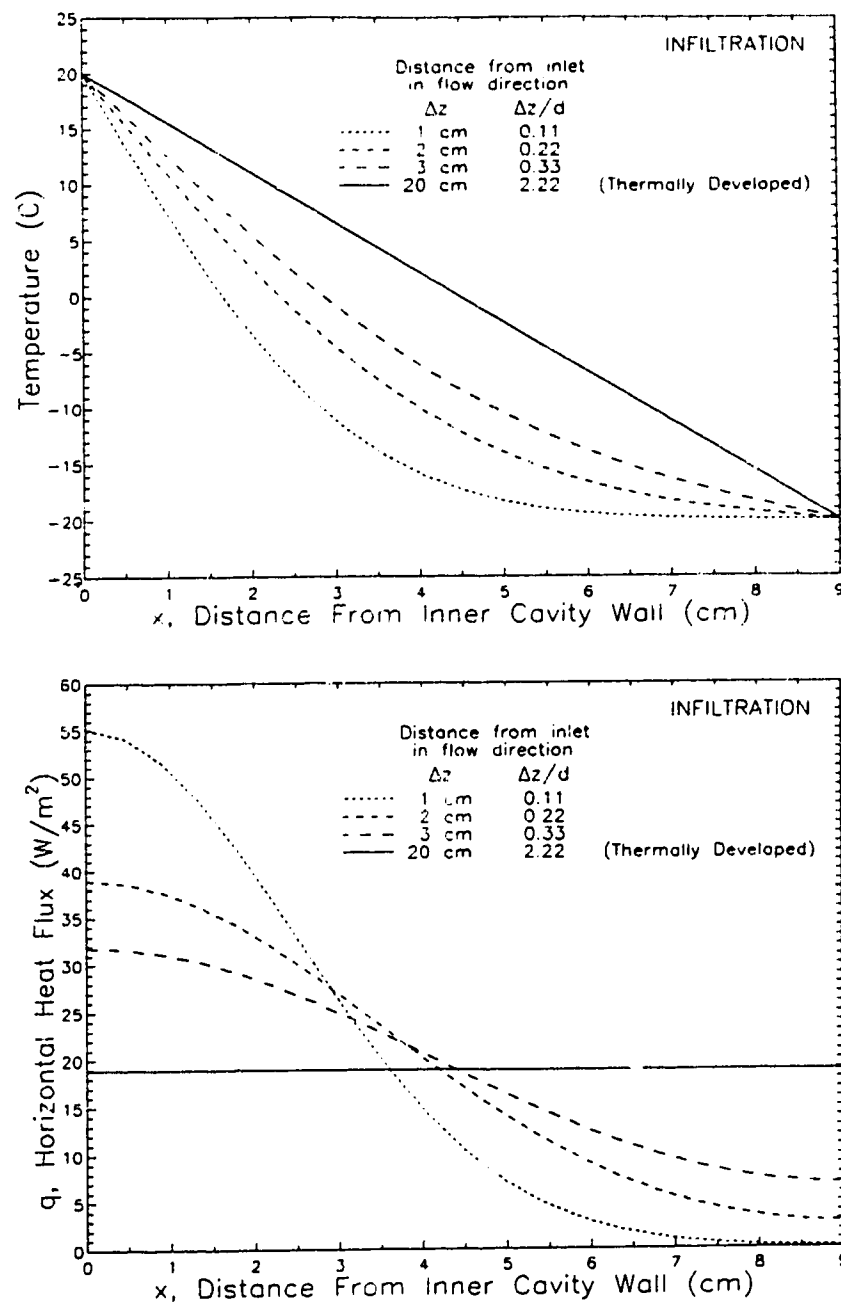


Figure 2.7 (a) Exact temperature profile for infiltrating flow through a porous medium filled wall cavity as the vertical distance from the inlet plane increases. (b) Horizontal heat flux corresponding to the gradient of the temperature profiles shown in (a). The flow becomes thermally developed approximately 20 cm from the inlet.

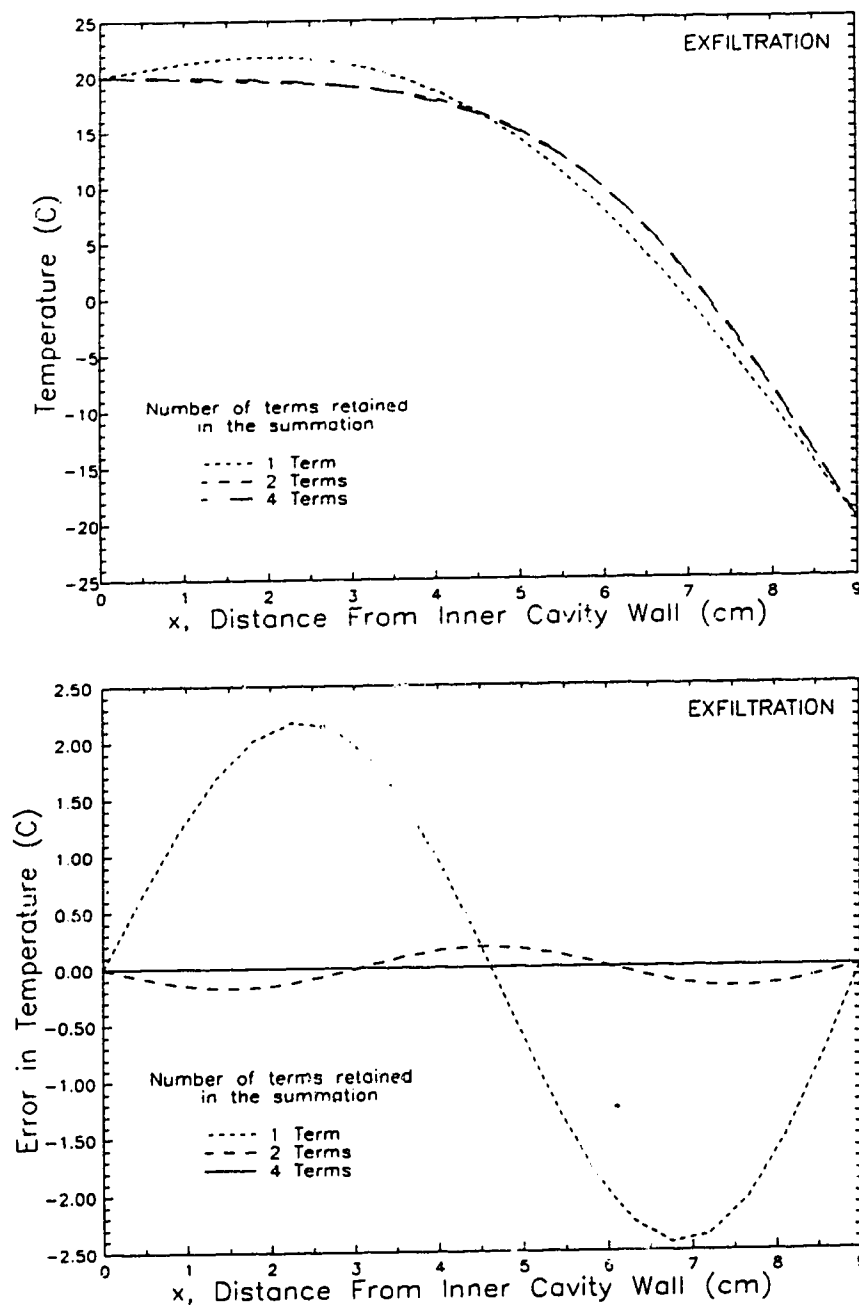


Figure 2.8 (a) Temperature profiles evaluated with varying the number of terms retained in Eqn. (2.33) (b) Error in temperature caused when retaining a small number of terms. The curves were evaluated 1 cm from the inlet. The base solution retained 20 terms ($N = 20$).

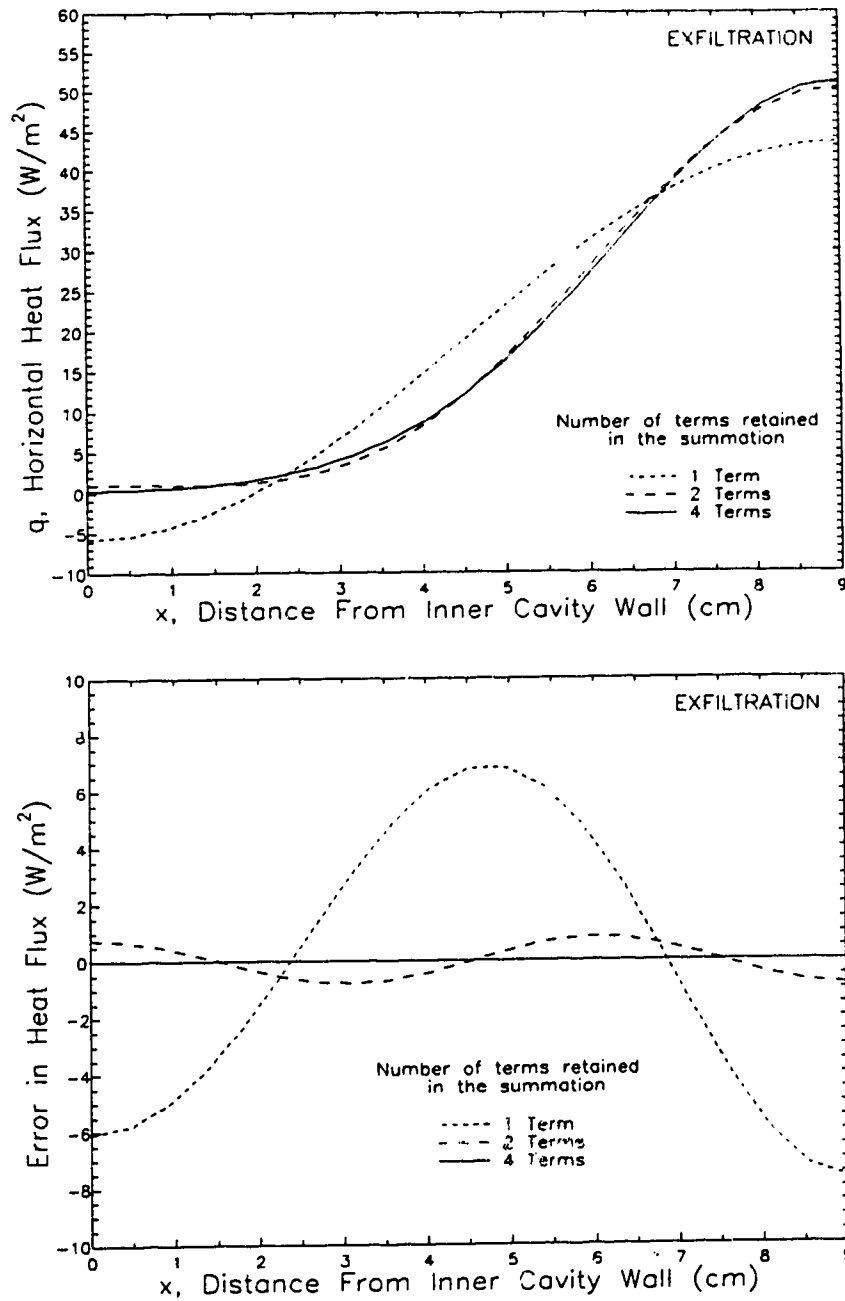


Figure 2.9 (a) Horizontal heat flux determined from the slope of the temperature profiles when evaluated using an increasing number of retained terms in Eqn. (2.34). (b) Error in heat flux caused when retaining a small number of terms. The curves were evaluated 1 cm from the inlet. Thermal conductivity for the porous medium was $0.0425 \text{ W} \cdot \text{m}^{-1} \cdot \text{K}^{-1}$. The base solution retained 20 terms ($N = 20$).

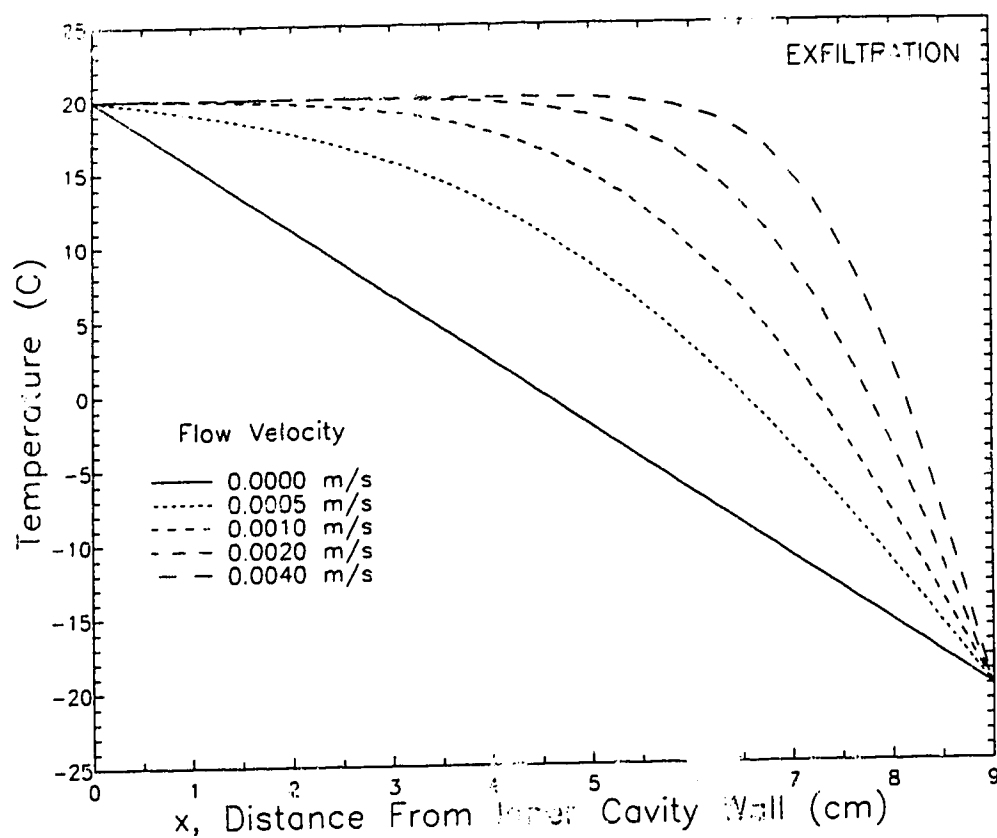


Figure 2.10 Effect on temperature profiles of increasing the exfiltrating flow velocity. With an increased flow rate the temperature profiles are more horizontal indicating a larger temperature difference from the conduction solution (zero flow). Evaluated at 1 cm from the inlet.

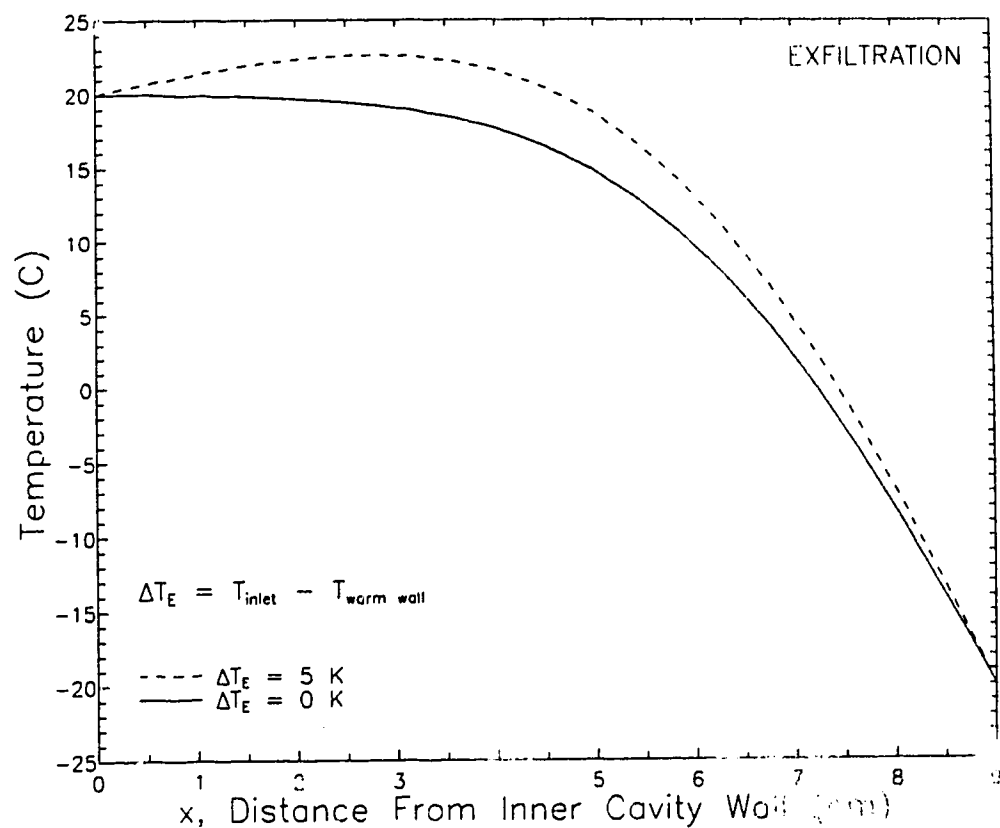


Figure 2.11 Temperature profiles for exfiltrating flow when the inlet temperature is greater than the warm wall temperature. Flow entering with a temperature higher than the warm wall boundary temperature will cause a bowing of the temperature profile. Evaluated at 1 cm from the inlet.

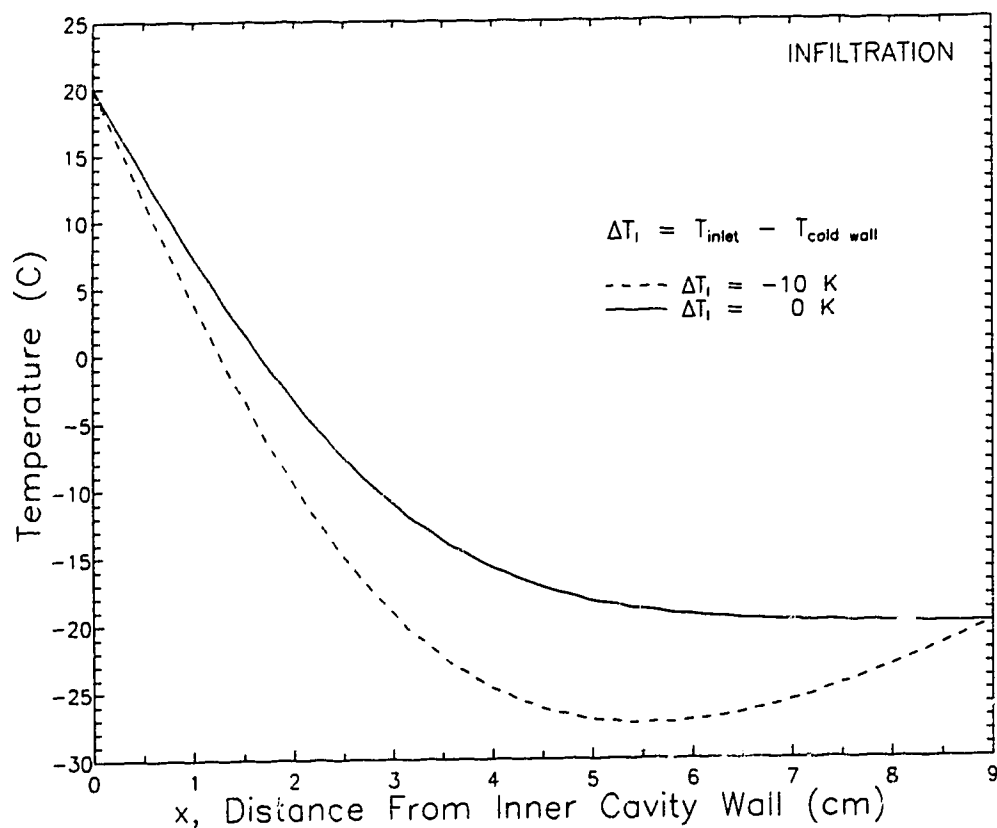


Figure 2.12 Temperature profiles for infiltrating flow when the inlet temperature is less than the cold wall temperature. Flow entering with a temperature lower than the cold wall boundary temperature will cause a bowing of the temperature profile. Evaluated at 1 cm from the inlet.

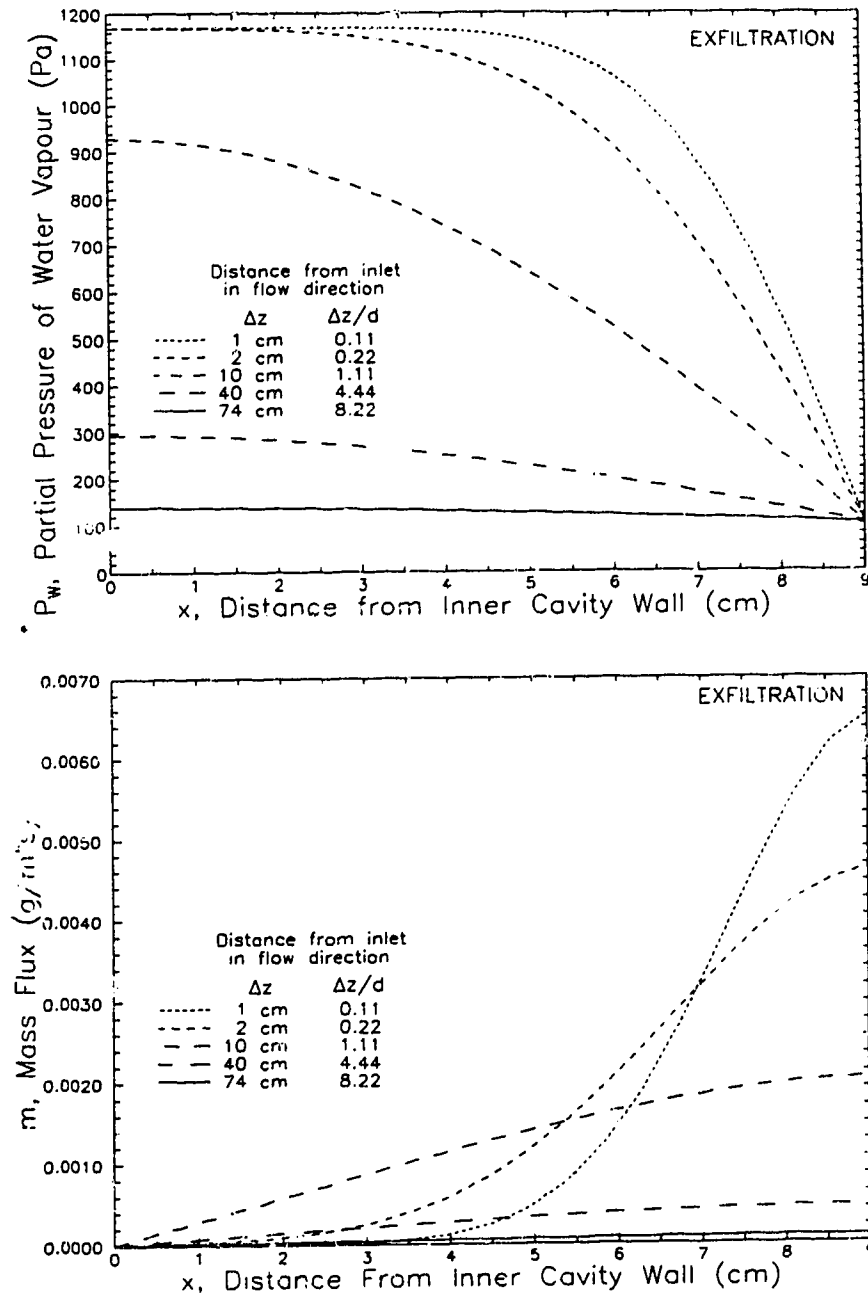


Figure 2.13 (a) Partial pressure profiles for exfiltrating flow through a porous medium filled wall cavity. (b) Mass flux of moisture through the porous medium. (Exfiltration: $T_{room} = 20^\circ\text{C}$; $\phi_{room} = 50\%$; $T_c = -20^\circ\text{C}$; $\phi_c = 100\%$; $w = 0.001 \text{ m}\cdot\text{s}^{-1}$; $D = 2.56 \cdot 10^{-5} \text{ m}^2\cdot\text{s}^{-1}$; $N = 20$)

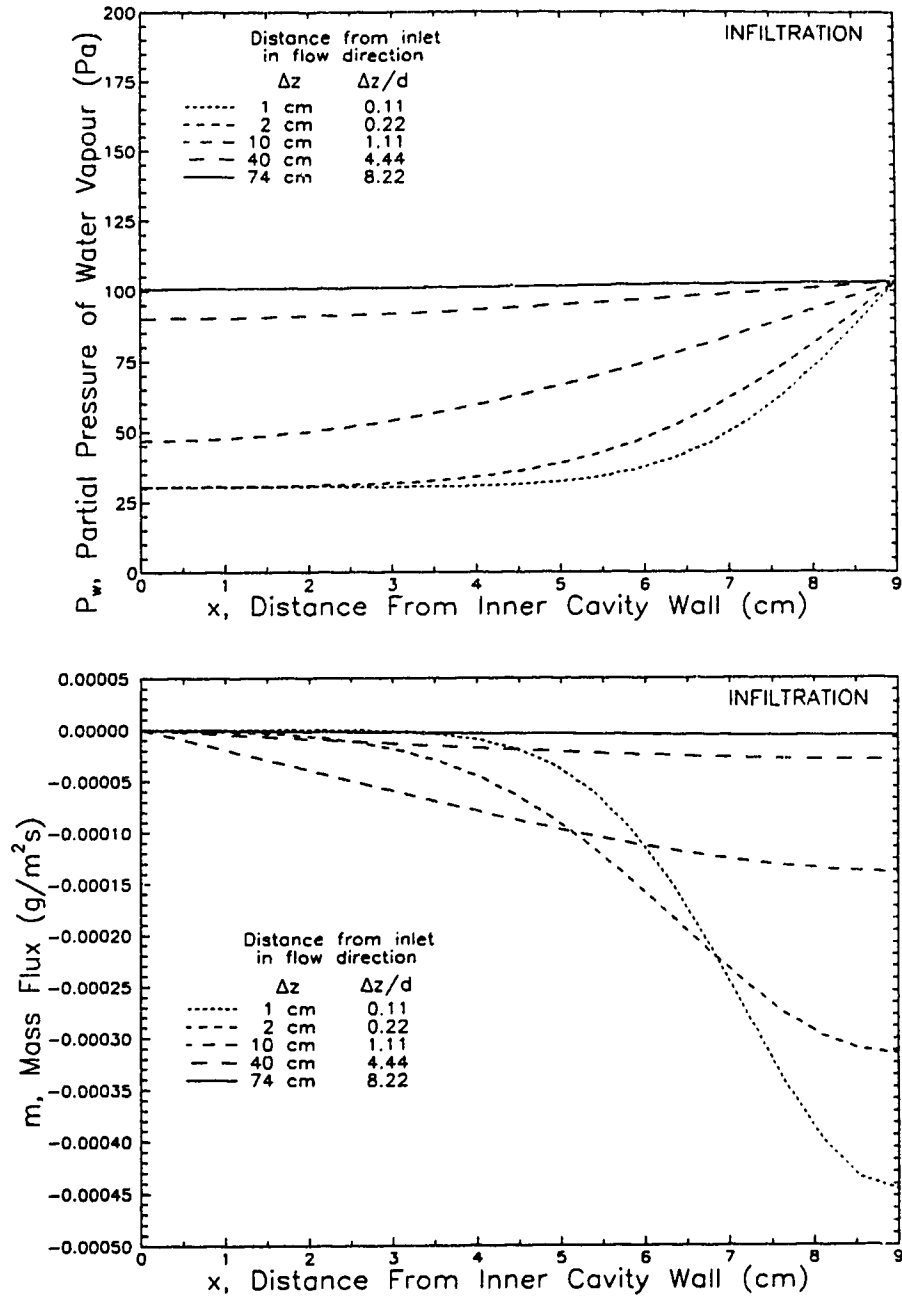


Figure 2.14 (a) Partial pressure profiles for infiltrating flow through a porous medium filled wall cavity. (b) Mass flux of moisture through the porous medium. (Infiltration: $T_{out} = -30^\circ\text{C}$; $\phi_{out} = 80\%$; $T_c = -20^\circ\text{C}$; $\phi_c = 100\%$; $w = 0.001 \text{ m}\cdot\text{s}^{-1}$; $D = 2.56 \cdot 10^{-5} \text{ m}^2\cdot\text{s}^{-1}$; $N = 20$)

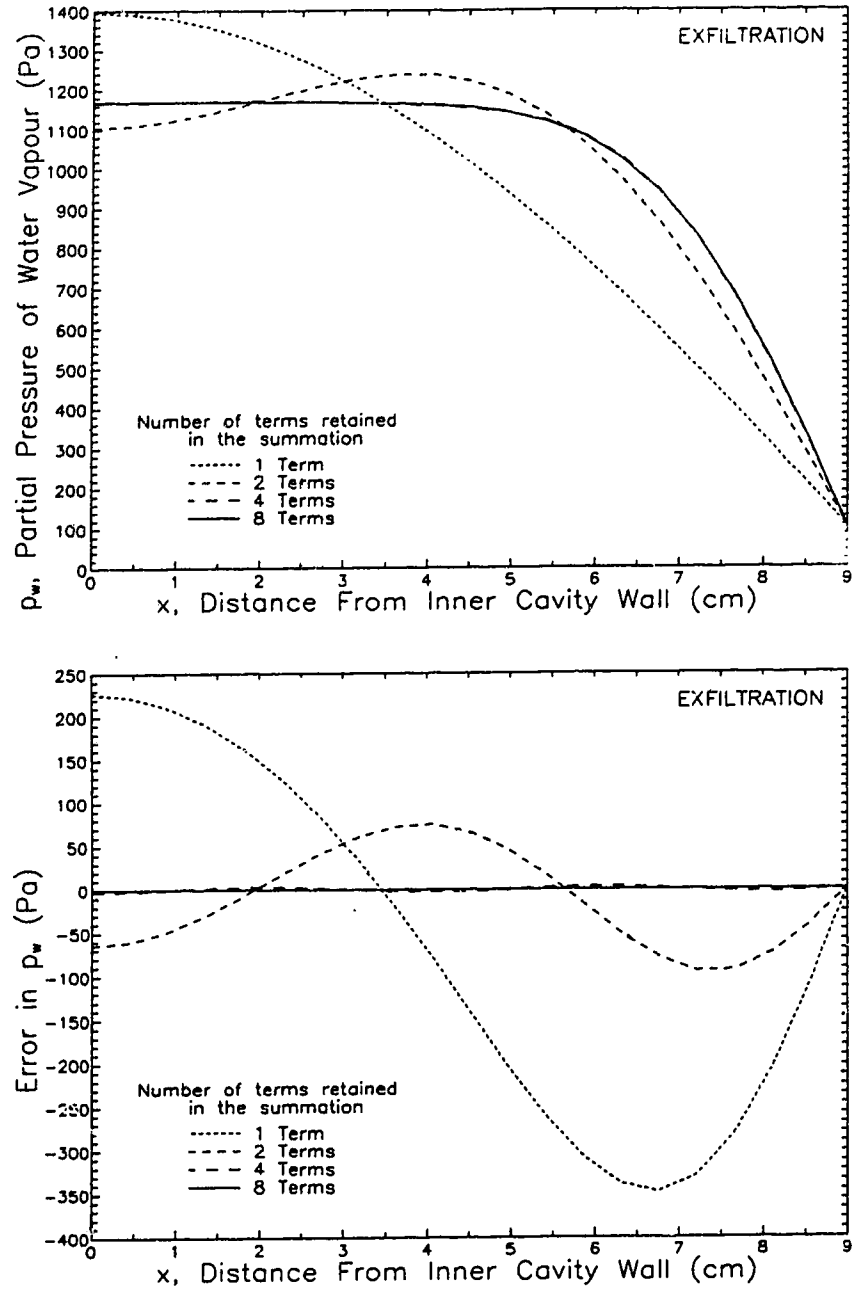


Figure 2.15 (a) Variation in the partial pressure profile (Eqn. (2.73)) when retaining an increasing number of terms. (b) Error in the calculated partial pressures. (Exfiltration: $T_{room} = 20^\circ\text{C}$; $\phi_{room} = 50\%$; $T_c = -20^\circ\text{C}$; $\phi_c = 100\%$; $w = 0.001 \text{ m}\cdot\text{s}^{-1}$; $D = 2.56 \cdot 10^{-5} \text{ m}^2\cdot\text{s}^{-1}$; $\Delta z = 1 \text{ cm}$)

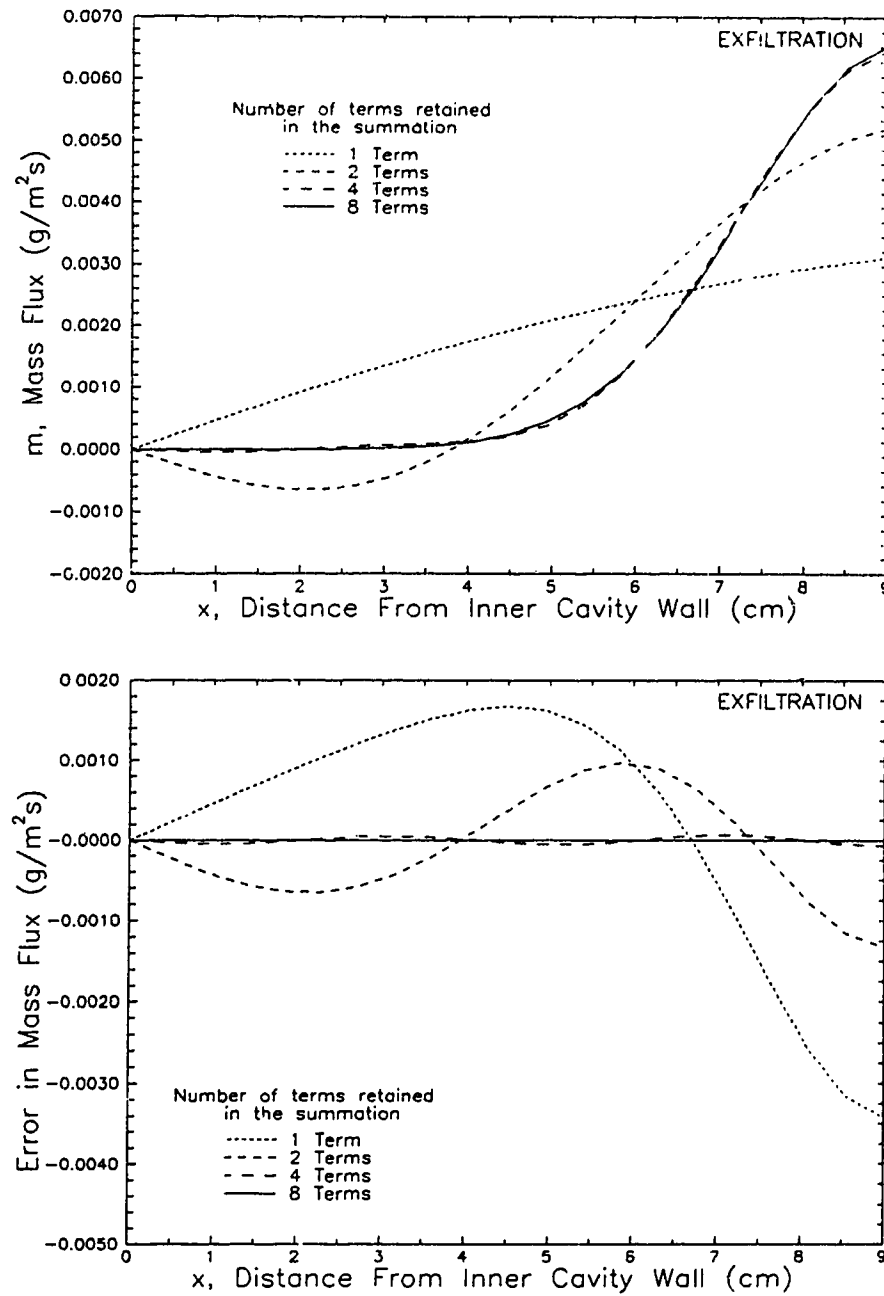


Figure 2.16 (a) Variation in mass flux (Eqn. (2.74)) when retaining an increasing number of terms. (b) Error in the calculated mass fluxes. (Exfiltration: $T_{room} = 20^\circ\text{C}$; $\phi_{room} = 50\%$; $T_c = -20^\circ\text{C}$; $\phi_c = 100\%$; $w = 0.001 \text{ m}\cdot\text{s}^{-1}$; $D = 2.56 \cdot 10^{-5} \text{ m}^2\cdot\text{s}^{-1}$; $\Delta z = 1 \text{ cm}$)

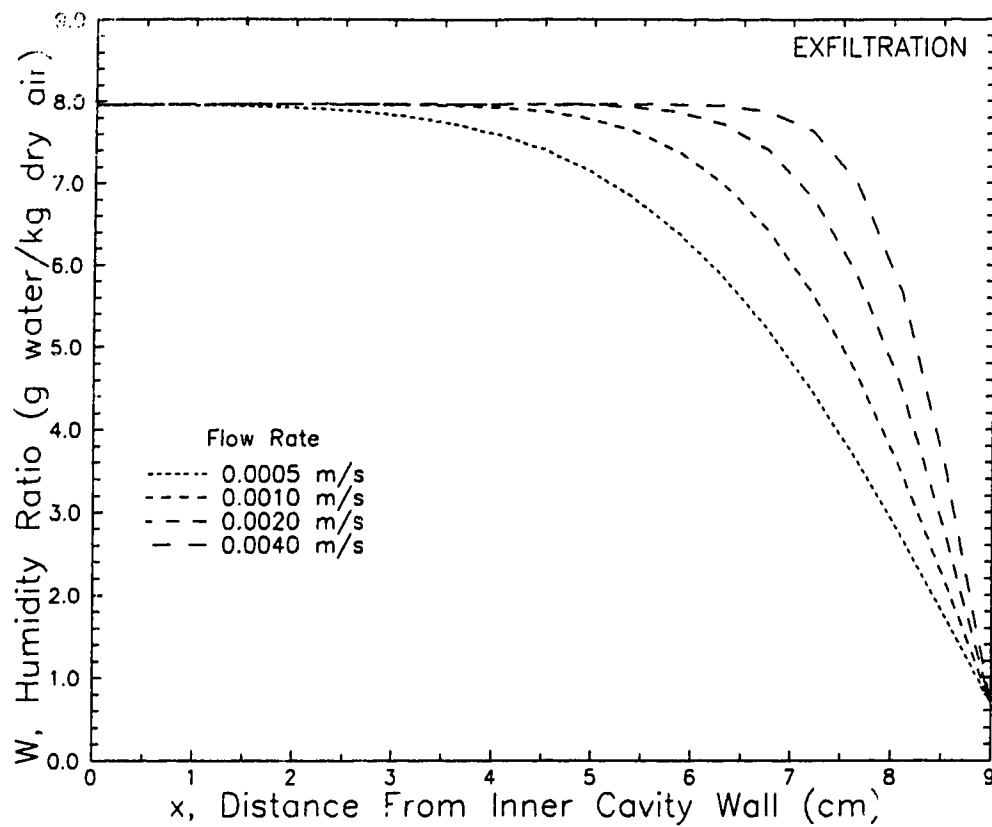


Figure 2.17 Variation in humidity ratio profiles for increasing exfiltration velocity.
 (Exfiltration: $T_{room} = 20^{\circ}\text{C}$; $\phi_{room} = 50\%$; $T_c = -20^{\circ}\text{C}$; $\phi_c = 100\%$;
 $D = 2.56 \cdot 10^{-5} \text{ m}^2 \cdot \text{s}^{-1}$; $n = 20$; $\Delta z = 1 \text{ cm}$)

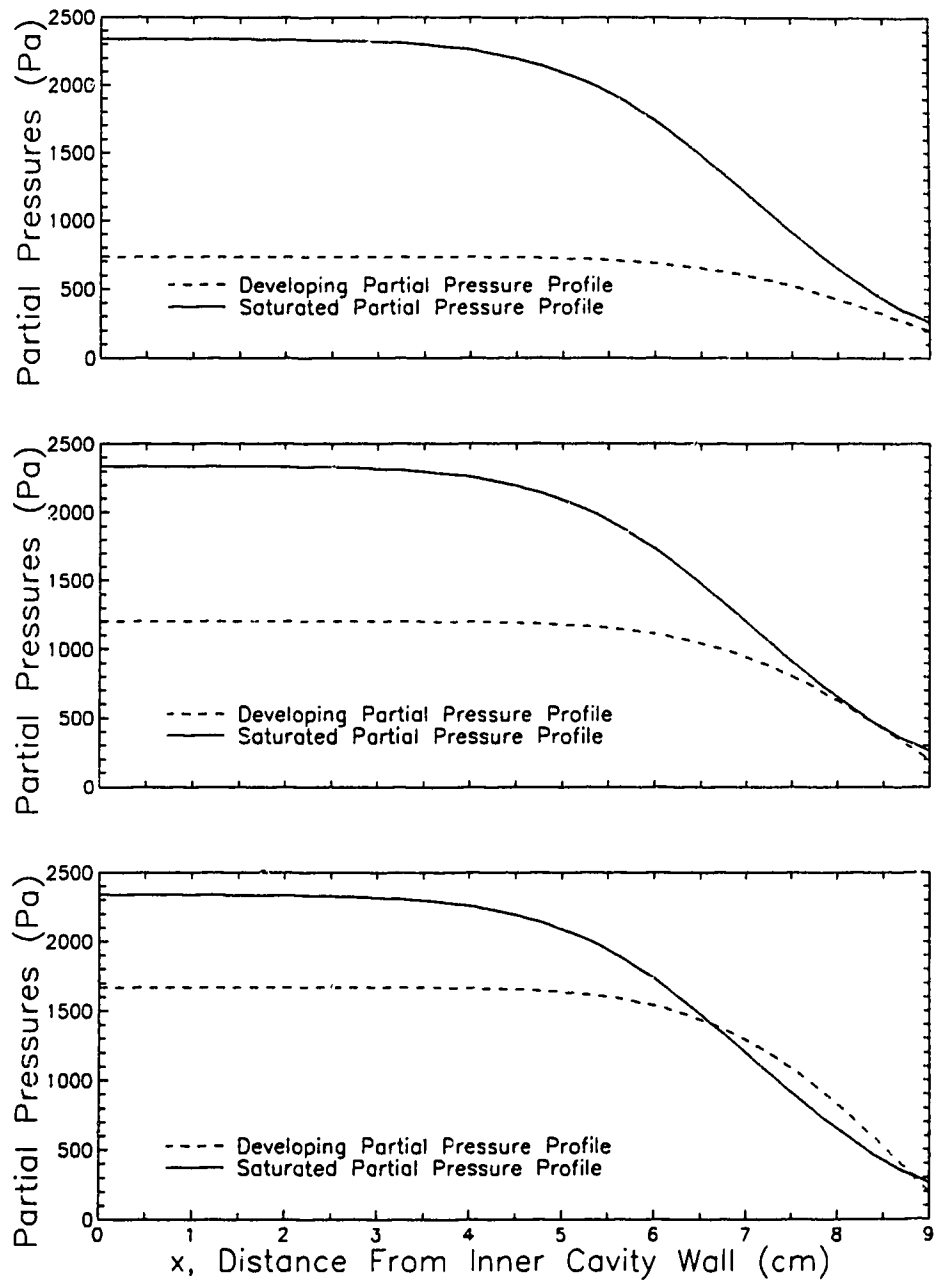


Figure 2.18 Three possible partial pressure profile conditions within the wall cavity. (a) shows that the model is valid and deposition occurs at the outer cavity wall ($\phi_{inlet} = 30\%$). (b) shows the transition point where deposition in the insulation may occur ($\phi_{inlet} = 50\%$). (c) indicates that the model is invalid and deposition will occur within the insulation ($\phi_{inlet} = 70\%$).

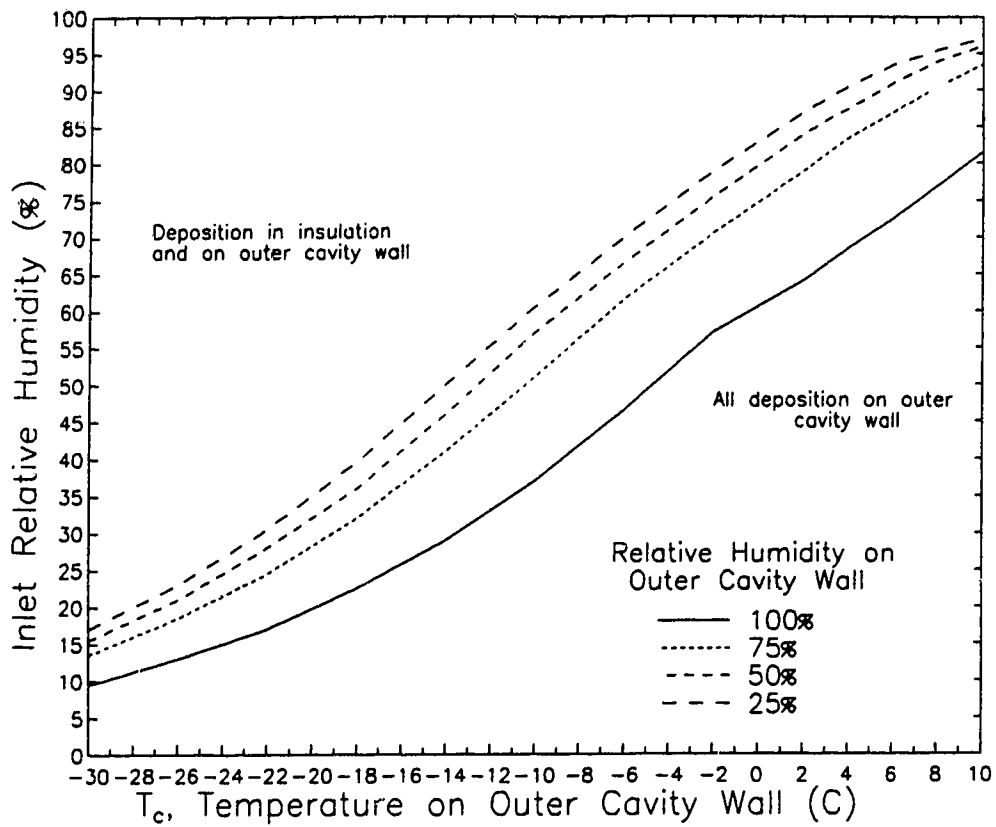


Figure 2.19 Region of validity for the moisture deposition model for very high exfiltration velocity. (Exfiltration: $T_{room} = 20^{\circ}\text{C}$; $D = 2.56 \cdot 10^{-5} \text{ m}^2 \cdot \text{s}^{-1}$; $N = 20$; $w = 0.01 \text{ m} \cdot \text{s}^{-1}$)

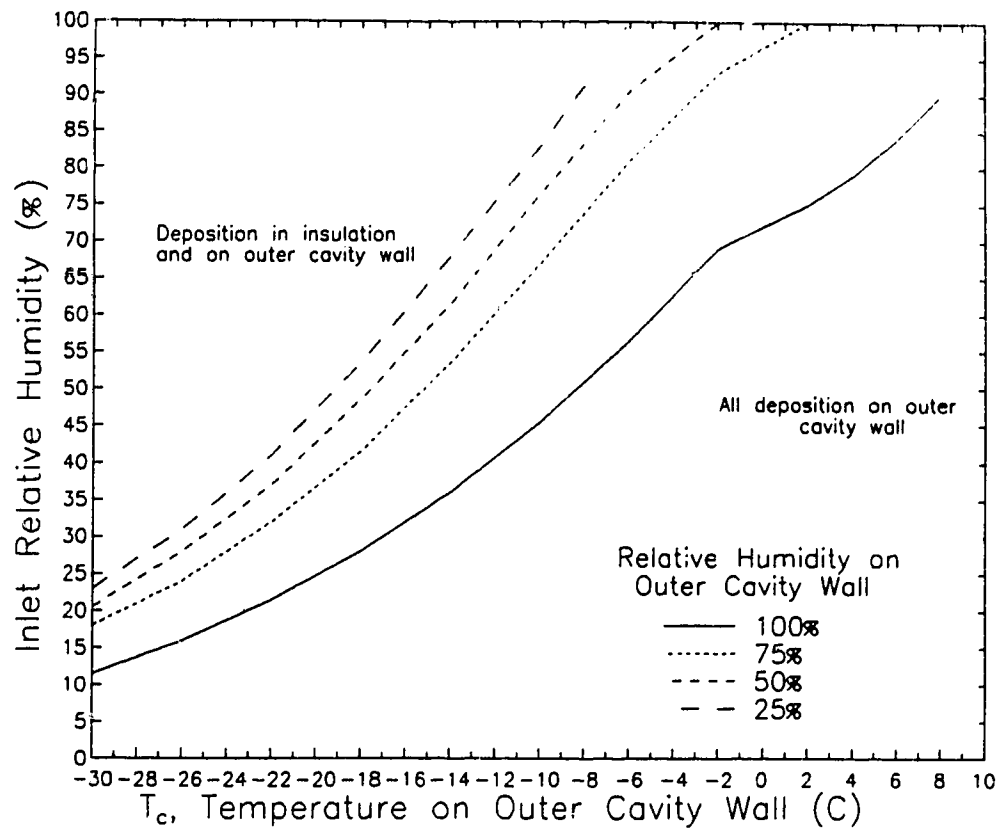


Figure 2.20 Region of validity for the moisture deposition model for slow flow rates. (Exfiltration: $T_{room} = 20^\circ\text{C}$; $D = 2.56 \cdot 10^{-5} \text{ m}^2 \cdot \text{s}^{-1}$; $N = 20$; $w = 0.0001 \text{ m} \cdot \text{s}^{-1}$)

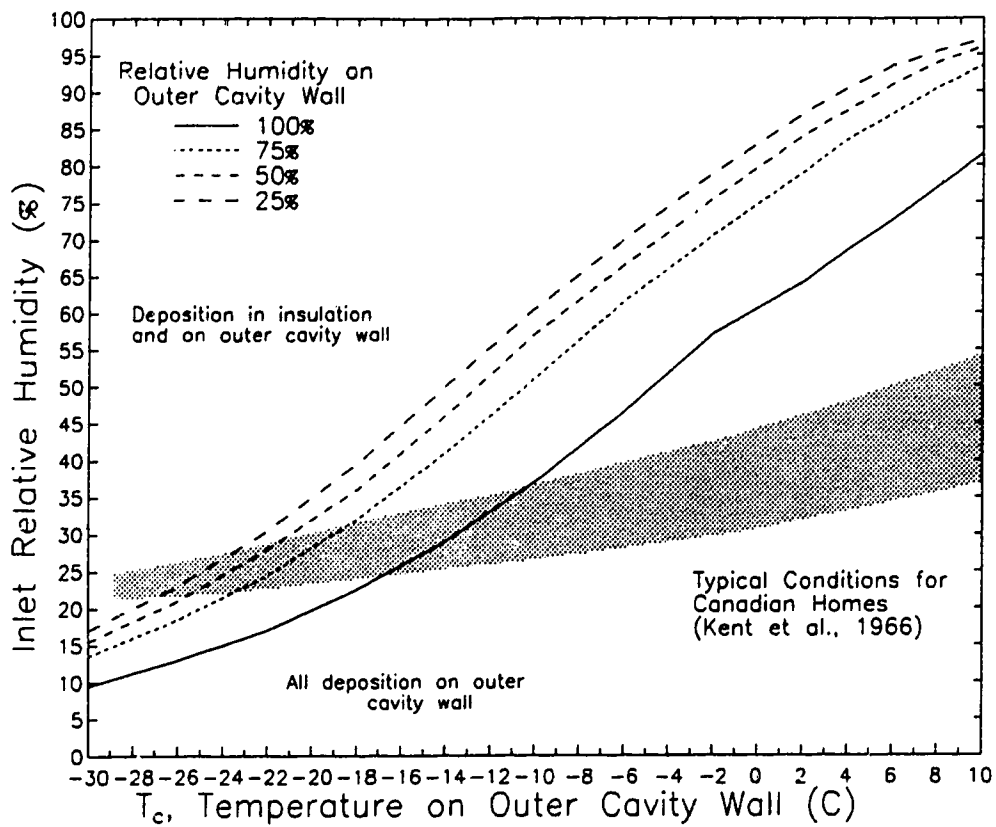


Figure 2.21 Typical relative humidities and temperature distributions for Canadian homes, Kent *et al.* (1966), superimposed on the region of validity for the moisture deposition model. ($T_{room} = 20^\circ\text{C}$; $w = 0.01 \text{ m}\cdot\text{s}^{-1}$)

CHAPTER 3

EXPERIMENTAL METHODS AND MODEL EVALUATION

The heat transfer and moisture deposition models developed in Chapter 2 will be evaluated using measurements obtained at the Alberta Home Heating Research Facility (AHHRF) during the 1987/1988 heating season. The AHHRF consists of six unoccupied, single-zone houses located in a rural area south of Edmonton, Alberta. The houses have been operated continuously by the Mechanical Engineering Department of the University of Alberta since 1980.

Initially the method of testing and the pertinent data obtained from the testing will be reviewed. Next, the temperature model will be compared to actual measured temperature data. The moisture deposition model will then be compared to actual measured moisture deposition data.

3.1 Review of Experimental Apparatus, Method, and Data Obtained

The heat and moisture models developed in Chapter 2 will be tested against data obtained from AHHRF Test House 6. The single-story wood framed house is depicted in Fig. 3.1, from Wilson and Dale (1985), indicating basic dimensions, location of doors and windows, and house orientation. Table 3.1, adapted from Forest (1989) and Walker (1991), lists the construction details, materials, and insulation levels of the various components of House 6.

Testing was conducted during the 1987/88 heating season. Hourly averaged data was obtained continuously for 550 hours extending from 1400h, 26 January to 1100h, 18 February 1988; this was a portion of more extensive data that had been collected over a two year period. No data was recorded for a 26 hour period extending from 1200h on 28 January to 1400h on 29 January. Another single hour gap in the data occurred at 0900h, 10 February. The data gaps are clearly shown in Fig.

3.10. The limited time period was chosen since it corresponded to a period of large indoor-outdoor temperature difference (Section 3.1.3) and large exfiltration flows (Section 3.1.5), both of which contribute to increased moisture deposition.

3.1.1 Description of the wall test panel

Two removable wall panels were constructed and installed in the north and south walls of House 6, as shown in Fig. 3.2. The test panels measured 1170 mm × 2340 mm × 100 mm (46" × 92" × 4") and were divided into three vertical sections. Figure 3.3 shows a front view of the north test panel, indicating the general dimensions, construction, and the three vertical sections. Each vertical section measured 340 mm × 2300 mm × 90 mm. Only the centre section of the north test panel was used to test the models. The south panel was not used, except for comparing air flow leakage data and outer cavity wall temperatures.

Figure 3.4 shows a side view of the centre section of the north test panel which has been further divided into an upper wall section (or cavity) and a lower wall section (or cavity). The upper wall section was 750 mm high and the lower wall section was 1550 mm high. Each section was 90 mm deep. The aspect ratio (H/d) for the upper cavity was 8.33 and for the lower cavity, 17.2. The overall aspect ratio for the entire cavity was 25.6. Along the interior wall, inside the cavity, was a polyethylene vapour barrier, shown in Fig. 3.4. All seams were sealed to prevent moisture or air from leaking through the barrier. The cavity was completely filled with glass fibre insulation.

At the point where the cavity was divided, 1550 mm from the base of the wall, was a 9.5 mm orifice plate flowmeter (see Fig. 3.4). The flowmeter was located in the interior wall and acted as the interior leakage site for air flowing into or out of the cavity. Opposite the flowmeter, as shown in Fig. 3.4, the vapour barrier was cut to allow air flow to enter the insulation. The edges of the vapour barrier were sealed to the interior wall to prevent air from flowing between the wall and the vapour barrier. The pressure difference across the flowmeter was measured by an

automated data acquisition system in order to determine the flow rate of air into and out of the cavity.

Located on the exterior side of the cavity were two long, slender cracks. One crack was located at the top of the upper wall cavity and the other was located at the bottom of the lower wall cavity. During normal construction of wood framed houses, it is not uncommon to find small cracks along the upper and lower edges where the exterior sheathing meets the wooden house frame. If these cracks are not sealed, air may be able to flow into or out of the cavity. The actual configuration of the cracks present in the exterior of the test cavity were not accurately recorded. For the purposes of this work it was assumed that the cracks extended the width of the cavity (340 mm) and were 0.5 mm high. It was assumed that the cracks acted as orifices.

3.1.2 Measuring moisture deposition

Moisture collection plugs were installed in the exterior sheathing. These plugs could be removed and weighed in order to determine the amount of moisture deposition on the outer cavity wall. By using removable plugs the measurement of moisture accumulation could be accomplished without disrupting further testing. The placement of the moisture plugs relative to the interior orifice is shown in Fig. 3.3, Forest (1989). The wooden plugs were cut out of the exterior sheathing and were each 50 mm in diameter and 9.5 mm thick, the same thickness as the exterior sheathing. Extending into the cavity from each moisture plug was 25 mm of glass fibre insulation. On the exterior side of the plugs were attached small wooden handles to facilitate removal of the plugs from the wall. Around the circumference of each plug was a neoprene seal which prevented air from leaking out around the plug. At the beginning of the test period, the initial weight of each plug was determined. Each week during the three week test period, the plugs were removed from the wall and weighed. During the weighing process the moisture plugs were kept in a cold, insulated box which prevented the accumulated moisture from thawing and migrating

unnaturally, Forest (1989). The plugs were returned to their original positions after weighing.

For the purpose of this analysis, the moisture plugs were numbered and grouped into six zones of three plugs each, according to Fig. 3.5. Zones 1, 2, and 3, containing moisture plugs 1 to 9, were located in the upper wall cavity, immediately above the inlet orifice as shown in Fig. 3.5. The three zones beneath the inlet orifice, zones 4, 5, and 6, containing moisture plugs 10 to 18, were in the lower wall cavity as shown in Fig. 3.5. The lower wall cavity had three additional zones, 7, 8, and 9, which were not used in this study.

Three plugs were used per zone in order to determine a more accurate moisture accumulation for each zone. One moisture plug was located in the middle of each zone and the other two were adjacent to the right and left edges of the centre vertical section, shown in Fig. 3.5. The distance of each zone from the leakage sites is shown in Fig. 3.5. Zone 1 was located 140 mm from the interior orifice plate and 610 mm from the upper wall leakage crack. Zone 2 was 420 mm from the orifice and 330 mm from the upper leakage crack. Zone 3 was 700 mm from the orifice and 50 mm from the upper leakage crack. In the lower wall section, zone 4 was 140 mm from the orifice plate and 1410 mm from the lower leakage crack. Zone 5 was 420 mm from the orifice plate and 1130 mm from the lower leakage crack. Zone 6 was 700 mm from the orifice plate and 850 mm from the lower leakage site.

At the start of testing the wood moisture content of plug 8, located in zone 1 directly above the orifice, and plug 11, located in zone 4 directly below the orifice, were determined to be 7% by weight, Forest (1989). Appendix A, Tables A.1 to A.3, lists the actual measured moisture depositions for the removable moisture plugs. The mass deposited per square meter was calculated for the deposition on each plug and it is this value, multiplied by the surface area of the zone (50 mm × 340 mm) in which each plug was located, that will be used in Section 3.3 to compare actual results to the predicted results of the moisture deposition model.

3.1.3 Measuring temperatures

Temperatures were measured using copper-constantan thermocouples connected to an automated, computer controlled data acquisition system. The system sampled eighty times each minute and then calculated and recorded the hourly average as well as the standard deviations. The system allowed for continuous monitoring of the indoor (T_{room}), inner cavity wall (T_b), outer cavity wall (T_o), and outdoor (T_{out}) temperatures for both the north and south wall test panels.

Shown in Fig. 3.6 is the daily averaged indoor-outdoor temperature difference over the testing period. The indoor temperature was maintained at $20^\circ \pm 1.5^\circ\text{C}$. This 550 hour testing period was chosen since it corresponded to a time with large indoor-outdoor temperature difference. A large temperature difference between indoors and outdoors indicates a large thermal buoyancy driving force across the wall cavity which may induce exfiltration through the wall cavity (see Section 3.1.5). Exfiltration will be shown to be the major source of moisture entering a wall cavity.

The inner and outer cavity wall temperatures were measured at only one location along the wall, directly opposite the inlet orifice. For the outer cavity wall, it was assumed that the temperature measured opposite the inlet orifice was representative of the temperature along the height of the cavity. This assumption will be shown to be realistic in Section 3.2. The south facing test panel was exposed to direct and diffuse solar radiation while the north wall test panel was exposed to only diffuse solar radiation. Solar radiation would act to increase the temperature within the cavity.

3.1.4 Indoor and outdoor relative humidity and humidity ratios

The computer controlled data acquisition system used to measure temperature data also measured the indoor and outdoor relative humidity continuously over the testing period. The relative humidity was measured directly using relative humidity probes. From the relative humidity and temperature data, the partial pressure of water vapour can be determined from

$$\phi = \frac{p_w}{p_{ws}} \quad (3.1)$$

where ϕ is the relative humidity, p_w is the partial pressure of water vapour, and p_{ws} is the saturated partial pressure of water vapour at the same temperature. The humidity ratio can be calculated according to

$$W = 0.622 \frac{p_w}{p_{atm} - p_w} \times 1000 \quad (3.2)$$

which is the same as Eqn. (2.78). Shown in Fig. 3.7 are the indoor and outdoor average daily humidity ratios for the test period. During the test, the indoor humidity ratio was nearly constant since the indoor relative humidity and temperature were carefully controlled. The indoor relative humidity was maintained at $40\% \pm 3\%$ by use of a rotating drum humidifier connected to a 250ℓ reservoir, and the indoor temperature was $20^\circ \pm 1.5^\circ\text{C}$. The outdoor humidity ratios responded to changes in the environment. The lowest humidity ratios occurred on days for which the indoor-outdoor temperature difference was at its highest.

A large difference between the indoor and outdoor humidity ratios indicates a large potential for moisture deposition. During exfiltration, the warm, moist room air will lose moisture through condensation and its humidity ratio will drop until equilibrium with the outdoor conditions is obtained. Not all of the moisture in the air-vapour flow will necessarily deposit within the wall, some moisture may still be retained in the flow as it leaves the cavity.

3.1.5 Flow through the wall cavities

Air flow through wall cavities is driven by a pressure differential between the indoor and outdoor environments. The two main factors influencing the pressure differential are indoor-outdoor temperature difference, and changing wind speed and wind direction, Walker (1991). Generally, the stack effect, caused by indoor-outdoor temperature differences, influences the air flow less than changing wind speed and

wind direction. The pressure difference across the wall cavity can cause either exfiltration or infiltration through the wall.

As mentioned in Section 3.1.1, the test panel wall cavity had one leakage site on the interior side (the orifice plate flowmeter) and two leakage sites in the exterior wall (two long, slender cracks at the top and bottom edges). The hourly average flow rate through the orifice plate flowmeter was recorded by the same data acquisition system used to record temperature and humidity data. Figure 3.8 shows the hourly average flow rates through the north wall cavity from 1400h, 26 January until 1100h, 18 February. Figure 3.9 shows the hourly average flow rates through the south wall test panel over the same time period.

The average infiltration rate for the north wall over the 550 hour testing period was $0.11 \text{ m}^3 \cdot \text{h}^{-1}$, which was over twice as large as its average exfiltration rate of $0.05 \text{ m}^3 \cdot \text{h}^{-1}$. The average infiltration rate for the south wall panel was $0.14 \text{ m}^3 \cdot \text{h}^{-1}$, while the average exfiltration rate was $0.02 \text{ m}^3 \cdot \text{h}^{-1}$. By comparing Figs. 3.8 and 3.9, it can be seen that during hours of high south wall infiltration, 0 to 40 hours and 330 to 380 hours, there was a corresponding increase in north wall exfiltration. Conversely, when there was north wall infiltration there was south wall exfiltration.

These results indicate that the measured data follows the correct trends: a south wind produces a positive pressure coefficient on the south wall, due to stagnation flow, forcing air in the house through the south wall; a south wind produces a negative pressure coefficient on the north wall, due to wake flow, driving air out through the north wall. The two figures, 3.8 and 3.9, do not match precisely, indicating that there were other leakage sites within the house since all of the flow entering through one wall did not leave directly through the other wall. For 228 of the 523 hours for which flow data exists, the north and south panels experienced both infiltration and exfiltration. This phenomena can clearly be seen in Fig. 3.8 for hours greater than 490.

Since the cavity was sealed, except for the interior and exterior cracks, all flow passing through the flowmeter must have passed through the two exterior cracks. Since the flow through each crack was not monitored, the exact flow distribution

between the upper and lower sections of the wall cavity is not known. However, based on the properties of the porous medium within the wall cavity and the assumed sizes of the exterior cracks, it is possible to predict what the flow distribution should be. According to Darcy's Law (Eqn. (2.1)) flow in porous medium is proportional to the pressure difference across the medium, and resistance to flow is proportional to length. A flow analysis on the test wall was performed (see Appendix B) with results showing that 2/3 of the total flow measured at the flowmeter passed through the upper wall section and 1/3 of the total flow passed through the lower wall section. The main resistance to the flow was due to the porous medium, not the cracks. It was assumed that the flow distribution did not change during the duration of the test. Tables 3.2 and 3.3 summarize the flow data for the north and south panel for both the upper and lower wall cavities assuming 2/3 of the total flow passed through the upper wall cavities. The measured flow rates were recorded as hourly averages. The model assumes that the flow entering the cavity for any particular hour was constant for the entire hour.

A question may arise as to whether or not the north wall experienced infiltration or exfiltration during the missing 26 hours of testing. By referring to Figs. 3.8 and 3.9 one cannot infer whether the north wall panel experienced either strong infiltration or exfiltration. In an attempt to better clarify the missing data, other data sets containing temperature and wind speed/direction data for the same time period were analyzed. The results were inconclusive, therefore, it will be assumed that the flow during the missing time periods was weak and the effect of the missing 26 hours will be omitted.

3.2 Heat Transfer Model Testing

Testing of the heat transfer model developed in Section 2.2 will be carried out in two parts. First, the actual measured temperatures for the outer cavity wall recorded at the AHHRF will be compared to two variations of the ASHRAE-based steady-

state model, neither of which include forced convective heat transfer within the cavity. Actual data and the ASHRAE models will then be compared to the heat transfer model developed in Section 2.2 which does include forced convective heat transfer within the cavity.

3.2.1 The ASHRAE-based steady-state heat transfer models

The ASHRAE-based steady-state heat transfer models were developed using the methods presented in the ASHRAE Fundamentals Handbook (1989). Two ASHRAE-based models were developed: a basic model and a modified model. The basic model neglected the effects of solar radiation and used a constant heat transfer coefficient for the exterior wall. The modified model used solar radiation data and an algorithm based on wind speed to calculate the heat transfer coefficient for the exterior wall. The reason for developing two ASHRAE-based models was that by comparing the results of the models it could be determined if it was necessary to include solar radiation effects and a wind speed dependent heat transfer coefficient in order to accurately predict interior cavity temperatures. If the basic model, without solar and wind effects, closely predicted the outer cavity wall temperature, then the moisture deposition model could be applied to buildings even in the absence of solar or wind data. Both the basic and the modified models solve for the overall heat flux through the wall assembly. Since the same heat flux must pass through each constituent part of the wall, individual surface temperatures can be determined.

3.2.1.1 The basic ASHRAE heat transfer model

The basic ASHRAE steady-state heat transfer model was developed in a manner analogous to that presented in Section 2.2.7 when developing the overall heat balance for a cavity with convective flow was discussed. The overall heat transfer equation for pure conduction through the multi-layered wall assembly shown in Fig. 3.4 is given by

$$q'' = \frac{T_{room} - T_{out}}{\frac{1}{h_a} + R_I + \frac{d}{k} + R_{II} + \frac{1}{h_d}} \quad (3.3)$$

where q'' is the heat flux for the entire wall and d/k is the thermal resistance of the insulation filling the cavity. The convective heat transfer coefficient for the exterior wall, h_d , was considered to be constant. ASHRAE (1989) gives a heat transfer coefficient of $34.0 \text{ W}\cdot\text{m}^{-2}\cdot\text{K}^{-1}$ for an exterior wall exposed to a winter wind of $24 \text{ km}\cdot\text{h}^{-1}$. Knowing the heat flux from Eqn. (3.3), the temperature of the outer cavity wall, T_c , can be determined from

$$T_c = q'' \left(R_{II} + \frac{1}{h_d} \right) + T_{out} \quad (3.4)$$

3.2.1.2 The modified ASHRAE heat transfer model

The modified ASHRAE-based steady-state heat transfer model was also developed in a manner analogous to Section 2.2.7 and the basic ASHRAE model presented in Section 3.2.1.1. However, unlike the basic ASHRAE model, the modified model uses a wind speed dependent exterior heat transfer coefficient and the solar radiation equations presented in Section 2.2.7. The overall steady-state heat transfer equation for the modified ASHRAE model can be written as

$$q'' = \frac{T_{room} - T_{out} - \frac{\alpha_d}{h_d} I_T}{\frac{1}{h_a} + R_I + \frac{d}{k} + R_{II} + \frac{1}{h_d}} \quad (3.5)$$

where h_d is the wind speed dependent exterior heat transfer coefficient defined in Eqn. (2.42) and α_d is the absorptance coefficient for the exterior wall and I_T is the total

solar radiation incident on the exterior wall. The temperature of the outer cavity wall, T_c , can be determined from

$$T_c = q'' \left(R_{II} + \frac{1}{h_d} \right) + T_{out} + \frac{\alpha_d}{h_d} I_T \quad (3.6)$$

3.2.1.3 Comparing the basic and modified ASHRAE heat transfer models

The temperature of the outer cavity wall, T_c , determined by the basic and modified ASHRAE heat transfer models, is shown in Fig. 3.10 for the north test panel and in Fig. 3.11 for the south test panel. The square symbols in both figures represent the actual measured data recorded from a single thermocouple placed on the outer cavity wall, directly across from the orifice plate flowmeter (see Section 3.1.3). The temperature for the outer cavity wall is used for comparing the models, since the outer cavity wall temperature affects the partial pressure of the wall, which in turn affects the moisture depositing on the wall. The data in Figs. 3.10 and 3.11 show a pattern in which the temperature has a local maximum every 24 hours. This corresponds to periods of increased solar radiation or daylight hours.

The solid lines in Figs. 3.10 and 3.11 represent the predicted temperatures for the outer cavity wall using the basic ASHRAE model. The temperatures predicted for the north wall test panel, Fig. 3.10, closely match those that were measured, except during daylight hours (10° was the maximum temperature difference between the actual data and the basic model). The basic model, however, does not accurately predict the outer cavity wall temperature for the south wall test panel, as shown in Fig. 3.11. Large discrepancies in temperatures occurred every 24 hours, with the largest difference being $\approx 55^\circ$. The basic model is unable to predict increases in the temperature of the test cavity caused by solar radiation. Because the south panel was exposed to direct solar radiation during the daytime and the north panel only experienced diffuse solar radiation, higher temperatures were recorded for the south wall than for the north wall test panel.

During periods of no solar radiation, i.e. at night, the basic ASHRAE model tracked the actual temperatures in the north and south walls reasonably well as can be seen in Figs. 3.10 and 3.11. The solar radiation models developed here do not include any losses due to night radiation. By including night radiation, the small discrepancy in nighttime temperatures could probably be rectified.

The modified ASHRAE model, which does include solar radiation terms, was able to track the variations in south outer cavity wall temperatures caused by increased solar radiation, as shown by the dashed line in Fig. 3.11. The modified ASHRAE model has a tendency to over-predict the measured temperatures, although the maximum discrepancy was less than 14° , whereas the basic model under-predicted the wall temperature by 55° . On the north wall, Fig. 3.10, the temperatures predicted by the modified model were higher during daylight hours than those that were actually measured, particularly in the later hours of the test (375 to 550). The reason for these errors is not readily apparent. A possible cause is that the real wall does not immediately react to the increased solar radiation on the exterior wall. The heat has to migrate inwards to the outer cavity wall before being recorded as an increased temperature. The modified ASHRAE model assumes that the effect of increased radiation on temperatures is immediate. This is because the ASHRAE model is a steady state calculation which does not include real transient effects.

Regardless of the slight discrepancies, the two models do predict the temperature of the outer cavity wall in the north test panel reasonably well. The use of solar data should be considered whenever accurate surface temperatures are required. It was determined that the wind speed dependent heat transfer coefficient did not contribute significantly to the overall performance of the modified ASHRAE model. Using the single ASHRAE value of $34.0 \text{ W}\cdot\text{m}^{-2}\cdot\text{K}^{-1}$ for the exterior heat transfer coefficient would be adequate for most typical winter applications.

3.2.2 Comparing the modified ASHRAE heat transfer model to the internal forced convective heat transfer model

The heat transfer model developed and discussed in Section 2.2 is a steady-state heat transfer model which allows for conduction and forced convective heat transfer between the walls of a porous medium filled cavity. The model includes solar and wind speed effects on the outer cavity wall. The convective aspect of the model accounts for the variable heat flux occurring in the entry length of the wall. It was shown in Section 2.2.3 that air flowing through a porous media filled wall cavity increased the rate of heat transfer in the thermally developing region above that for steady-state conduction. When the flow becomes thermally developed the heat transfer is entirely steady-state conduction driven. The thermally developing region was shown to be small in comparison with the overall cavity height. It will be shown that the thermally developing region plays a minor part in the overall cavity heat balance. In order to predict a single temperature for the outer cavity wall, heat flux through the wall was integrated over the wall height as shown in Eqns. (2.46) and (2.47). From this can be determined an average temperature for the outer cavity wall which corresponds to the imposed boundary condition of isothermal side walls.

The internal forced convection heat transfer model was compared to the modified ASHRAE-based steady-state heat transfer model and to measured data for the north wall panel. Figure 3.12 shows the actual measured temperatures on the outer cavity wall (square symbols), the predictions by the modified ASHRAE model (dashed line), and the predictions of the internal forced convection model developed in Section 2.2 (solid line). The results for the modified ASHRAE model and the forced convection model were nearly identical, indicating that the use of the simpler modified ASHRAE model yields the same solution as the more complex forced convection model. Both models tended to over-predict temperatures during daylight hours, but tracked the nighttime temperatures reasonably well, as shown in Fig. 3.12. The maximum daytime error in temperatures between the ASHRAE model and the internal forced convection model was 10° and occurred at 240 hours.

The testing of the heat transfer model developed in Section 2.2 has not been rigorous or complete. However, Fig. 3.12 does show that the effect of forced convective heat transfer on the overall wall heat balance is minimal within the test wall cavity filled with glass fibre insulation. Neglecting the effects of air flow-induced heat transfer in wall cavities appears to be reasonable; therefore, it follows that the thermally developing region plays a minor part in the overall cavity heat balance. The assumption that a single temperature can characterise the entire wall is reasonable. The single temperature can be determined from a steady-state heat transfer analysis which includes the effects of solar radiation. Further studies are required to better characterise the factors which have caused the heat transfer models to over-predict daytime temperatures.

3.3 Testing the Moisture Deposition Model

The basis of the moisture deposition model is diffusion of water vapour, which has been convected into the cavity, to a region of low vapour pressure. The derivation of the partial pressure gradient was discussed previously in Section 2.3.2 and shown in Eqn. (2.74). Fick's law for diffusion of water vapour through porous medium was also discussed in Section 2.3.2 and expressed in Eqn. (2.52). From these derivations a model was developed to calculate the deposition of moisture on the outer cavity wall of the test panel (Fig. 3.4).

The moisture deposition model integrated the exact partial pressure gradient over the height of each zone, as shown in Eqn. (2.76), to determine the mass of moisture deposited in each zone per hour of flow. The predicted moisture deposition was then compared to the actual measured deposition data obtained from the AHHRF House 6 north wall test panel for each individual zone (1 to 6 in Fig. 3.5). The method of obtaining the measured data was outlined in Section 3.1. This deposition data is listed in Appendix A, Tables A.1 to A.3.

3.3.1 The outer cavity wall boundary condition

When the partial pressure profile and mass flux equations were examined in Section 2.3.4, the partial pressure boundary condition for the outer cavity wall, specified in Section 2.3.1, was chosen to correspond to saturation ($p_{w,c} = p_{w,s,c}$). In many cases, however, the outer cavity wall would not be saturated and therefore, choosing a saturated boundary condition would not accurately represent the deposition of moisture on the wall. A method of assigning a sub-saturated partial pressure boundary condition to the wall would be to use the wall's wood moisture content. The USDA (1982) defines the moisture content of wood as "the weight of water in wood expressed as a fraction, usually as a percentage, of the weight of oven dry wood." Most woods are considered to be saturated when the wood moisture content exceeds approximately 30% (also referred to as the point of fibre saturation). The wood moisture content can be measured easily using resistance-type moisture meters. However, wood moisture content cannot be used directly as a boundary condition. The concept of an internal moisture limit (IML) will now be introduced in order to relate the wood moisture content to wall relative humidity, which can then be related to a partial pressure boundary condition.

3.3.1.1 The internal moisture limit concept

A novel feature of the present model is the internal moisture limit (IML). The IML is based on the concept that an "active layer" within the wall acts to regulate the absorption and desorption of moisture. If wood moisture content (by percent weight, MC_w) was directly linked to wall relative humidity (ϕ_c) then 30% wood moisture content would correspond to 100% wall relative humidity. This boundary condition may be appropriate if the entire wall (all sides simultaneously) were in direct contact with the depositing moisture.

In real walls, however, moisture deposits on only one side and then migrates towards the opposite side. A thin layer of the wall, next to the surface where deposition is occurring, represents the active layer. Moisture enters the active layer by

diffusion from the air-vapour flow at a faster rate than it leaves. This results in a higher wood moisture content in the active layer than in the rest of the wall. It is the moisture content of the active layer which regulates the boundary condition for the wall. If the active layer were thicker than ≈ 6 mm, the wood moisture content of the layer could be determined using resistance-type moisture pins (the depth of standard moisture pins is ≈ 6 mm). However, the active layer is extremely thin, and therefore, the use of moisture pins is impractical. It could be argued that the active layer is only a few water molecules thick and the surface would always be at saturation since moisture is condensing at the surface. This argument may be correct at the molecular level, but imposing a saturated condition on the surface of the wall may not accurately represent the ability of the wall to absorb moisture. On the other hand, using the overall wood moisture content of the wall overestimates the ability of the wall to absorb moisture. The internal moisture limit concept was developed as a way to convert measured wood moisture content into a boundary condition which incorporates the effects of the active layer.

The wood moisture content of a sample can be related to the relative humidity of the surrounding air, however, the relationship is not linear. Tveit (1966) studied the non-linear relationship and discovered that wood products typically behaved according to the functional form (fitted by the author),

$$MC_v(\%) = a' \left(\frac{\phi(\%)}{100 - \phi(\%)} \right)^b \quad (3.7)$$

where MC_v is the wood moisture content (by percent volume), ϕ is the percent relative humidity of the ambient air, and a' and b are empirical constants. Use of Eqn. (3.7) requires the determination of separate coefficients (a' and b) for each building material studied. Unfortunately, Tveit did not conduct tests on many of the more common North American building materials such as Douglas fir plywood or particle board. Since most woods behaved in a similar fashion, as described by Eqn. (3.7), it was decided to approximate Tveit's non-linear curve with a linear ramp function. A linear function, the internal moisture limit, would represent the connection between

wood moisture content and relative humidity, while the slope of the internal moisture limit function would model the behaviour of the active layer.

The internal moisture limit ramp function is of the form,

$$\begin{aligned} MC_w < IML : \phi_c &= \left(\frac{1}{IML} \right) MC_w \\ MC_w \geq IML : \phi_c &= 1 \end{aligned} \quad (3.8)$$

where IML is the internal moisture limit, MC_w is the averaged wood moisture content for the entire wall including the active layer, and ϕ_c is the outer cavity wall relative humidity, all of which are expressed as decimal values rather than percentages. The internal moisture limit fixes the point where wood moisture content reaches a saturated condition, that is, for $MC_w \geq IML$, $\phi_c = 100\%$.

Figure 3.13 shows the linear ramp function expressed in Eqn. (3.8) which corresponds to an internal moisture limit of 20%. The term "internal moisture limit" should not be confused with the definition of "wood moisture content." The internal moisture limit refers to a value which is used solely as a limit to fix the ramp function shown in Fig. 3.13, so that the actual wood moisture content can be utilized to determine a surface relative humidity. The partial pressure boundary condition can be determined by using the definition of relative humidity, which is,

$$\phi_c = \frac{P_{w,c}}{P_{ws,c}} \bigg|_{T,p} \quad (3.9)$$

By selecting different internal moisture limits, the effect on moisture deposition in the active layer can be altered. Small IMLs, less than 30%, corresponding to wood fibre saturation, would result in steep ramp functions. For a steep ramp, a small increase in wood moisture content corresponds to a large increase in relative humidity. This would act to increase the partial pressure boundary condition and therefore reduce further mass deposition by reducing the partial pressure gradient driving moisture deposition. This corresponds to an active layer which has a high moisture content and is unable to absorb more moisture. The active layer is por-

trayed as if it is saturated, while in fact it may not be. By choosing a larger IML, greater than 30%, a large amount of moisture depositing on the wall would correspond to a small increase in relative humidity. Selecting a large IML gives the wall the ability to absorb moisture beyond its fibre saturation point. This is similar to having an active layer which is sub-saturated, although the rest of the wall may be near saturation. It is suspected that one would rarely require the use an IML greater than the fibre saturation point for modelling deposition in wooden walls. A comparison of various internal moisture limits and their effect on moisture deposition is discussed in Section 4.2.

3.3.1.2 Selecting an appropriate internal moisture limit and calculating moisture deposition boundary conditions

The internal moisture limit selected to be used in testing the moisture deposition model was 20%, a value less than the fibre saturation point of most common woods used in construction. The moisture deposition model requires that a single partial pressure be assigned as the boundary condition on the outer cavity wall for each hour of the test. The partial pressure for the wall can be determined from using Eqns. (3.8) and (3.9) and the average wood moisture content for the wall.

The wood moisture content for each of the three zones in the upper wall section was found to be initially 7% MC_w , Forest (1989), which, by using Eqn. (3.8) and a 20% IML, resulted in an initial relative humidity for the wall of 35%. The temperature of the wall, which must be known in order to convert relative humidity into a partial pressure, was measured directly during the test. Therefore, the heat transfer model developed in Section 2.3 was not used to determine cavity temperatures in the moisture deposition model although it was shown that the heat transfer model predicts sheathing temperatures quite well. Using the moisture deposition model, the amount of moisture deposited in each zone was predicted. Each zone contained three moisture plugs and was the height of a moisture plug (50 mm) and the width of the wall cavity (340 mm). The mass of moisture which deposited on each zone per hour was used to calculate a new average wood moisture content for the

three zones. The average wood moisture content was used in Eqns. (3.8) and (3.9) to determine the wall boundary condition for the next hour.

Figure 3.14 shows the outer cavity wall relative humidity and the wood moisture content for the upper wall section as predicted from the moisture deposition model using a 20% IML. Figure 3.15 shows the same information for the lower wall section. The upper and lower wall sections do not use the same relative humidity boundary condition curve since they are exposed to different air flows and deposition rates. Figure 3.14 indicates that when a 20% IML was used to regulate the wall boundary condition, the outer cavity wall reached a maximum of 75% relative humidity and 15% MC_w . For the lower wall section, the maximum relative humidity was less than 50% and less than 10% MC_w .

3.3.2 Moisture deposition in the upper wall zones

The actual mass of moisture deposited on each plug located in the upper wall section was determined according to the method outlined in Section 3.1.2, with the upper wall receiving two thirds of the total flow through the cavity, as discussed in Section 3.1.5. The placement of zones 1, 2, and 3 was indicated in Fig. 3.5. The moisture deposition model was run with 550 hours of data obtained from the north wall test panel. The results for the three upper wall zones are shown in Figs. 3.16 to 3.18. Each zone was 50 mm high and 340 mm long and contained three moisture plugs, each plug had a diameter of 50 mm. The model used an internal moisture limit set at 20% in order to calculate the wall partial pressure boundary condition. The model was compared to the measured data at three points, 169, 314, and 501 hours after testing began. A summary of the predicted and actual depositions is presented in Table 3.4.

Figure 3.16 shows the mass of water deposited in zone 1 on a cumulative basis during the 550 hour test period. The deposition in zone 1 increased from its initial value of zero to a maximum of 9.0 g after 550 hours. The increase in deposition was continuous and at no time was there any evaporation or sublimation of water from the

wall. The symbols shown in Fig. 3.16 indicate the moisture deposited in each zone (50 mm × 340 mm) based on the assumption that the mass measured in each plug, in the zone, was representative of the moisture deposited in the entire zone. For example, if 0.67 g of moisture was deposited on one plug ($35.7 \text{ g} \cdot \text{m}^{-2}$), then for the entire zone, the moisture deposited would be 0.61 g (see Section 3.1.2 and Appendix A). At the first evaluation point, 169 hours, the model predicted a mass deposition of 2.0 g, 26% less than the actual average deposition of 2.7 g. After 314 hours, the predicted mass increased to 5.0 g, 25% less than the measured value of 6.7 g. Near the end of the test, at 501 hours, the predicted mass deposition was 9.0 g, 20% less than the actual value of 11.3 g. Although the errors appear to be large, the depositions predicted from the model follow the upward trend of the measured data. It appears from Fig. 3.16 that if the missing data from hours 45 to 70 were present, the predicted depositions would be closer to the measured data.

Plotted above the zone 1 moisture deposition curve, Fig. 3.16, are the total flow rates through the north wall, 2/3 of which flowed through the upper wall section. As expected, during exfiltration, the moisture deposition increased, as shown during the period from 340 to 370 hours. Deposition increased during exfiltration since warm, moist air was entering the cavity and was depositing on the outer cavity wall as the air-vapour flow proceeded through the cavity. Large periods of infiltration, such as those from 30 to 100 hours, showed no moisture deposition or evaporation. This adds support to the claim that exfiltration is the main source of moisture entering wall cavities. Infiltrating flow did not deposit or remove any moisture in zone 1 since the infiltrating flow partial pressure had already reached equilibrium with the wall partial pressure before reaching zone 1.

Figure 3.17 shows the moisture deposition in zone 2 for the 550 hour test period and the corresponding flow rates through the north wall panel. The deposition curve produced from the model shows a general increase in mass deposition until, at the 430 hour mark, a small, rapid amount of evaporation occurred. This evaporation corresponded to a sudden increase in infiltration. During earlier hours of infiltration, 250 to 300, no evaporation occurred since the infiltrating air had a partial pressure

greater than the wall, thus the corresponding mass flux was positive. At 430 hours and later, the infiltrating air had a lower partial pressure than the wall, the mass flux became negative, and moisture was removed from the wall. From 480 to 550 hours, there was a small, gradual amount of evaporation since the infiltrating air had a vapour pressure lower than the wall vapour pressure. The measured data followed the same trend as predicted by the model: initial deposition followed by evaporation during the later hours. The model under-predicted the deposition at 169 hours by 0.4 g (57%). At 314 hours, the model also under-predicted deposition by 0.4 g (40%). However, at 501 hours, the model over-predicted mass deposition by 0.2 g (20%). A sudden increase in mass deposition occurred during a 50 hour period of high exfiltration starting at 330 hours. The final amount of moisture in zone 2 after 550 hours was 1.2 g or 7.5 times less than the amount that had deposited in zone 1.

The measured data recorded from each moisture plug in zone 2 is more consistent than in zone 1. At 501 hours in zone 1, Fig. 3.16, the measured mass depositions of the three plugs varied from 8.3 g to 15.4 g, a difference of 7.1 g. However, in zone 2, Fig. 3.17, the deposition varied from 0.9 g to 1.0 g, a difference of only 0.1 g. These differences may be contributed to the flow through the cavity being more evenly distributed when further away from the leakage site. Zone 2 was 420 mm from the exfiltration orifice whereas zone 1 was only 140 mm away. The measured depositions across each zone in the cavity were closer in magnitude during the early hours, as shown for zone 1 in Fig. 3.16, with the range of differences in depositions being 0.8 g and 2.7 g for hours 169 and 314, respectively. The high exfiltration rate recorded between 330 and 380 hours may have accounted for the wide difference in mass depositions at the 501 hour mark (7.1 g). The high influx of air would have distributed itself across the cavity width before reaching zone 2 and 3 and therefore the measured range of depositions were much narrower in these zones than in zone 1. Appendix A, Tables A.1 to A.3., list the complete deposition data for all the zones.

In zone 3, Fig. 3.18, the model consistently over-predicted the moisture deposition at each evaluation point, although the model continued to follow the general

trend in the measured data, including evaporation in the later hours. Table 3.4 lists the predicted mass deposition and the actual mass deposition at the three evaluation points shown in Fig. 3.18. The moisture deposition curve for zone 3, Fig. 3.18, shows different deposition features than either zone 1 or 2. In zone 1, Fig. 3.16, during the first 20 hours of the test, deposition increased from 0 to 0.8 g due to exfiltrating flow. Zone 2, Fig. 3.17, indicated a considerably smaller increase during the first 20 hours from 0 to less than 0.1 g. However, zone 3, Fig. 3.18, showed no increase in moisture deposition during the first 20 hours but showed a large increase at 40 hours, an increase not realized in zone 1. This indicates that the deposition in zone 1 is not controlled by the same flow regime as in zone 3.

Moisture deposition in zone 1 was shown to be dominated by exfiltration only, infiltration had no affect on the deposition curve shown in Fig. 3.16. Figure 3.18 shows that, during periods of infiltration, the moisture deposition either increased or decreased but during hours of exfiltration there was little to no increase in moisture deposition. This leads to the conclusion that in zone 3 the deposition or evaporation of moisture was dominated by infiltration. Figure 3.19 shows the contribution to the total moisture deposition in zone 3 by exfiltration and infiltration. Up until 350 hours, the deposition of moisture was entirely by infiltration. At 350 hours, zone 3 experienced a slight increase in moisture deposition, due to a large increase in exfiltration. After 350 hours, infiltration began to desorb moisture from the wall, thus the downward slope in the infiltration and total deposition curves in Fig. 3.19. Evaporation from the wall occurs when the wall partial pressure is greater than the infiltrating partial pressure and only occurs in the later hours of the test period. The close proximity of zone 3 to the exterior crack (50 mm away) makes zone 3 highly susceptible to infiltration deposition and insensitive to exfiltration deposition which enters the cavity 700 mm away from zone 3. During periods of exfiltration, the warm, moist room air would deposit most of its moisture near the inlet, leaving little moisture to be deposited in the rest of the wall, including zone 3.

3.3.3 Moisture deposition in the lower wall zones

The lower wall zones, zones 4, 5, and 6, exhibited moisture deposition characteristics quite different from the upper wall zones. The results from running the model on the three lower zones are shown in Figs. 3.20 to 3.22. The flow rate through the lower zones was 1/3 of the total flow rate through the wall (Section 3.1.5). The internal moisture limit was set at 20%. The model was compared to the measured data at three points, 169, 314, and 501 hours after testing began.

In each of the lower zones, the model under-predicted moisture deposition as compared to the measured values. Table 3.5, which summarises the predicted and actual moisture deposition in zones 4, 5, and 6, shows that the predicted deposition in zone 4 at 501 hours was 2.9 g compared to the actual average deposition of 12.4 g, a 9.5 g difference. The differences between the predicted and actual values were smaller in zones 5 and 6 (1.45 g and 0.66 g, respectively) only because the overall magnitude of the deposition decreased. Although the moisture predictions were in error, the predicted moisture deposition curve in all three zones (Figs. 3.20, 3.21, and 3.22), followed the general trend in the measured data. As time progressed, the amount of deposition increased in each zone. Only zone 6, Figure 3.22, indicated any moisture evaporation, however, the amount was small and it was hard to determine whether or not it was true evaporation or experimental error.

Since the model did follow the trend of the data and only the magnitude of the depositions were incorrect, it was possible that the model may have had incorrect initial parameters. A smaller flow rate was assumed for the lower cavity than the upper cavity which led directly to less moisture being available to deposit in the lower wall section. A sensitivity analysis was conducted in Chapter 4 which evaluates the changes in moisture deposition due to changing the flow distribution between the upper and lower sections. A sensitivity study is also conducted in Chapter 4 on the effects of changing the internal moisture limit on moisture deposition.

3.3.4 Effect of the moisture deposition model's region of validity on the test results

Discussed previously, in Section 2.3.7, was the concept of a region where the moisture deposition model was valid and a region where the model was invalid due to potential deposition in the insulation rather than on the wall. The region depended on three items: inlet relative humidity, outer cavity wall temperature, and outer cavity wall relative humidity. When the criteria (the wall relative humidity and temperature relationship) outlined earlier based on the theoretical wall (Section 2.3.7) was applied to the test data, interesting results occurred. Of the 523 hours for which data was collected, the model failed 27% of the time (142 hours) when using the maximum airflow velocity ($w = 0.01 \text{ m}\cdot\text{s}^{-1}$) plot (Fig. 2.19). By switching to the slower air-flow velocity ($w = 0.0001 \text{ m}\cdot\text{s}^{-1}$) plot (Fig. 2.20), when possible, the model failed 24% of the time (126 hours).

But did the model actually fail? Reviewing the actual data and the predicted depositions (Figs. 3.16 to 3.22), it can be seen that in the upper zones the model closely predicted the deposition in the cavity even though the model was strictly invalid for 142 hours. This indicates that the model "failure" is gradual and that the errors produced are small. Another possible explanation is that the ice accumulation within the insulation, which affects the flow distribution through the cavity, may not be as significant a factor as first assumed. More investigations are required in this area to better determine the reason why the model was able to predict reasonable results when the model was strictly invalid.

3.3.5 Summary of the moisture deposition model testing

Some interesting observations from testing the moisture deposition model were:

- The air-vapour flow entering the cavity, whether by exfiltration or infiltration, will tend to deposit the majority of its moisture near the point of entry. The exfiltration flow will typically carry more moisture into

the cavity than the infiltrating flow since the exfiltrating flow has a higher moisture content.

- The moisture deposition model is capable of handling either deposition or evaporation of moisture due to either exfiltrating or infiltrating flow.
- Using an internal moisture limit to set the partial pressure boundary conditions for the outer wall did enable the model to follow the trends shown in the measured data.
- The moisture deposition model is valid for dry air up to the point where humidity in the air causes moisture to deposit in the insulation rather than on the wall. Figure 2.21 shows the range of relative humidities for which the model is valid for increasing wall temperatures. The model predicted actual moisture depositions with reasonable accuracy and was able to follow the various trends in the data, even though the model was strictly invalid for 27% of the test period.

Table 3.1 Construction details of Alberta Home Heating Research Facility test House 6.*

Floor Area:	6250 x 6860 mm -- 42.88 m ²
Wall Height:	2440 mm
Basement Height:	2440 mm, 1830 mm below grade
Walls:	9.5 mm pre-stained Rough Tex Plywood 90 mm glass fibre batt insulation, RSI 1.7 50 x 100 mm nominal studs, 400 mm centres 0.102 mm polyethylene vapour barrier 13 mm painted gypsum wallboard
Wall area / Floor area:	1.39
Windows:	North: 990 x 1950 mm double glazed sealed South: none East: 1000 x 1950 mm double glazed opening West: 1000 x 1950 mm double glazed opening
Window area / Floor area:	11.9%
Ceiling:	9.5 mm plywood sheathing RSI 2.1 glass fibre batt insulation 0.102 mm polyethylene vapour barrier 13 mm painted gypsum wallboard
Roof:	CMHC approved trusses with 760 mm stub 210# asphalt shingles 9.5 mm plywood Ext. GD sheathing
Basement:	13 mm preservative treated plywood to 600 mm below grade 50 mm rigid insulation, RSI 1.7, to 600 mm below grade 200 mm concrete wall 100 mm concrete slab on 0.152 mm polyethylene vapour barrier
Door:	910 x 2030 mm insulated metal
Electric furnace capacity:	7.5 kW
Humidifier:	Rotating drum connected to reservoir

*Table adapted from Forest (1989) and Walker (1991).

Table 3.2 Summary of velocity flow data and calculated flow velocities in the north wall test cavity. The upper wall cavity had 2/3 of the total flow.

	Infiltration	Exfiltration
Average flow rate through orifice meter ^a [m ³ h ⁻¹]	0.1104	0.0458
Number of flow hours [h]	383	363
Average flow rate (reduced hour average) ^b [m ³ h ⁻¹]	0.1510	0.0650
Maximum flow rate through orifice meter [m ³ h ⁻¹]	0.9426	0.3725
Average cavity velocity ^b , w [m s ⁻¹]	upper cavity	0.0009
	lower cavity	0.0005
Maximum cavity velocity, w [m s ⁻¹]	upper cavity	0.0057
	lower cavity	0.0029
Superficial crack velocity ^c , u , [m s ⁻¹]	0.9863	0.4245

^aAverage flow rate through the wall including hours where there was no flow.

^bReduced hour average does not include any hours in which there was zero flow.

^cSuperficial crack velocity is defined as $u_s = Q/(0.6 \times \text{orifice area})$.

Table 3.3 Summary of velocity flow data and calculated flow velocities in the south wall test cavity. The upper wall cavity had 2/3 of the total flow.

	Infiltration	Exfiltration
Average flow rate through orifice meter ^a [m ³ h ⁻¹]	0.1350	0.0220
Number of flow hours [h]	460	355
Average flow rate (reduced hour average) ^b [m ³ h ⁻¹]	0.1540	0.0320
Maximum flow rate through orifice meter [m ³ h ⁻¹]	1.1864	0.1538
Average cavity velocity ^b , w [m s ⁻¹]	upper cavity	0.0009
	lower cavity	0.0005
Maximum cavity velocity, w [m s ⁻¹]	upper cavity	0.0072
	lower cavity	0.0036
Superficial crack velocity ^c , u , [m s ⁻¹]	1.0058	0.2090

^aAverage flow rate through the wall including hours where there was no flow.

^bReduced hour average does not include any hours in which there was zero flow.

^cSuperficial crack velocity is defined as $u = Q/(0.6 \times \text{orifice area})$.

Table 3.4 Comparison of the measured moisture deposition in each zone of the upper wall section and the predictions of the moisture deposition model.

Zone	Hour of Evaluation	Predicted Mass Deposition (g)	Measured Mass Deposition (g)	Percent Error (%)	Error (g)
1	169	2.0	2.7	-26	-0.7
	314	5.0	6.7	-25	-1.7
	501	9.0	11.3	-20	-2.3
2	169	0.3	0.7	-57	-0.4
	314	0.6	1.0	-40	-0.4
	501	1.2	1.0	+20	0.2
3	169	1.0	0.6	+67	0.4
	314	1.2	0.9	+33	0.3
	501	1.1	0.3	+267	0.8

Table 3.5 Comparison of the measured moisture deposition in each zone of the lower wall section and the predictions of the moisture deposition model.

Zone	Hour of Evaluation	Predicted Mass Deposition (g)	Measured Mass Deposition (g)	Percent Error (%)	Error (g)
4	169	0.4	1.4	-71	-1.0
	314	1.1	4.5	-76	-3.4
	501	2.9	12.4	-77	-9.5
5	169	0.00	0.5	--	-0.5
	314	0.01	0.7	-99	-0.69
	501	0.15	1.6	-90	-1.45
6	169	0.00	0.5	--	-0.5
	314	0.16	0.7	-77	-0.54
	501	0.04	0.7	-94	-0.66

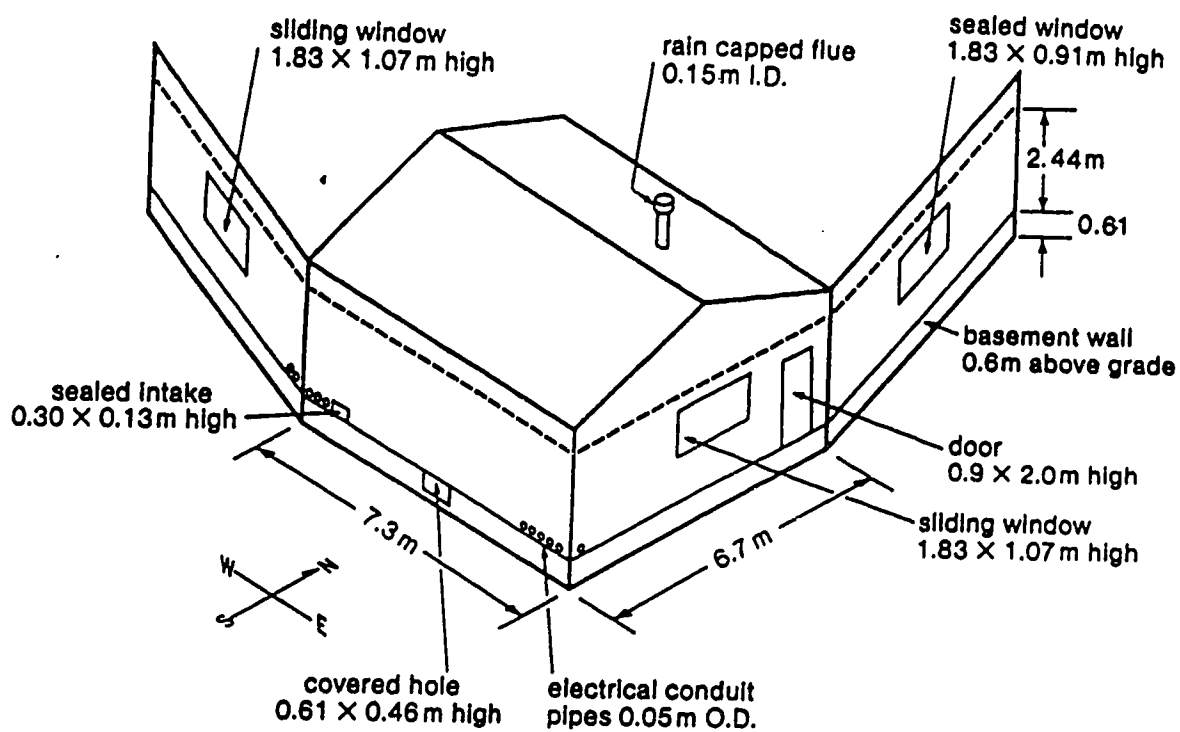


Figure 3.1 Alberta Home Heating Research Facility House 6 used in experimentally validating the moisture deposition model.

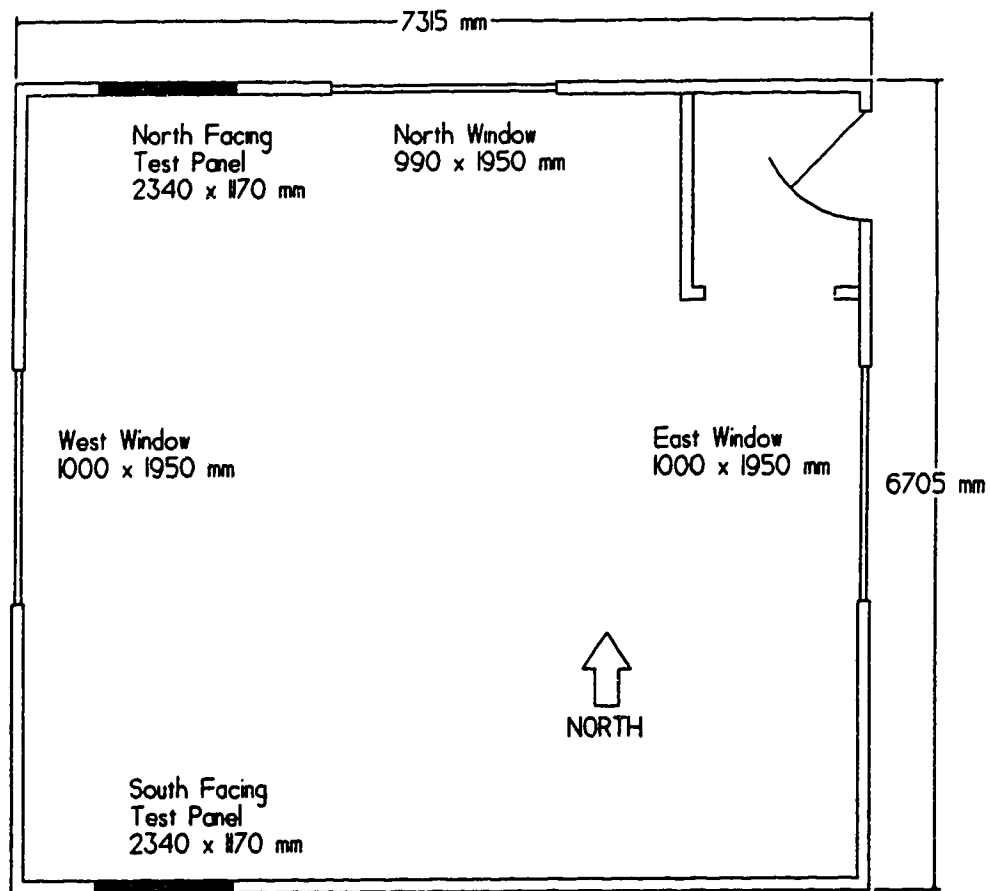


Figure 3.2 Plan view of House 6 at the Alberta Home Heating Research Facility showing the location of the wall test panels in the north and south walls.

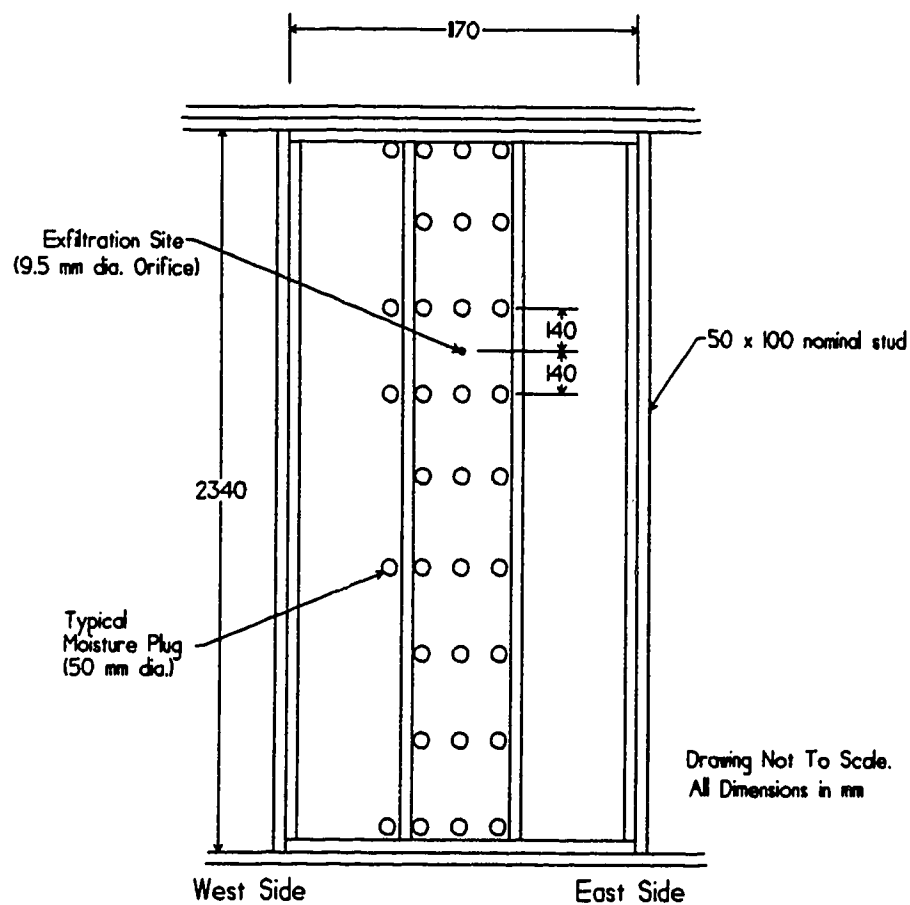


Figure 3.3 Front view of the north wall test panel showing construction details, placement of the moisture plugs, and the location of the exfiltration site.

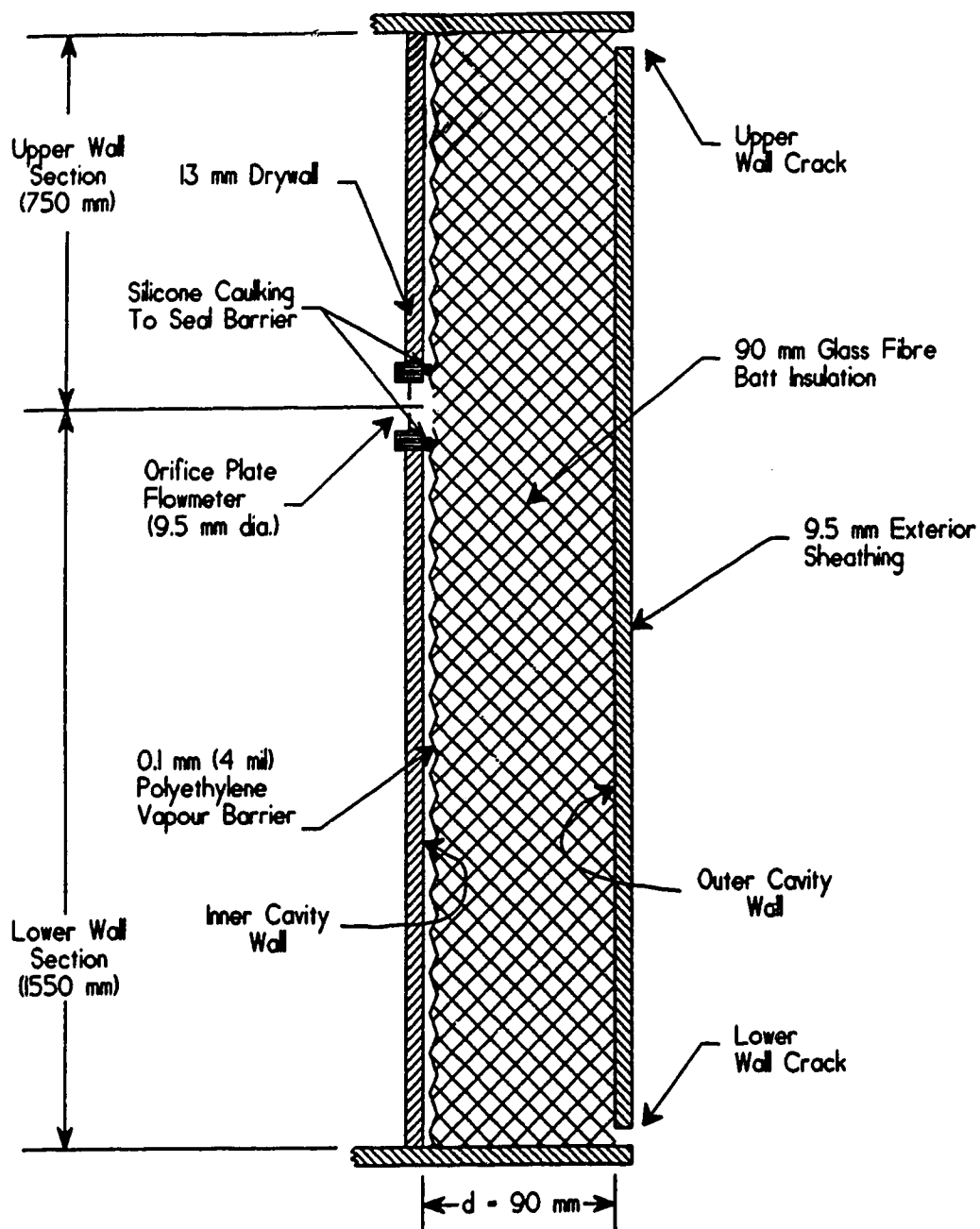


Figure 3.4 Side view and construction details of the north wall test panel. The annular slit orifice plate flowmeter acts as the exfiltration site on the interior wall of the test panel.

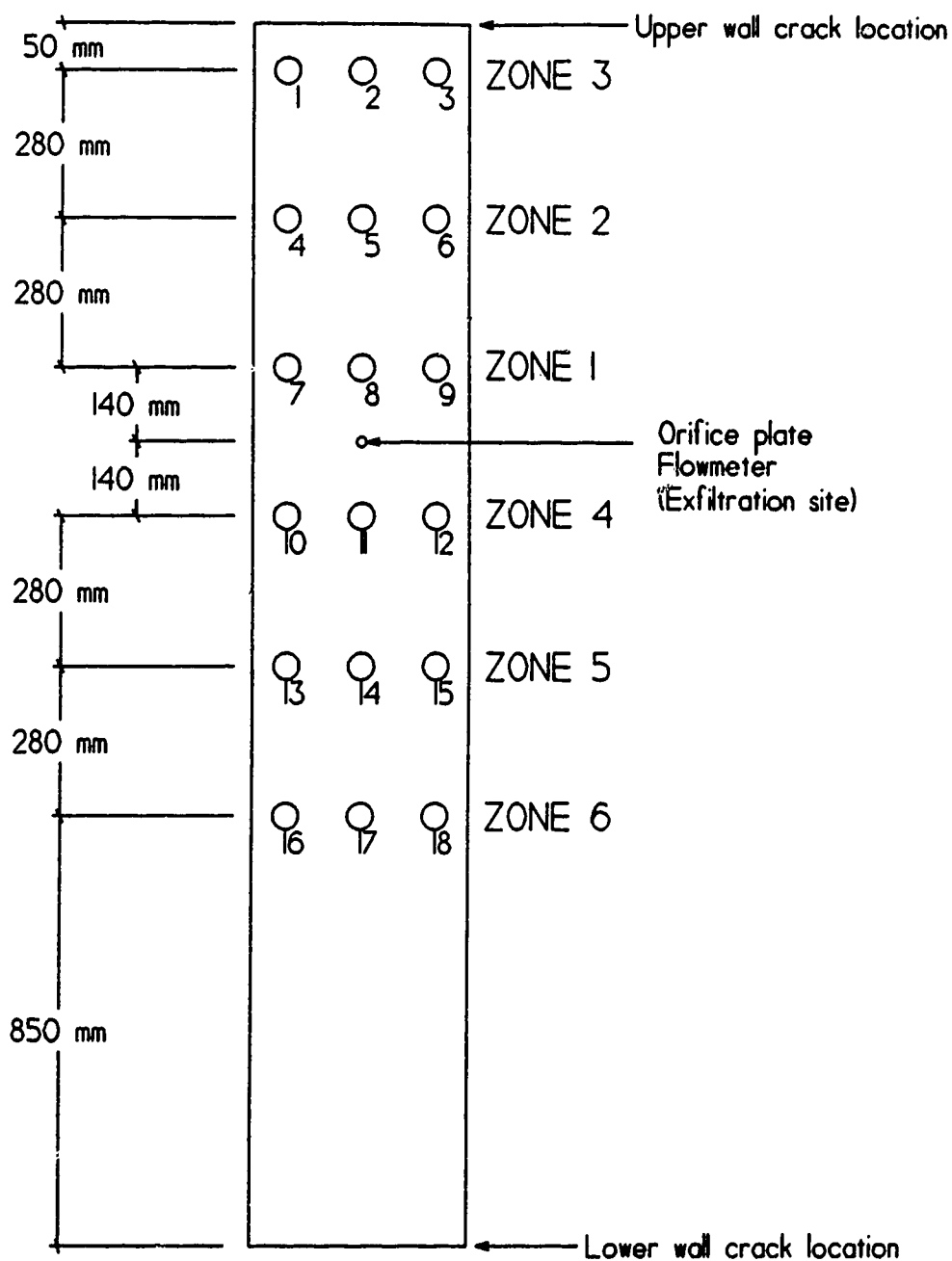


Figure 3.5 Labelling of the individual moisture plugs and grouping of the plugs into zones. Each zone consists of three horizontal plugs. Zones 1 to 3 constitute the upper wall section while zones 4 to 6 constitute the lower wall section.

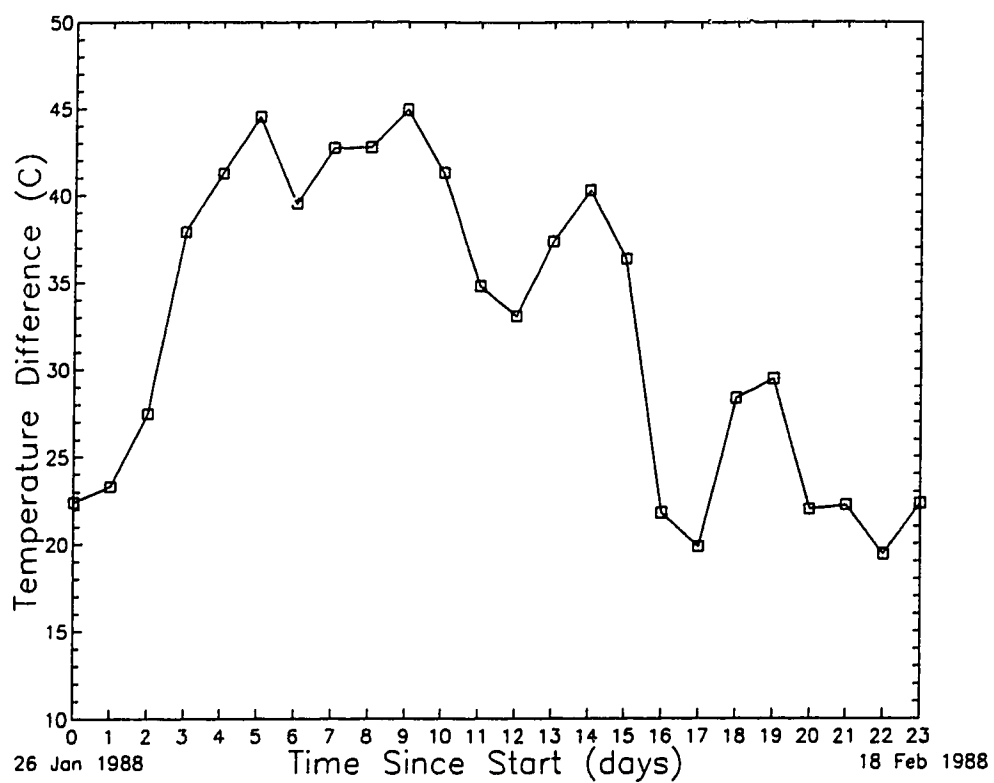


Figure 3.6 Daily averaged indoor—outdoor temperature difference for AHHRF House 6 from 26 January to 18 February 1988. The indoor temperature was maintained at $20^{\circ}\text{C} \pm 1.5^{\circ}\text{C}$.

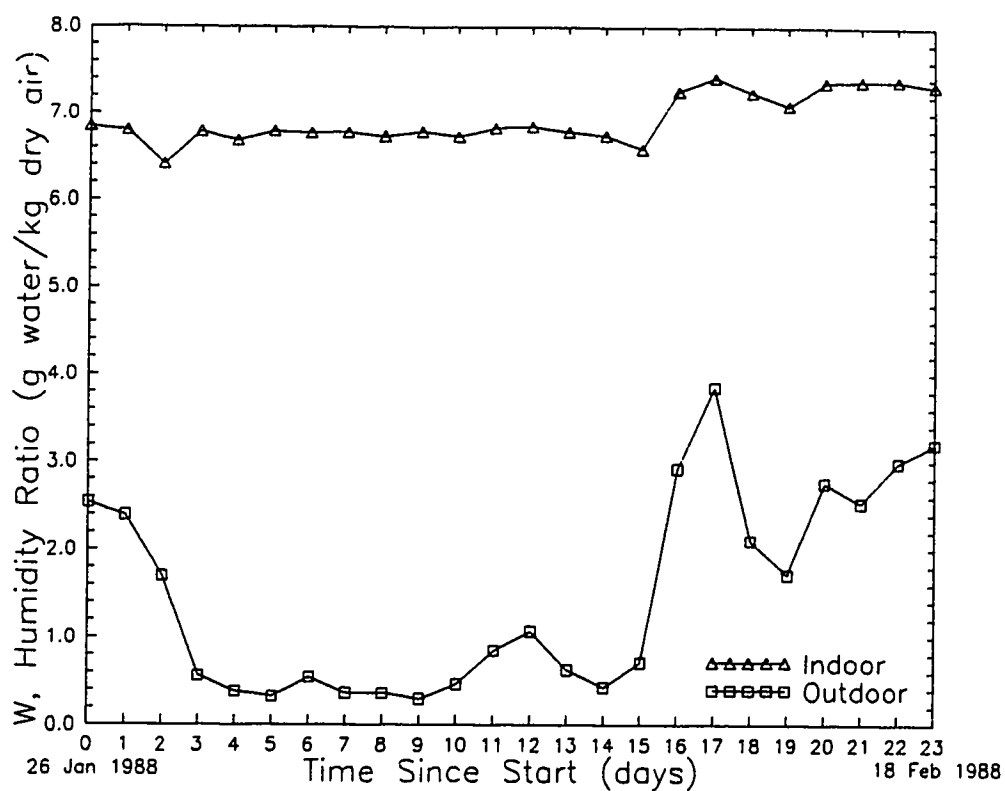


Figure 3.7 Daily averaged indoor and outdoor humidity ratios for House 6 at the AHHRF from 26 January to 18 February 1988. The indoor relative humidity was maintained at $40\% \pm 3\%$ while the indoor temperature was maintained at $20^{\circ}\text{C} \pm 1.5^{\circ}\text{C}$.

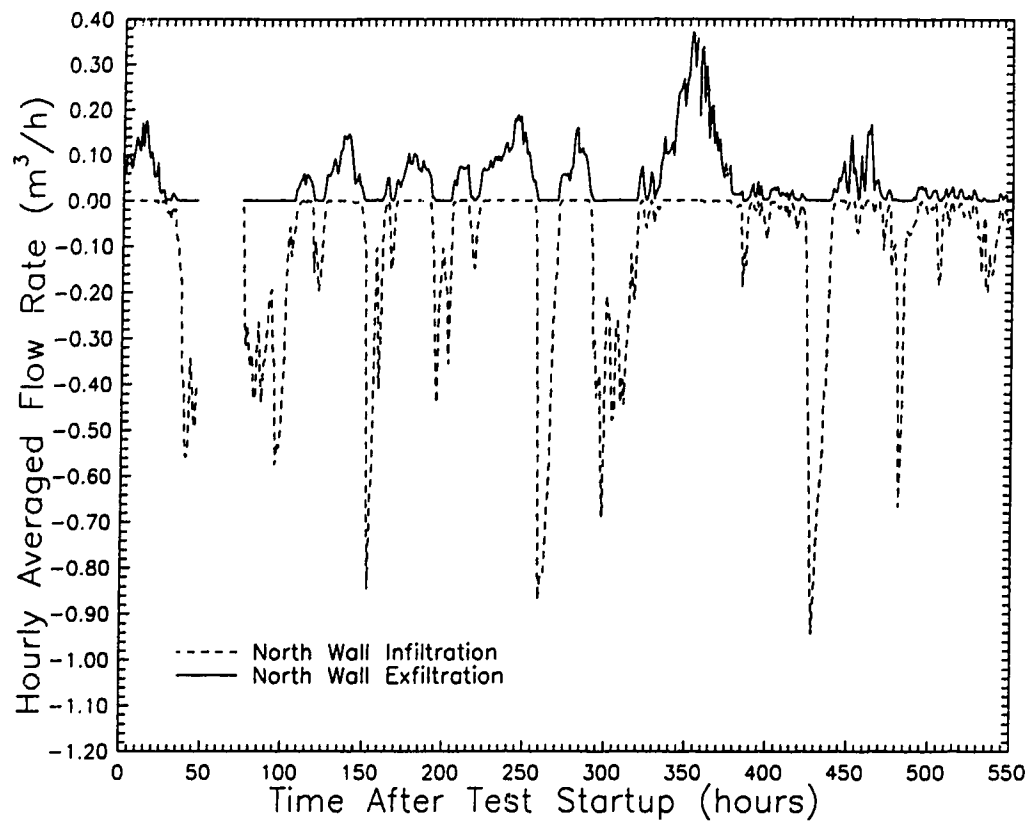


Figure 3.8 The flow rate of moist air through the north wall cavity in House 6 at the AHHRF from 1400h, 26 January 1988 to 1100h, 18 February 1988. Data was recorded eighty times each hour and then averaged over the hour.

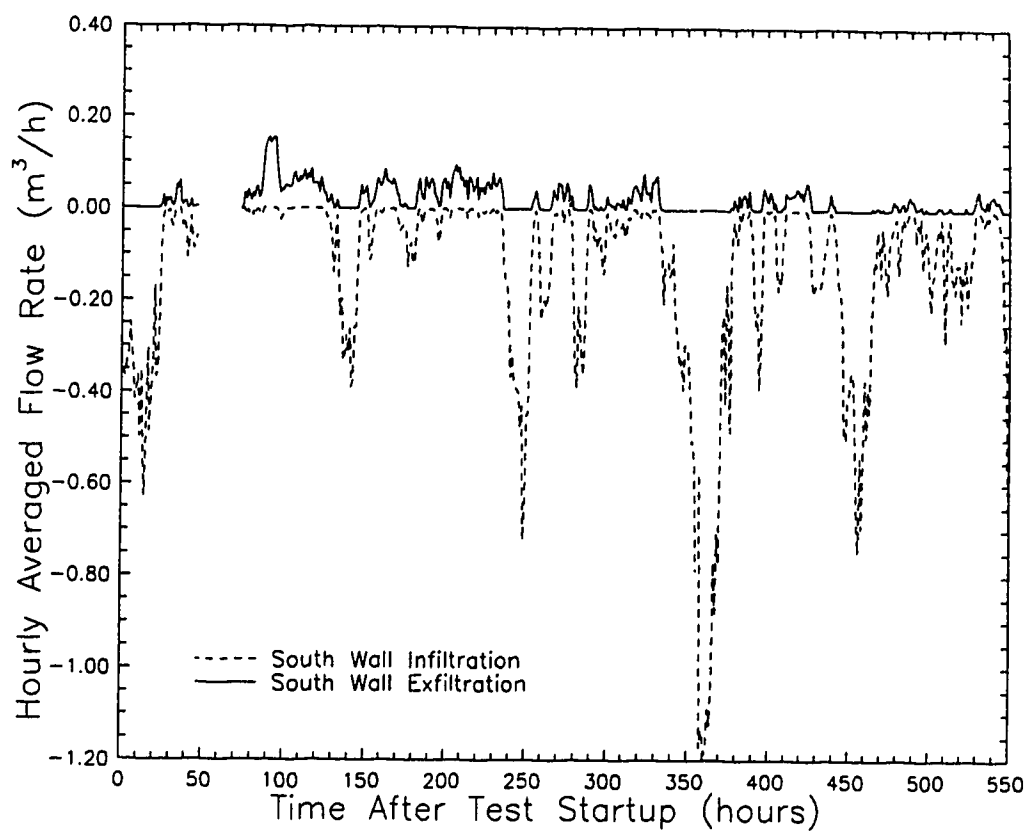


Figure 3.9 The flow rate of moist air through the south wall cavity in House 6 at the AHHRF from 1400h, 26 January 1988 to 1100h, 18 February 1988. Data was recorded eighty times each hour and then averaged over the hour.

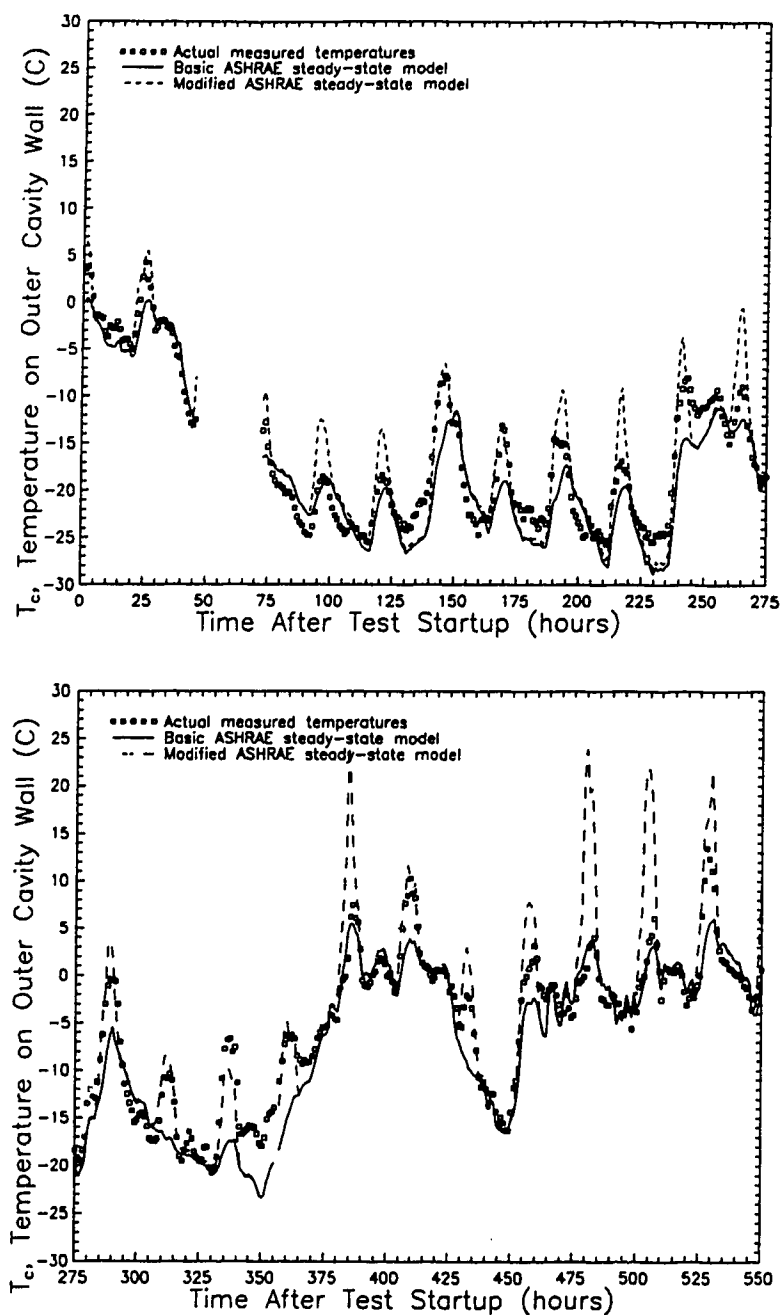


Figure 3.10 A comparison of the actual measured temperatures on the outer cavity wall for the north test panel with the ASHRAE-based models. The basic model used no solar data while the modified model used solar data.

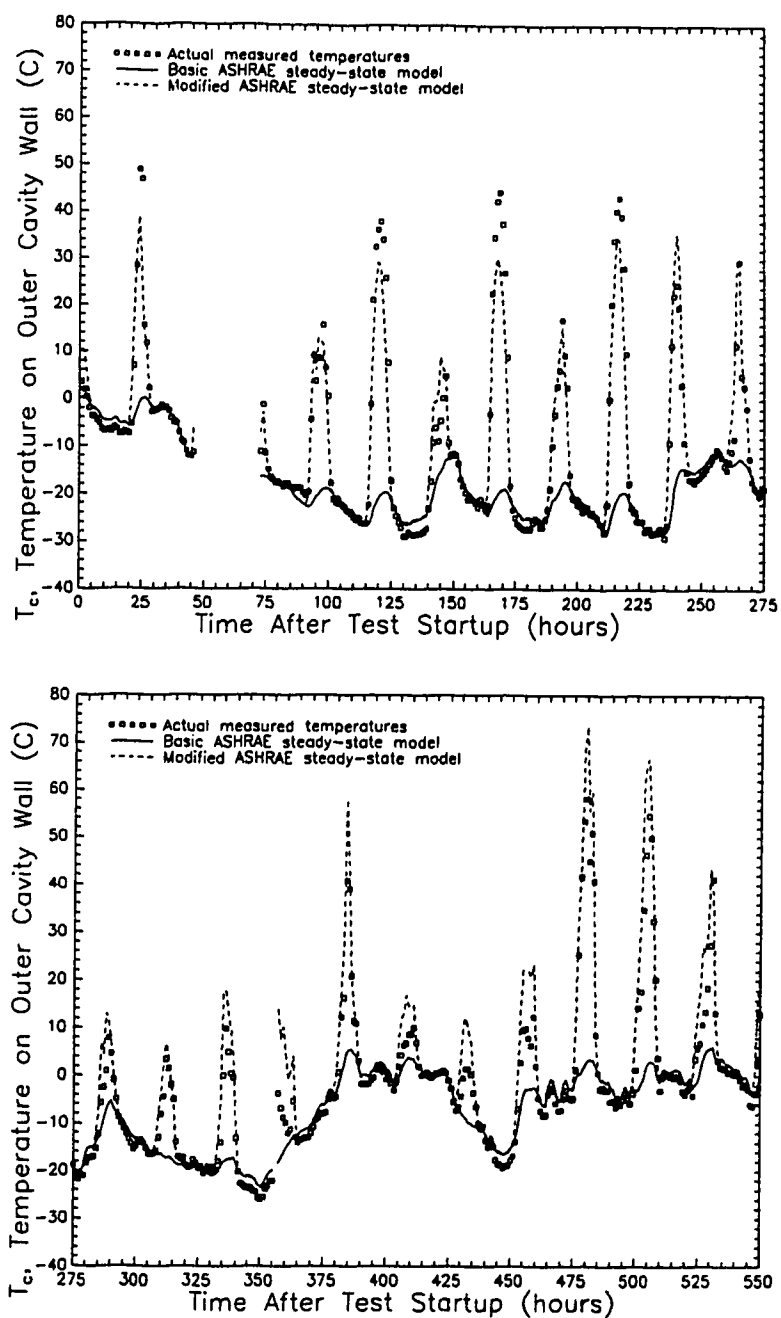


Figure 3.11 A comparison of the actual measured temperatures on the outer cavity wall for the south test panel with the ASHRAE-based models. The basic model used no solar data while the modified model used solar data.

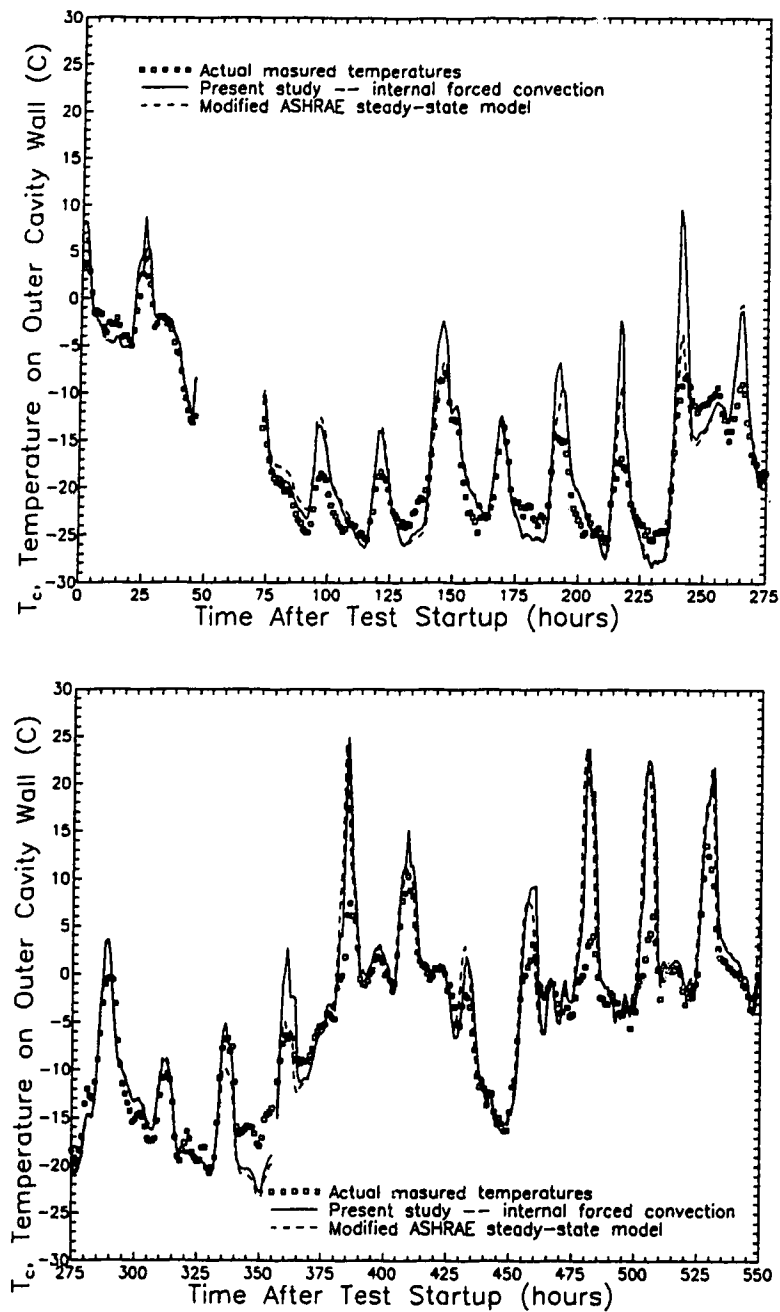


Figure 3.12 Comparison of measured temperatures on the outer cavity wall with predictions made using the internal convection (non-steady state) model and the modified ASHRAE steady-state model. Both models include solar radiation and wind speed effects.

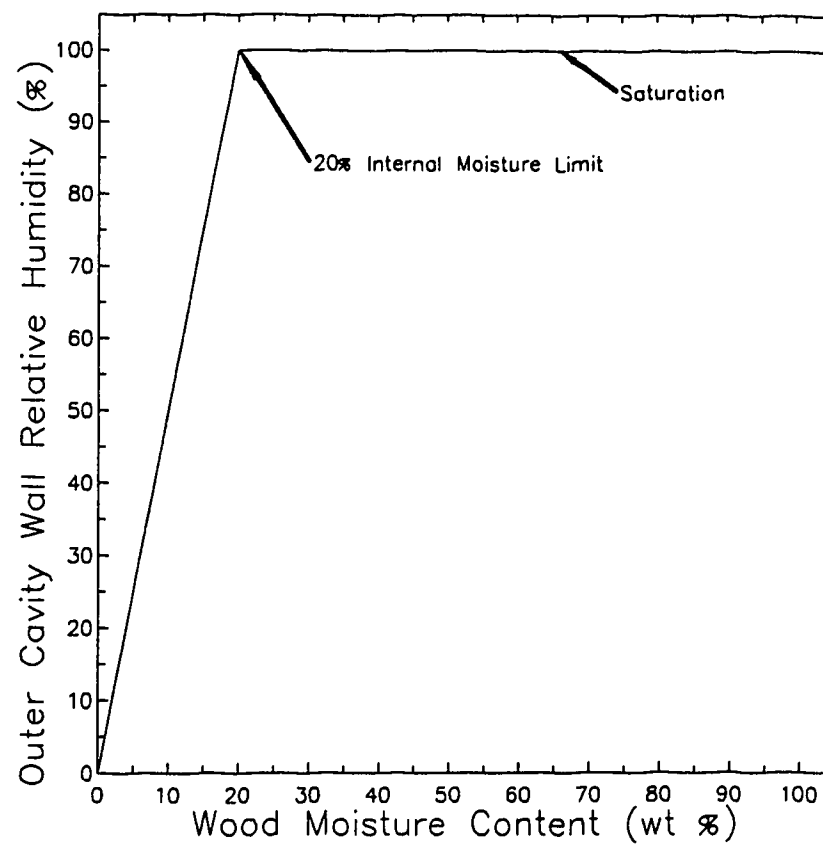


Figure 3.13 The 20% internal moisture limit ramp function used for determining the relative humidity on the outer cavity wall given wood moisture contents. Saturated conditions are reached when the wood moisture content exceeds 20%.

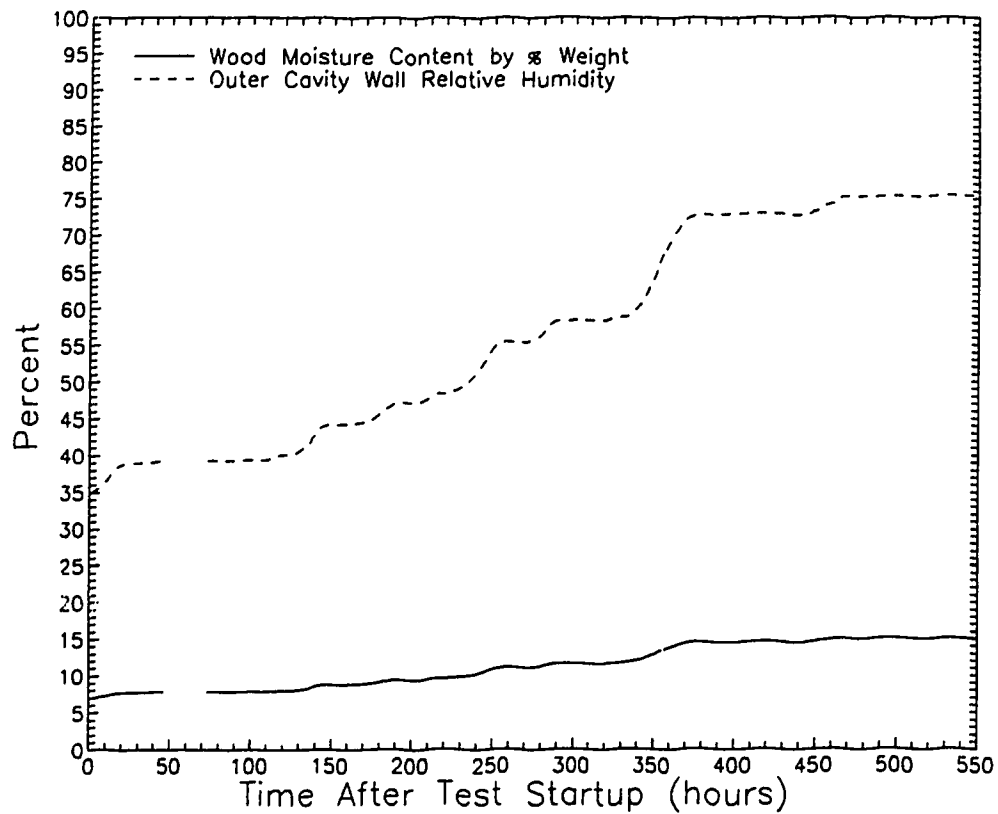


Figure 3.14 Outer cavity wall wood moisture content and corresponding relative humidity using a 20% internal moisture limit. Curves are for the upper section of the north wall test panel.

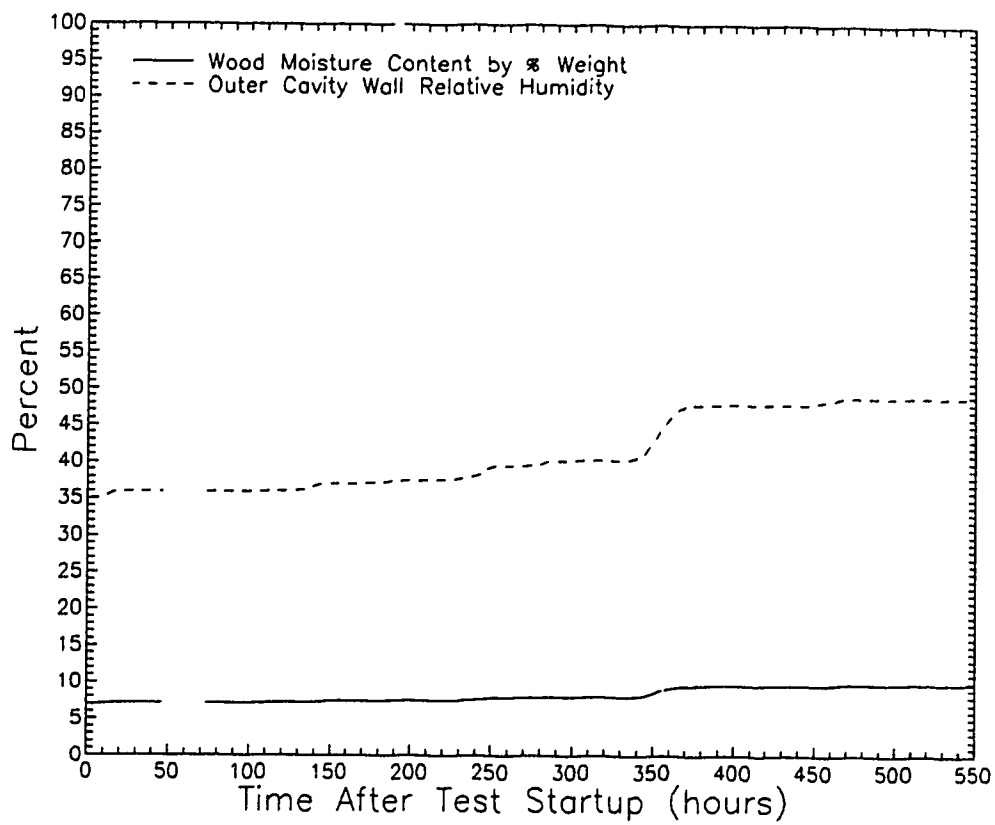


Figure 3.15 Outer cavity wall wood moisture content and corresponding relative humidity using a 20% internal moisture limit. Curves are for the lower section of the north wall test panel.

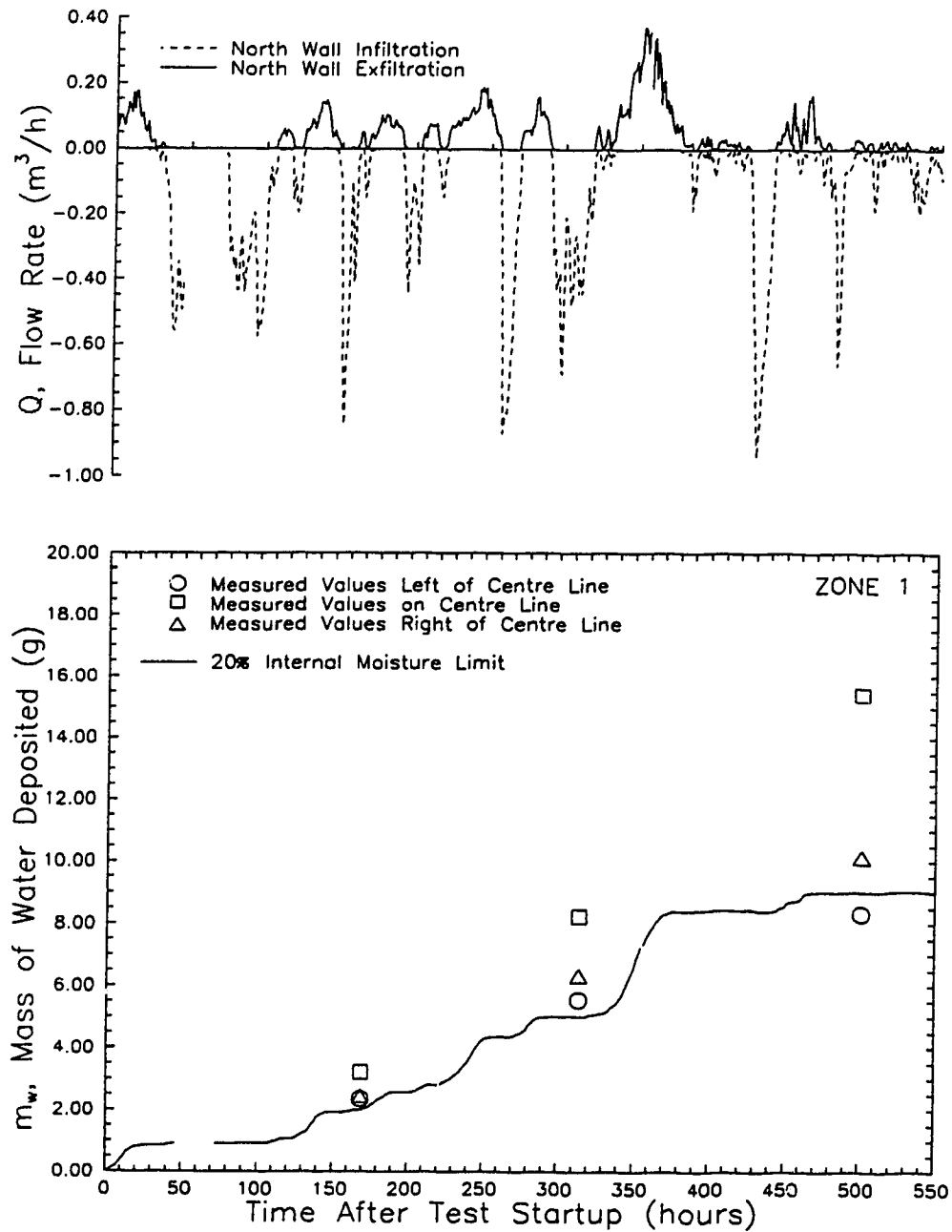


Figure 3.16 Cumulative moisture deposition on the north test panel outer cavity wall in zone 1 when using a 20% internal moisture limit. The solid line indicates the model predicted depositions. Shown also is the corresponding total flow rate through the north test panel.

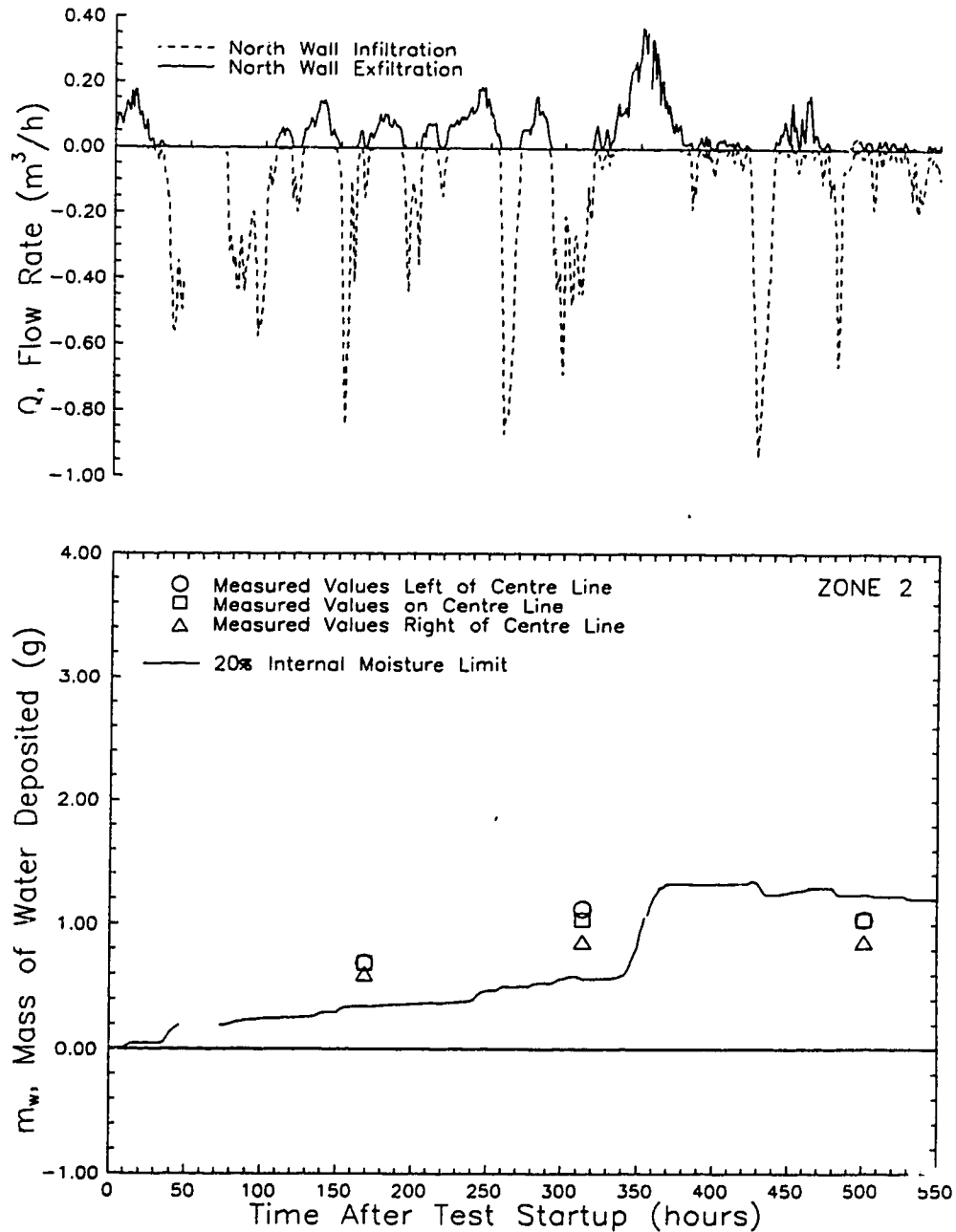


Figure 3.17 Cumulative moisture deposition on the north test panel outer cavity wall in zone 2 when using a 20% internal moisture limit. The solid line indicates the model predicted depositions. Shown also is the corresponding total flow rate through the north test panel.

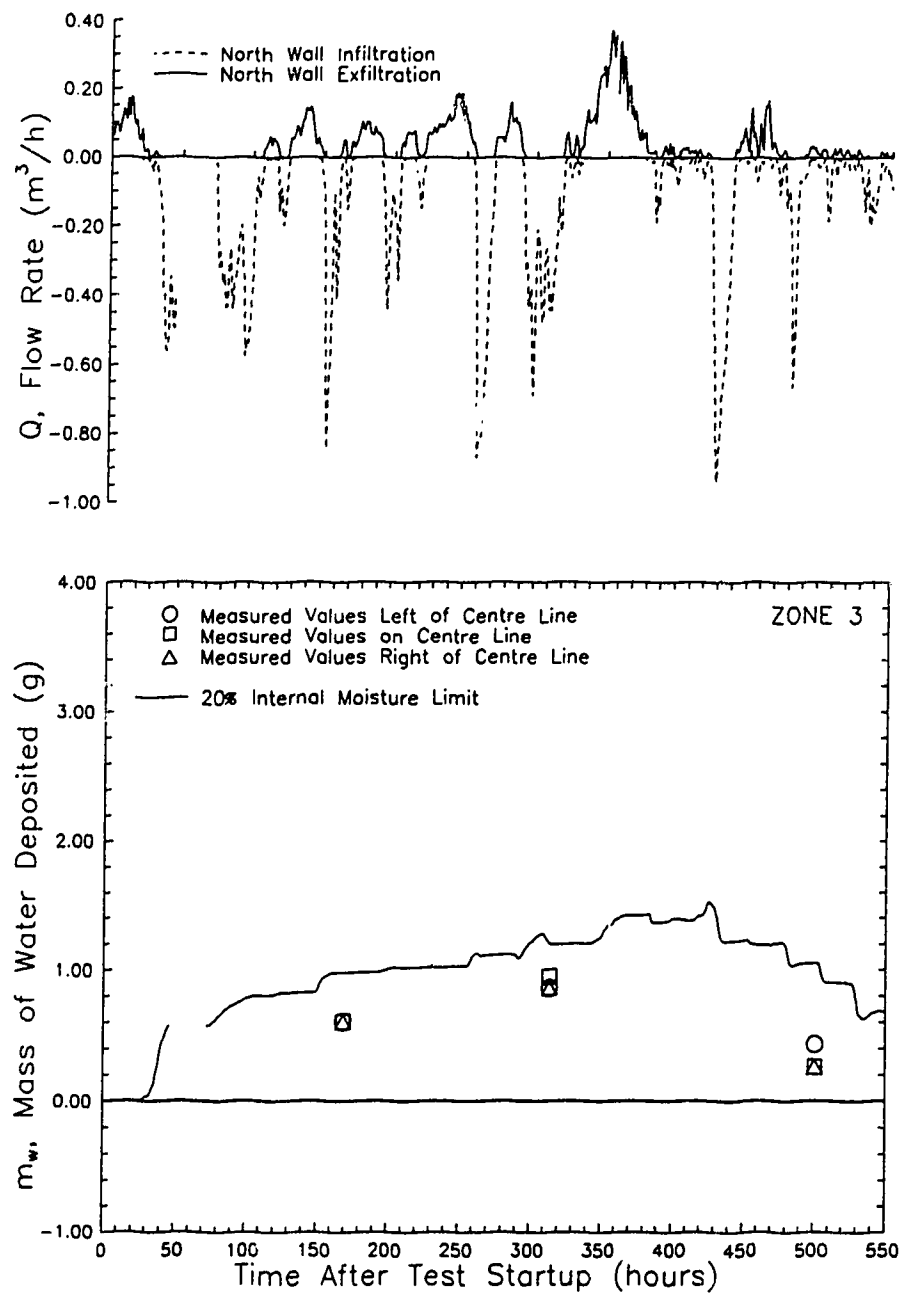


Figure 3.18 Cumulative moisture deposition on the north test panel outer cavity wall in zone 3 when using a 20% internal moisture limit. The solid line indicates the model predicted depositions. Shown also is the corresponding total flow rate through the north test panel.

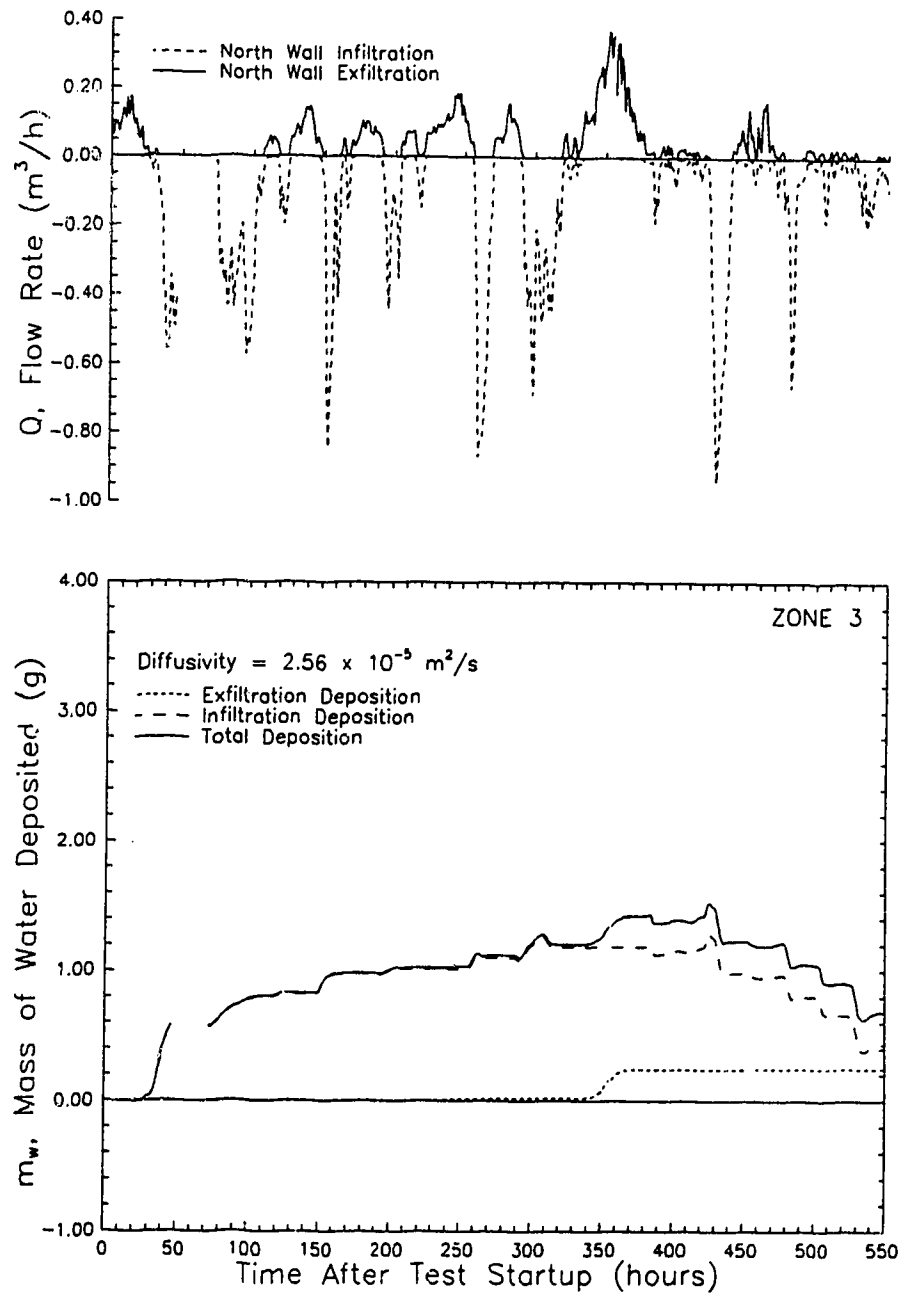


Figure 3.19 Contribution of exfiltration and infiltration to cumulative moisture deposition in zone 3 during the test period.

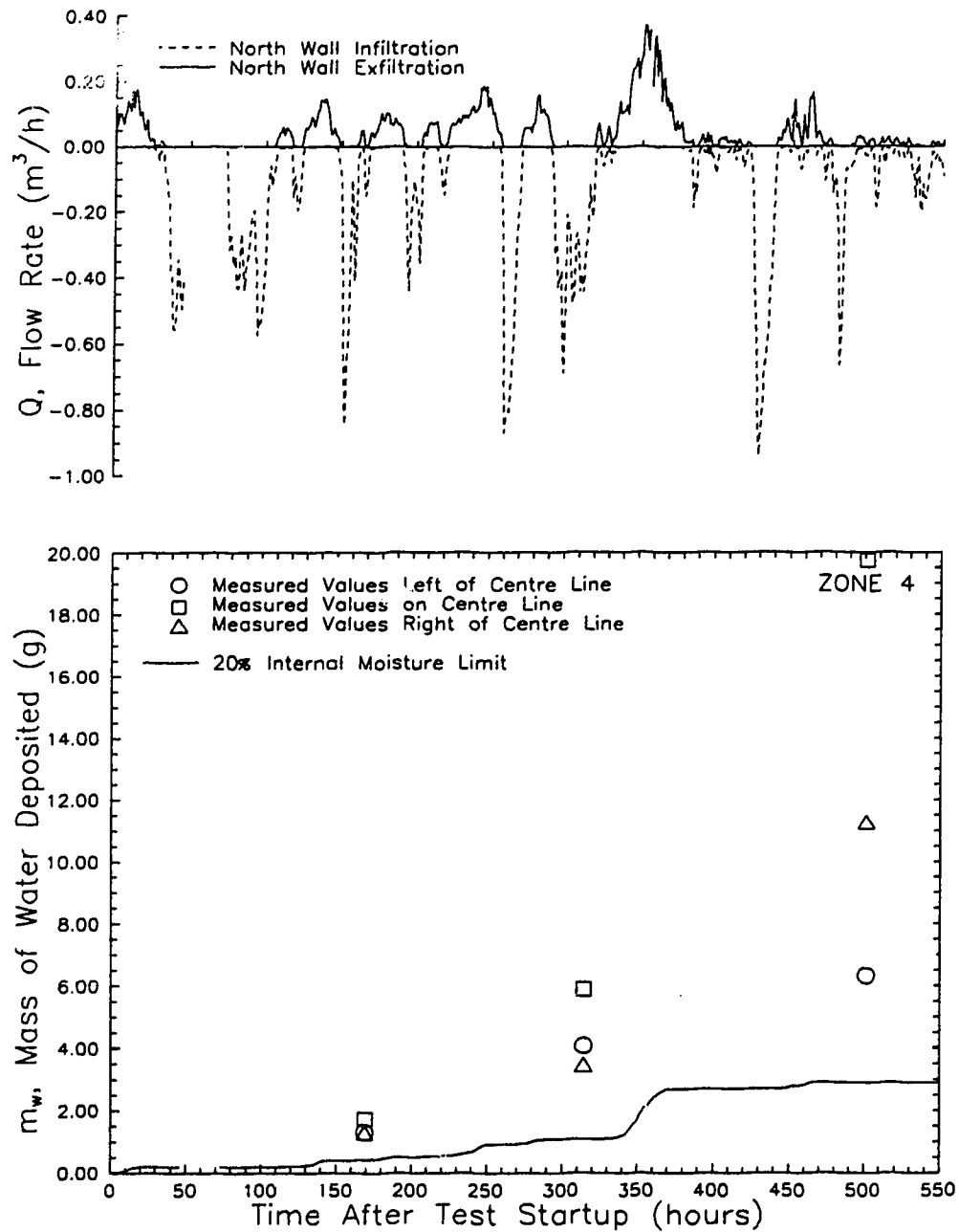


Figure 3.20 Cumulative moisture deposition on the north test panel outer cavity wall in zone 4 when using a 20% internal moisture limit. The solid line indicates the model predicted depositions. Shown also is the corresponding total flow rate through the north test panel.

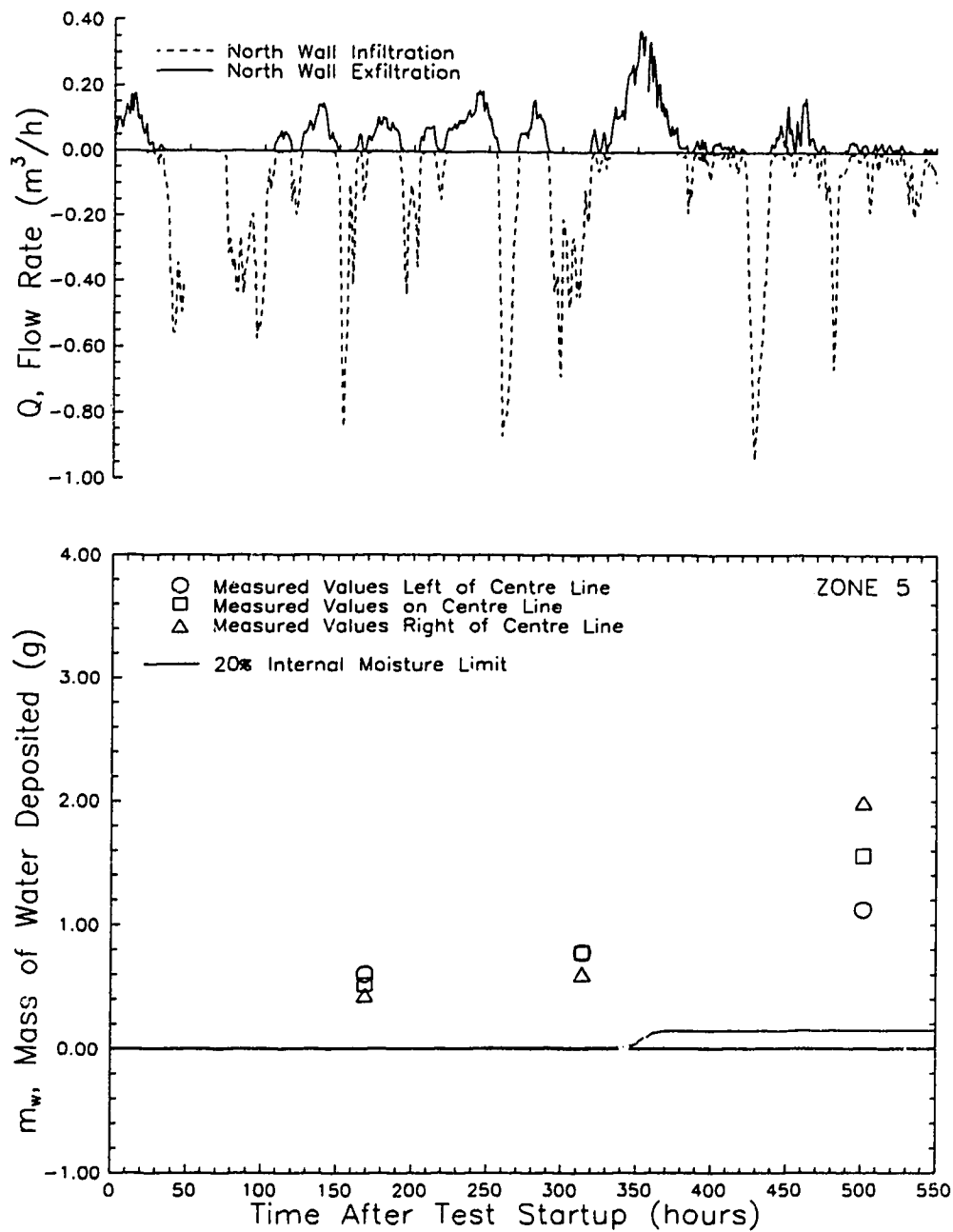


Figure 3.21 Cumulative moisture deposition on the north test panel outer cavity wall in zone 5 when using a 20% internal moisture limit. The solid line indicates the model predicted depositions. Shown also is the corresponding total flow rate through the north test panel.

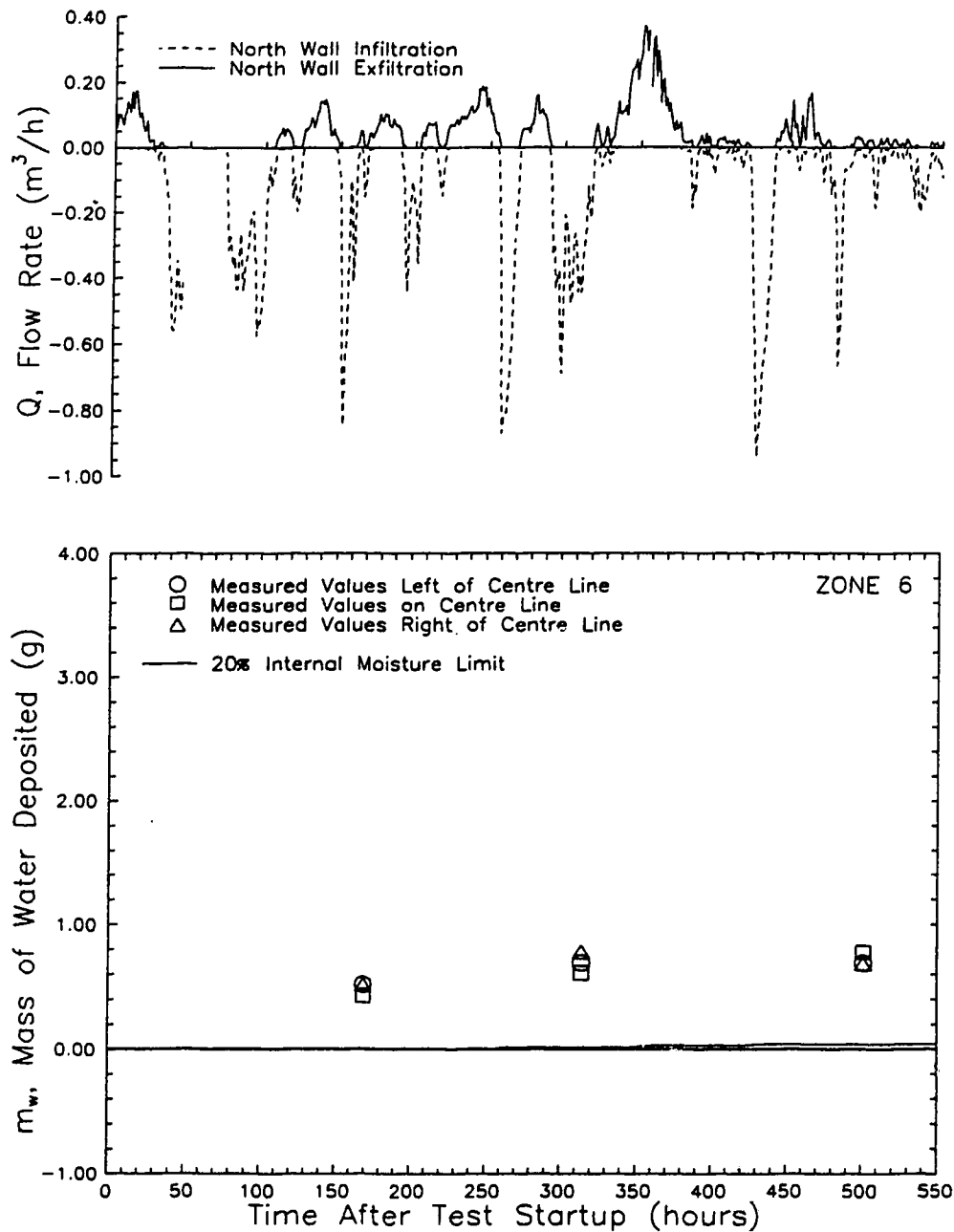


Figure 3.22 Cumulative moisture deposition on the north test panel outer cavity wall in zone 6 when using a 20% internal moisture limit. The solid line indicates the model predicted depositions. Shown also is the corresponding total flow rate through the north test panel.

CHAPTER 4

PARAMETRIC STUDIES OF THE SENSITIVITY OF THE MOISTURE DEPOSITION MODEL TO VARIATIONS IN INPUT PARAMETERS

In order to quantify the effects of the input variables on moisture deposition, a sensitivity study was undertaken. Five parameters were investigated: internal moisture limit (IML), flow rate, mass diffusivity, cavity height, and cavity width. The internal moisture limit is user-specified, and is related to the nature of the exterior sheathing. The flow rate is dependent on environmental conditions and may change considerably during actual testing. The last three parameters: mass diffusivity of the porous medium, cavity height, and cavity width, are physical characteristics of the wall assembly. Each of the five parameters will be varied independently of the others.

Zones 1 and 3 located in the outer cavity wall of the upper section of the north wall test panel, Fig. 3.5, will be used for comparing the effects of changing the input variables. The behaviour in zone 2 was found in all cases to be similar to zone 1 and will not be discussed separately. The lower section of the north wall test panel was not used for the sensitivity studies except for comparisons using the internal moisture limit. Varying the input parameters affected the lower wall section in the same manner as the upper wall section; however, the magnitude of the change was smaller and therefore difficult to notice. It was decided to show and discuss only the more pronounced responses in the upper wall section. The lower wall section will be discussed only when its behaviour differed from the upper section.

4.1 Initial Parameters for the Sensitivity Study

The wall assembly used to conduct the parametric studies was the north wall test panel from AHHRF House 6, shown previously in Figs. 3.3, 3.4, and 3.5. Table 4.1 lists the base-case parameters used in the sensitivity study. The height, width, and depth correspond to the actual dimensions of the upper section of the test

panel. The flow rate was divided between the upper and lower wall sections according to an analysis of the pressure losses occurring in porous insulation and through cracks. The results of the analysis (presented in Appendix B) estimated that the upper wall section received 2/3 of the total flow passing through the wall cavity.

The mass diffusivity chosen as the initial value corresponds to the value for water vapour diffusing through air ($2.6 \times 10^{-5} \text{ m}^2 \cdot \text{s}^{-1}$). The choice of this mass diffusivity value was discussed in Section 2.1.8. The initial wood moisture content by weight, MC_w , of the wall was determined earlier to be 7%, Forest (1989), which, when using an internal moisture saturation limit of 20%, shown in Fig. 4.1, yielded an initial wall relative humidity of 35%. All temperature, relative humidity, and flow data used in the sensitivity analysis was the actual data recorded at the test house from 26 January to 18 February 1988. The predicted total moisture deposition in each zone (shown in Fig. 3.5) after 550 hours was calculated using the base values listed in Table 4.1 and results are shown in Table 4.2.

4.2 The Effect of Varying the Internal Moisture Limit on Moisture Deposition

The internal moisture limit (IML) was defined in Section 3.3.1.1 as a novel way to define a linear ramp function that specifies the relationship between wood moisture content and relative humidity. The internal moisture limit corresponds to the maximum wood moisture content allowed in the sheathing; however, the IML may or may not correspond to the actual wood fibre saturation point for the sheathing material. The IML's main purpose is to allow for the selection of a partial pressure for water vapour depositing on the sheathing surface. This reflects the fact that the overall average sheathing moisture content might not be the same as the active layer next to the porous medium. As long as the wood moisture content is below the internal moisture limit, then the boundary condition for the sheathing is below saturation. For wood moisture contents above the IML, then the boundary condition for the sheathing is saturation. For example, if the actual wood moisture content was 22%

and the IML was 20%, then the boundary condition for the wall would be held at saturation even though the wood moisture content is less than the fibre saturation point ($\approx 30\% MC_w$).

Moisture deposition is dependent on the partial pressure difference (Δp_w) between the air-vapour flow and the outer cavity wall where deposition takes place. By selecting different IMLs, the partial pressure specified at the outer cavity wall can be altered. This has a direct effect on the amount of moisture absorbed or desorbed from the wall. Assigning a high internal moisture limit to a wall results in more moisture being absorbed by the material than if a low IML is used. A material such as fibreboard sheathing, which readily absorbs moisture, would have a large IML. Materials such as polystyrene sheathing, which does not absorb moisture, would have a low IML, indicating that the material reaches a saturated state very rapidly. In order to study a wide range of possible building materials, four IMLs ranging from 15 to 60% were chosen for comparison. The characteristics of the chosen IML ramp functions are shown in Fig. 4.1. A 20% IML was taken as the base value against which the other IMLs were compared. Reducing the IML to 15% resulted in smaller moisture deposition than for the base 20% IML; increasing the IML to 30% and 60% yielded higher moisture depositions.

4.2.1 The effect of internal moisture limits on wall relative humidity

Figure 4.2 shows how the outer wall cavity relative humidity boundary condition was changed by using different IML ramp functions. At the beginning of the test period, the wall had a wood moisture content of 7%. Using a 20% IML, a wood moisture content of 7% corresponded to an initial wall relative humidity of 35%. Reducing the IML to 15% increased the initial wall relative humidity to 47%. Increasing the IML to 60% reduced the initial wall relative humidity to 12%.

As the test proceeded, moisture began to deposit on the outer cavity wall and be absorbed into the sheathing, which resulted in an increase in the average wood moisture content for the sheathing. An increase in wood moisture content leads di-

rectly to an increase in wall relative humidity, as shown by the relationship in Fig. 4.1. An increase in wall relative humidity decreases the driving force for moisture deposition (Δp_w gets smaller) during exfiltration, and increases the driving force for moisture desorption from the wall during infiltration. This occurs since the wall partial pressure could be greater than the inlet air-vapour partial pressure.

Selecting a small IML (15%) reduces the amount of moisture depositing on the outer cavity wall since the partial pressure difference between the air-vapour flow and the wall is small. The slope of the 15% IML function (shown in Fig. 4.1) is steep indicating that only a small amount of moisture is required to drive the boundary condition to saturation which further reduces the amount of deposition. Moisture is more likely to desorb from the exterior sheathing when a small IML is chosen because the wall partial pressure is more likely to be higher than the inlet partial pressure.

Selecting a large IML (60%), as expected, would have opposite effects to selecting a small IML. A large IML increases the amount of moisture that is able to deposit and subsequently be absorbed into the wall. The increase in wood moisture content is large, but due to the shallow nature of the selected IML function (shown in Fig. 4.1) the progress up the ramp is slow. The wall relative humidity boundary condition changes slowly thereby leaving a large partial pressure difference between the wall and the air-flow.

Figure 4.2 shows how rapidly the wall relative humidity increases for an IML of 15% compared to the gradual increase in relative humidity for 60% IML. Figure 4.2 also shows that for none of the internal moisture limits tested does the outer wall reach saturation (100% relative humidity). Over this period of time, one would not expect to see any visible moisture (either liquid water or frost) at the sheathing/insulation interface.

4.2.2 Choosing an internal moisture limit below the base case 20% IML

One internal moisture limit below the base case IML was used in this sensitivity analysis. Choosing a 15% IML resulted in a ramp function with a steeper slope than the base case, which led to less moisture deposition than for the base case.

Progress up the steep 15% IML ramp function, shown in Fig. 4.1, towards higher wall relative humidities, was rapid, as shown in Fig. 4.2.

Figures 4.3 to 4.8, representing zones 1 to 6 respectively, all show a lower moisture deposition for the 15% IML than for the base case 20% IML. In zone 1, at 550 hours, the 15% IML curve predicted a moisture deposition of 8.3 g, which was 0.7 g less than the 20% IML curve. In zone 2 the difference between the two IML predictions decreased to 0.6 g, but in zone 3 the difference increased to 2.7 g. In zone 4 the difference in predicted depositions between the 15% and 20% IMLs after 550 hours was 0.1 g. In zone 5 and 6 the difference was 0.01 g and 0.02 g, respectively. The effect of decreasing the IML in the lower zones (4, 5, and 6) was similar in nature to zone 1, except that the magnitude of the change was smaller due to the smaller flow rates in the lower wall section.

An interesting consequence of choosing a small IML was that when flow infiltrated through the cavity, the partial pressure of the exterior sheathing became higher than the inlet air-vapour partial pressure. This led to moisture being desorbed from the sheathing. The effects of infiltration-dominated moisture desorption are shown most prominently in zones 2 and 3 on Figs. 4.4 and 4.5 respectively, since these zones were located closer to the exterior crack, which for infiltration was the inlet crack, than zone 1. Zone 1 was completely dominated by exfiltration and showed only a small amount of moisture desorption in the later hours. The reduction in accumulated moisture in zone 2 began at 420 hours although there was a slight reduction in moisture at 310 hours. Up until 420 hours, the moisture deposition in zone 2 was caused by both exfiltration and infiltration, but as the partial pressure of the exterior sheathing rose, the desorption of moisture by the infiltrating air flow began to dominate. In zone 3, almost all of the moisture deposition and desorption was infiltration

dominated, as was discussed in Section 3.3.2, and shown in Fig. 3.19. Because infiltration dominated in zone 3, up until 250 hours infiltration caused deposition but after 250 hours, infiltration caused the desorption of moisture as shown in Fig. 4.5. At the end of the test, 550 hours, the sheathing was drier than at the beginning of the test. The drying of the sheathing was the reason why the moisture deposition predicted by the 15% IML in zone 3 after 550 hours was 2.7 g less than the predicted deposition using the 20% IML (refer to Fig. 4.5).

4.2.3 Choosing an internal moisture content above the base case 20% IML

Choosing an internal moisture limit higher than the standard case meant that the slope of the ramp function became more shallow. Figure 4.1 shows the slopes for the 30% and 60% IMLs as compared to the base case 20% IML. For shallow slopes, a large increase in wood moisture content would be required for a small increase in wall relative humidity. This kept the partial pressure on the wall at a low level, as shown in Fig. 4.2, where the 30% and 60% IML curves increased slowly over time, allowing the driving force for moisture deposition to remain large. The wall relative humidity never reached the point where the corresponding partial pressure was high enough for desorption to occur with infiltrating flow.

In all of the zones, Figs. 4.3 to 4.8, moisture deposition increased when the internal moisture limit was larger than 20%. In zone 1, Fig. 4.3, the increased deposition over the base 20% IML at 550 hours was 0.6 g for the 30% IML and 1.5 g for the 60% IML. In zone 2, Fig. 4.4, the depositions were 0.6 g and 1.3 g greater than the base 20% IML, using 30% and 60% IMLs, respectively. Zone 3 behaved in a different manner than either zone 1 or 2. As discussed in Section 3.3.2, moisture deposition in zone 3 was dominated by infiltration rather than by exfiltration. Figure 4.5 shows that in zone 3 the deposition of moisture when using a 30% or 60% IML was far greater than for the base case 20% IML. At 420 hours, the amount of water deposited decreased in zone 3 and the 20% IML curve began to show desorption. The 30% and 60% IML curves showed moisture deposition for the duration of the

test period with no moisture desorption due to infiltration. This was because the wood moisture content never became high enough to impose a partial pressure on the wall which was higher than the infiltrating partial pressure. Therefore, a driving force for moisture deposition onto the wall always existed, even during infiltration. The moisture deposited in zone 3 after 550 hours for the 30% IML was 3.5 g, which was 2.8 g more than for the 20% IML. For the 60% IML, the maximum amount of moisture deposited was 6.5 g, which was 5.8 g more than for the 20% IML. In zones 2 and 3 the measured moisture depositions were best predicted using the 20% IML, while in zone 1, the 30% IML better predicted the measured results.

The moisture deposition in zones 4, 5, and 6, Figs. 4.6, 4.7, and 4.8 respectively, were not greatly affected by increasing the IML. The maximum difference between the 20% IML curve and the 60% IML curve in zone 4 was less than 0.2 g. In zone 5 the difference in deposition between the 20% IML and the 60% IML was less than 0.02 g. In zone 6, the 60% IML curve predicted a deposition of 0.08 g while the base 20% IML predicted a deposition of 0.04 g. Although the percentage difference in zone 6 appeared to be large (100%), the actual difference was only 0.04 g, a value which is difficult to measure in real walls. The effect of increasing the IML in the lower zones (4, 5, and 6) was similar in nature to zone 1, discussed previously, except that the magnitude of the change was smaller due to the lower flow rates in the lower wall section.

In summary, the internal moisture limit (IML) is the physical link between wood moisture content and relative humidity. The selection of an appropriate IML is dependent on the properties of the material to be modeled. The characteristic behaviour of the IML curves depend greatly on flow rate and flow direction as well as the climatic conditions being modeled. In warm climates infiltration will predominantly remove moisture from the wall cavity while in colder climates moisture deposition is a more common occurrence.

4.3 Dependence of Moisture Deposition on Changes in Distribution of Flow

The amount of moisture depositing in the wall cavity can be influenced by changing the flow distribution through the cavity. For the wall cavity tested in Chapter 3, the flow was initially split such that $2/3$ of the total flow passed through the upper wall section and $1/3$ passed through the lower wall section. This flow distribution was based on the relationship between flow resistance in porous medium and the height of each wall section. Since it has been shown that air-vapour exfiltration and infiltration rates greatly affect the prediction of moisture deposition, it was decided to vary the original flow distribution in order to quantify the changes. Changing the flow distribution corresponded to fixing the internal-external pressure difference and varying the height of the interior leakage site. The total flow rate through the wall cavity was held constant while the upper wall section had its share of the distribution increased by 10% which resulted in a decrease in flow in the lower wall cavity of 20%. An decrease in flow distribution in the upper cavity of 10% resulted in an increase in flow in the lower cavity of 20%.

Figure 4.9 shows the effect of increasing and decreasing the flow rate in zones 1 and 3. By increasing the flow rate in zone 1 by 10%, Fig. 4.9(a), moisture deposition increased from 9.0 g to 10.1 g at 550 hours, an increase of 12%. Furthermore, the moisture deposition was always larger than the base case over the entire 550 hour test period. A decrease in flow rate in zone 1 caused a decrease in moisture deposition for the entire 550 hour test period. At 550 hours, the amount of moisture deposited dropped from 9.0 g to 7.9 g, a decrease of 12%. In zone 1, which was located 140 mm above the interior orifice, moisture deposition was governed by exfiltration, so that as more moist air exfiltrated, more deposition occurred. In zone 3, the effect of increasing flow rate followed a similar trend as that shown in zone 1: increased flow rate led to increased moisture deposition from 0 to 420 hours. However, since zone 3 was located close to the exterior leakage site (50 mm away), the deposition of moisture was dominated by infiltration rather than by exfiltration. In Fig. 4.9(b), until 300 hours, a 10% increase in flow rate corresponded to an increase

in moisture deposition. After 300 hours, the wall partial pressure became larger than the infiltrating partial pressure and moisture began to be removed from the wall. Accordingly, increased infiltration led to higher rates of desorption, as shown in Fig. 4.9(b), after 420 hours. At 550 hours, the increased flow rate through zone 3 had deposited 0.3 g of water on the outer cavity wall, as opposed to the base case flow rate which deposited 0.7 g.

Decreasing the flow rate through the upper wall section by decreasing the flow distribution by 10% caused a reduction in moisture deposition. In zone 1 the amount of moisture deposited after 550 hours dropped from 9.0 g for the base case to 7.9 g due to the reduced flow rate. In zone 2 the base case deposition after 550 hours was 1.20 g compared to the reduced flow rate deposition of 1.0 g. Zone 3 experienced an increase in moisture deposition at 550 hours because, as mentioned previously, flow in zone 3 was infiltration dominated. The infiltrating flow was removing moisture from the flow in the later hours, as can be seen in Fig. 4.9(b), at a slower rate for the decreased flow rate than for the base flow rate. This left a greater amount of moisture in the sheathing at the end of the test period.

The critical point at which infiltration began to dominate, i.e. desorption became prominent, began sooner for large flow rates than for small flow rates. The reason for this was that with large flow rates more moisture was initially deposited in each zone, thus increasing the wood moisture content. Increased wood moisture content led to higher wall partial pressures which reduced the driving force for moisture deposition during exfiltration but increased the driving force for desorption during infiltration. If large amounts of moisture are deposited early on, then the partial pressure will rise rapidly and infiltration will remove moisture from the wall. If only small amounts of moisture are deposited during periods of exfiltration, then the partial pressure on the wall will not rise above the infiltrating partial pressure and deposition will occur during infiltration.

As mentioned in the opening paragraph, by changing the flow distribution through the wall, the flow rates in both the upper and lower wall sections change. Figure 4.10 shows the change in deposition in zones 4 and 6 caused by increasing and

decreasing the flow distribution in the upper wall section by 10%. The effect on the lower zones, was that the flow rate was effectively reduced by 20%. For zone 4, Fig. 4.10(a), an increase in flow rate corresponded to an increase in moisture deposition and a decrease in flow rate corresponded to a decrease in moisture deposition. For zone 6, Fig. 4.10(b), the same results hold as for zone 4, except, that the change in deposition is difficult to resolve. Generally, since the lower zones had a smaller overall flow rate than the upper zones, the effects of changes in flow distribution were less pronounced.

4.4 Effect of Changing Mass Diffusivity on Moisture Deposition

The mass diffusivity term, D , is an empirical constant that must be determined for each particular building material. Changing the mass diffusivity can greatly affect the mass flux since mass flux equals the mass diffusivity multiplied by the concentration gradient, as expressed in Fick's Law, Eqn. (2.52). The relationship between the mass diffusivity and the partial pressure gradient is non-linear, as can be seen in Eqn. (2.74), where the mass diffusivity appears in the exponential term of the partial pressure gradient expression. Generally when mass diffusivity is reduced, moisture deposition decreases as less moisture diffuses to the outer wall. When the diffusivity is increased, more moisture will diffuse towards the outer wall and measured deposition should increase. Shown in Fig. 4.11 is the effect of changing mass diffusivity on moisture deposition in zones 1 and 3. The range of diffusivities tested was from one-half to twice the base value of $2.56 \times 10^{-5} \text{ m}^2 \cdot \text{s}^{-1}$.

In zone 1, Fig. 4.11(a), decreasing the base mass diffusivity term by one-half caused the amount of moisture deposited to increase by 0.6 g (6%) at 550 hours. By doubling the base mass diffusivity the amount of moisture deposited on the outer cavity wall decreased by 3.3 g (36%) at 550 hours. These results appear to directly contradict the previous statements that indicated that decreased diffusivity should lead to decreased mass flux and hence less moisture deposition. However, this contradic-

tion can be easily explained. Using a smaller mass diffusivity than the base case did decrease the amount of moisture depositing on the outer cavity wall, but only in the area between the inlet orifice and zone 1 (see Fig. 3.5). Since less moisture had deposited, more moisture remained in the air flow as it entered zone 1. The partial pressure of water vapour in the air flow entering zone 1 was higher than the base case, which made the driving force for moisture deposition ($\partial p_w / \partial x$) in zone 1 large. The amount of moisture depositing in zone 1 increased since the net effect of multiplying the smaller mass diffusivity value by the larger partial pressure gradient, as expressed in Eqn. (2.52), was a larger mass flux than for the base case diffusivity. The reverse argument is true when increasing the mass diffusivity. Increased diffusivity led to more moisture depositing in the area between the inlet and zone 1. The air flow entering zone 1 had less moisture than the base flow and the mass flux term was smaller in overall magnitude although the mass diffusivity term was larger. It can be seen in zone 1, Fig. 4.11(a), that the increase in mass diffusivity had a larger effect on moisture deposition than did the decrease in mass diffusivity because the mass flux—mass diffusivity relationship is non-linear.

Moisture deposition in zone 3 behaved differently than in zone 1. While moisture deposition in zone 1 was exfiltration dominated, in zone 3 moisture deposition and desorption was infiltration dominated because of zone 3's close proximity to the exterior crack. As can be seen by comparing the depositions in zone 1 and zone 3 in Fig. 4.11, the sharp increases in moisture deposition in zone 1 did not correspond to increases in moisture deposition in zone 3. For example, at hours 30 and 430 zone 3 experienced an increase in the amount of moisture deposited due to infiltration, while zone 1 experienced no change.

At first glance, the moisture deposition curves shown for zone 3, Fig. 4.11(b), do not appear to behave in a manner consistent with the arguments presented for deposition in zone 1. A large diffusivity in zone 3 showed a higher moisture deposition than the base case but in zone 1, a large diffusivity resulted in decreased deposition. A similar difference is noted for smaller diffusivities where in zone 1 the deposition was greater than the base case but in zone 3 deposition was less than the base

case. These apparent differences from the behaviour in zone 1 can be contributed to the location of zone 3 with respect to the exfiltration and infiltration inlets. Zone 3 was located 700 mm from the interior orifice and 50 mm from the exterior crack (refer to Fig. 3.5). During periods of exfiltration, moisture was able to deposit on 700 mm of wall before reaching zone 3, leaving little moisture in the air-vapour flow to deposit in zone 3. However, during periods of infiltration, moisture can only deposit over 50 mm before reaching zone 3. Therefore, the deposition of moisture in zone 3 due to infiltration can be large. Figure 3.19 shows the contributions to the total deposition from exfiltration and infiltration for the base case mass diffusivity. When the mass diffusivity was reduced to one-half the base value, less moisture was deposited during exfiltration throughout the wall cavity, which left more moisture in the air-vapour flow as it entered zone 3. As shown in Fig. 4.12(a), the deposition in zone 3, although not dominated by exfiltration, became more influenced by exfiltration as compared to the base case diffusivity (Fig. 3.19). After 380 hours, the total accumulated moisture began to drop. This was due to the infiltrating air-vapour flow removing moisture from the outer cavity wall.

When the mass diffusivity was increased to twice the base value, the moisture accumulation curve in zone 3 became solely infiltration dominated. This is apparent in Fig. 4.12(b), which shows the contributions of exfiltration and infiltration on the total moisture deposition in zone 3. High mass diffusivity drew more moisture onto the lower part of the wall during exfiltration thus leaving little to no excess moisture in the flow to deposit in zone 3. For the same reason, during infiltration, moisture was drawn to the outer cavity wall, and since zone 3 was located close to the infiltration inlet, large amounts of moisture deposited. Although there were certain times when moisture desorbed from the outer cavity wall (310, 430, 500, and 530 hours), the general trend during the test period was for increased deposition. Large amounts of desorption of moisture from zone 3 did not occur for high diffusivities because the partial pressure on the outer cavity wall did not exceed the inlet partial pressure for any great length of time.

As discussed in Section 3.3.1.2, the outer cavity wall partial pressure boundary condition was calculated based on the average moisture deposited in each of the upper zones. By changing the diffusivity, the vertical distribution of the deposited moisture changed. It was shown that for high diffusivities the moisture deposited increased in the regions next to the inlet or outlet cracks. Since zone 1 was located 140 mm from the inlet orifice, the deposition in zone 1 decreased from the base value. In zone 2, which was not discussed earlier, the moisture deposited also decreased since zone 2 was more influenced by exfiltration than infiltration. Zone 3 was shown to have increased deposition due to infiltration. By averaging the depositions in each zone to determine the overall wall boundary condition, the effect of increased deposition in zone 3 is overshadowed by decreased deposition in zones 1 and 2. This effectively keeps the wood moisture content from raising, by way of the IML function, the wall relative humidity condition. The wall partial pressure is kept below the inlet partial pressures for both exfiltration and infiltration, which leads to deposition being dominant as opposed to desorption.

In summary, increasing the mass diffusivity results in increased mass deposition in the region near to the inlet opening and a reduction in mass deposition throughout the rest of the cavity. For decreased mass diffusivity, less moisture will deposit in the region near to the inlet and more will deposit throughout the rest of the cavity. The effects are the same for exfiltration and infiltration.

4.5 The Effect of Changing Wall Height on Moisture Deposition

Since the height of the wall cavity is measured from the interior wall leakage site to the exterior wall leakage site, tall cavities will have the inlet and outlet leakage sites farther apart than shorter cavities. In order to study the effect of increasing the wall cavity height, it was decided to increase the height of only the upper wall section. By doing so, the flow distribution should be modified to account for the increase in flow resistance added to the upper wall section. However, changing the

flow distribution also affects moisture deposition (Section 4.3). In order not to have any conflicting effects, it was decided to fix the flow distribution so that the upper wall section continued to have 2/3 of the total flow. This type of analysis corresponds to allowing the internal-external pressure difference across the cavity to change in order to maintain the base flow distribution.

When comparing the effect of moisture deposition by changing wall heights, it is important to realize the differences contributed by the location of the measurement zone. Moisture deposition in zones which are located close to inlet or outlet openings will be more influenced by the direction of the flow than zones located a far distance from either opening. For the purpose of this comparison, the zones in the upper wall section were fixed relative to the interior wall orifice as shown in Fig. 3.5. Zone 1 was located 140 mm above the interior wall orifice plate and 610 mm from the upper exterior wall crack located at the top of the upper wall section. Zone 3 was located 700 mm from the interior wall orifice plate and only 50 mm from the exterior wall crack. In order to test the effect of increasing wall height, the exterior wall crack was moved progressively further away from the interior orifice. Initially, the upper wall section was 750 mm high. Its height was then increased by 10% to 830 mm and by 20% to 900 mm. This meant the distance between the exterior wall crack and zones 1 and 3 increased by 80 mm and 150 mm, respectively.

Figure 4.13 shows the effect of increasing the height of the upper wall section by 10% and 20%. In zone 1, Fig. 4.13(a), the change in moisture deposition for the increased wall height was less than 0.1 g or 1% of the total deposition recorded. Because zone 1 was located far from the exterior wall crack, moisture deposition was not strongly affected by increasing the wall height, as the deposition in zone 1 was exfiltration dominated. In zone 3, Fig. 4.13(b), the change in wall height, and therefore the location of the exterior crack, did affect moisture deposition because infiltration dominates in this zone. As the exit crack in the upper section was moved further away from zone 3, a decrease in moisture deposition in zone 3 resulted. For the base case wall height of 750 mm, the total predicted deposition after 550 hours was 0.70 g. When the wall height was increased to 830 mm, the predicted deposition

decreased to 0.51 g, a decrease of 0.19 g or 27%. A further increase in wall height to 900 mm reduced the predicted deposition to 0.46, a total decrease of 0.24 g or 34%. As the wall height is increased further, the moisture deposition in zone 3 becomes progressively less affected by infiltration and the moisture deposition profile settles down to a minimum.

The reason for the decrease in the amount of moisture depositing in zone 3 was that as the wall section becomes taller, zone 3 was located progressively further away from the exterior crack. When the flow begins to infiltrate, the exterior crack becomes the inlet crack. During infiltration, moisture which previously deposited on the outer cavity wall 50 mm from the inlet, would still deposit 50 mm into the cavity; however, zone 3 is no longer located 50 mm into the cavity. Zone 3 is still the same distance from the interior orifice but zone 3 is now further away from the top of the cavity. Therefore, less moisture was present in the infiltrating air-vapour flow when it reached zone 3. Exfiltrating flow would continue to deposit the same amount of moisture in zone 3 regardless of cavity height since the position of zone 3 relative to the interior orifice did not change. As the wall height is increased further, the moisture deposition in zone 3 becomes progressively less affected by infiltration and the moisture deposition profile settles down to a minimum dominated by exfiltration.

The model is only sensitive to changes in the wall height for measurement positions close to the inlet or outlet cracks.

4.6 The Effect of Changing Cavity Width on Moisture Deposition

Changing the width of the cavity also affects the amount of moisture depositing within the wall cavity. A change in cavity width affects flow velocity and the method which is used to calculate the wood moisture content which is then used in determining the outer cavity wall boundary condition.

As a wall cavity is made narrower, the flow velocity increases for the same given pressure differential across the wall. This occurs because the same amount of

flow must now pass through a smaller cross-sectional area. By increasing the flow velocity, moisture is pushed further along the cavity before diffusing to the outer cavity wall. In Fig. 4.14 the mass depositions in zones 1 and 3 are shown as the wall width is reduced from 340 mm by one-half cavity depth to 295 mm and then one full cavity depth to 250 mm.

In zone 1, Fig. 4.14(a), the net effect of decreasing the wall cavity width was negligible. The maximum difference in moisture deposition between the 340 mm cavity (full width) and the 250 mm cavity was less than 0.5 g. Since the maximum amount of moisture deposited in zone 1 was 9.0 g, the difference in moisture deposition was less than 5%. In zone 3, Fig. 4.14(b), a decrease in cavity width corresponds to a decrease in moisture deposition. This was again due to deposition in zone 3 being dominated by infiltration and the cavity wall boundary condition being such that infiltration led to moisture desorption. Increased velocity through the upper wall section added to the increase in moisture deposition shown in zone 1, Fig. 4.14(a), and the increase in moisture desorption shown in zone 3, Fig. 4.14(b).

A change in wall width also changes the mass of wall used in determining the wood moisture content. Wood moisture content is the weight of water contained in a sample of initially dry wood. If the volume of wood used in determining the wood moisture content decreases then a small amount of water added to the wood sample would correspond to a large increase in wood moisture content. Increasing the wood moisture content affects the wall relative humidity and hence the wall's partial vapour pressure boundary condition. This reduces the partial pressure gradient driving deposition during exfiltration and increases the desorption during infiltration.

The analysis shows that the model is weakly dependent on cavity width. Thus cavity widths need only be determined to less than 1/2 cavity depth to ensure a reasonably realistic solution.

4.7 Summary of Sensitivity Study

The results of the sensitivity study indicate four main items:

- Moisture deposition is highly sensitive to the proper selection of an internal moisture limit. The ideal range for IML appears to be between 20 and 30%. Internal moisture limits above 30% should not be used since they are unable to reasonably model moisture deposition.
- Changing the distribution of flow between the upper and lower wall sections affects the amount of deposition occurring. Flow rates must be accurately known in order to ascertain reasonable moisture deposition predictions.
- Mass diffusivity affects moisture deposition throughout the entire cavity. Increasing the diffusivity increases moisture deposition near the inlets and reduces deposition further along the cavity.
- Varying the physical cavity properties, height and width, did not greatly affect the deposition of moisture. Altering the cavity height only affected moisture deposition during infiltration in the zone closest to the exterior crack. Narrow cavities show increased moisture deposition although the effect of reducing the cavity width by one cavity depth was not significant.

Table 4.1 Base case parameters used in the sensitivity analysis for the north wall test panel, upper and lower sections.

Symbol		Upper Wall Cavity	Lower Wall Cavity
<i>H</i>	Height	0.75 m	1.55 m
<i>L</i>	Width	0.34 m	0.34 m
<i>d</i>	Depth	0.09 m	0.09 m
Division of Flow Rate (percentage of total flow)		67	33
IML	Internal Moisture Limit	20%	
<i>D</i>	Mass Diffusivity	$2.56 \times 10^{-5} \text{ m}^2 \cdot \text{s}^{-1}$	

Table 4.2 Mass accumulation predicted on the outer cavity wall after 550 hours using the base case parameters.

Zone Number	Predicted Mass Deposition (g)
1	9.02
2	1.20
3	0.67
4	2.90
5	0.15
6	0.04

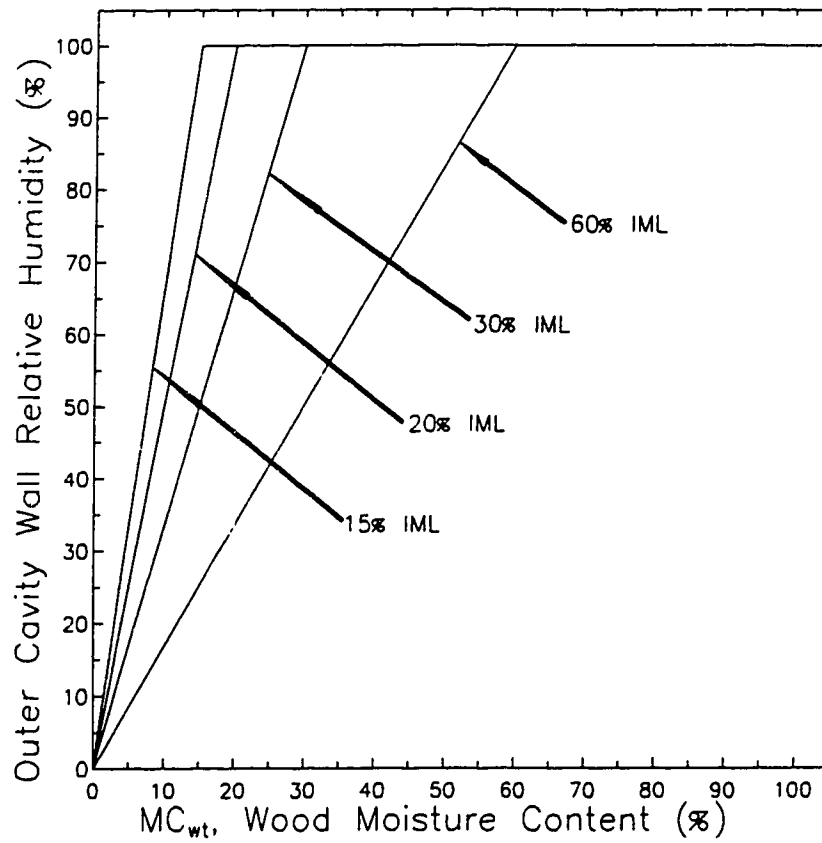


Figure 4.1 The internal moisture limit ramp functions used for comparing the sensitivity of the moisture deposition model to changes in the outer cavity wall boundary conditions.

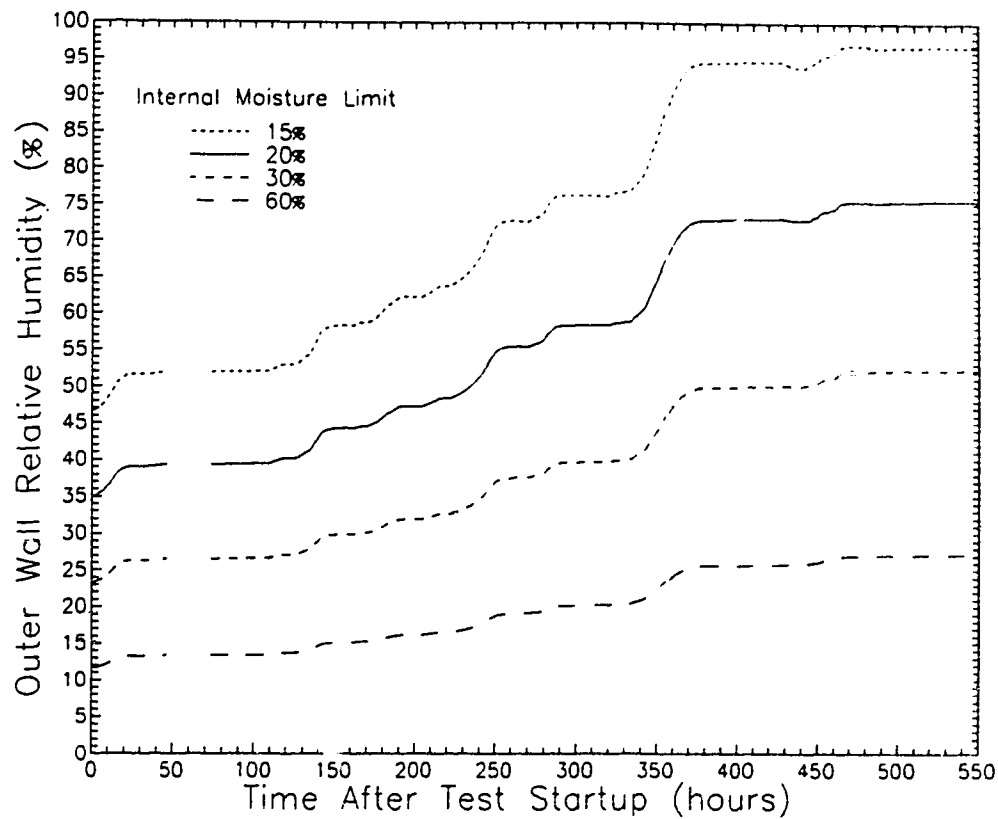


Figure 4.2 A comparison of the relative humidity boundary conditions for various internal moisture limits used in the sensitivity studies. Each curve corresponds to a prescribed internal moisture limit for the upper wall section where the base case has an internal moisture limit of 20%.

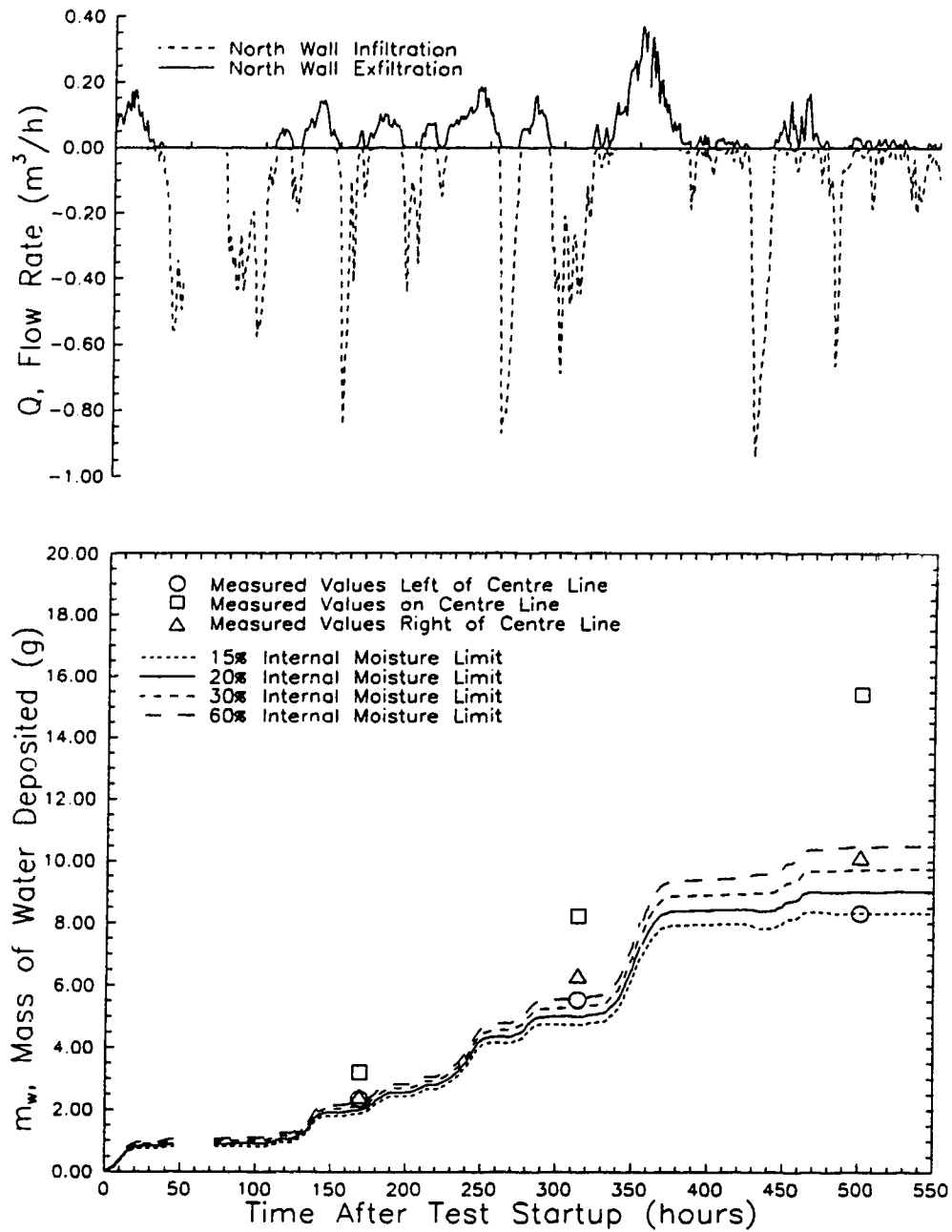


Figure 4.3 Cumulative moisture deposition in zone 1 as the internal moisture limit is increased from 15% to 60%. The upper cavity had 2/3 of the total flow shown in the upper graph.

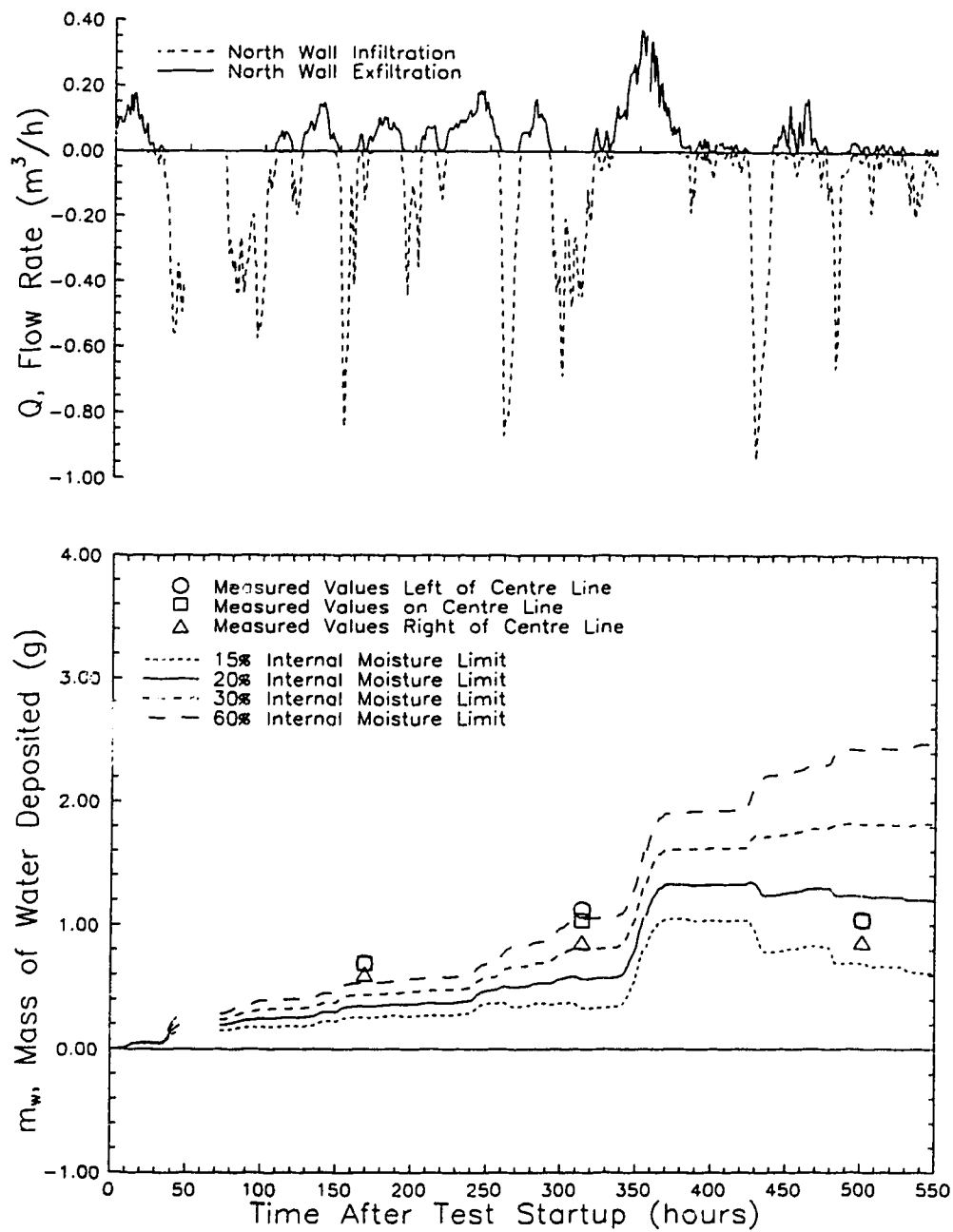


Figure 4.4 Cumulative moisture deposition in zone 2 as the internal moisture limit is increased from 15% to 60%. The upper cavity had 2/3 of the total flow shown in the upper graph.

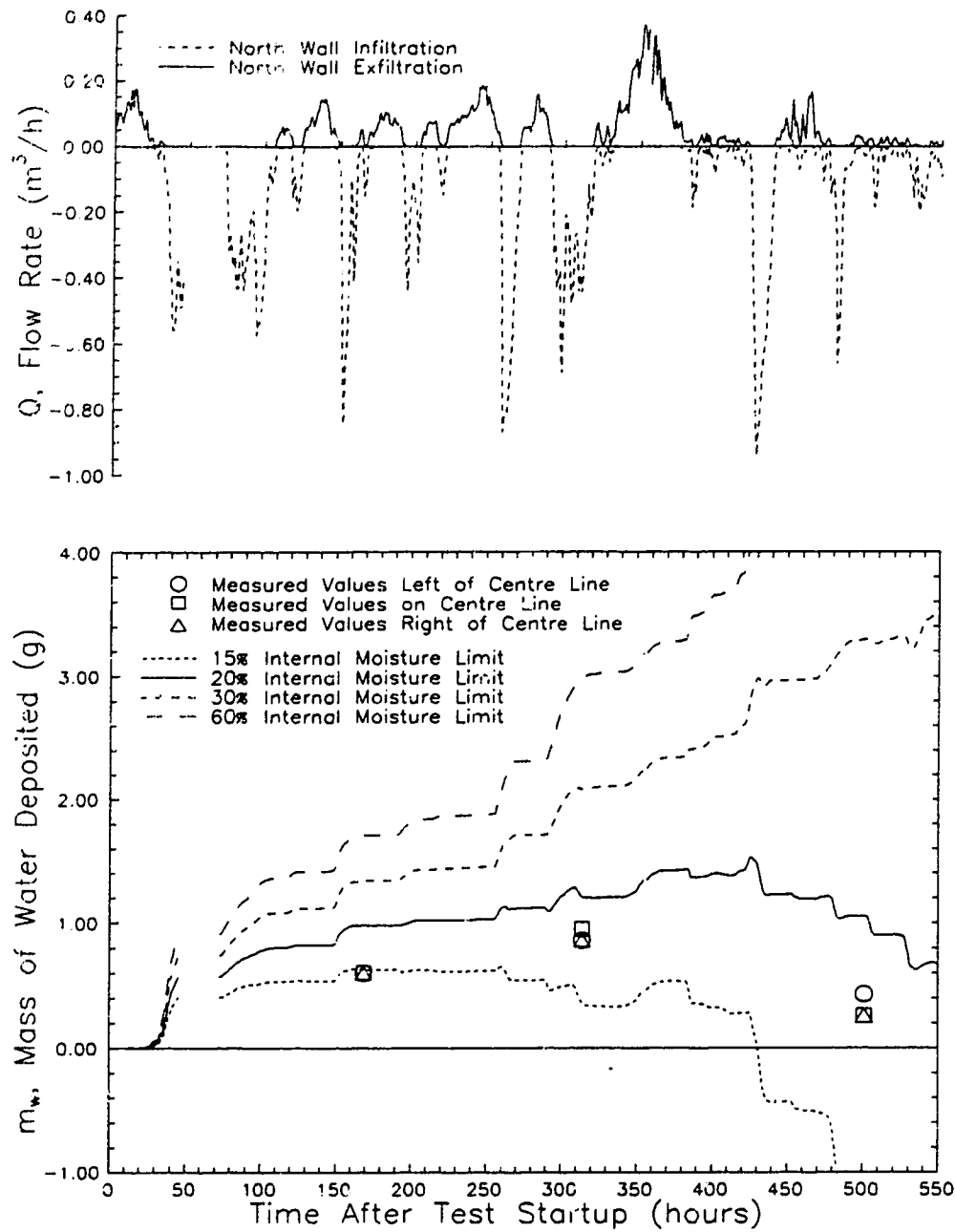


Figure 4.5 Cumulative moisture deposition in zone 3 as the internal moisture limit is increased from 15% to 60%. The upper cavity had 2/3 of the total flow shown in the upper graph.

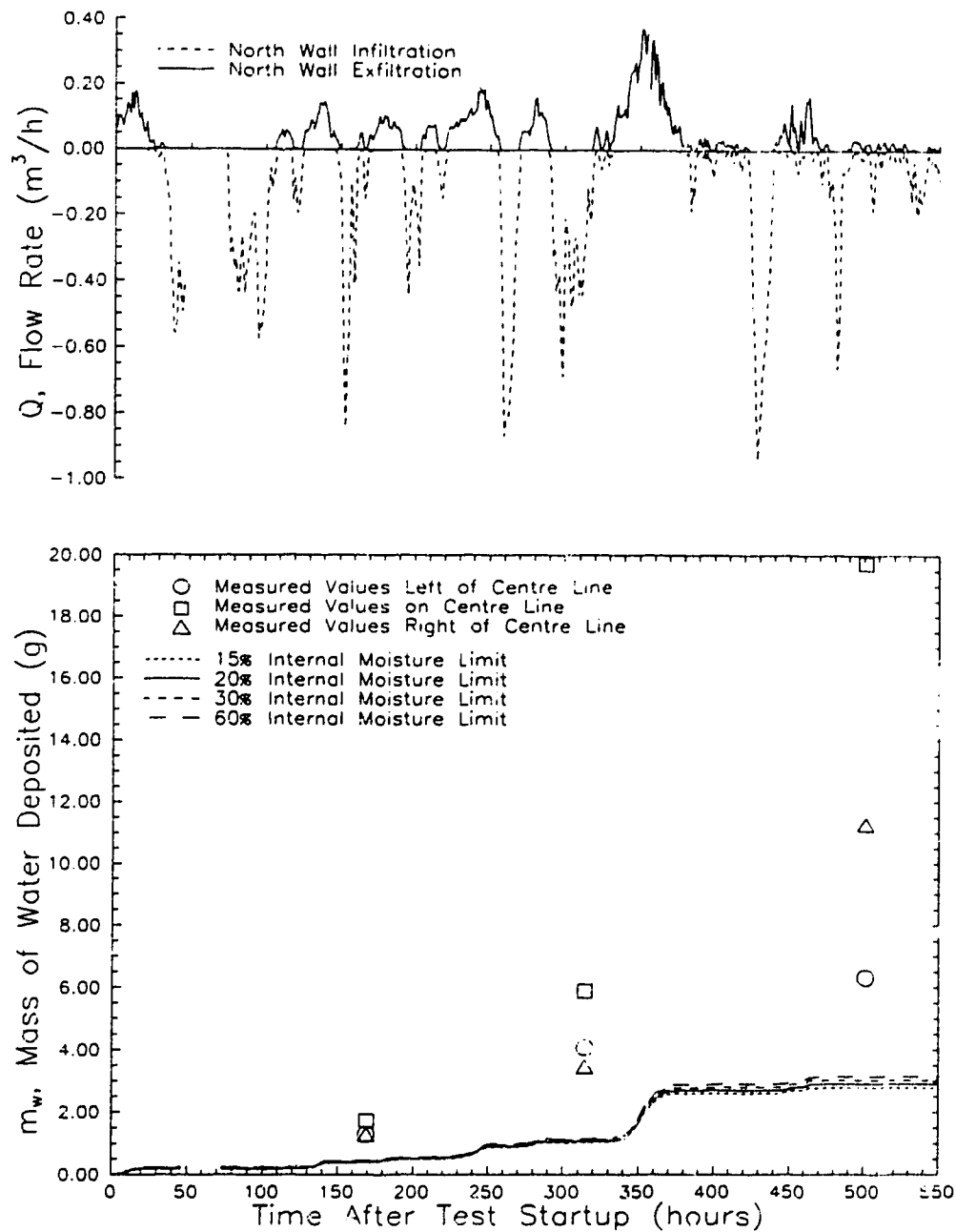


Figure 4.6 Cumulative moisture deposition in zone 4 as the internal moisture limit is increased from 15% to 60%. The lower cavity had 1/3 of the total flow shown in the upper graph.

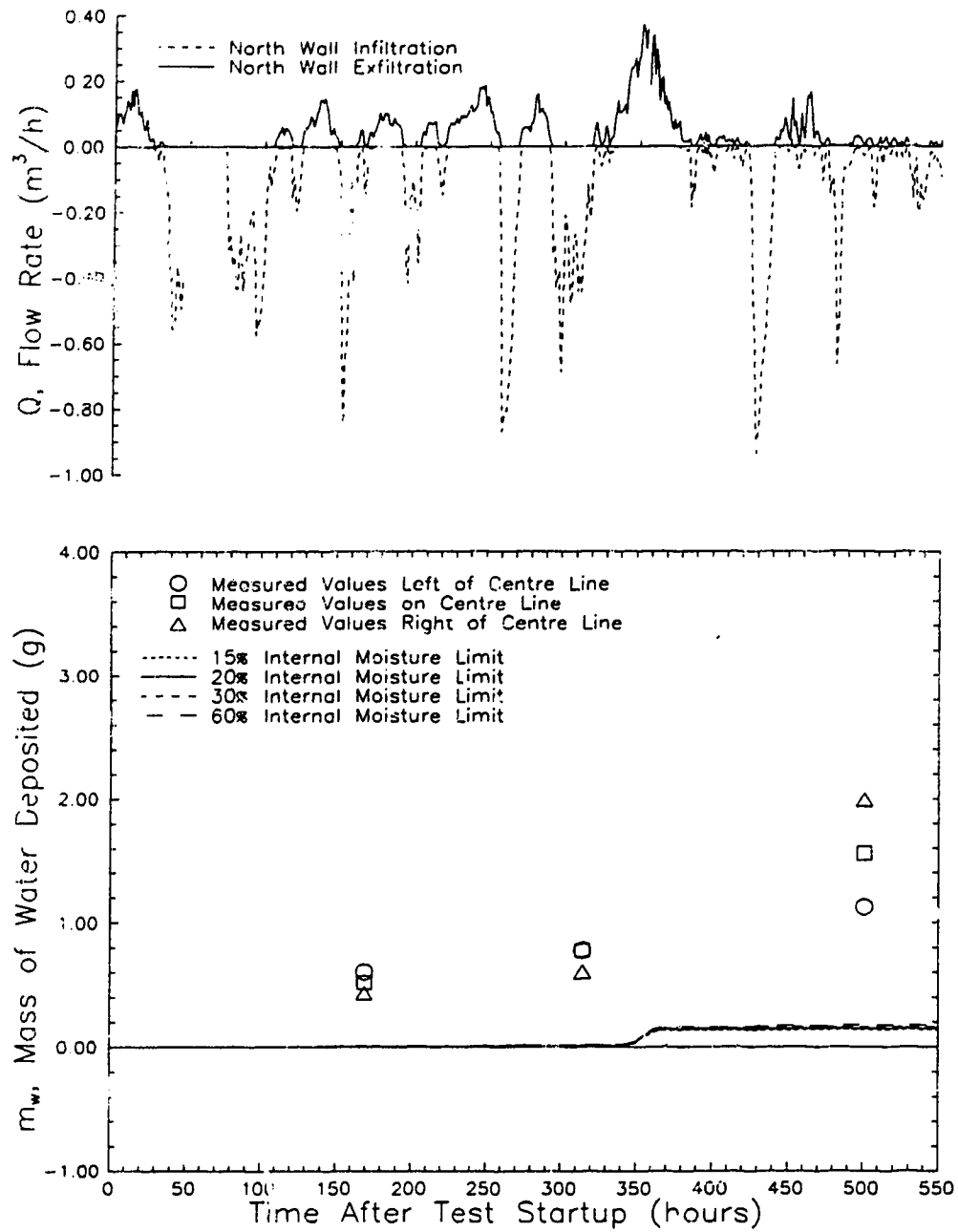


Figure 4.7 Cumulative moisture deposition in zone 5 as the internal moisture limit is increased from 15% to 60%. The lower cavity had 1/3 of the total flow shown in the upper graph.

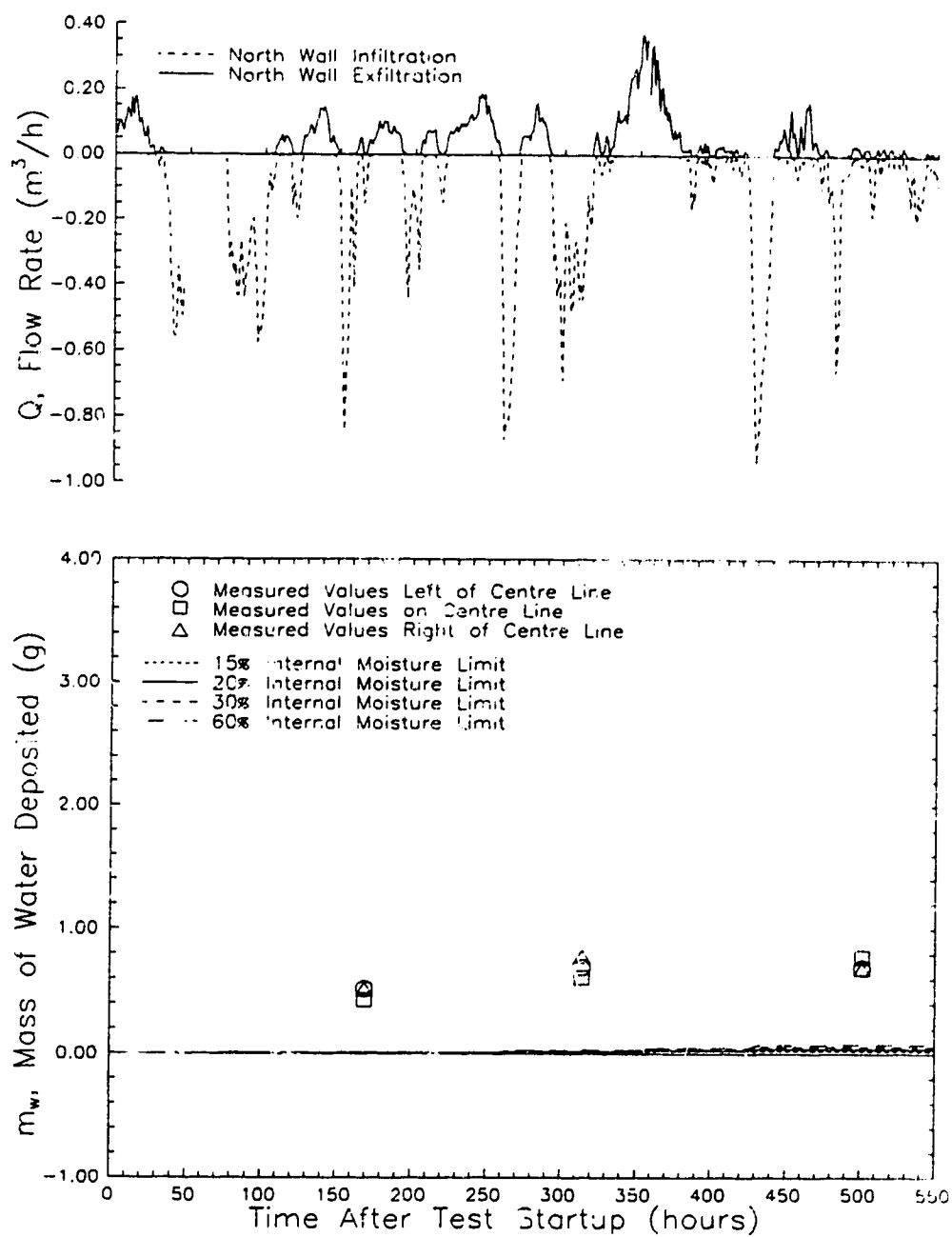


Figure 4.8 Cumulative moisture deposition in zone 6 as the internal moisture limit is increased from 15% to 60%. The lower cavity had 1/3 of the total flow shown in the upper graph.

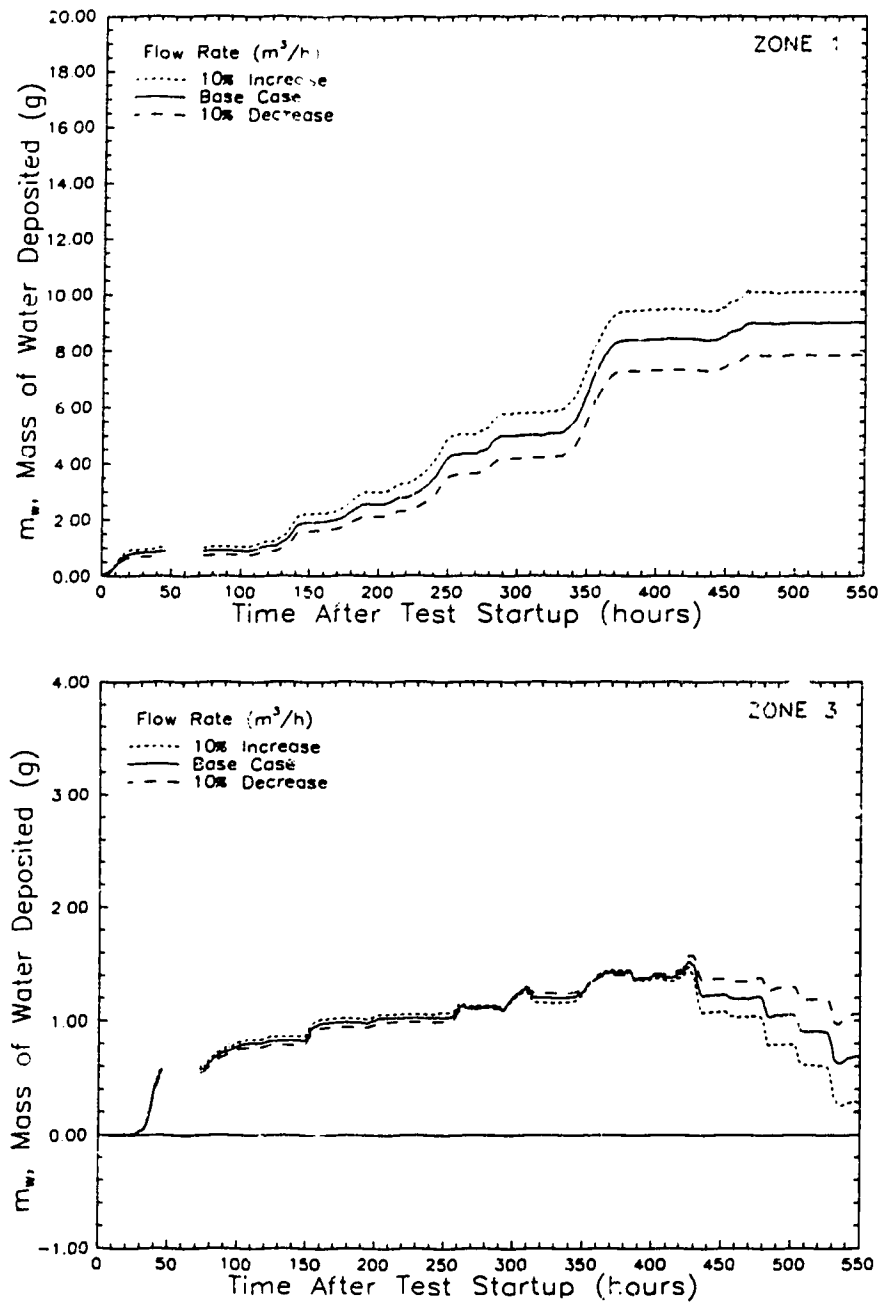


Figure 4.9 Cumulative moisture deposition in (a) zone 1 and (b) zone 3 for increasing and decreasing the total flow rate by 10%. An increased flow rate in the upper wall section increases moisture deposition and moisture evaporation. (IML = 20%)

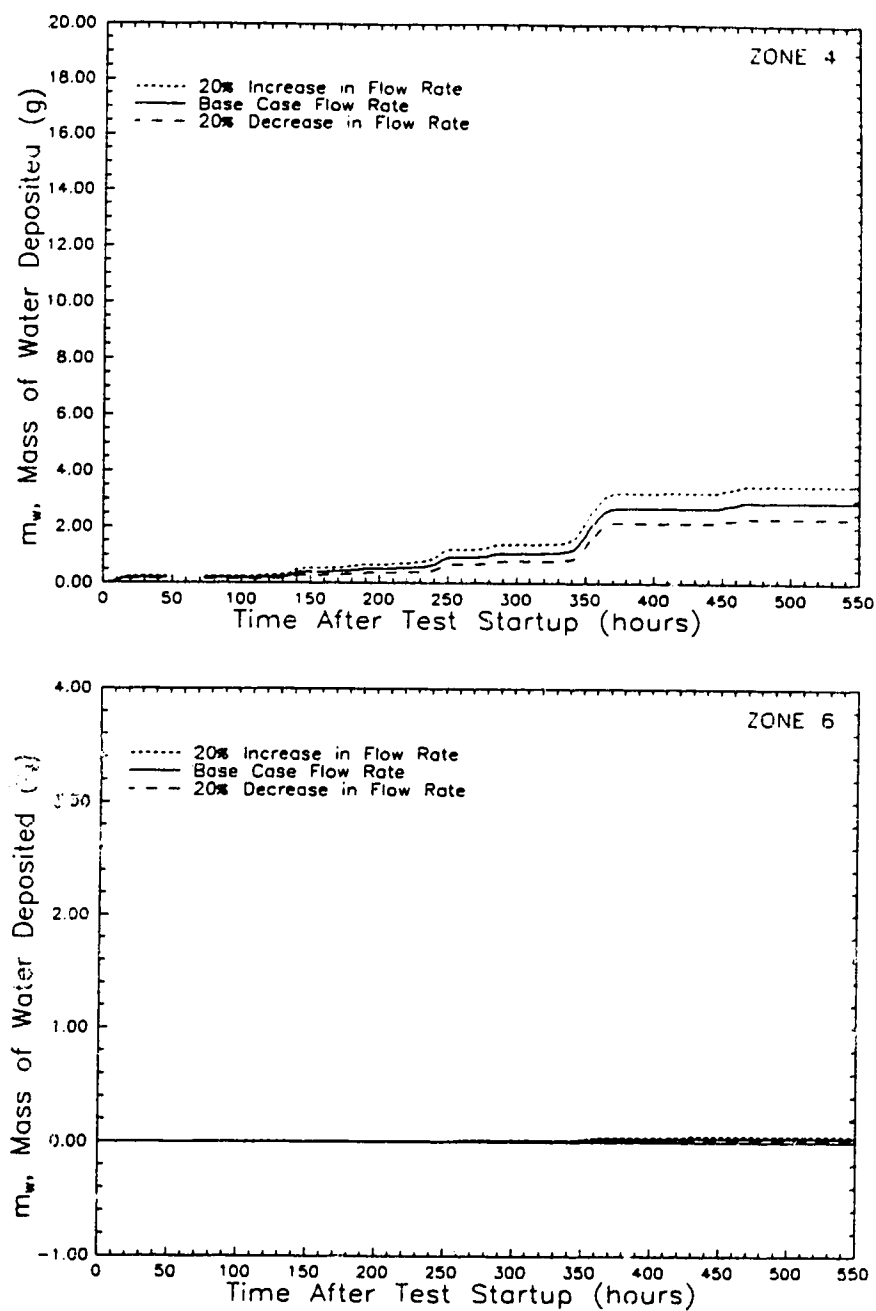


Figure 4.10 Cumulative moisture deposition in (a) zone 4 and (b) zone 6 for increasing and decreasing the total flow rate by 10%. Increasing the flow in the lower wall section correspondingly decreases the flow in the upper wall section.

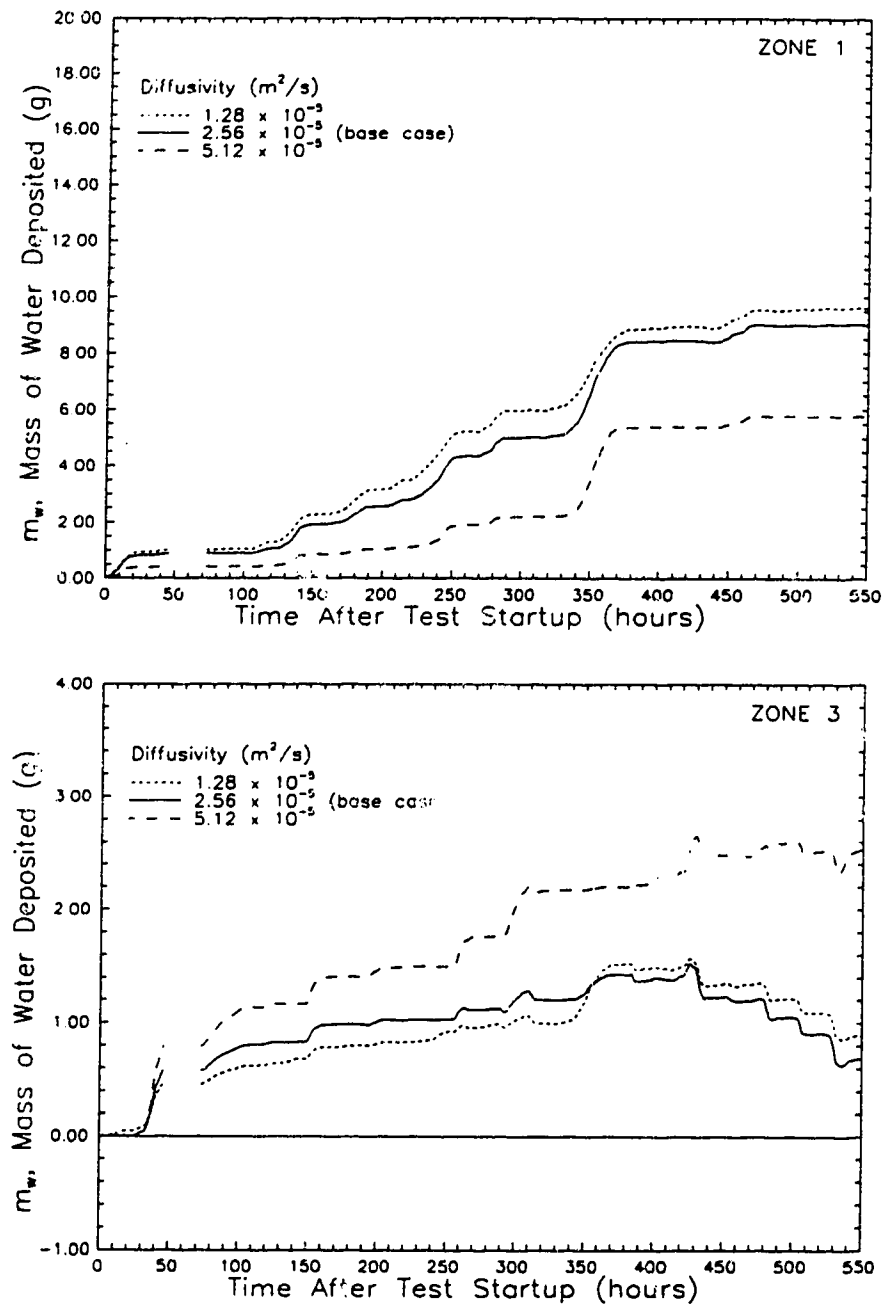


Figure 4.11 Cumulative moisture deposition in (a) zone 1 and (b) zone 3 for doubling and halving the mass diffusivity (D). Deposition in zone 1 is dominated by exfiltration while deposition in zone 3 is dominated by infiltration. (IML = 20%)

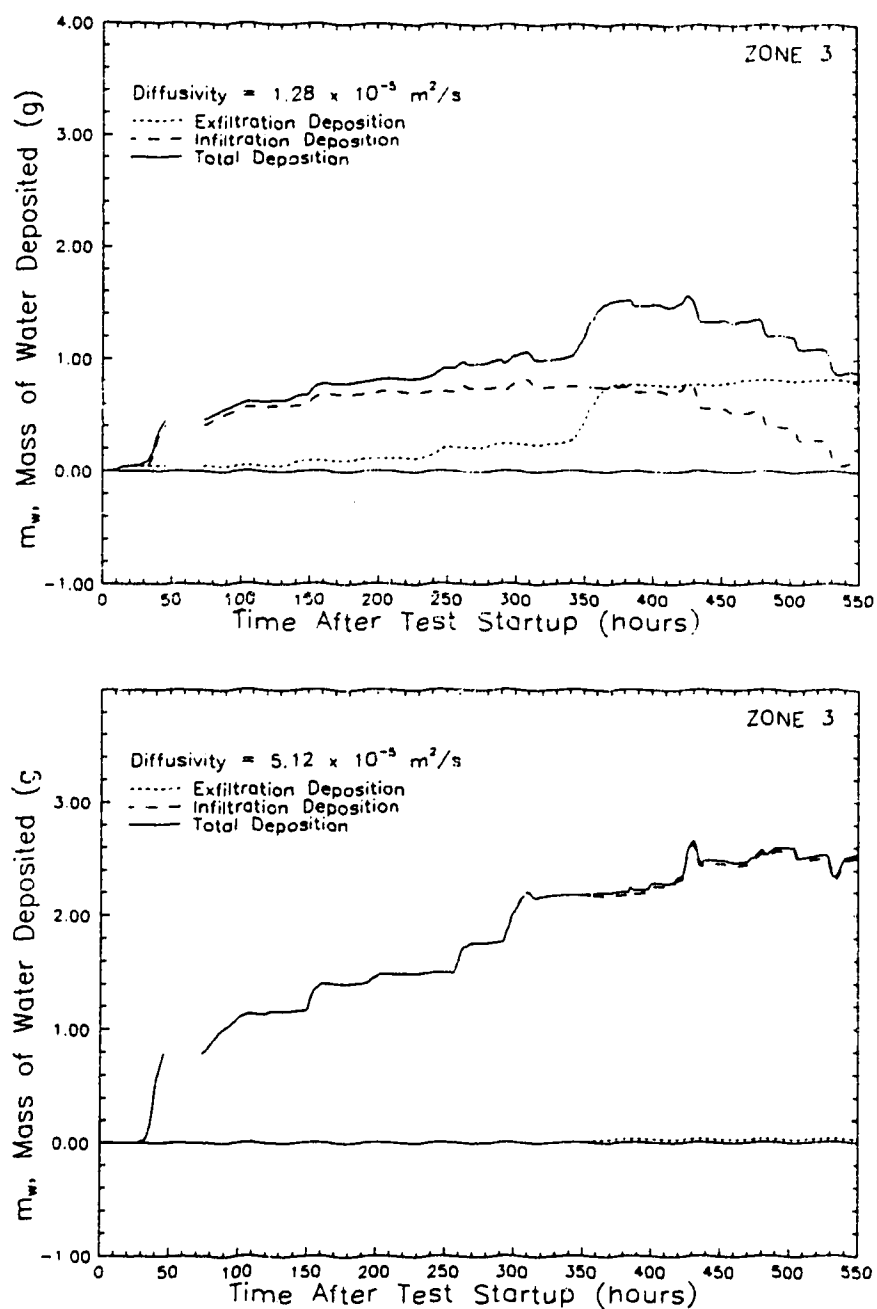


Figure 4.12 Cumulative moisture deposition in zone 3 for (a) one-half and (b) twice the standard mass diffusivity. Each graph shows the contribution to the total moisture deposition by exfiltration and infiltration. For low diffusivities exfiltration is prominent. For high diffusivities moisture deposition by infiltration dominates.

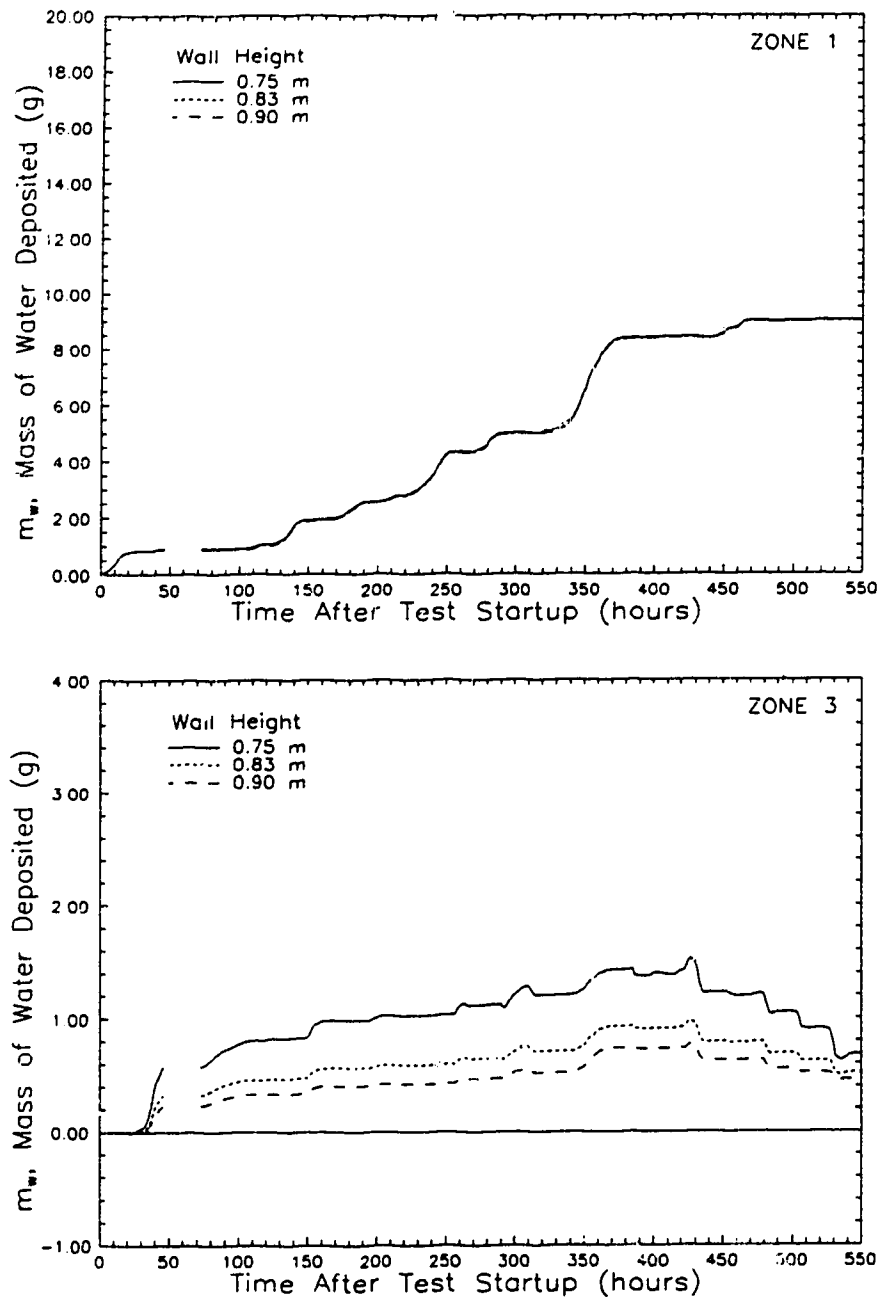


Figure 4.13 Cumulative moisture deposition in (a) zone 1 and (b) zone 3 for increasing wall height. Increasing the wall height moves zone 3 further from the upper leakage site and therefore reduces the effect of infiltration on moisture deposition. Zone 1 is unaffected by changing the wall height. (IML = 20%)

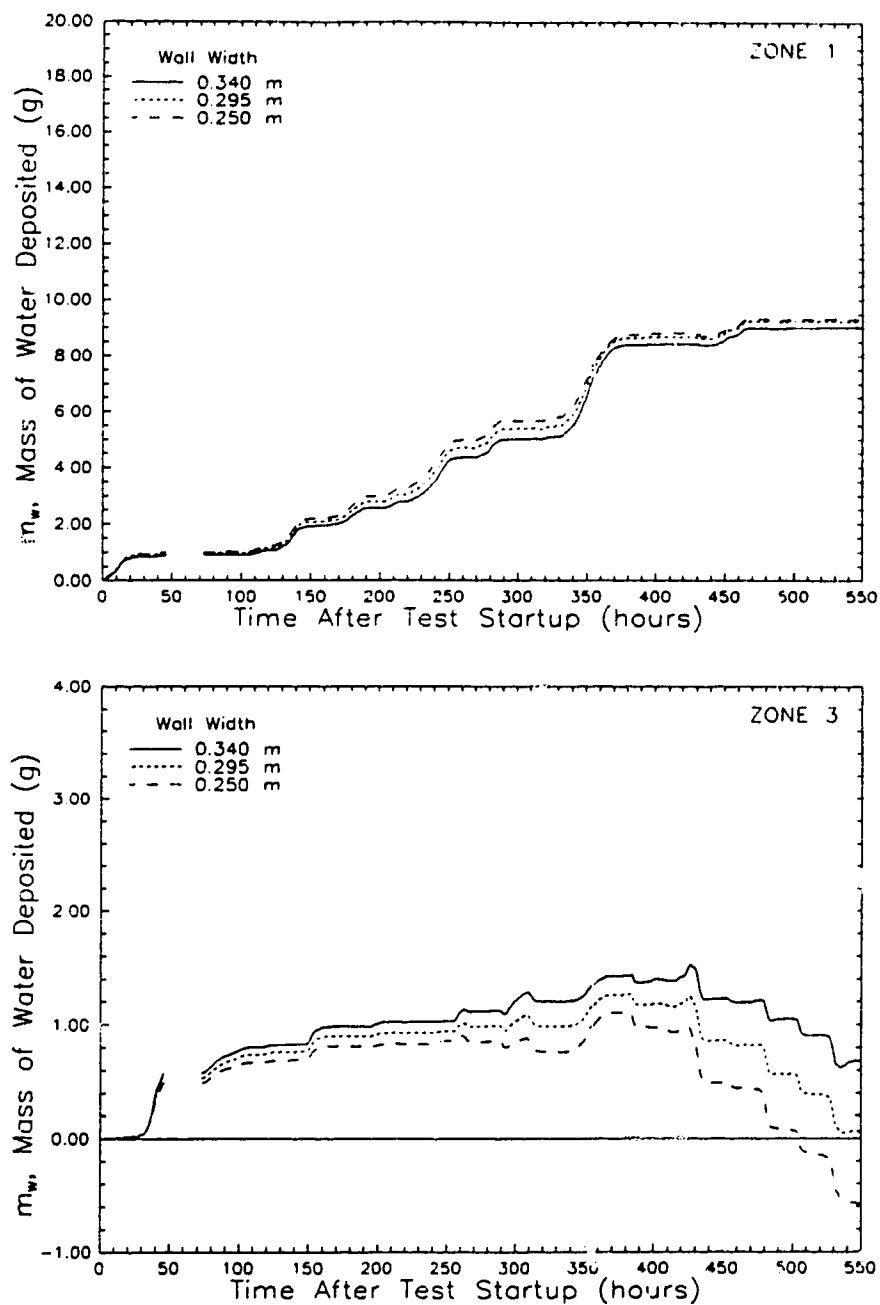


Figure 4.14 Cumulative moisture deposition in (a) zone 1 and (b) zone 3 for decreasing cavity width. A narrower cavity increases the mass flux causing increased deposition in the lower zone and increased evaporation in the upper zone. (IML = 20%)

CHAPTER 5

CONCLUSIONS AND RECOMMENDATIONS

A model capable of predicting the heat transfer and moisture deposition in a porous medium filled vertical wall cavity with forced air flow was developed. It has been shown that a reasonable prediction of moisture deposition can be obtained by using an analytical solution to the governing differential equations coupled with approximate boundary conditions.

The test data used to verify the model was initially part of a larger study of the effects of high indoor humidity in cold climates. The wall test data was not recorded with the intention of producing a moisture deposition model and thus some key aspects were missing (exact location of exit cracks and amount of flow through each exit crack). However, although the data was not "ideal", the model was able to track the moisture deposition trends inherent in the measured data and closely predict the actual depositions. The model is capable of comparing the relative differences in moisture deposition within wall cavities subjected to varying external and internal conditions.

Some observations and conclusions arising from the study are:

Heat Transfer Model

1. Walls subjected to a forced internal flow have a different temperature profile in the thermal developing region than that predicted by steady-state theory. After the flow has become fully developed, conduction is the only means of heat transfer from one side of the cavity to the other and the resulting temperature profile is linear. For the wall cavity studied, which typically had an internal flow velocity less than $0.04 \text{ m}\cdot\text{s}^{-1}$, the flow became thermally developed in less than $1/3$ of the cavity height, and therefore, steady-state theory can be used.

2. The solution to the analytical equation for the temperature profile (Eqn. (2.36)) and the temperature profile gradient (Eqn. (2.37)) in a porous medium required a minimum of 4 terms in the summation (in addition to the steady-state term) in order to yield results within 5% of the exact solution, calculated using 20 terms. Physical cavity geometry, flow rate, and properties of the porous medium greatly influenced the number of terms required for convergence.
3. The modified ASHRAE-based steady-state temperature model, which included the effects of solar radiation but not internal flow, predicted internal wall cavity surface temperatures as effectively as the present heat transfer model which includes the effects of internal forced convection as well as solar radiation.

Moisture Deposition Model

4. The infinite series solution for the partial pressure profile of water vapour (Eqn. (2.73)) and the partial pressure gradient (Eqn. (2.74)) in a porous medium filled vertical cavity required a minimum of 4 terms in the summation. The error in partial pressure was less than 2% when using four terms, as compared to the base solution which used 20 terms.
5. The assumption that moisture will tend to deposit on the exterior sheathing, at the insulation/sheathing interface, has been shown to be correct for most weather conditions. The vertical distribution of moisture on the wall indicates that the majority of moisture is deposited, either by exfiltration or infiltration, close to the point of entry of the air-vapour flow.
6. The deposition of moisture has been shown to be very sensitive to variations in flow rate. The flow rate through the cavity must be accurately known in order to produce reasonable results.

7. The new concept of using an internal moisture limit, which links the overall average wood moisture content of the exterior sheathing to a relative humidity boundary condition, appears to be capable of modelling the performance of a real wall subjected to increasing and decreasing moisture content.
8. The mass deposition model has been shown to be valid over a wide range of inlet relative humidities and wall surface temperatures. Although the model was verified with data that suggested that deposition could occur within the insulation for a quarter of all measured hours, the model was able to predict reasonable moisture depositions in the upper wall section. This leads to the conclusion that the model is more flexible than would appear from its boundary condition limits and is able to function under conditions more severe than indicated. The moisture deposition model can be used in the wide range of environmental conditions found in Canada.

Recommendations

1. A method of selecting the correct internal moisture limit for various types of sheathing has not been formulated. More studies are required in this area.
2. An experiment should be conducted in which the wall cavity design more closely resembles the assumptions used in developing the model (i.e. two isothermal sides, one side impermeable, air flow entering cavity with a uniform profile). This would allow for a more rigorous verification of the heat and mass transfer models.
3. The moisture deposition model is well suited for parametric studies of differing wall assemblies. Comparisons can be made between a "standard" wall configuration and altered wall configurations in order to determine the amount of change in moisture deposition each alteration causes.

4. The moisture deposition model depends heavily on knowing the air-vapour flow rate through the wall cavity. For most applications, the exact flow data is not known, simply because field testing to obtain flow data is not practical. However, by utilizing an air infiltration model which can predict air flows through walls, the usefulness of the moisture deposition model can be enhanced. An air infiltration model particularly well suited for this application is being developed by Walker (1991). Walker's single zone air infiltration model calculates the pressure differential across each element of the building envelope (ie. open doors, open windows, flues, ceiling, floor, and walls). The mass flow of air through each part of the building envelope can then be calculated from the pressure differential.

REFERENCES

- ASHRAE (1968): "Proposed Procedure for Determining Heating and Cooling Loads for Energy Calculations — Algorithms for Building Heat Transfer Subroutines." American Society of Heating, Refrigerating and Air-Conditioning Engineers, Inc., New York. pp. 35.
- ASHRAE (1988): **Equipment Handbook**, American Society of Heating, Refrigeration and Air Conditioning Engineers, Inc. Atlanta, GA.
- ASHRAE (1989): **Fundamentals Handbook, S.I. edition**. American Society of Heating, Refrigeration and Air Conditioning Engineers, Inc. Atlanta, GA.
- Bankvall, C.G. (1972): "Natural Convective Heat Transfer in Insulated Structures," Lund Institute of Technology, Sweden, Report #38.
- Bejan, A. (1980): "A Synthesis of Analytical Results for Natural Convection Heat Transfer Across Rectangular Enclosures." *Int. J. Heat Mass Transfer* 23, pp. 723-726.
- Bejan, A. (1984): **Convection Heat Transfer**. Wiley-Interscience, John Wiley & Sons, New York.
- Burns, P.J. and Tien, C.L. (1978): "Effects of Infiltration on Heat Transfer Through Vertical Slot Porous Insulation." *Energy Conservation in Heating, Cooling, and Ventilating Buildings*. C.J. Hoogendoorn and N.H. Afgan (eds.). Hemisphere Publishing Co., Washington. pp. 93-105.
- Burns, P.J.; Chow, L.C.; and Tien, C.L. (1977): "Convection in a Vertical Slot Filled With Porous Insulation." *Int. J. Heat Mass Transfer* 20, pp. 919-926.
- Forest, T.W. (1989): "Moisture Transfer Through Walls." In: *Proceedings, ASHRAE/DOE/BTECC/CIBSE Conference on the Thermal Performance of the Exterior Envelopes of Buildings IV*, December, 1989, Orlando, Florida. pp. 532-542.
- Jackson, G.W. and James, D.F. (1986): "The Permeability of Fibrous Media." *The Canadian Journal of Chemical Engineering* 64, pp. 364-374.
- Kent, A.D.; Handegord, G.O. and Robson, D.R. (1966): "A Study of Humidity Variations in Canadian Houses." *ASHRAE Transactions*, Vol. 72, Part II, pp. 1.1-1.8.

- Kohonen, R. (1986): "Thermal Effects of Airflows and Moisture on Exterior Wall Structures." In: *Proceedings, ASHRAE/DOE Conference on Thermal Performance of the Exterior Envelopes of Buildings III*, December 1985, Clearwater Beach, FLA. ASHRAE SP 39. Atlanta, GA: ASHRAE, pp. 583-605.
- Lundberg, R.E.; McCuen, P.A. and Reynolds, W.C. (1963): "Heat Transfer in Annular Passages. Hydrodynamically Developed Laminar Flow with Arbitrarily Prescribed Wall Temperatures or Heat Fluxes." *Int. J. Heat Mass Transfer*, Vol. 6, pp. 495-529.
- McCuen, P.A. (1962): "Heat Transfer with Laminar and Turbulent Flow between Parallel Planes with Constant and Variable Wall Temperature and Heat Flux." Stanford University Ph.D. Thesis, Engineering Mechanics.
- Ogniewicz, Y. and Tien, C.L. (1981): "Analysis of Condensation in Porous Insulation." *Int. J. Heat Mass Transfer* 24, pp. 421-429.
- Ojanen, T. and Kohonen, R. (1989): "Hygrothermal (sic) Influence of Air Convection in Wall Structures." In: *Proceedings, ASHRAE/DOE/BTECC/CIBSE Conference on the Thermal Performance of the Exterior Envelopes of Buildings IV*, December 1989, Orlando, Florida. pp. 234-249.
- Perry, R.H. and Chilton, C.H. (eds.) (1973): *Chemical Engineers' Handbook*. McGraw-Hill, New York. 5th edition.
- Powers, D.L. (1979): *Boundary Value Problems*. Academic Press, New York.
- Reynolds, W.C.; Lundberg, R.E. and McCuen, P.A. (1963): "Heat Transfer in Annular Passages. General Formulation of the Problem for Arbitrarily Prescribed Wall Temperatures or Heat Fluxes." *Int. J. Heat Mass Transfer*, Vol. 6, pp. 483-493.
- Schuyler, G.D.; Swinton, M. and Lankin, J. (1989): "WALLDRY—A Computer model that Simulates Moisture Migration through Wood Frame Walls—Comparison to Field Data." In: *Proceedings, ASHRAE/DOE/BTECC/CIBSE Conference on the Thermal Performance of the Exterior Envelopes of Buildings IV*, December 1989, Orlando, Florida. pp. 492-505.
- Sparrow, E.M.; Hallman, T.M.; and Siegel, R. (1958): "Turbulent Heat Transfer in the Thermal Entrance Region of a Pipe with Uniform Heat Flux." *Applied Scientific Research*, Section A, Vol. 7, pp. 37-52.

- Sterling, E.M.; Arundel, A.; and Sterling, T.D. (1985): "Criteria for Human Exposure to Humidity in Occupied Buildings." *ASHRAE Transactions* **91**, Pt. 1, p. 611.
- TenWolde, A. (1985): "Steady State One-Dimensional Water Vapor Movement by Diffusion and Convection in a Multi-layered Wall." *ASHRAE Transactions* **91**, Part 1A, pp. 322-342.
- TenWolde, A. and Suleski, J.C. (1984): "Controlling Moisture in Houses," *Solar Age* **9**, No. 1, pp. 34-37.
- Timusk, J. and Doshi, H. (1985): "Effect of Insulating Sheathing on Heat and Moisture Flow." *Proceedings of the 3rd CSCE Conference on Building Science and Technology*, Toronto, Nov. 1985.
- Tveit, A. (1966): **Measurements of Moisture Sorption and Moisture Permeability of Porous Materials.** Norwegian Building Research Institute, Oslo, Norway. Report no. 45.
- USDA Forest Products Laboratory (1974): **Wood Handbook: Wood as an Engineering Material.**, U.S. Department of Agriculture Forest Service Handbook No. 72, Rev.. Chpt. 3 & 17.
- Walker, I. (1991): Ph.D. Thesis in progress, University of Alberta, Edmonton, Alberta.
- Wilson, D.J. and Dale, J.D. (1985): "Measurement of Wind Shelter Effects on Air Infiltration" In: *Proceedings, ASHRAE/DOE Conference on Thermal Performance of the Exterior Envelopes of Buildings III*, December 1985, Clearwater Beach, FLA. ASHRAE SP 39. Atlanta, GA.

APPENDICES

APPENDIX A

Results of the Moisture Deposition Measurements

The average moisture accumulated over the cavity width is used to compare the output of the moisture deposition model to the actual measured data. The measured data consists of three discrete samples of moisture deposited on five centimetre diameter removable plugs. The mass deposited on each plug was determined by weighing the plug and subtracting the initial dry weight of the plug, Forest (1989).

Tables A.1 to A.3 list the moisture data for the individual plugs and the average moisture deposition values over the cavity width. The columns in the tables were generated as follows (example is for Table A.1, row 1):

Column 3: Actual measured moisture accumulated on each individual plug (g)

Column 4: Mass of moisture deposited on plug surface area (g/m²)

$$\begin{aligned}
 \text{col. 4} &= \frac{\text{mass deposited per plug}}{\text{area of plug}} \\
 &= \frac{0.07}{\pi \frac{0.05^2}{4}} \\
 &= 35.65 \frac{\text{g}}{\text{m}^2}
 \end{aligned}$$

Column 5: Average of column 4 (g/m²)

Column 6: Moisture that would have deposited in the entire zone if the amount of moisture depositing on the plug was representative of the entire zone (g)

$$\begin{aligned}
 \text{col. 6} &= (\text{mass deposited per plug area}) \cdot (\text{zone area}) \\
 &= 35.65 \cdot (0.05 \cdot 0.34) \\
 &= 0.61 \text{ g}
 \end{aligned}$$

Column 7: Average of column 6 (g)

Table A.1 Moisture accumulated at the moisture plugs in the north wall 169 hours (seven days) after testing began.

Zone number	Moisture plug number	Mass deposited on plug (g)	Mass deposited on plug (g/m ²)	Average mass deposited (g/m ²)	Mass spread over wall width (g)	Average mass over wall width (g)
3	1	0.07	35.65		0.61	
	2	0.07	35.65	35.65	0.61	0.61
	3	0.07	35.65		0.61	
2	4	0.08	40.74		0.69	
	5	0.08	40.74	39.05	0.69	0.66
	6	0.07	35.65		0.61	
1	7	0.27	137.51		2.34	
	8	0.37	188.44	156.18	3.20	2.66
	9	0.28	142.60		2.42	
4	10	0.15	76.39		1.30	
	11	0.20	101.86	84.88	1.73	1.44
	12	0.15	76.39		1.30	
5	13	0.07	35.65		0.61	
	14	0.06	30.56	30.56	0.52	0.52
	15	0.05	25.46		0.43	
6	16	0.06	30.56		0.52	
	17	0.05	25.46	28.86	0.43	0.49
	18	0.06	30.56		0.52	
	19	0.05	25.46		0.43	
	20	0.06	30.56	28.86	0.52	0.49
	21	0.06	30.56		0.52	
	22	0.05	25.46		0.43	
	23	0.06	30.56	30.56	0.52	0.52
	24	0.07	35.65		0.61	

Table A.2 Moisture accumulated at the moisture plugs in the north wall 314 hours (thirteen days) after testing began.

Zone number	Moisture plug number	Mass deposited on plug (g)	Mass deposited on plug (g/m ²)	Average mass deposited (g/m ²)	Mass spread over wall width (g)	Average mass over wall width (g)
3	1	0.10	50.93	52.63	0.87	0.89
	2	0.11	56.02		0.95	
	3	0.10	50.93		0.87	
2	4	0.13	66.21	59.42	1.13	1.01
	5	0.12	61.12		1.04	
	6	0.10	50.93		0.87	
1	7	0.64	325.95	393.86	5.54	6.70
	8	0.95	483.83		8.23	
	9	0.73	371.79		6.32	
4	10	0.47	239.37	263.14	4.07	4.47
	11	0.68	346.32		5.89	
	12	0.40	203.72		3.46	
5	13	0.09	45.84	42.44	0.78	0.72
	14	0.09	45.84		0.78	
	15	0.07	35.65		0.61	
6	16	0.08	40.74	40.74	0.69	0.69
	17	0.07	35.65		0.61	
	18	0.09	45.84		0.78	
	19	0.05	25.46	28.86	0.43	0.49
	20	0.06	30.56		0.52	
	21	0.06	30.56		0.52	
	22	0.05	25.46		0.43	
	23	0.06	30.56		0.52	
	24	0.07	35.65		0.61	

Table A.3 Moisture accumulated at the moisture plugs in the north wall 501 hours (twenty-one days) after testing began.

Zone number	Moisture plug number	Mass deposited on plug (g)	Mass deposited on plug (g/m ²)	Average mass deposited (g/m ²)	Mass spread over wall width (g)	Average mass over wall width (g)
3	1	0.05	25.46	18.67	0.43	0.32
	2	0.03	15.28		0.26	
	3	0.03	15.28		0.26	
2	4	0.12	61.12	57.72	1.04	0.98
	5	0.12	61.12		1.04	
	6	0.10	50.93		0.87	
1	7	0.96	488.92	663.78	8.31	11.28
	8	1.78	906.55		15.41	
	9	1.17	595.88		10.13	
4	10	0.73	371.79	731.69	6.32	12.44
	11	2.28	1161.19		19.74	
	12	1.30	662.08		11.26	
5	13	0.13	66.21	91.67	1.13	1.56
	14	0.18	91.67		1.56	
	15	0.23	117.14		1.99	
6	16	0.08	40.74	42.44	0.69	0.72
	17	0.09	45.84		0.78	
	18	0.08	40.74		0.69	
	19	0.05	25.46	32.26	0.43	0.55
	20	0.08	40.74		0.69	
	21	0.06	30.56		0.52	
	22	0.05	25.46	52.63	0.43	0.89
	23	0.19	96.77		1.65	
	24	0.07	35.65		0.61	

APPENDIX B

Determining the Flow Division Between the Upper and Lower Wall Sections.

The total amount of flow going through the wall test panels was measured during testing, however, the flow division or split between the upper section and the lower section of the wall cavity was not known. The wall assemblies were initially designed to reflect the current construction practises found in regular residential walls. As such, the exact leakage sites on the exterior surface were not accurately characterized. It is possible, however, to make certain assumptions regarding flow through cracks and porous medium such that a reasonable flow split can be determined.

The leaks at the top and bottom of the wall assembly were assumed to be long slender cracks running the entire width of the wall cavity (0.34 m) located where the exterior sheathing met the frame of the house. Both the top and bottom leaks were assumed to be identical. Flow through the crack was treated as orifice type flow with a flow coefficient of $n = 1/2$. The indoor-outdoor pressure differential driving the flow through the cavity was not measured during the experiment. This analysis will use 1, 4, and 10 Pa as a reasonable range of driving forces.

The resistances to air flow through the cavity can be modelled as a parallel and series flow arrangement as schematically shown in Figure B.1. For the insulation, assuming laminar Darcy Flow yields the following equation for the pressure drop:

$$\Delta P_m = \frac{w\mu h}{K} \quad (\text{B.1})$$

where ΔP_m is the pressure drop across the porous media [Pa], w is the velocity through the porous media [$\text{m}\cdot\text{s}^{-1}$], μ is the dynamic viscosity [$\text{kg}\cdot\text{m}^{-1}\cdot\text{s}^{-1}$], h is the height of the insulation [m], and K is the permeability of the porous media [$\text{m}^2\cdot\text{s}^{-1}$].

Since the velocity is unknown but the cross sectional area is known, and the desired quantity is the flow rate, by letting $w = Q/A_m$ one arrives with the desired equation:

$$\Delta P_m = \frac{Q}{A_m} \frac{\mu h}{K} \quad (\text{B.2})$$

where Q is the flow rate through the insulation [$\text{m}^3 \text{s}^{-1}$], and A_m is the cross sectional area of the insulation, perpendicular to the flow [m^2]. Equation (B.2) will take the same form for the upper insulation and the lower insulation except for the changing height term.

As mentioned previously, the long slender crack may be treated as flow through a round orifice which has the following characteristic pressure drop equation:

$$Q = C \Delta P_c^n \quad (\text{B.3})$$

where n is the flow coefficient ($1/2$ for turbulent flow), ΔP_c is the pressure drop across the crack [Pa], and C is the orifice coefficient [$\text{m}^3 \text{Pa}^{-n} \text{s}^{-1}$]

The orifice coefficient can be described by

$$C = A_c \left(\frac{2}{\rho} \right)^{\frac{1}{2}} \quad (\text{B.4})$$

where A_c is the area of the crack [m^2]. The pressure drop across the crack now equals,

$$\Delta P_c = \left(\frac{Q}{A_c \left(\frac{2}{\rho} \right)^{\frac{1}{2}}} \right)^{\frac{1}{2}} \quad (\text{B.5})$$

When the total pressure drop from inside to outside is prescribed, it is possible to calculate the amount of flow passing through each leg in Figure B.1. By calculating the pressure drop across the orifices and comparing it to the pressure drop across

the porous insulation one can determine which has the greatest resistance to flow.

This allows for an assessment of the flow distribution. The resistance due to the installed flow meter orifice was neglected since it has no effect on the distribution of flow but only effects the magnitude of the flow. The values shown in Table B.1 were used to calculate the flow distribution.

For a 10 Pa indoor-outdoor pressure drop, the equation representing the series pressure drop in the upper path, shown in Figure B.1, was,

$$\Delta P_{wall} = \Delta P_{insulation} + \Delta P_{crack} \quad (B.6)$$

substituting from Table B.1,

$$\Delta P_{wall} = \frac{Q(1.8 \times 10^{-5})(0.75)}{(0.0306)(31 \times 10^{-10})} + \left(\frac{Q}{(170 \times 10^{-6}) \left(\frac{2}{1.21} \right)^{1/2}} \right)^{1/2} \quad (B.7)$$

hence,

$$10 = 142.3 \times 10^3 Q + 67.6 \sqrt{Q} \quad (B.8)$$

therefore $Q = 6.56 \times 10^{-5} \text{ m}^3 \cdot \text{s}^{-1}$ ($0.24 \text{ m}^3 \cdot \text{h}^{-1}$) in the upper wall section. The calculations for the lower wall section are the same except for the height term, therefore,

$$10 = 294.1 \times 10^3 Q + 67.6 \sqrt{Q} \quad (B.9)$$

and $Q = 3.26 \times 10^{-5} \text{ m}^3 \cdot \text{s}^{-1}$ ($0.12 \text{ m}^3 \cdot \text{h}^{-1}$). It can be seen that, under a 10 Pa driving force, the flow through the upper wall cavity was 2/3 of the total flow and the flow through the lower wall cavity was 1/3 of the total.

The pressure drop across the upper and lower wall sections' porous insulation

was, using the results from the previous equations, were 9.3 and 9.6 Pa, respectively. The main restriction to flow is the insulation not the cracks. The results of the analysis for the other driving forces is presented in Table B.2.

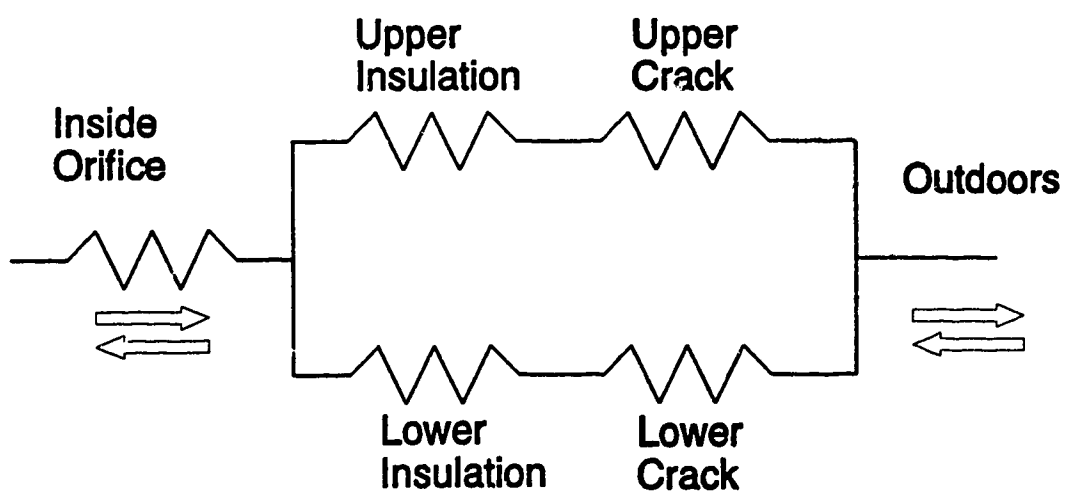


Figure B.1 Schematic of an analogous resistance diagram for flow through the wall cavity.

Table B.1 Physical properties used in evaluating the flow division through the wall cavity.

Symbol	Description	Value
K	Permeability	$31 \times 10^{-10} \text{ m}^2 \cdot \text{s}^{-1}$
μ	Dynamic viscosity	$1.8 \times 10^{-5} \text{ kg m}^{-1} \cdot \text{s}^{-1}$
H	Height: Upper	0.75 m
	Lower	1.55 m
A_c	Crack area	$170 \times 10^{-6} \cdot \text{m}^2$ (0.5 mm \times 340 mm)
A_m	Cross sectional area of the insulation	0.0306 m^2
n	Flow coefficient for turbulent orifice flow	0.5

Table B.2 Summary of flow distributions with various driving pressures and crack sizes.

Driving Pressure [Pa]	Crack Size [mm x mm]	Flow Through the Upper Path
1	0.5 x 340	66.5 %
4	0.5 x 340	67.0 %
10	0.5 x 340	66.8 %

APPENDIX C

ASHRAE-Based Calculations

C.1 Steady-State Heat Transfer

Presented in Section 2.2.7 was the method of determining a heat balance on a wall cavity using the heat flux terms derived in Section 2.2.2 when forced convection exists within the wall cavity. Presented here are the steady-state calculations based on ASHRAE methods for determining the temperatures within a wall cavity while neglecting both solar effects and convective heat transport.

The basic equations will not be derived here but the author refers the reader to the ASHRAE Fundamentals Handbook (1989), Chapters 3 & 22, for a full explanation. Shown below is the overall heat flux equation through a multi-layered wall section typically found in Canadian housing. The indoor and outdoor temperatures are prescribed as are all the thermal resistances of the layers. The overall heat flux is given by,

$$q'' = \frac{T_{room} - T_{out}}{\frac{1}{h_a} + R_I + \frac{d}{k} + R_{II} + \frac{1}{h_d}} \quad (C.1)$$

where by substituting the appropriate values from Table C.1 the heat flux can be calculated to be,

$$q'' = 16.64 \frac{W}{m^2}$$

Using this heat flux and by breaking the main heat flux equation into its constitutive parts and remembering that the heat flux through each layer must be the same as the heat flux through the entire wall, it is possible to determine the temperatures at each interface. These results are presented in Table C.2. The results clearly indicate that the largest temperature drop occurs across the insulation.

Table C.1 Parameters used for the example ASHRAE steady state conduction temperature calculations.

Symbol	Description	Value	Units
h_a	Indoor wall convective heat transfer coefficient for a non-reflective surface, still air, vertical surface	8.29	$\text{W m}^{-2} \text{K}^{-1}$
h_d	Outdoor wall convective heat transfer coefficient for a winter air velocity of 6.7 m s^{-1}	34.08	$\text{W m}^{-2} \text{K}^{-1}$
R_i	Interior wall: thermal resistance for 12.70 mm gypsum wallboard	0.079	$\text{m}^2 \text{K W}^{-1}$
R_u	Exterior wall: thermal resistance for 9.53 mm plywood	0.083	$\text{m}^2 \text{K W}^{-1}$
k	Thermal conductivity of glass fibre insulation	0.0425	$\text{W m}^{-1} \text{K}^{-1}$
d	Wall cavity depth	0.09	m

Table C.2 Calculated temperatures and temperature drops between the layers of a typical multi-layered wall.

Position	Temperature [K]	Temperature Difference [K]	
Room	293.15	2.01	1.32
Inside Wall	291.14		
Inner Cavity Wall	289.82	34.81	1.38
Outer Cavity Wall	255.01		
Outside Wall	253.63	0.48	
Outdoors	253.15		
Total temperature drop from indoor to outdoor		40.00	

C.2 Steady-State Moisture Diffusion

Moisture can travel through a medium either by convective transport or by diffusion. This thesis presents a method to handle the convective transport while ASHRAE presents in their Fundamentals Handbook (1989) a method to calculate the steady-state diffusion of moisture across a wall cavity. A sample calculation using the ASHRAE methods will now be presented.

The ASHRAE method is based on the equation,

$$\dot{m} = MA_v \Delta p_w \quad (\text{C.3})$$

where \dot{m} is the total mass of vapour transmitted, M is the permeance coefficient [$\text{ng} \cdot \text{s}^{-1} \cdot \text{m}^{-1} \cdot \text{Pa}^{-1}$ or perms], and A_v is the area of cross section of the flow path [m^2].

The wall being analyzed is of the same construction as that presented in the thesis. Table C.3 shows the temperature, relative humidity, and partial pressures for the surfaces making up a typical wall. The temperatures were calculated using the steady-state temperature analysis previously described in Appendix C.

Before applying Eqn. (C.3), the pressure drops must be calculated between the room, the outer cavity wall, and the outdoors. From Table C.3 the drop in partial pressure between the room and the outer cavity wall was determined to be 1044.5 Pa. The pressure drop from the outer cavity wall to the outdoors was 42.26 Pa.

From the ASHRAE Fundamentals Handbook, Chapter 22, Table 7, the vapour resistance between the room and the outer cavity wall was determined to be 0.218 perms (gypsum drywall, vapour retarder, insulation). The vapour resistance from the outer cavity wall to the outdoors was calculated to be 0.025 perms (plywood).

The difference between the vapour diffusing to the outer cavity wall and the vapour diffusing away from the outer cavity wall, is the amount of moisture that accumulates at the wall. By applying Eqn. (C.3) one can calculate the vapour diffusing through the wall. These values are shown in Table C.4. The net result is the accumulation of moisture at the outer cavity wall at the rate of $3.1 \cdot 10^9 \text{ kg} \cdot \text{m}^{-2} \cdot \text{s}^{-1}$, which corresponds to about $0.011 \text{ g} \cdot \text{h}^{-1}$ for a typical $2.4 \text{ m} \times 0.4 \text{ m}$ wall.

Table C.3 Temperature, relative humidity, and partial pressures on the surfaces of a typical wall cavity.

Position	Temperature [K]	Relative Humidity [%]	Partial Pressure [Pa]
Room	293.15	50	1169.4
Indoor Wall	291.14		
Inner Cavity Wall	289.82		
Outer cavity wall	255.01	100	124.9
Outdoor Wall	253.63		
Outdoors	253.15	80	82.64

Table C.4 Calculated vapour diffusion through the wall cavity using the ASHRAE steady state method.

	Vapour flow [$\text{kg} \cdot \text{m}^2 \cdot \text{s}^{-1}$]
Moisture diffusing to the outer cavity wall	4.8×10^{-9}
Moisture diffusing away from the outer cavity wall	1.7×10^{-9}
Moisture accumulating at the outer cavity wall	3.1×10^{-9}

C.3 Determining the Mass of Water Entering the Cavity by Convection

The mass of water entering the cavity can be determined by performing a simple psychrometric analysis of the inlet air stream. The incoming air is assumed to have both a constant and uniform temperature, T , and relative humidity, ϕ .

The first step is to determine the humidity ratio defined as,

$$W = 0.62198 \frac{p_w}{p_{atm} - p_w} = \frac{m_w}{m_{air}} \quad (C.4)$$

and expressed in units of kilograms of water per kilogram of dry air. p_w can be determined from the relative humidity since,

$$\phi = \frac{p_w}{p_{ws}} \quad (C.5)$$

and p_{ws} can be determined from the equations presented in Appendix C.4 or from psychrometric tables. The mass of dry air can be determined from,

$$\dot{m}_{air} = \frac{Q}{v} \quad (C.6)$$

where Q is the volume flow rate of air and v is the specific volume of the air. The specific volume of moist air can be calculated from,

$$v = \frac{R_{air} T_{air}}{p_{atm} - p_w} \quad (C.7)$$

By combining Eqns. (C.4), (C.5), and (C.7), the mass of water entering the cavity can be determined by solving,

$$\dot{m}_w = 0.62198 \frac{p_w Q}{R_{air} T_{air}} \quad (C.8)$$

where m_w is the mass of water expressed in kg or kg/time if flow rate is used instead of volume.

EXAMPLE:

The inlet conditions are:

$$\begin{aligned} T_{air} &= 293.15 \text{ K (} 20^{\circ}\text{C)} \\ \phi &= 50\% \\ Q &= 0.11 \text{ m}^3 \text{ h}^{-1} \\ R_{air} &= 287.055 \text{ J kg}^{-1} \text{ K}^{-1} \end{aligned}$$

One can determine the saturated pressure at 293.15 K from psychometric tables.
Using this information one can determine that:

$$p_w = p_{ws} \frac{\phi}{100} = 2338.9 \frac{50}{100} = 1169.4 \text{ Pa}$$

From Eqn. (C.8):

$$\dot{m}_w = 0.62198 \frac{p_w \cdot Q}{R_{air} \cdot T_{air}} = 0.62198 \frac{1169.4 \cdot 0.1102}{287.055 \cdot 293.15} = 0.00095 \frac{\text{kg}}{\text{h}}$$

The amount of moisture entering the cavity by convection is almost 100 times greater than the amount of moisture entering the cavity by diffusion.

C.4 Determining the Saturated Partial Pressure

The saturated partial pressure can be determined by using two equations from ASHRAE Fundamentals Handbook (1989), Chapter 6. One equation is for temperatures below freezing and the other equation is for temperatures above freezing.

The saturated partial pressure for water vapour in air over ice is given by,

$$\ln(p_{ws}) = \frac{C_1}{T} + C_2 + C_3T + C_4T^2 + C_5T^3 + C_6T^4 + C_7\ln(T) \quad (C.9)$$

for the range $173.15 \text{ K} < T < 273.15 \text{ K}$. The saturated partial pressure for water vapour in air over liquid water is given by,

$$\ln(p_{ws}) = \frac{C_8}{T} + C_9 + C_{10}T + C_{11}T^2 + C_{12}T^3 + C_{13}\ln(T) \quad (C.10)$$

for the range $273.15 \text{ K} < T < 473.15 \text{ K}$. The coefficients C_1 to C_{13} are defined in Table C.5.

The partial pressure at any point within the cavity is given by,

$$\frac{\partial p_w(x, z)}{\partial x} = (p_{inlet} - p_{w, c}) \sum_{n=1}^{\infty} \frac{-2 \sin \lambda_n}{d} \sin\left(\frac{\lambda_n x}{d}\right) \exp\left[-\frac{D \lambda_n^2 z}{w d^2}\right] \quad (C.11)$$

which was developed in Section 2.3.

Table C.5 Values of the coefficients used to determine the water vapour saturation pressure and gradient.

Coefficient	Value
C_1	-5674.5359
C_2	6.3925247
C_3	$-0.9677843 \cdot 10^{-2}$
C_4	$0.62215701 \cdot 10^{-6}$
C_5	$0.20747825 \cdot 10^{-8}$
C_6	$0.9484024 \cdot 10^{-12}$
C_7	4.1635019
C_8	-5800.2206
C_9	1.3914993
C_{10}	-0.04860239
C_{11}	$0.41764768 \cdot 10^{-4}$
C_{12}	$-0.14452093 \cdot 10^{-7}$
C_{13}	6.5459673

APPENDIX D

Estimating the Amount of Energy Released by Condensation

In Section 2.1.4 it was stated that the effect of latent heat due to condensation and subsequent freezing of water vapour was to be neglected in the development of the moisture diffusion model. In order to substantiate this claim, an estimate of the amount of energy released by the change in state of the depositing moisture will be calculated and compared to steady-state conduction (Appendix C.1)

In zone 1 the maximum measured moisture deposition was 15.4 g after 501 hours of testing. This corresponded to an average deposition rate of $31 \times 10^{-6} \text{ kg} \cdot \text{h}^{-1}$. If this deposition rate occurred over the entire wall ($0.75 \text{ m} \times 0.34 \text{ m} = 0.255 \text{ m}^2$), the deposition flux would be $3.4 \times 10^{-8} \text{ kg} \cdot \text{m}^{-2} \cdot \text{s}^{-1}$.

The average heat of fusion for water is $2500 \text{ kJ} \cdot \text{kg}^{-1}$.

The energy released is the mass flux multiplied by the heat of fusion which equals $0.085 \text{ W} \cdot \text{m}^{-2}$. The steady-state heat conduction is $\approx 17 \text{ W} \cdot \text{m}^{-2}$. These two terms differ by 3 orders of magnitude. Therefore, the assumption that the latent heat generated by the condensation and freezing of the water vapour is insignificant, can be considered reasonable.

APPENDIX E

Alternate Solutions to the Governing Differential Equation for Heat Transfer

In order to solve the governing differential equation for heat transfer (Eqn. (2.19)) in Section 2.2.1, the method of separation of variables, Powers (1979), was introduced. The separation constant, λ^2 , was chosen to be strictly negative and the resulting solution for the governing differential equation was presented. However, two other possible solutions also exist. The separation constant could have been chosen to be either zero or a positive real number instead of a negative real number. It will now be shown that only using a negative real separation constant will result in a physically realistic solution.

The governing differential equation was given in Eqn. (2.19) and is,

$$\frac{\partial \bar{\theta}}{\partial \bar{z}} + \frac{\alpha H}{wd^2} \frac{\partial^2 \bar{\theta}}{\partial \bar{x}^2} = 0 \quad (\text{E.1})$$

with the homogeneous boundary conditions given as (Eqn. (2.17)),

$$\bar{\theta}(0, \bar{z}) = 0 ; \quad \bar{\theta}(1, \bar{z}) = 0 ; \quad \bar{\theta}(\bar{x}, 0) = \frac{[-(T_I - T_H)\bar{x} + T_I] - T_c}{T_b - T_c} = 1 + \bar{x} \quad (\text{E.2})$$

Using the method of separation of variables results in

$$\bar{\theta}(\bar{x}, \bar{z}) = X(\bar{x}) Z(\bar{z}) \quad (\text{E.3})$$

so that Eqn. (E.1) becomes two ordinary differential equations in Z and X , expressed as,

$$\frac{wd^2}{\alpha H} \frac{1}{Z} \frac{dZ}{d\bar{z}} = -\lambda^2 \quad (\text{E.4})$$

$$\frac{1}{X} \frac{d^2 X}{d\bar{x}^2} = -\lambda^2 \quad (\text{E.5})$$

Soln. 1: Separation constant, $\lambda^2 = 0$

If the separation constant is chosen to be zero then, Eqn. (E.4) becomes

$$\frac{w d^2}{\alpha H} \frac{1}{Z} \frac{dZ}{d\bar{z}} = 0 \quad (\text{E.6})$$

which results in $Z(\bar{z}) = \text{constant}$ and Eqn. (E.5) becomes

$$\frac{1}{X} \frac{d^2 X}{d\bar{x}^2} = 0 \quad (\text{E.7})$$

which results in $X(\bar{x}) = C_1 \bar{x} + C_2$ where C_1 and C_2 are constants. Therefore, by multiplying the two solutions together as shown in Eqn. (E.3), the resulting solution to Eqn. (E.1) is

$$\bar{\theta}(\bar{x}, \bar{z}) = F(\bar{x}) + G \quad (\text{E.8})$$

where F and G are constants. Applying the first boundary condition in Eqn. (E.2) results in $G = 0$. The second boundary condition results in $F = 1$. The last boundary condition results in $\bar{x} = 0$ for all \bar{x} which is not a possible solution. Therefore, choosing the separation constant, λ^2 , to be zero is not a realistic solution.

Soln. 2: Separation constant, $\lambda^2 > 0$

If the separation constant is chosen to be strictly positive, then the solution to Eqn. (E.4) becomes,

$$Z(\bar{z}) = C_1 \exp\left[\frac{\alpha}{w} \lambda^2 \bar{z}\right] \quad (\text{E.9})$$

where C_1 is a constant; the solution to Eqn. (E.5) becomes

$$X(\bar{x}) = C_2 \exp[\lambda \bar{x}] + C_3 \exp[-\lambda \bar{x}] \quad (\text{E.10})$$

where C_2 and C_3 are constants. By multiplying the solutions for X and Z together, as shown in Eqn. (E.3), the result is another possible solution to Eqn. (E.1),

$$\bar{\theta}(\bar{x}, \bar{z}) = \exp\left[\frac{\alpha}{w} \lambda^2 \bar{z}\right] \left(A \cosh[\lambda \bar{x}] + B \sinh[-\lambda \bar{x}] \right) \quad (\text{E.11})$$

where A and B are constants.

Applying the three boundary conditions:

$$1. \bar{\theta}(0, \bar{z}) = 0$$

$$0 = \exp\left[\frac{\alpha}{w} \lambda^2 \bar{z}\right] A \quad (\text{E.12})$$

which leads to $A \equiv 0$.

$$2. \bar{\theta}(1, \bar{z}) = 0$$

$$1 = \exp\left[\frac{\alpha}{w} \lambda^2 \bar{z}\right] B \sinh(\lambda) \quad (\text{E.13})$$

$$3. \bar{\theta}(\bar{x}, 0) = 0$$

$$0 = B \sinh[\lambda \bar{x}] \quad (\text{E.14})$$

which leads to $\lambda \equiv 0$ since the constant B is arbitrary.

Boundary condition #2 and #3 are in conflict. If $\lambda = 0$, which it must be, then boundary condition #2 cannot equal 1, which it must. Therefore, choosing the separation constant, λ^2 , to be strictly positive is not a realistic solution.